MODEL BASED CONTROL OPTIMISATION OF RENEWABLE ENERGY BASED HVAC SYSTEMS

- SOLAR DRIVEN ABSORPTION AND OPEN DESICCANT EVAPORATIVE COOLING –

Dirk Pietruschka

A thesis submitted in partial fulfilment of requirements of De Montfort University for the degree of Doctor of Philosophy (PhD)

March 2010

Institute of Energy and Sustainable Development
De Montfort University Leicester

Faculty of Civil Engineering, Building Physics and Economics
University of Applied Sciences Stuttgart

ABSTRACT

During the last 10 years solar cooling systems attracted more and more interest not only in the research area but also on a private and commercial level. Several demonstration plants have been installed in different European countries and first companies started to commercialise also small scale absorption cooling machines. However, not all of the installed systems operate efficiently and some are, from the primary energy point of view, even worse than conventional systems with a compression chiller. The main reason for this is a poor system design combined with suboptimal control. Often several non optimised components, each separately controlled, are put together to form a 'cooling system'. To overcome these drawbacks several attempts are made within IEA task 38 (International Energy Agency Solar Heating and Cooling Programme) to improve the system design through optimised design guidelines which are supported by simulation based design tools. Furthermore, guidelines for an optimised control of different systems are developed. In parallel several companies like the SolarNext AG in Rimsting, Germany started the development of solar cooling kits with optimised components and optimised system controllers. To support this process the following contributions are made within the present work:

- For the design and dimensioning of solar driven absorption cooling systems a detailed and structured simulation based analysis highlights the main influencing factors on the required solar system size to reach a defined solar fraction on the overall heating energy demand of the chiller. These results offer useful guidelines for an energy and cost efficient system design.
- Detailed system simulations of an installed solar cooling system focus on the influence of the system configuration, control strategy and system component control on the overall primary energy efficiency. From the results found a detailed set of clear recommendations for highly energy efficient system configurations and control of solar driven absorption cooling systems is provided.

- For optimised control of open desiccant evaporative cooling systems (DEC) an innovative model based system controller is developed and presented. This controller consists of an electricity optimised sequence controller which is assisted by a primary energy optimisation tool. The optimisation tool is based on simplified simulation models and is intended to be operated as an online tool which evaluates continuously the optimum operation mode of the DEC system to ensure high primary energy efficiency of the system. Tests of the controller in the simulation environment showed that compared to a system with energy optimised standard control the innovative model based system controller can further improve the primary energy efficiency by 19 %.

DECLARATION

The research presented in this thesis is the original work of the author except where otherwise specified, or where acknowledgements are made by references. The contents of the work have not been submitted for any academic or professional award. I acknowledge that this thesis is submitted according to the conditions laid down in the regulations. Furthermore, I declare that the work was carried out as a part of the course for which I was registered. I draw attention to any relevant considerations of rights of third parties.

ACKNOWLEDGEMENTS

This research was carried out at the Institute of Energy and Sustainable Development at De Montfort University Leicester in collaboration with the Faculty of Civil Engineering, Building Physics and Economics at the University of Applied Sciences Stuttgart.

I would like to take this opportunity to express my gratitude to my supervisiors Prof. Dr. Victor Hanby and Prof. Dr. Ursula Eicker for their valuable help, revision and encouragement throughout the period of study.

I would also like to extend my thanks to Dr. Jürgen Schumacher who gave me significant support during the utilisation of his software INSEL which plays a major role in this work. Furthermore, I am grateful to my colleagues at the Faculty of Civil Engineering, Building Physics and Economics at the University of Applied Sciences Stuttgart for their assistance, especially to Martin Huber, Petra Fischbach and Silke Schmidt who planned, organised and did the hardware installation of the new setup of the DEC system. Furthermore, I'd like to thank Siegfried Riedel who helped me with the cabling work on the DEC system.

The SolarNext AG in Rimsting, Germany offered me the possibility to work on their chilli® solar cooling system. They provided me with all the data of the installation and with measured performance data of the system which I used for the validation of the developed simulation models. Especially, I'd like to thank Dr. Uli Jakob, the former head of the Solar Cooling Division of the SolarNext AG, who supported me with my work on their installation and who revised chapter 4 of this work.

Finally – wondering that I am still married – I would like to express special thanks to my wife Simone for her patience, encouragement and her understanding of the fact that a lot of common leisure time and many, many weekends were necessary to complete this work.

TABLE OF CONTENT

APPENDIX

NOMENCLATURE

Latin letters

A	[m²]	surface, area
a_1	[W m^{-2}K^{-1}]	heat loss coefficient
a_2	[W m^{-2}K^{-2}]	temperature dependent heat loss coefficient
C	[J kg^{-1} K^{-1}]	specific heat of liquids and solids
c_p	[J kg^{-1} K^{-1}]	specific heat of gases at constant pressure
C_{eff}	[J m^{-2} K^{-1}]	effective or area related heat capacity
C_k	[-]	cooling tower constant
$\dot{C}$	[J s^{-1} K^{-1}]	capacity flow
d	[m]	diameter
D	[°dH]	Hardness of the fresh water (1°dH = 0.18 mol m^{-3})
d_z	[°dH]	Hardness of the circulated water
G	[$W\ m^{-2}$]	Solar radiation
H	[m]	Height
h	[J/kg]	specific enthalpy
h_c	[W m^{-2}K^{-2}]	convective heat transfer coefficient
h_r	[W m^{-2}K^{-2}]	irradiative heat transfer coefficient
$K_{\theta b}$	[-]	incident angle modifier for beam radiation
$K_{\theta d}$	[-]	incident angle modifier for diffuse radiation
l	[m]	Length
L	[m]	characteristic length (for *Nu*, *Sh* and *Re*)
l_0	[$kg\ kg^{-1}$]	effective air to water mass flow rate
l_{min}	[$kg\ kg^{-1}$]	minimum air to water mass flow rate
m	[kg]	Mass
$\dot{m}$	[$kg\ s^{-1}$]	mass flow
M	[$kg\ mol^{-1}$]	specific molar mass
Nu	[-]	Nusselt-number (heat transmission)
P	[Pa]	(total) pressure
P_{el}	[W]	electrical power

PEF	[-]	Primary energy factor
PER	[-]	Primary energy ratio
Pr	[-]	Prandtl-number (heat transmission)
p_v	[*Pa*]	partial vapour pressure (in this study always $p_v \mathrel{\hat{=}} p_{v,H_2O}$)
Q	[*J*] or [kWh]	thermal energy / heat
$\dot{Q}$	[*W*]	Heat flow
R	[*J/kg K*]	specific gas constant
Re	[-]	Reynolds-number (flow: laminar, turbulent)
RH	[-] / [%]	relative humidity
R_m	[*J/mol K*]	general/molar gas constant (8.3145 J/mol K)
Sc	[-]	Schmidt-number (mass transmission)
Sh	[-]	Sherwood-number (mass transmission)
T	[°C]	(internal) Temperature
*t_*	[°*C*]	(external) temperature
t	[*s*]	Time
U	[W $m^{-2}K^{-1}$]	heat loss coefficient
u	[*m*]	circumference
U_{eff}	[W $m^{-2}K^{-1}$]	effective heat loss coefficient
V	[m^3]	Volume
$\dot{V}$	[m^3h^{-1}]	volume flow rate
v	[*m/s*]	flow velocity
W	[m]	Width
$\dot{W}$	[kg s^{-1}]	water consumption
x	[*kg/kg*]	absolute humidity of air
X	[$kg_{LiBr}/kg_{solutiion}$]	Concentration of LIBr solution

Greek Letters

α	$[W/m^2\,K]$	heat transmission coefficient
β	$[m/s]$	mass transmission coefficient
$\Delta...$	[-]	difference
δ_{eff}	$[m^2/s]$	effective diffusion coefficient (gas diffusion in porous solid material)
δ	[-]	Boolean switch parameter (0,1)
δ_N	$[m^2/s]$	normal gas diffusion coefficient (gas in gas)
γ	[-]	ratio area of rips
η	$[Pa\,s]$/[-]	dynamic viscosity / efficiency
η_0	[-]	zero-loss collector efficiency
φ	[-]	relative humidity of air
λ	$[W/m\,K]$	heat conductivity
λ_a	[-]	air ratio
μ_p	[-]	gas diffusion resistance coefficient of porous solid materials
ν	$[m^2/s]$	kinetic viscosity
Θ	[°]	incident angle
ρ	$[kg/m^3]$	density

Subscripts

a	absorber plate of air collector
A	Axis
A	absorber / air
ad	additional / adsorption
amb	Ambient
b	back cover of air collector
C	condenser / convective
Cc	convection and conduction
col	Collector
con	Convective
d	design conditions

e	evaporator
el	electrical
ev	evaporation
f	Fluid
fc	forced convection
fi	Fins
fl	liquid phase
g	generator
h	horizontal surface / heat
H_2O	Water
hc	convective heat transfer
hl	heat lossed
i / n	Index (0,1,2...) / number
in	Inlet
iso	isolation
l	linear
m	motor
m	mean value
max	maximal / maximum
min	minimal / minimum
out	outlet
r	rich LiBr solution
reg	regeneration
ret	return
s	storage
s	saturation
st	stored
sup	supply
t	tilted surface
tot	total
v	ventilator
V	Water vapour
W	Water

wb	wet bulb

Abbreviations

ACM	**A**bsorption **C**ooling **M**achine
COP	**C**oefficient **O**f **P**erformance
CPC	**C**ompound **P**arabolic **C**oncentrator
DEC	**D**esiccative and **E**vaporative **C**ooling

1. INTRODUCTION

Solar or waste heat driven closed absorption or adsorption chillers and open desiccant evaporative cooling systems (DEC) offer the potential to provide summer comfort conditions in buildings at low primary energy consumption (Henning, 2004). As a consequence of the climate change debate and the common goal to reduce the CO_2 emissions in the European Union by at least 20% until 2020, interest in these innovative technologies has increased significantly during the last ten years. Several test and demonstration plants of the different technologies have been installed. However, not all of the installed systems operate in an energy efficient way. From the primary energy point of view some are even worse than comparable conventional systems with compression chillers (Sparber, et al., 2009; Núnez, et al., 2009; Vitte et al., 2008). Reasons for this are insufficiently designed solar systems and badly dimensioned hydraulics with inefficient or over dimensioned pumps or fans or badly controlled heat rejection systems. This leads to high additional heating energy and electricity consumption and in consequence significantly reduces their primary energy efficiency. Consequently, the requirement of appropriate design tools and integrated energy efficient system control is attracting more and more attention in research and development and therefore are main topics of IEA task 38 (International Energy Agency Solar Heating and Cooling Programme).

1.1 SOLAR DRIVEN ABSORPTION CHILLERS

For the often used single effect absorption chillers, the ratio of cold production to input heat (COP) is in the range of 0.5-0.8, while electrically driven compression chillers today work at COPs around 3.0 or higher. Solar fractions on the heating energy demand of the absorption chillers therefore need to be higher than about 50% to start saving primary energy (Mendes, et al., 1998). The exact value of the minimum solar fraction required for primary energy saving not only depends on the performance of the thermal chiller, but also on the electricity consumption of the other components such as the cooling tower:

a thermal cooling system with an energy efficient cooling tower performs better than a compression chiller at a solar fraction of 40%, a low efficiency cooling tower increases the required minimum solar fraction to 63%. These values were calculated for a thermal chiller COP of 0.7, a compressor COP of 2.5 and an electricity consumption of the cooling tower between 0.02 or 0.08 kWh_{el} per kWh of cold (Henning, 2004).

Double effect absorption cycles have considerably higher COPs at around 1.1 - 1.4, but require significantly higher driving temperatures between 120°C and 170°C (Wardono and Nelson, 1996), so that the energetic and economical performance of the solar thermal cooling system is not necessarily better (Grossmann, 2002).

Several authors published detailed analyses of the absorption cycle performance for different boundary conditions, which showed the very strong influence of cooling water temperature, but also of chilled water and generator driving temperature levels on the coefficient of performance (Engler, et al., 1997; Kim, et al., 2002). Most models resolve the internal steady state energy and mass balances in the machines and derive the internal temperature levels from the applied external temperatures and heat transfer coefficients of the evaporator, absorber, generator and condenser heat exchangers. To simplify the performance calculations, characteristic equations have been developed (Ziegler, 1998), which are an exact solution of the internal energy balances for one given design point and which are then used as a simple linear equation for different boundary conditions. The disadvantages of the characteristic equation can be easily overcome, if dynamic simulation tools are used for the performance analysis and internal enthalpies are calculated at each time step - an approach, which is chosen here (see chapter 2.1.2.1) using the simulation environment INSEL (Schumacher, 1991).

The available steady state models of the absorption chillers provide a good basis for planners to dimension the cooling system with its periphery such as

fans and pumps, but they do not give any hint for the dimensioning of the solar collectors or any indication of the solar thermal contribution to total energy requirements. This annual system performance depends on the details of the collector, storage and absorption chiller dimensions and efficiencies for the varying control strategies and building load conditions. An analysis of the primary energy savings for a given configuration with renewable energy heat input requires a complete model of the cooling system coupled to the building load with a time resolution of at least one hour. Very few results of complete system simulations have been published. In the IEA task 25 several design methods have been evaluated and a simplified design tool is currently under development in IEA task 38. In the simplest approach a building load model provides hourly values of cooling loads and the solar fraction is calculated from the hourly produced collector energy at the given irradiance conditions. Excess energy from the collector can be stored in available buffer volumes without however considering specific temperature levels. Different building types were compared for a range of climatic conditions in Europe with cooling energy demands between 10 and 100 kWh per square meter conditioned space and annum. Collector surfaces between 0.2 - 0.3 m^2 per square meter of conditioned building space combined with 1 - 2 kWh of storage capacity gave solar fractions above 70% (Henning, 2004). System simulations for an 11 kW absorption chiller using the dynamic simulation tool TRNSYS gave an optimum collector surface of only 15 m^2 for a building with 196 m^2 gross floor area and 90 kWh per m^2 annual cooling load, i.e. less than 0.1 m^2 per square meter of building surface. A storage volume of 0.6 m^3 was found to be optimum (40 litre per m^2 collector), which at 20K useful temperature level only corresponds to 14 kWh total or 0.07 kWh per square meter of building gross floor area (Florides, et al., 2002). Another system simulation study (Atmaca, et al., 2003) considered a constant cooling load of 10.5 kW and a collector field of 50 m^2. 75 liters of storage volume per square meter of collector surface were found to be optimum. Larger storage volumes were detrimental to performance. The main limitation of these models is that the storage models are very simple and only balance energy flows, but do not consider stratification of temperatures. This

explains the performance decrease with increasing buffer volume, if the whole buffer volume has to be heated up to reach the required generator temperatures.

Also, attempts have been made to relate the installed collector area to the installed nominal cooling power of the chillers in real project installations. The collector areas varied between 0.5 and 5 m² per kW of cooling power with an average of 2.5 m² per kW. To summarise the available solar cooling simulation literature, there are detailed thermal chiller models available, which are mainly used for chiller optimisation and design and not for annual system simulation. Solar thermal systems on the other hand, have been dynamically modelled mainly for heating applications.

A detailed monitoring of installed solar driven absorption and adsorption cooling systems within IEA task 38 showed that the electricity consumption of the ACM itself, the external pumps and especially of the heat rejection system clearly influence the primary energy efficiency reached. Systems with over dimensioned pumps and badly controlled heat rejection system (constant fan speed) reach primary energy ratios (PER) which are below 1.0 in the worst case (Sparber, et al., 2009; Núnez, et al., 2009). For comparison, systems with good compression chillers in the same power range with dry heat rejection typically reach average electrical system COP of 3.0 and primary energy ratios which are slightly above 1.0 (Yu, et al., 2004). This clearly demonstrates that solar driven absorption chillers are not necessarily better than standard systems with compression chillers. Therefore, improved and standardised control strategies and the development of system kits with improved hydraulics and highly efficient pumps are required. Most of the installed solar driven absorption and adsorption cooling systems are operated with independent controllers for the solar system, the absorption chiller and the cooling tower. New control strategies try to optimise the primary energy efficiency at part load conditions through increased temperature setpoints for the heat rejection system (with fan speed control) if sufficient solar heat is available (Albers, 2008). However, for

the implementation of such improved control strategies and control algorithms new system controllers need to be developed, which are able to control the whole solar cooling system.

Purely solar driven absorption cooling systems often suffer from a delayed system startup in the morning caused by the relatively high inertia of the collector field and of the hot water storage tank. To overcome this problem actual research work focuses on direct solar driven absorption chillers without hot water storage (Kühn, et al., 2008, Safarik, 2008). These systems operate very well on cloudless days and if the cooling load of the building is constantly nearly equal or higher than the cooling capacity of the absorption chiller. Other conditions lead to several shutdowns and startups of the chiller and in consequence result in low energy efficiencies. These problems of direct solar driven absorption chillers can be reduced if a hot water storage with storage bypass can be implemented in the systems. However, intelligent storage charge and discharge strategies are required to ensure an early system startup and a stable operation of the absorption chiller on partly cloudy days.

1.2 SOLAR DRIVEN OPEN DESICCANT EVAPORATIVE COOLING SYSTEMS (DEC)

Desiccant cooling systems are an interesting technology for sustainable building climatisation, as the main required energy is low temperature heat, which can be supplied by solar thermal energy or waste heat. Desiccant processes in ventilation mode use fresh air only, which is dehumidified, precooled and humidified to provide inlet air at temperature levels between 16 and 19°C. Crucial for the process is an effective heat exchange between the dried fresh air and the humidified exhaust air, as the outside air is dried at best in an isenthalpic process and is warmed up by the heat of adsorption. For a rather high heat exchanger efficiency of 85%, high humidification efficiencies of 95% and a dehumidification efficiency of 80%, the inlet air can be cooled from design condition of 32°C and 40% relative humidity to below 16°C, which is already slightly below the comfort limit.

The concept of desiccant cooling was developed in the 1930s and early attempts to commercialize the system were unsuccessful. Pennington patented the first desiccant cooling cycle (Pennington, 1955), which was then improved by Carl Munters in the 1960s (Munters, 1960). Good technology overviews are given by Mei, Lavan and others (1992) or Davanagere, et al. (1999). The most widely used desiccants are silica gel, lithium chloride or molecular sieves, for example zeolites. Solid desiccants such as silica gel adsorb water in its highly porous structure. Lithium chloride solution is used to impregnate for example a cellulose matrix or simpler cloth based constructions and can then be used to absorb water vapor from the air stream (Hamed, et al., 2005). Apart from cooling applications with adiabatic humidification, desiccant systems have been proposed for air drying only. Recent studies consider for example museum buildings with high requirements on air properties (Ascione, et al., 2009).

Although the technology is known for decades, there are only a few demonstration plants which are powered by solar energy, so that operational experience from such plants is very scarce. To introduce the technology into the market, information about the energy performance (efficiency, heat and electricity consumption), water consumption and maintenance issues need to be provided.

Compared to closed cycle cooling systems, where the thermal energy efficiency is simply defined by the ratio of produced cold to the input heat, open cycle system efficiency can either be related to the removed cooling load of the building (room air) or to the enthalpy decrease of ambient air.

For the hygienically needed fresh air supply, the enthalpy difference between ambient air and room supply air can be considered as useful cooling energy. If the building has higher cooling loads than that can be covered by the required fresh air supply, the useful cooling energy has to be calculated from the enthalpy difference between room exhaust and supply air, which is mostly

lower. The thermal COP is obtained from the enthalpy ratio. Related to ambient air, the thermal COP can be near to 1.0, if regeneration temperatures are kept low, and reduces to 0.5, if the ambient air has to be significantly dehumidified. Thermal COP's obtained from room exhaust to supply air are lower between 0.35 and 0.55 (Eicker, 2003).

Under conditions of 35°C ambient air temperature and 40% relative humidity, defined by the American Air conditioning and Refrigeration Institute (so called ARI conditions), reversible thermal COP´s of 2.6 and 3.0 were calculated for ventilation and recirculation mode (Kanoglu, 2007). The real process, however, has highly irreversible features such as adiabatic humidification. Furthermore, the specific heat capacity of the desiccant rotor increases the heat input required.

Simple models have been used to estimate the working range of desiccant cooling systems, for example to provide room conditions not just for one set point, but for a range of acceptable comfort conditions (Panaras, et al., 2007). The performance of the desiccant rotor itself can be evaluated by complex heat and mass transfer models based on Navier Stokes equations (Maclaine-Cross, 1988; Gao, et al., 2005). This allows the evaluation of the influence of flow channel geometry, sorption material thickness, heat capacity, rotational speed, fluid velocity etc. They are mostly too time consuming to be used in full system simulations including solar thermal collectors, where mostly simpler models are available, based either on empirical fits to measured data (Beccali, et al., 2003) or on models of dehumidification efficiency.

Different control strategies have been compared by Ginestet, et al. (2003) to study the influence of air volume flow and regeneration temperature. As the increase of regeneration temperature does not linearly lower the supply air temperature, the study concluded that increased air flow rates are preferable to increased thermal input by auxiliary heaters, if the cooling demand is high.

Mean calculated thermal COP´s for the climatic conditions of Nice were between 0.3 and 0.4. Henning and others also remarked that increasing the air flow is useful in desiccant cooling mode, but that the minimum acceptable flow rate should be used in adiabatic cooling or free ventilation mode to reduce electricity consumption (Henning, et al., 1999; Vitte, et al., 2008).

Common problems of many installed DEC systems are very low solar system efficiencies of the installed collector fields (Eicker, et al., 2006) and moderate primary energy ratios[1] with values between 1.2 and 1.7 (Henning, et al., 2002; Vitte, et al., 2008). For comparison, standard air handling units with compression chillers reach primary energy efficiencies in the region of one or slightly below one (Vitte, et al., 2008). The low solar system efficiencies of the collector fields of DEC systems are an attribute to the fact that for dry climatic conditions indirect or combined humidification is often sufficient to cover the required cooling load, especially if the system is operated at maximum air flow rate. In consequence, the sorption wheel is very seldom in operation. In some control strategies, fixed regeneration temperatures are implemented although often much lower regeneration temperatures would be sufficient to cover the required cooling load (Schürger, et al., 2006). This significantly increases the amount of required additional heating energy. Systems with primary energy optimised control therefore should operate at variable regeneration temperatures between 45°C and 90°C. Additionally, the regeneration mode should be activated with priority to the increase of the air flow rate if sufficient solar energy is available and the cooling load cannot be covered with combined humidification at the lowest possible air flow rate.

DEC systems are typically controlled by sequence controllers which switch on or off the system components dependening on the ambient and room air conditions. In case of a primary energy improved control strategy at cool and

[1] The primary energy ratio is defined as the ratio between the cooling power provided to the room divided by the primary energy consumption caused by additional heating and electricity for the pumps and fans of the system.

dry ambient air conditions first the return air humidifier and the heat exchanger between supply and return air are activated for indirect evaporative cooling. Afterwards the supply air humidifier is switched on and the system operates in combined humidification mode. If the room air temperature still increases, sufficient solar energy is available and the supply air temperature is above the lower limit, the regeneration mode is activated. If this is still not sufficient to cover the cooling load, as a next control option the air volume flow is increased. The additional heater is considered as the last control option to increase the regeneration air temperature if at full desiccant mode and full air flow rate the provided cooling power is still too low to keep the room air conditions within comfort limits. However, common control problems of installed DEC systems mainly result from an insufficient consideration of the inertia of the components especially of the humidifiers. Typical contact matrix or hybrid humidifiers take about 5 to 10 minutes after activation until they reach their full humidification efficiency. If they are deactivated after full operation it takes more than 15 minutes until a significant decrease in humidification efficiency becomes visible and more than 45 minutes until they are completely dried. A too fast activation of the components can lead to uncomfortable supply air conditions which result in several control reactions to increase the supply air temperature again. In consequence the DEC system is operated inefficiently at fluctuating operation modes (Eicker, et al., 2003). A too slow activation of the humidifiers and humidifier stages on the other hand can lead to uncomfortable room air conditions and in consequence to an activation of the DEC mode with increased air volume flow although not strictly required.

1.3 RESEARCH AIMS AND OBJECTIVES

As shown in chapter 1.1 and 1.2 solar cooling systems often do not reach the expectations on their overall energy efficiency. The main problems found can be attributed to insufficient system design, system configuration, control strategy selection and system control. The present work aims to give assistance to overcome these shortcuts of this innovative and promising technology. Therefore, the mentioned four main problems found are addressed and

analysed in different levels of detail. Dynamic system simulations are used for the analyses of the complex systems in the simulation environment INSEL. The main tasks and objectives of the presented work can be summarised as follows:

- Dimensioning strategies for solar driven absorption cooling systems

The aim of chapter 3 of this work is to analyse and highlight the influencing factors on the design of solar driven absorption cooling systems. The factors addressed are different cooling load characteristics caused by high or low internal loads, different building orientations and locations. Furthermore, the influence of different system configurations (high / low temperature cold distribution, dry or wet heat rejection) and the influence of different control strategies (constant or variable generator inlet temperatures) on the system design are addressed. A detailed cooling cost analysis highlights applications and configurations which offer the potential for a cost effective implementation of the innovative technology in the near future.

- Model based control strategy optimisation of solar driven absorption cooling systems

Chapter 4 of this work aims to give a clear set of recommendations on the control strategies and system configurations required for a highly energy efficient operation of solar driven absorption cooling systems. Therefore, detailed analyses are performed to highlight the influence of different control strategies and system configurations on the overall primary energy efficiency. These controls strategies and system configurations are analysed in the simulation environment for a solar cooling system installed in Germany. The main influencing factors addressed are the cooling tower type (dry or wet), its temperature setpoint and the implementation of a fan speed control. Furthermore, the control of the generator inlet temperature (constant / variable) and the implementation of a mass flow control of the cold distribution pump are analysed.

For purely solar driven absorption chillers additionally strategies for an early systems startup and a high solar cooling fraction on the cooling energy demand of the building are developed. Here different hot water storage charge and discharge strategies with storage bypass and / or storage segmentation are analysed and compared.

- **Model based development of primary energy optimised control strategies for open desiccant evaporative cooling systems (DEC)**

The main aim of chapter 5 is to develop a control strategy which efficiently avoids the typical control problems found for installed desiccant evaporative cooling systems in order to improve their primary energy efficiency. An electricity optimised standard sequence controller is used with control support from a primary energy optimisation tool. The aim of this newly developed primary energy optimisation tool is a continuously evaluation of the optimum operation mode for the actual weather and room air conditions. This tool is supposed to be operated as ‘online tool’ which allows or blocks possible operation modes in the sequence controller. Furthermore, it includes a control support for the supply air humidifier to ensure a stable and efficient operation.

2. MODEL DEVELOPMENT FOR SOLAR COOLING COMPONENTS

2.1 INTRODUCTION

There are several modular dynamic simulation tools available for the simulation of HVAC and solar heating and cooling systems like TRNSYS, HVACSIM+, Energy Plus, Simulink-Simad, INSEL and others.

TRNSYS (2004) in the version 16.1 provides a full set of simulation models required for the simulation of solar hot water systems. For hot water driven single effect absorption chillers there are two types of models available. TRNSYS Type 107 is a model of a single-effect hot water driven absorption chiller which uses a lookup approach from a performance data file to predict the part load performance. This model is based on normalised performance characteristics derived from large single effect absorption chillers (>200 kW). Therefore it could in principle be applied also to small scale single effect absorption chillers. During the work in IEA Task 25 also a TRNSYS Type 107 has been developed for TRNSYS-15 (Albers, 2002). To avoid conflicts the Type number has been changed in TRNSYS-16 to Type 177. This Type uses the method of characteristic equations (Schweiger, et al., 1999), which can be used to describe the part load behaviour of ad- and absorption chillers. The main problem of this model is the difficulty to generate the required model parameters of the chiller, which requires a set of detailed measured performance data (Witte, et al., 2006). For open desiccant evaporative cooling systems there are models for all required components (sorption wheel, heat exchangers, solar air collectors, humidifiers, etc.) available in TRNSYS. Most of these standard models do not consider the inertia of the components.

HVACSIM+ (open source) is also a modular simulation tool specially designed for the simulation of HVAC systems and HVAC controls (Park, 1985). There are models available for solar heating systems, all HVAC components including sorption wheels and some absorption chillers. The modular structure of HVACSIM+ is based on the methodology used in TRNSYS. Some of models developed in HVACSIM+ can be also used in TRNSYS. However, HVACSIM+

does not provide a graphical programming interface, which makes the model development of complex models difficult. Further disadvantages are missing meteorological functions which are required e.g. to calculate the solar radiation on different orientated façades and long calculation times when solving simultaneous simulations.

EnergyPlus (open source) is a very powerful building simulation program (open source) which includes building heat balance simulations as well as building system simulations like HVAC or PV systems etc. and offers interfaces to HVACSIM+ and other advanced software. The main disadvantage is the high level computer literacy required and a missing structured free ware graphical interface. A commercial graphical interface is provided by DesignBuilder which makes the model development in EnergyPlus much easier.

SIMBAD Building and HVAC-Toolbox performs transient simulations of HVAC plants with short time steps. SIMBAD Building and HVAC Toolbox is a HVAC toolbox for the MATLAB/Simulink environment. The toolbox provides a large number of ready to use HVAC models and related utilities to perform dynamic simulation of HVAC plants. This toolbox in connection with other existing toolboxes (Neural network, fuzzy logic, optimisation etc.) offers a powerful and efficient tool for design and test of controllers. The weakness of this toolbox is that there are no models available for solar heating and cooling systems. Furthermore there are no detailed meteorological functions included.

INSEL 7.0 is a modular simulation environment, with software to understand, plan, monitor, and visualize energy systems. For this purpose, INSEL provides state-of-the-art functions as blocks for the simulation of meteorological data, electrical and thermal energy components. These blocks can be interconnected to a detailed model of a specific simulation problem. For the interconnection of the INSEL blocks a runtime version of HP VEE can be used as graphical interface. In the newer version INSEL 8.0 HPVEE is replaced by a new integrated graphical interface. INSEL provides very detailed mathematical and meteorological tool sets and basic simulation tools for solar thermal heating and cooling systems.

In the present work INSEL was chosen as simulation environment to perform all the simulations required within this work for the detailed analysis and control strategy optimisation of the solar cooling systems. There are three main reasons for the choice of INSEL:

- INSEL provides all the required functionality required for the complex simulation tasks
- In INSEL the physical models of each component are solved within each single block. Therefore, there is no need for a common equations solver. This makes the simulations of complex models much faster compared to the other tools
- INSEL offers interfaces like OPC or DataSocket for a direct communication between INSEL and building management or other plant control systems. For future work, this offers the opportunity of a direct coupling of the primary energy optimisation tool for open desiccant evaporative cooling systems (DEC) developed in chapter 5 of this work with the control unit of the installed DEC-system at the University of Applied Sciences in Stuttgart.
- INSEL has been developed by Dr. Schumacher (1991) in Oldenburg and is now further developed in Stuttgart. The direct contact to the developer of INSEL was considered to be very helpful for the solution of the complex simulation tasks.

Altogether, there was some additional need for model development in INSEL compared to other software like TRNSYS or EnergyPlus. However, due to other significant advantages stated above it was considered to be worth while to spend some additional time in model development.

At the start of the work in INSEL some models for the simulation of solar systems, like simple collector, heat exchanger and storage models for water based systems and a static and dynamic air collector model for air based systems were available. For the simulation of open desiccant systems an existing desiccant wheel model and a simple humidifier model could also be used. Models for the simulation of closed absorption cooling machines were not included in INSEL. Since the topic of this work was to perform detailed

simulation based analyses on control strategies of solar cooling systems, new and more detailed models of the components of solar cooling systems needed to be developed. Within this chapter the developed models like dynamic solar collector, heat storage with stratification, solar heat exchanger, absorption chiller static and dynamic, dry and wet heat rejection systems, sorption wheel and dynamic humidifier are described in detail.

2.2 CLOSED SOLAR DRIVEN ABSORPTION COOLING SYSTEMS

Closed solar driven absorption cooling systems consist apart from the absorption chiller typically of a liquid based solar system which provides the required driving heat for the system. The solar system consists of solar collectors, a solar heat exchanger and a hot water storage tank. For heat rejection either wet cooling towers or dry heat rejection systems are used. On the cold distribution side most systems operate with smaller or larger cold water storage. In case of insufficient solar heat supply an auxiliary heating device is connected to most of the systems. **Fig. 2-1** shows a scheme of a solar driven absorption cooling system.

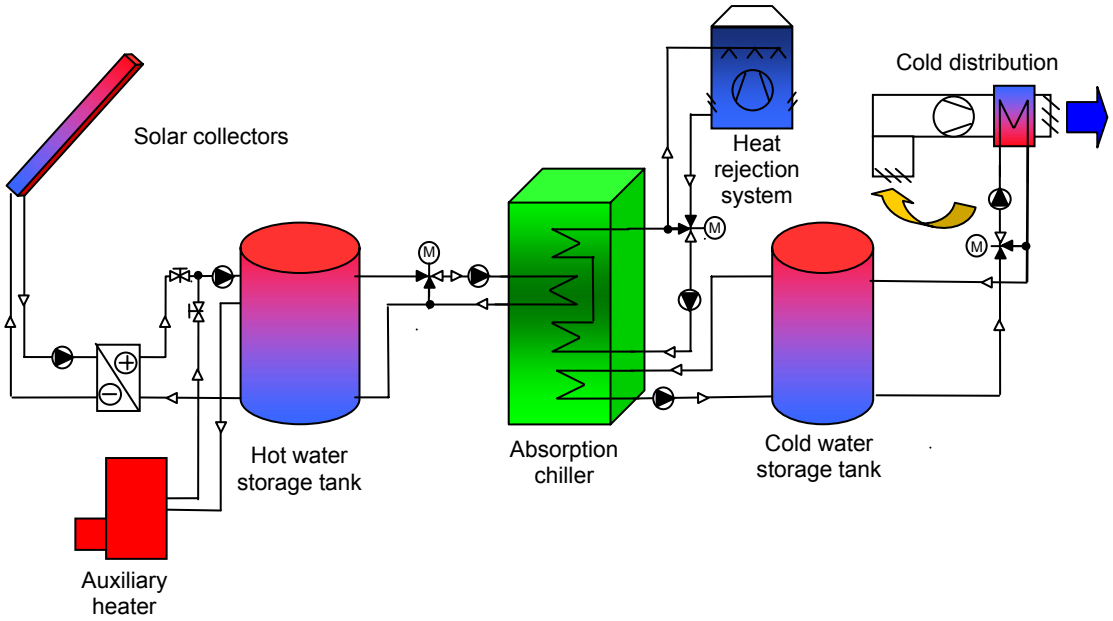

Fig. 2-1: Scheme of a solar driven absorption cooling system

Within chapter 2.2 models of all components of the solar driven absorption cooling system are described in detail.

2.2.1 SOLAR THERMAL SYSTEM

2.2.1.1 Solar Collectors

There are a number of different solar collectors available on the market, like flat plate collectors with single or double glazing or vacuum tube collectors with and without compound parabolic concentrator (CPC). It is very difficult to develop detailed dynamic simulation models for each available single collector type with product specific variations. Therefore, in this chapter a simplified dynamic simulation model is developed, which is based on the parameters of the harmonised collector test procedure described in EN 12975-2:2001 – part 2. Since these parameters are available for nearly all collectors, the developed model can be easily adapted to different collector types of different producers.

a) Static collector model

In the simplest static case without consideration of the thermal mass of the collector, the collector equation is given by

$$\dot{q}_{col} = \eta_0 \cdot \left(K_{\Theta b}(\Theta) \cdot G_b + K_{\Theta d}(\Theta) \cdot G_d\right) - a_1\left(T_{col,m} - T_{amb}\right) - a_2\left(T_{col,m} - T_{amb}\right)^2 \quad (2.2.1\text{-}1)$$

If the incident angle modifiers $K_{\Theta b}(\Theta)$ and $K_{\Theta d}(\Theta)$ are considered to be used externally for the calculation of a total solar irradiation on the collector field of G_t the equation simplifies to

$$\dot{q}_{col} = \eta_0 \cdot G_t - a_1\left(T_{col,m} - T_{amb}\right) - a_2\left(T_{col,m} - T_{amb}\right)^2 \quad (2.2.1\text{-}2)$$

and the overall collector efficiency is:

$$\eta_{col} = \eta_0 - a_1 \frac{\left(T_{col,m} - T_{amb}\right)}{G_t} - a_2 \frac{\left(T_{col,m} - T_{amb}\right)^2}{G_t} \quad (2.2.1\text{-}3)$$

If the collector mean temperature $T_{col,m}$ is approximated by the mean temperature of the collector inlet $T_{col,in}$ and collector outlet $T_{col,out}$

$$T_{col,m} = \frac{T_{col,in} + T_{col,out}}{2} \ , \quad (2.2.1\text{-}4)$$

the useful heating power of the collector is given by

$$\dot{Q}_{col} = \eta_{col} \cdot G_t \cdot A = \dot{m}_{fluid} c_{fluid} \cdot \left(T_{col,out} - T_{col,in}\right) \quad (2.2.1\text{-}5)$$

The solution of equation 2.2.1-3 and 2.2.1-5 for the collector outlet temperature leads to a quadratic equation with the solutions

$$T_{col,out\,1/2} = -\frac{p}{2} \pm \sqrt{\left(\frac{p}{2}\right)^2 - q} \quad (2.2.1\text{-}6)$$

and the coefficients:

$$p = \frac{2a_1}{a_2} + 2T_{col,in} - 4T_a + \frac{2\dot{m}_{fluid} \cdot c_{fluid}}{A \cdot a_2} \quad (2.2.1\text{-}7)$$

$$q = \left(\frac{2a_1}{a_2} - 4T_a + T_{col,in} - \frac{2\dot{m}_{fluid} \cdot c_{fluid}}{A \cdot a_2}\right) \cdot T_{col,in} - 4 \cdot \left(\frac{G_t \eta_0}{a_2} + \frac{a_1 Ta}{a_2} + T_a^2\right) \quad (2.2.1\text{-}8)$$

This simple model requires only the efficiency parameters of the collector zero efficiency η_0, linear heat loss coefficient a_1, and quadratic heat loss coefficient a_2 together with the reference gross aperture or absorber area. These values are provided on the product datasheet of the collectors. This block was already available and is called ‘SCETA’ and can be found in the thermal tool box of INSEL.

b) Simple one node dynamic collector model

With the new collector test procedure of EN 12975-2:2001 – part 2 the specific thermal capacity of the collectors is determined in form of an area related effective thermal capacity C_{eff} given in kJ $m^{-2}K^{-1}$. This thermal mass is considered in the collector equation in the general form:

$$\dot{q}_{col} = \eta_0 \cdot \left(K_{\Theta b}(\Theta) \cdot G_b + K_{\Theta d}(\Theta) \cdot G_d\right) - a_1\left(T_{col,m} - T_{amb}\right) - a_2\left(T_{col,m} - T_{amb}\right)^2 - C_{eff}\,\frac{dT_{col,m}}{dt} \qquad (2.2.1\text{-}9)$$

If we again assume that the incident angle modifiers $K_{\Theta b}(\Theta)$ and $K_{\Theta d}(\Theta)$ are considered externally we get

$$\dot{q}_{col} = \eta_0 \cdot G_t - a_1\left(T_{col,m} - T_{amb}\right) - a_2\left(T_{col,m} - T_{amb}\right)^2 - C_{eff}\,\frac{dT_{col,m}}{dt} \qquad (2.2.1\text{-}10)$$

If we further assume the collector mean temperature $T_{col,m}$ to be approximately equal to the mean temperature of the collector inlet and outlet temperature

$$T_{col,m} = \frac{T_{col,in} + T_{col,out}}{2} \qquad (2.2.1\text{-}11)$$

the collector equation can be written as

$$\begin{aligned}
&\frac{\dot{m}_{fluid} c_{fluid}}{A}\left(T_{col,out} - T_{col,in}\right) = \eta_0 \cdot G_t - a_1\left(T_{col,m} - T_{amb}\right) - a_2\left(T_{col,m} - T_{amb}\right)^2 - C_{eff}\,\frac{dT_{col,m}}{dt} \\
&\frac{2\dot{m}_{fluid} c_{fluid}}{A}\left(T_{co,ml}(t) - T_{col,in}\right) = \eta_0 \cdot G_t - a_1\left(T_{col,m}(t) - T_{amb}\right) - a_2\left(T_{col,m}(t) - T_{amb}\right)^2 - C_{eff}\,\frac{dT_{col,m}(t)}{dt} \\
&C_{eff}\,\frac{dT_{col,m}(t)}{dt} = \left(\eta_0 \cdot G_t + a_1 T_{amb} - a_2\left(T_{col,m}(t) - T_{amb}\right)^2 + \frac{2\dot{m}_{fluid} c_{fluid} T_{col,in}}{A}\right) \\
&\qquad\qquad - \left(a_1 + \frac{2\dot{m}_{fluid} c_{fluid} T_{col,m}(t)}{A}\right)
\end{aligned} \qquad (2.2.1\text{-}12)$$

With the simplifications

$$\begin{aligned}
a &= \eta_0 \cdot G_t + a_1 T_{amb} - a_2\left(T_{col,m}(t) - T_{amb}\right)^2 + \frac{2\dot{m}_{fluid} c_{fluid} T_{col,in}}{A} \\
b &= a_1 + \frac{2\dot{m}_{fluid} c_{fluid} T_{col,m}(t)}{A}
\end{aligned} \qquad (2.2.1\text{-}13)$$

this differential equation has the form:

$$C_{eff}\,\frac{dT_{col,m}(t)}{dt} = a - b \cdot T_{col,m}(t) \qquad (2.2.1\text{-}14)$$

Considering the initial condition: $T_{col,m}(0) = T_{col,m,0}$ the solution of this equation is:

$$T_{col,m}(t) = \frac{e^{-\frac{b\cdot t}{C_{eff}}}\left(b \cdot T_{col,m,0} + a \cdot e^{-\frac{b\cdot t}{C_{eff}}} - a\right)}{b} \qquad (2.2.1\text{-}15)$$

The collector outlet temperature is then calculated from equation 2.2.1-11. The dynamic model has been programmed in FORTRAN as INSEL block. To compare the efficiency of the static model and of the dynamic one node model an INSEL model has been developed with varying solar radiation and on / off switching of the collector mass flow. The results are shown in Fig. 2.2.

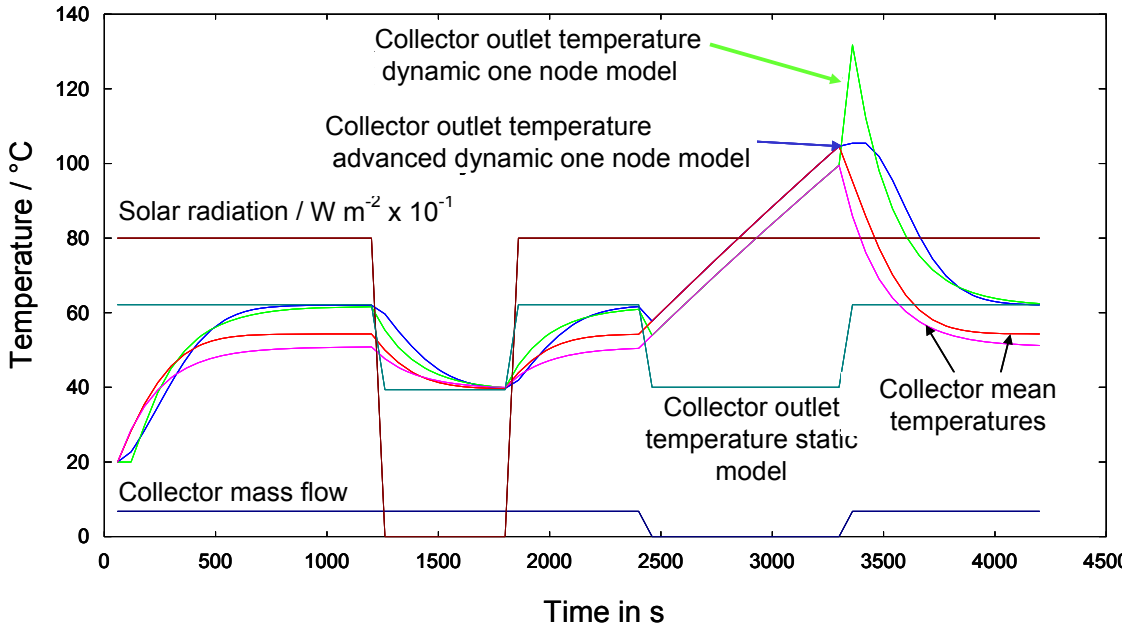

Fig. 2-2: Comparison of the performance of a static and a one node dynamic collector model

The difference between the static model and the dynamic one node model is clearly visible. The static model increases immediately to the steady state outlet temperature as soon as solar irradiation is on the collector plane and drops immediately down to the collector inlet temperature as soon the solar radiation

is off. For the dynamic one node model the temperature increases and decreases much slower, but finally reaches the same outlet temperature as the static model. However, if after a period without mass flow in the collector, the collector pump is switched on a large peak in the outlet temperature of the simple dynamic one node collector model is visible. This temperature peak increases significantly above the collector mean temperature before the pump is switched on. The reason for this unrealistic behavior is, that during the stand-still phase the collector temperature increases quite fast to a high value. When the collector pump is switched on the collector outlet temperature is then simply calculated form the cold collector inlet temperature and the collector mean temperature. Due to a large temperature difference between collector inlet temperature and collector mean temperature, a very high outlet temperature is calculated from Equation 2.2.1-11. To overcome this problem an improved model was developed which simply divides the collector model internally into a number of simple finite segments with same absorber area (whole absorber area divided by number of segments). The calculations are then done for each of the segments where the segment inlet temperature is set equal to the segment outlet temperature of the segment before. With this advanced dynamic one node model, the peak after a phase without collector mass flow is avoided and a realistic behavior is simulated.

2.2.1.2 Hot Water Storage Tank

For the solar storage of the solar driven cooling systems a storage tank model with ideal stratification has been developed. For a fully mixed solar storage tank the energy balance can be written as follows:

$$m_s c_s \frac{dT_s}{dt} = \dot{Q}_{h,col} + \dot{Q}_{h,ad} - \dot{Q}_{load} - \dot{Q}_{loss}$$

$$m_s c_s \frac{dT_s}{dt} = \delta_{col} \cdot \dot{m}_{col} \cdot c_{col} \cdot \left(T_{col,out} - T_s\right) + \dot{Q}_h - \delta_{load} \dot{m}_{load} \cdot c_{load} \cdot \left(T_s - T_{load,ret}\right) - U_{eff} A \cdot \left(T_s - T_{amb}\right) \quad (2.2.1\text{-}16)$$

Since neither the load Boolean switch δ_{load} nor the additional heating $\dot{Q}_h$ are continuous functions of the time, it is not possible to solve the differential equation analytically. Therefore, a simple forward differences method is used, which enables the calculation of the storage temperature for the actual time step n from the values of the previous time step (n-1) and equation (2.2.1-16) can be written as:

$$T_s(t_n) = T_s(t_{n-1}) + \frac{\Delta t}{m_s c_s}\begin{pmatrix} \delta_{col} \cdot \dot{m}_{col} \cdot c_{col} \cdot (T_{col,out} - T_s) + \dot{Q}_h \\ - \delta_{load} \dot{m}_{load} \cdot c_{load} \cdot (T_s - T_{load,ret}) \\ - U_{eff} A \cdot (T_s - T_{amb}) \end{pmatrix} \qquad (2.2.1\text{-}17)$$

For the storage tank with stratification (Fig. 2-3) the equation becomes more complex since for each layer an energy balance is required and additional effects like convective heat transfer and heat conduction between the layers needs to be considered. Since the exact mathematical model development is difficult for convective heat flows, the convection and conduction between the layers are approximated by a common effective heat conductivity λ_{eff}. According to Eicker (2001) for good constructed hot water storage tanks without internal heat exchangers this effective heat conductivity is in the region of the heat conductivity of water and can be approximated by a value of λ_{eff} = 0.644 W m^{-1} K^{-1}. For heat storages with internal heat exchangers effective heat conductivity is in the region of λ_{eff} = 1.0 - 1.5 W m^{-1}. With this the heat flow between layer i-1 and 1 or between i and i-1 is calculated according to the Fourier equation and the heat flow between one layer and the two adjacent layers caused by heat convection and heat conduction can be written as:

$$\begin{aligned} \dot{Q}_{cc,i} &= \dot{Q}_{cc,i-1\to i} - \dot{Q}_{cc,i\to i+1} \\ &= -A_s \frac{\lambda_{eff}}{z}(T_{s,i} - T_{s,i-1}) - \left(-A_s \frac{\lambda_{eff}}{z}(T_{s,i+1} - T_{s,i})\right) \\ &= A_s \frac{\lambda_{eff}}{z}(T_{s,i+1} - 2T_{s,i} + T_{s,i-1}) \end{aligned} \qquad (2.2.1\text{-}18)$$

Since only some of the layers are connected to external or active connections the energy balance needs to be developed for each of the layers, in the simplest case for layers without external connections the heat capacity flows are equal and the heat flow caused by forced convection is equal to:

$$\begin{aligned}\dot{Q}_{fc} &= \dot{m}_{i-1} \cdot c \cdot \left(T_{i-1} - T_i\right) + \dot{m}_i \cdot c \cdot \left(T_i - T_{i+1}\right) \\ &= \dot{m}_i \cdot c \cdot \left(T_{i-1} - T_{i+1}\right)\end{aligned} \qquad (2.2.1\text{-}19)$$

For layers with external connections the external energy flows need to be considered separately. If **stratification charge equipment** is used, the position of the external energy flow input depends on the temperature of the layers. The energy balance for one layer of the storage tank can then be written as:

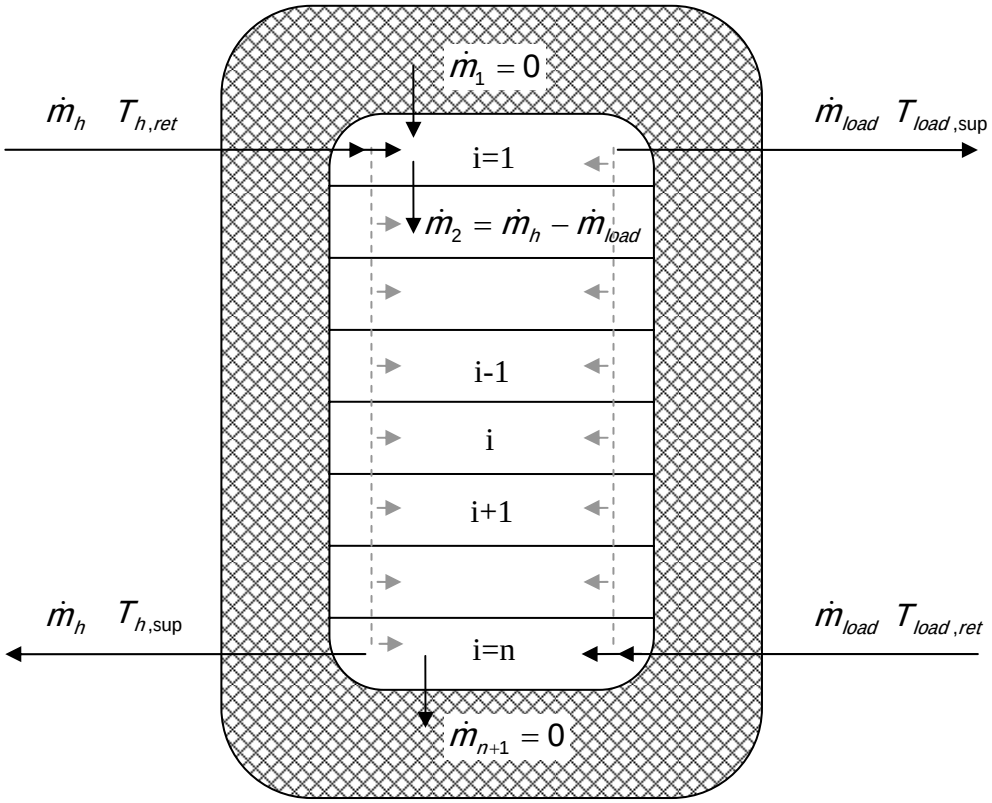

Fig. 2-3: Heat storage with stratification

$$m_s c_s \frac{dT_s}{dt} = \dot{Q}_{h,col,i} + \dot{Q}_{h,ad,i} - \dot{Q}_{load,i} - \dot{Q}_{loss,i} + \dot{Q}_{cc,i} + \dot{Q}_{fc,i} \qquad (2.2.1\text{-}20)$$

For the calculation of the energy exchange between the layers from top (i=1) to bottom (i=n) first the effective mass flows are calculated. For two connections (supply and return) of the heat source side and two connections (supply and return) of the load side with typically counter flow arrangement (supply to the heat source from the bottom and supply to the load from the top), the effective mass flow between the layers is calculated from the difference between both mass flows. For the first and the last layer the effective mass flow is zero.

In the developed model ideal stratification charge systems are considered for both, the heat supply and the return flow of the load. Therefore, in the model first the temperature profile of the storage tank of the previous time step is evaluated and compared to the actual heat supply and load return temperature. The heat supply is then fed into the highest possible node with a temperature less or equal to the actual heat supply temperature. The load return is fed into the highest possible node with a temperature equal or grater to the actual load return temperature. In the model the mass flow control of the heat supply and load return is controlled by load Boolean switch parameters δ_i^h (heat supply) and δ_i^{load} (load return).

Once the two layers with direct mass flow are known the mass flows between the layers are calculated. From the new mass flows and the inlet temperatures of the two sources the new temperature of each layer is calculated.

$$\dot{m}_i = \dot{m}_h \cdot \delta_i^h - \dot{m}_{load} \cdot \delta_i^{load} \qquad for\ i = 2,N \qquad (2.2.1\text{-}21)$$

$$\dot{m}_i = 0 \qquad for \qquad i = 1\ and\ i = N \qquad (2.2.1\text{-}22)$$

A positive effective mass flow with energy gain from layer i-1 to layer i is considered by the parameter $\delta_i^+ = 1$. For no or negative mass flow $\delta_i^+ = 0$. A

negative effective mass flow (larger load mass flow) is considered by the parameter δ_i^- = -1. For no or positive mass flow δ_i^- = 0. The energy balance of the storage can then be written as:

$$\begin{aligned} m_s c_s \frac{dT_{s,i}}{dt} = {} & \delta_i^h \cdot \dot{m}_h \cdot c \cdot \left(T_{h,ret} - T_{s,i}\right) + \dot{Q}_h \\ & - \delta_i^{load} \dot{m}_{load} \cdot c \cdot \left(T_{s,i} - T_{load,ret}\right) - U_{eff} A_i \cdot \left(T_{s,i} - T_{amb}\right) \\ & + \delta_i^+ \dot{m}_i \cdot c \cdot \left(T_{s,i-1} - T_{s,i}\right) + \delta_i^- \dot{m}_{i+1} \cdot c \cdot \left(T_{s,i} - T_{s,i+1}\right) \\ & - A_s \frac{\lambda_{eff}}{z} \cdot \left(T_{s,i} - T_{s,i-1}\right) \end{aligned} \qquad (2.2.1\text{-}23)$$

A_i is the outer tank wall area and A_s is the cross sectional area of the tank at the actual node. The Boolean switch parameters used above for the mass flow control in each layer are defined as follows:

$$\delta_i^h = \begin{cases} 1 & \text{for } T_i \le T_{h,ret} \\ & \text{means collector return in the layer i} \\ 0 & \text{for } T_i > T_{h,ret} \end{cases}$$

$$\delta_i^{load} = \begin{cases} 1 & \text{for } T_i \ge T_{load,ret} \\ & \text{means load return in the layer i} \\ 0 & \text{for } T_i < T_{load,ret} \end{cases}$$

$$\delta_i^+ = \begin{cases} 1 & \text{for } \dot{m}_i > 0 \\ & \text{means load energy flow from layer i-1 to layer i} \\ 0 & \text{for } \dot{m}_i \le 0 \end{cases}$$

$$\delta_i^- = \begin{cases} 1 & \text{for } \dot{m}_{i+1} < 0 \\ & \text{means load energy flow from layer i-1 to layer i} \\ 0 & \text{for } \dot{m}_{i+1} \ge 0 \end{cases}$$

2.2.1.3 Solar Heat Exchanger

Since in solar collector systems often water glycol mixtures are used as fluid to avoid freezing in winter a heat exchanger is required between the solar circuit and the heating circuit of the solar cooling system or building. For a high efficiency such heat exchanges should offer a sufficient transfer power in order

to ensure as low collector supply temperatures as possible. For an ideal heat exchanger the temperature of the cold fluid could be heated up to the inlet temperature of the cold fluid. The heat exchanger efficiency describes how close a heat exchanger comes to the ideal case and is therefore defined as the ratio between the maximum possible heat transfer and the actual heat transfer as shown in Equation 2.2.1-24.

$$\phi = \frac{\dot{m}_1 c_1 \left(T_{1,in} - T_{1,aus}\right)}{\dot{m}_1 c_1 \left(T_{1,in} - T_{2,in}\right)} = \frac{\dot{m}_2 c_2 \left(T_{2,aus} - T_{2,in}\right)}{\dot{m}_1 c_1 \left(T_{1,in} - T_{2,in}\right)} \qquad (2.2.1\text{-}24)$$

The heat exchanger effectiveness of the most common heat exchangers (counter flow, concurrent flow, cross flow) are functionally dependent on the ratio between the heat transfer power UA and the capacity flow $\dot{C} = \dot{m} \cdot c$. This ratio is called as number of transfer units NTU.

$$NTU = \frac{UA}{\dot{C}} \qquad (2.2.1\text{-}25)$$

The heat exchanger efficiency for counter flow heat exchangers is according to (Bosnjakovic, 1951) for heat capacity flows $\dot{C}_1 < \dot{C}_2$ as follows:

$$\phi = \frac{1 - e^{-\left(1 - \frac{\dot{C}_1}{\dot{C}_2}\right) \cdot \frac{UA}{\dot{C}_1}}}{1 - \frac{\dot{C}_1}{\dot{C}_2} e^{-\left(1 - \frac{\dot{C}_1}{\dot{C}_2}\right) \cdot \frac{UA}{\dot{C}_1}}} \qquad (2.2.1\text{-}26)$$

In INSEL a block called ‘HXS’ is already available based on the equations shown above. This block is used for the simulation of the counter flow heat exchangers of the solar systems analysed in Caper 3, 4 and 5.

2.2.1.4 Tubing

The heat losses of the collector tubing can be calculated by a linear heat loss coefficient U_l as shown in Equation 2.2.1-27. If mass flow is in the tubing the heat losses are equal to the temperature difference between tube inlet and tube outlet multiplied by the mass flow rate and the thermal capacity of the fluid. The energy balance can be solved for the outlet temperature of the tube as shown in Equation 2.2.1-28.

$$Q_{tube} = U_l \cdot l_{tube} \cdot \left(\overline{T}_w - T_a\right) = \dot{m}_w \cdot c_w \cdot \left(T_{w,in} - T_{w,out}\right) \qquad (2.2.1\text{-}27)$$

$$U_l \cdot l_{tube} \cdot \left(\frac{T_{w,in} + T_{w,out}}{2} - T_a\right) = \dot{m}_w \cdot c_w \cdot \left(T_{w,in} - T_{w,out}\right)$$

$$T_{w,out} = \frac{T_{w,in} \cdot \dot{m}_w \cdot c_w + 0.5 \cdot U_l \cdot l_{tube} \cdot \left(2 \cdot T_a - T_{w,in}\right)}{0.5 \cdot U_l \cdot l_{tube} + \dot{m}_w \cdot c_w} \qquad (2.2.1\text{-}28)$$

With the linear heat loss coefficient defined as:

$$U_l = \frac{\pi}{\frac{1}{2\lambda_{iso}} \cdot \ln\frac{d_{iso}}{d_{tube}} + \frac{1}{h_a \cdot d_{iso}}} \qquad (2.2.1\text{-}29)$$

With this quite simple model the heat loses of the collector tubing can be calculated with sufficient accuracy during operation of the collector field. This model was used for the annual simulations performed in Chapter 3.
However, in the simple model, losses during stand still of the collector pump and the storage capacity of the tube walls are not considered. These losses mainly occur at system startup when cold water from the tubing is pumped to the heat exchanger and into the collector which results in fluctuating outlet temperatures of the collector. For the detailed analysis of control strategies it is therefore important to consider these effects by a dynamic simulation model.

Two different cases need to be considered in this model, the standstill phase without mass flow in the tubes and the normal operation case with mass flow in the tubes. For the standstill phase the problem is similar to that of the fully mixed hot water storage model without external mass flows. Convection and conduction effects within the tubes are very complex and difficult to model and for the regarded application do not influence the accuracy significantly. These effects are therefore neglected and the problem can be written as:

$$\bar{C}_{tube}\frac{dT_{tube}}{dt} = -\left(U_{l,tube}\cdot l_{tube}\right)\cdot\left(T_{tube}(t) - T_{amb}\right) \qquad (2.2.1\text{-}30)$$

This differential equation can be solved if the initial condition that at t=0 the tube temperature is given after a phase with mass flow: $T_{tube}\big|_{t=0} = T_{tube,0}$

With this condition the temperature in the tube in dependence of the time is given as:

$$T_{tube}(t) = \left(T_{tube,0} - T_{amb}\right)\cdot\exp\left(-\frac{U_{l,tube}\cdot l_{tube}}{\bar{C}_{tube}}\cdot t\right) + T_{amb} \qquad (2.2.1\text{-}31)$$

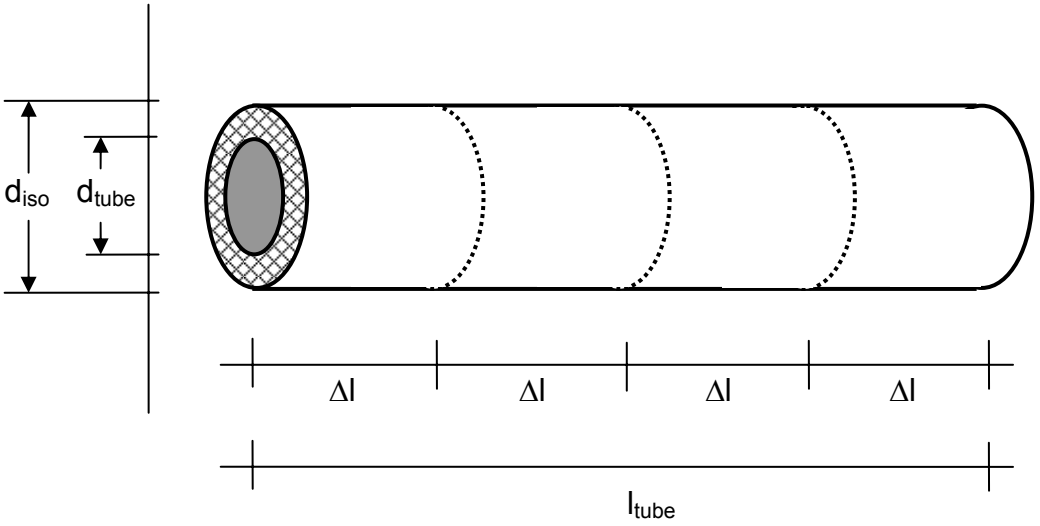

Fig. 2-4: Segmentation of a tube with heat isolation

During phases without mass flow no heat transfer is considered between the fluid and the tube walls. Therefore, both are on the same temperature level and a common heat capacity is considered, which is defined as:

$$\bar{C}_{tube} = m_{fl} \cdot c_{fl} + m_{tube} \cdot c_{tubel} \qquad (2.2.1\text{-}32)$$

For the normal operation case two temperature nodes are considered, one for the tube wall and one for the fluid. The problem is similar to the stratified storage case with the tubes divided into finite elements. At startup of the pump the tube wall and the fluid are at the same temperature for the whole tube. The energy balance of each element of the tube can be written as:

$$C_{tube\ wall} \frac{dT_{tube,i}}{dt} = \dot{m}_{fluid} \cdot c_{fluid} \cdot \left(T_{fluid,in} - T_{fluid,out}\right) - U_{l,tube} \cdot dl \cdot \left(T_{tube,i} - T_{amb}\right) \qquad (2.2.1\text{-}33)$$

$$\dot{m}_{fluid} \cdot c_{fluid} \cdot \frac{dT_{fluid}}{dx} = \frac{h_c \cdot dA}{2}\left(T_{fluid,in} + T_{fluid,out} - 2T_{tube,i} - dT_{tube,i}\right) \qquad (2.2.1\text{-}34)$$

A simple forward differences method enables the calculation of the tube wall temperature and the tube outlet temperature from the temperatures of the time step before. The energy balance can then be written as:

$$\frac{c_{tube,i} \cdot m_{tube,i}}{\Delta t}\left(T_{tube,i}(t-1) - T_{tube,i}(t)\right) = \dot{m}_{fluid} \cdot c_{fluid} \cdot \left(T_{fluid,in,i} - T_{fluid,out,i}\right) - U_{l,tube} \cdot \Delta l \cdot \left(\frac{T_{tube,i}(t-1) + T_{tube,i}(t)}{2} - T_{amb}\right) \qquad (2.2.1\text{-}35)$$

$$\dot{m}_{fluid} \cdot c_{fluid}\left(T_{fluid,in} - T_{fluid,out}\right) = \frac{h_c \cdot A}{2}\left(T_{fluid,in} + T_{fluid,out} - T_{tubel}(t-1) - T_{tubel}(t)\right) \qquad (2.2.1\text{-}36)$$

If this equation system is solved for $T_{tube,i}(t)$ and $T_{fluid,out,l}$ we get the following solution:

$$T_{tube,i}(t) = T_{tube,i}(t-1)\cdot\left(\frac{\frac{m_{tube,i}\cdot c_{tube,i}}{dt}+\frac{\left(\frac{hc\cdot A}{2}\right)^2}{\dot{m}_{fluid}\cdot c_{fluid}+\frac{hc\cdot A}{2}}-\frac{hc\cdot A}{2}}{\frac{m_{tube,i}\cdot c_{tube,i}}{dt}-\frac{\left(\frac{hc\cdot A}{2}\right)^2}{\dot{m}_{fluid}\cdot c_{fluid}+\frac{hc\cdot A}{2}}+\frac{hc\cdot A}{2}+\frac{U_{l,tube}\cdot \Delta l}{2}}\right)$$

$$+T_{fluid,in,i}\cdot\left(\frac{\frac{hc\cdot A}{2}+\dot{m}_{fluid}\cdot c_{fluid}\frac{hc\cdot A}{2}-\left(\frac{hc\cdot A}{2}\right)^2}{\frac{m_{tube,i}\cdot c_{tube,i}}{dt}-\frac{\left(\frac{hc\cdot A}{2}\right)^2}{\dot{m}_{fluid}\cdot c_{fluid}+\frac{hc\cdot A}{2}}+\frac{hc\cdot A}{2}+\frac{U_{l,tube}\cdot \Delta l}{2}}\right)$$

$$+\left(T_{amb}-\frac{T_{tube,i}(t-1)}{2}\right)\cdot\left(\frac{U_{l,tube}\cdot \Delta l}{\frac{m_{tube,i}\cdot c_{tube,i}}{dt}-\frac{\left(\frac{hc\cdot A}{2}\right)^2}{\dot{m}_{fluid}\cdot c_{fluid}+\frac{hc\cdot A}{2}}+\frac{hc\cdot A}{2}+\frac{U_{l,tube}\cdot \Delta l}{2}}\right) \quad \text{(2.2.1-37)}$$

$$T_{fluid,out,i} = T_{fluid,in,i}\cdot\left(\frac{\dot{m}_{fluid}\cdot c_{fluid}-\frac{hc\cdot A}{2}}{\dot{m}_{fluid}\cdot c_{fluid}+\frac{hc\cdot A}{2}}\right)$$

$$+\left(T_{tube,i}(t)+T_{tube,i}(t-1)\right)\cdot\left(\frac{\frac{hc\cdot A}{2}}{\dot{m}_{fluid}\cdot c_{fluid}+\frac{hc\cdot A}{2}}\right) \quad \text{(2.2.1-38)}$$

The Equations 2.2.1-37 and 2.2.1-38 are used for the programming of the model for the case with mass flow in the tubes. For the case without mass flow in the tubes the heat losses of the tubes are calculated from Equation 2.2.1-31.

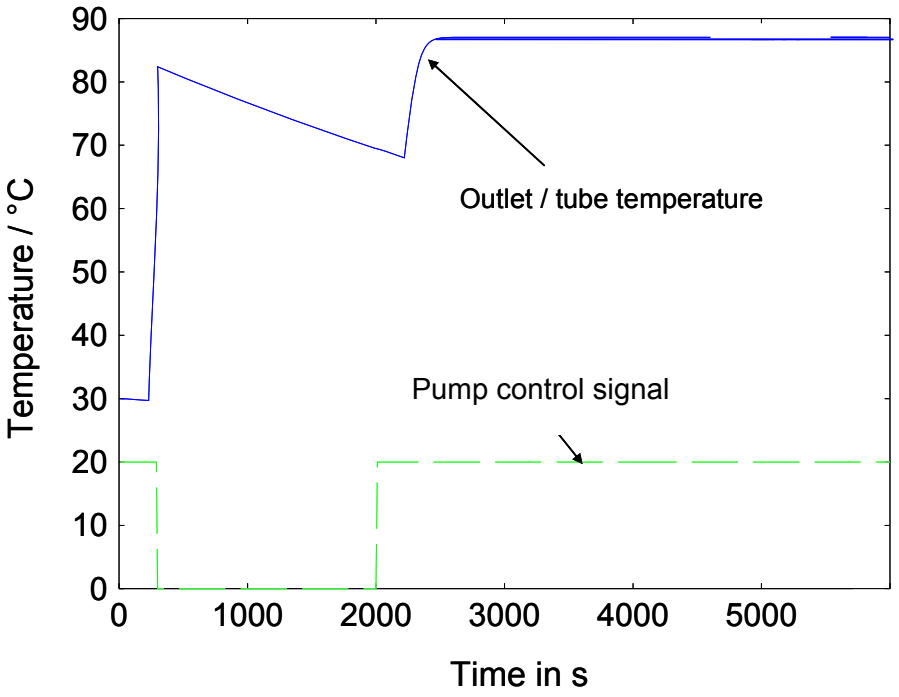

Fig. 2-5: Performance of the TUBLOD model, for 30°C starting and 90°C supply temperature

Since in this case only one node is considered for the tubing at shut down of the mass flow first the average temperature between the tube walls and the fluid in the tubes is calculated. This value is then used as starting temperature for the one node model for operation conditions without mass flow. At startup of the mass flow the fluid node and the tube wall node are set to the same average temperature which was calculated during the last time step without mass flow in the tubes. The fluid inlet temperatures of the single tube segments are set to the calculated outlet temperature of the previous segment calculated for the previous time step. For a stable and accurate operation of the model in mass flow mode, the internal time step is reduced to a value at which the water in the tube segments is exchanged exactly once. Fig. 2-5 shows the performance of the developed model for a tube with 30°C starting temperature and 90°C supply temperature with mass flow turned on for a while, then turned off and turned on again.

2.2.2 COOLING SYSTEM

2.2.2.1 Static Absorption Chiller Model

The performance of absorption cooling machines strongly depends on the external fluid temperatures and mass flow rates. Apart from the generator temperature the COP of absorption chillers at given cold water temperature is mainly influenced by the cooling water temperatures for the absorption and condensation process. For a description of the behaviour of absorption cooling machines a number of models have been developed during the last two decades. The most commonly used model is the so called characteristic equation which has been developed by (Ziegler, 1998) and is based on the internal mass and energy balances in all components. Detailed derivations of the characteristic equation with its coefficients were described in (Schweigler, et al., 1999). (Albers, et al., 2003) conclude that the application of one single equation is not sufficient for absorption chillers with thermally driven bubble pumps for internal solution transport.

The characteristic equation is derived from the heat transfer equations and the internal enthalpy balance. Internal temperatures are written with a capital T and standard t is used for all external temperatures. For simplification in the standard characteristic equation, all UA values and the internal enthalpy differences are calculated only for the design conditions and are assumed to be constants for the calculation of the cooling power for other external temperature conditions. Fig. 2-6 shows a system scheme of a single stage absorption chiller with all main components like the evaporator (E), the absorber (A), the generator (G) and the condenser (C) and the interconnection and flow directions between the components.

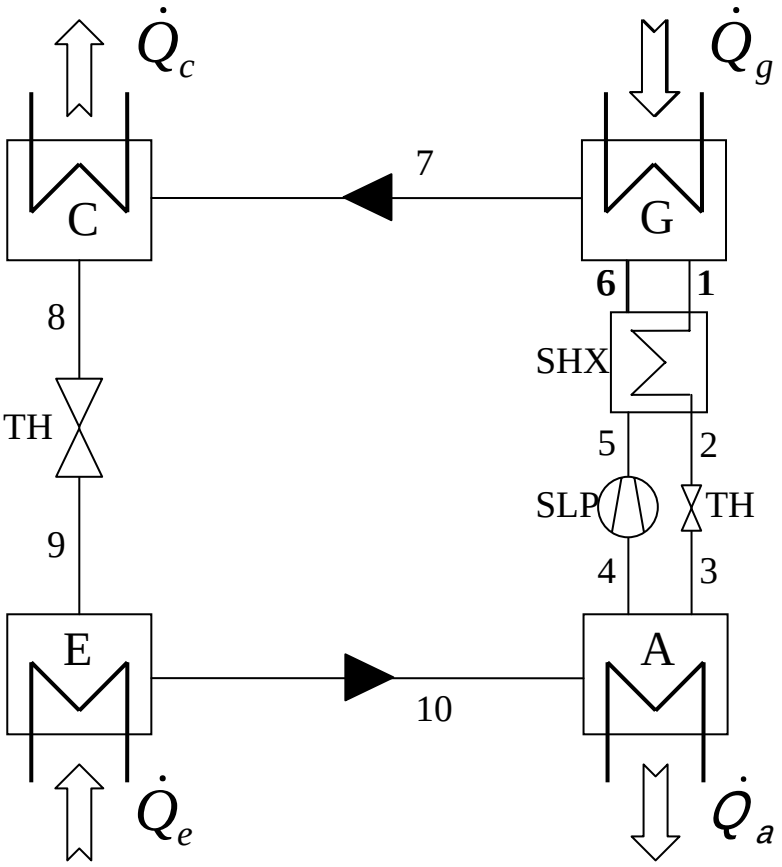

Fig. 2-6: System scheme with all external energy flows

In the evaporator water is evaporated at low pressure and low temperature. The required evaporation enthalpy is taken from the cold water circuit which e.g. cools a building. The water vapour flows into the absorber where it is absorbed in a concentrated LiBr solution. Since the water vapour changes from the vapour to the liquid phase during the absorption process the evaporation enthalpy is set free and needs to be rejected to the environment for a constant low absorber temperature. During the absorption process the LiBr solution gets more and more diluted and needs to be regenerated for a constant process and is therefore pumped into the generator. To reduce heat losses a heat exchanger is integrated to preheat the cool diluted solution from the absorber by the hot concentrated solution which is flowing from the generator back to the absorber. Due to the different pressure levels between absorber and generator a throttle is integrated in the back flow tubing. In the generator the diluted solution is

heated up and a part of the water is evaporated which increases the vapour pressure. The water vapour flows to the condenser where it is condensed at high vapour pressure and high condensation temperature. The condensed water is then led back to the evaporator for a closed cycle. Due to the pressure difference between condenser and evaporator a throttle is integrated in the back flow tubing. The heat of the condenser and of the absorber is rejected to the environment in a dry heat rejection system or an open wet cooling tower.

Evaporator

Fig. 2-7 shows the evaporator of the ACM model with the inlet and outlet conditions of the internal circuit.

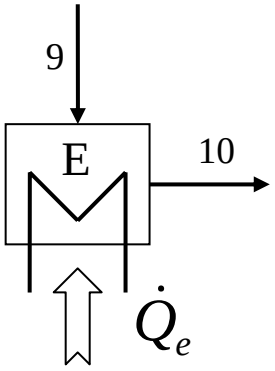

Fig. 2-7: Evaporator of the ACM model

The cooling capacity of the evaporator can be described by the mean temperature difference between the external and the internal temperature multiplied by the overall heat transfer coefficient of the heat exchanger which is equal to the internal evaporator enthalpy difference qe multiplied by the vapour mass flow rate.

$$\dot{Q}_e = \left(\bar{t}_e - T_e\right) U A_e = \dot{m}_V \, q_e \qquad (2.2.2\text{-}1)$$

The factor q_e is defined as the enthalpy difference between the produced water vapour h_{10} and the water entering the evaporator h_9.

$$q_e = h_{10} - h_9 \qquad (2.2.2\text{-}2)$$

The enthalpy of the water and water vapour are calculated from correlation described by empirical temperature dependent correlations provided by (Glück, B. 1991) which are shown in Appendix A, Paragraph 1.2.1.

Absorber

Fig. 2-8 shows the absorber of the ACM model with the inlet and outlet conditions of the internal and external circuits.

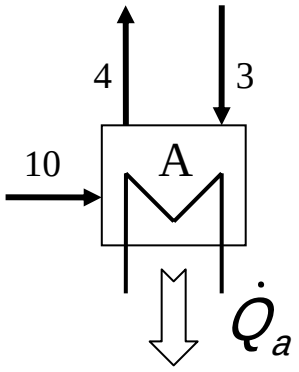

Fig. 2-8: Absorber of the ACM model

The amount of heat which needs to be removed from the absorber can be described by the temperature difference between the external and internal mean temperatures multiplied by the overall heat transfer coefficient of the heat exchanger. The required cooling power at the absorber results from the enthalpy input of the weak solution coming from the generator and by the enthalpy of the water vapour absorbed in the weak solution reduced by the enthalpy of the strong solution, which is pumped to the generator.

$$\begin{aligned}\dot{Q}_a &= \left(T_a - \bar{t}_a\right) U A_a = \dot{m}_V\, h_{10} - \dot{m}_r\, h_4 + \left(\dot{m}_r - \dot{m}_V\right) h_3 \\ &= \dot{m}_V \left(h_{10} - h_3\right) + \dot{m}_r \left(h_3 - h_4\right) = \dot{Q}_e\, A_E + \dot{Q}_{ax}\end{aligned} \qquad (2.2.2\text{-}3)$$

With:

Heat losses due to an imperfect solution heat exchanger:

$$\dot{Q}_{ax} = \dot{m}_r \left(h_3 - h_4\right) \qquad (2.2.2\text{-}4)$$

Since the solution mass flow rate within the most market available absorption chillers is constant these heat losses can be assumed to be constant as well.

The factor A_E is introduced for simplification and is defined by the enthalpy difference between the water vapour h_{10} and the weak solution h_3 entering the absorber divided by q_e.

$$A_E = \frac{(h_{10} - h_3)}{q_e} \tag{2.2.2-5}$$

The enthalpies of the weak and strong solution are calculated from correlations described by empirical temperature dependent correlations provided by (Mc Neely 1979) which are shown in Appendix A Chapter 1.2.2.

Generator

The model of the generator of the ACM is shown in Fig. 2-9 with the inlet and outlet conditions of the internal and external circuits.

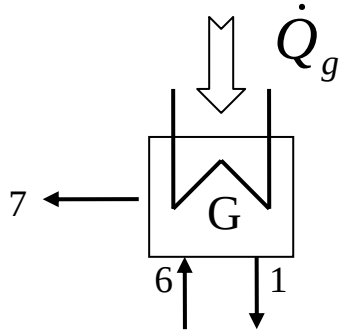

Fig. 2-9: Generator of the ACM model

The required heating capacity of the generator is calculated from the enthalpy difference between the strong solution entering the generator and the hot weak solution leaving the generator multiplied by the solution mass flow rate and the enthalpy difference between the weak solution and the water vapour extracted from the strong solution multiplied by the water vapour flow rate.

$$\begin{aligned}\dot{Q}_g &= (\bar{t}_g - T_g) U A_g = \dot{m}_V\, h_7 + (\dot{m}_r - \dot{m}_V) h_1 - m_r\, h_6 \\ &= \dot{m}_V (h_7 - h_1) + \dot{m}_r (h_1 - h_6) = \dot{Q}_e\, G_E + \dot{Q}_{gx}\end{aligned} \tag{2.2.2-6}$$

With:

Heat losses of the solution circuit due to imperfect solution heat exchanger:

$$\dot{Q}_{gx} = \dot{m}_r \left(h_1 - h_6 \right) \tag{2.2.2-7}$$

For constant solution mass flow rate as in most market available absorption chillers these heat losses are constant.

The factor G_E is introduced for simplification and is defined by the enthalpy difference between the water vapour and the weak solution leaving the generator, divided by q_e:

$$G_E = \frac{\left(h_7 - h_1 \right)}{q_e} \tag{2.2.2-8}$$

Condenser

The model of the condenser of the ACM is shown in Fig. 2-10 with the inlet and outlet conditions of the internal and external circuits.

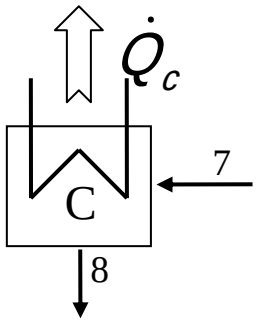

Fig. 2-10: Condenser of the ACM model

The amount of heat which needs to be removed from the condenser can be described by the temperature difference between the external and internal mean temperatures multiplied by the overall heat transfer coefficient of the heat exchanger. The required cooling power at the condenser results from the enthalpy input of the water vapour coming from the generator h_7 reduced by the enthalpy of the liquid water leaving the condenser h_8.

$$\dot{Q}_c = \left(T_c - \bar{t}_c\right) UA_c = \dot{m}_V \left(h_7 - h_8\right) = \dot{Q}_e \frac{h_7 - h_8}{q_e} = \dot{Q}_e \, C_E \qquad (2.2.2\text{-}9)$$

The factor C_E is introduced for simplification and is defined by the enthalpy difference between the water vapour entering the condenser h_7 and the liquid water leaving the condenser divided by q_e.

$$C_E = \frac{h_7 - h_8}{q_e} \qquad (2.2.2\text{-}10)$$

With the simplifications defined above we can write all heating and cooling capacities in dependence of the produced cooling capacity at the evaporator:

$$\dot{Q}_e = UA_e \left(\bar{t}_e - T_e\right) \qquad (2.2.2\text{-}11)$$

$$\dot{Q}_e \, C_E = UA_c \left(T_c - \bar{t}_c\right) \qquad (2.2.2\text{-}12)$$

$$\dot{Q}_e \, A_E - \dot{Q}_{ax} = UA_a \left(T_a - \bar{t}_a\right) \qquad (2.2.2\text{-}13)$$

$$\dot{Q}_e \, G_E - \dot{Q}_{gx} = UA_g \left(\bar{t}_g - T_g\right) \qquad (2.2.2\text{-}14)$$

In this equation system the main variables are the resulting cooling capacity of the evaporator and the driving temperature differences ΔT_i. The internal temperatures T_i are self regulating in dependence of the external mean temperatures t_i resulting from the application and the control system. Since the internal temperatures are bound to the solution field, the produced cooling power can be controlled by the external temperatures and the constants C_E, A_E, G_E and the heat losses Q_x and Q'_x. The geometry of the solution field according to Dühring rules gives:

$$T_g - T_a = \left(T_c - T_e\right) B$$

$$B = \frac{T_g - T_a}{T_c - T_e} \qquad (2.2.2\text{-}15)$$

The so called Dühring factor B is determined by the ratio of the internal temperature differences between the generator and the absorber and between the condenser and evaporator and thereby indicates the difference in the slope angle of the isosters in the Dühring chart. In general the Dühring factor B is slightly bigger than 1. For single-effect absorption chillers with working pair water/LiBr the value of the Dühring factor ranges from 1.1 to 1.2 for typical operation conditions (Albers, et al., 2003; Kohlenbach, et al., 2004).

The internal temperatures in equation (2.2.2-15) can be replaced by resolved equations (2.2.2-11) to (2-14) which gives

$$\bar{t}_c - \bar{t}_e + \dot{Q}_e\left(\frac{C_E}{UA_c} + \frac{1}{UA_e}\right)B = \bar{t}_g - \bar{t}_a - \dot{Q}_e\left(\frac{G_E}{UA_g} + \frac{A_E}{UA_a}\right) - \frac{\dot{Q}_{gx}}{UA_g} - \frac{\dot{Q}_{ax}}{UA_a} \tag{2.2.2-16}$$

From this a characteristic double temperature difference $\Delta\Delta t$ can be derived between the mean external generator and absorber temperatures t_g and t_a on the one hand and the external condenser and evaporator temperature t_c and t_e on the other hand.

$$\Delta\Delta t = \left(\bar{t}_g - \bar{t}_a\right) - \left(\bar{t}_c - \bar{t}_e\right)B \tag{2.2.2-17}$$

The dissipated energy between the generator and absorber through the solution circuit is determined by the efficiency of the heat exchanger and can be described as follows:

$$\Delta\Delta t_{\min,E} = \frac{\dot{Q}_{gx}}{UA_g} + \frac{\dot{Q}_{ax}}{UA_a} \tag{2.2.2-18}$$

Furthermore, all constants like the UA values, the Dühring factor and enthalpy difference ratios are summarised in the factor S_E:

$$s_E = \left[\left(\frac{C_E}{UA_c} + \frac{1}{UA_e} \right) B + \left(\frac{G_E}{UA_g} + \frac{A_E}{UA_a} \right) \right]^{-1} \quad (2.2.2\text{-}19)$$

With the factors and constants described above the characteristic equation can be written as follows:

$$\dot{Q}_E = s_E \left(\Delta\Delta t - \Delta\Delta t_{\min,E} \right) \quad (2.2.2\text{-}20)$$

With the assumption of constant enthalpy differences and heat transfer coefficients which are fixed with the dimensioning of the ACM the factors S_E and $\Delta\Delta t_{min,E}$ are constant and the cooling capacity therefore is only influenced by the characteristic temperature function which depends on the external mean temperatures.

However, in the characteristic equation so far only the external mean temperatures are used, which is not useful for dynamic system simulations. With the simplified assumption of a linear heat exchange the external mean temperatures can be written in dependence of the inlet and outlet temperature:

$$\bar{t}_i = \frac{\left(t_{i,in} + t_{i,out} \right)}{2}; \; t_{out,i} = 2\bar{t}_i - t_{in} \quad (2.2.2\text{-}21)$$

With this simplified correlation the equation system with the external and internal energy balances can be resolved for the unknown external mean temperatures. The solution is shown in Appendix A, paragraph 1.

Based on the equation system described above a simulation model has been programmed as INSEL Block in FORTRAN. In this model first all internal enthalpies are calculated from the internal temperatures at design conditions. With the internal enthalpies the parameters of the characteristic equation are calculated. Then the external mean temperatures and external heat flows at the evaporator, absorber, generator and condenser are calculated from the equation system shown in Appendix A. At this stage the model is exactly based on the characteristic equation with constant internal enthalpies.

To further improve this simple model an iteration process has been implemented to consider changing internal enthalpies with changing external temperatures. For this after the calculation of the external energy flows and the external mean temperatures the new internal temperatures are calculated from Equations (2.2.2-11) to (2.2.2-14) solved for the internal mean temperature as shown below:

$$T_e = \bar{t}_e - \frac{\dot{Q}_e}{UA_e} \tag{2.2.2-22}$$

$$T_c = \bar{t}_c + \frac{\dot{Q}_e C_E}{UA_c} \tag{2.2.2-23}$$

$$T_a = \bar{t}_a + \frac{\dot{Q}_e A_E - \dot{Q}_{ax}}{UA_a} \tag{2.2.2-24}$$

$$T_g = \bar{t}_g - \frac{\dot{Q}_e G - \dot{Q}_{gx}}{UA_g} \tag{2.2.2-25}$$

With this calculated new internal temperatures the whole calculation process is repeated in a loop. Due to slight inaccuracies in the enthalpy calculations no full convergence is reached. Therefore, the loop needs to be interrupted after certain amount of iterations. From detailed analyses it was found out, that a sufficient accuracy is reached if the loop is interrupted after ten iterations.

For validation of the developed ACM simulation model measured performance data from the manufacturers catalogue of a 10 kW Phönix Sonnenklima LiBr absorption chiller are used and compared to the simulated values. To demonstrate the advantage of a calculation of variable internal enthalpies compared to a model with fixed internal enthalpies the simulation results of both model types are shown in Fig. 2-11 in comparison with the measured performance data from the manufacturer catalogue.

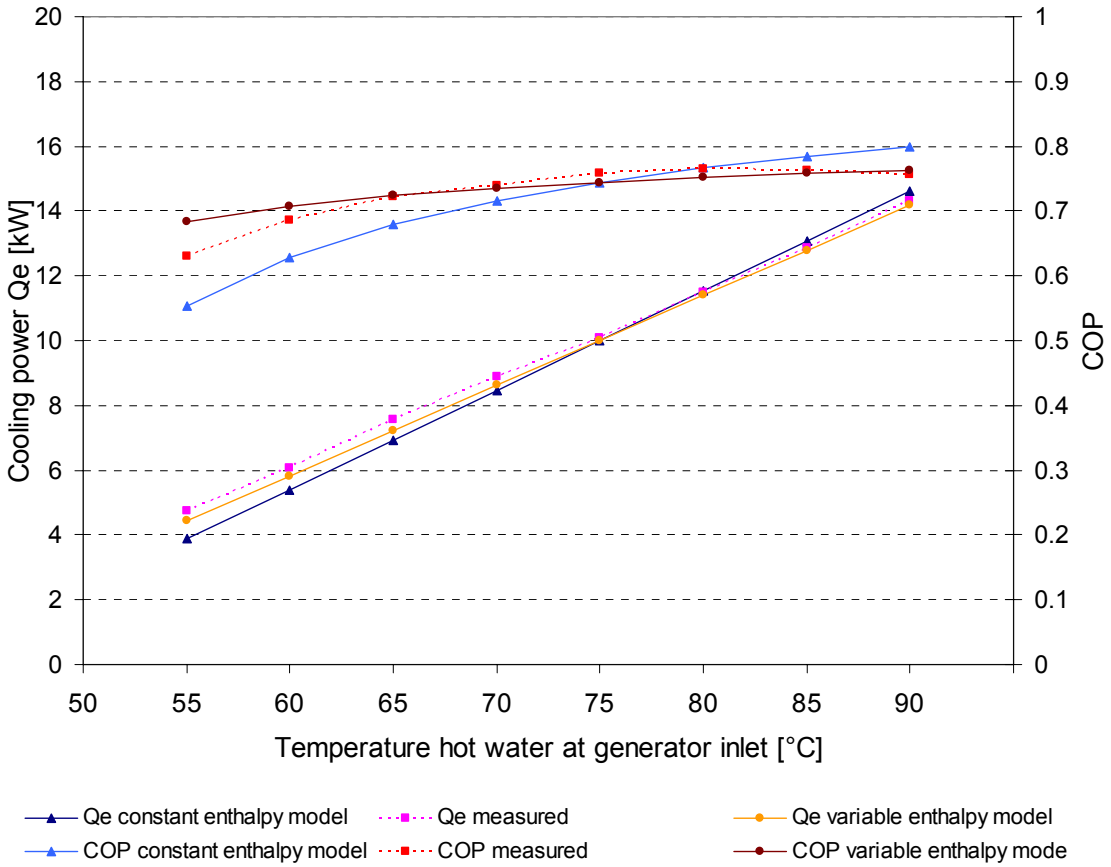

Fig. 2-11: Measured (taken from the manufacturer catalogue) and simulated cooling power and COP as a function of generator entry temperature for a 10 kW Phönix Sonnenklima LiBr absorption chiller

As visible from Fig. 2-11 the model based on the characteristic equations with constant enthalpy factors has a clearly decreasing accuracy for conditions which are not close to the design point. However, if an iteration process is implemented and the internal enthalpies are allowed to vary with the external temperatures the model accuracy can be significantly improved. With the improved model with variable enthalpies a very good accuracy is reached over a wide range of operation.

2.2.2.2 Parameter Identification for the Static Absorption Chiller Model

The main problem for the utilisation of the model based on the characteristic equations and variable enthalpies as described in chapter 2.2.2.1 is the availability of the required construction details. Especially the internal heat transfer coefficients UA, the solution flow rate, the solution heat exchanger efficiency and the internal temperatures need to be known. For the 10 kW Phönix Sonnenklima absorption chiller the required parameters were published and could therefore be used for the model. However, for most of the available absorption chillers this information is nearly impossible to get. To overcome this, an empirical parameter identification method has been developed on basis of the absorption chiller model to derive the required parameters only from the data sheet information of the absorption chillers. On the data sheets typically the cooling power of the evaporator, the heating power of the generator and the required power for the heat rejection of the absorber/condenser circuit is given together with the water inlet and outlet temperatures and water mass flow rates of the three circuits. All this information is given for the nominal operation point of the chiller together with the thermal COP reached at these operation conditions.

The developed model for the parameter identification is in principle a kind of inverse model of the absorption chiller model. As input the model gets the inlet temperature of the three circuits and the cooling capacity of the absorption chiller. The parameters of the model are the temperature spread between the external and internal mean temperature of the evaporator, absorber, generator and condenser. These values are guessed or set to typical values of known machines and later need to be adapted. The fifth parameter is the solution heat exchanger efficiency which is typically also not known and therefore needs to be guessed as well. The last three parameters are the known temperature spreads of the three external circuits (heating, cooling and cold water circuit).

With these parameters in the model first the external mean temperatures are calculated. With the assumption of a linear heat transfer this is quite easily done for the evaporator and the generator. For the heat rejection circuit of the absorber and condenser only the inlet temperature at the absorber and the outlet temperature at the condenser are known. In a first approximation it is therefore assumed that half of the total temperature spread is caused in each of the two components and the external mean temperatures are calculated as follows:

$$\bar{t}_a = \left(t_{a,in} + \frac{\Delta t_{ac}}{4} \right) \tag{2.2.2-26}$$

$$\bar{t}_c = \left(t_{a,in} + \frac{\Delta t_{ac}}{2} + t_{c,out} \right) \cdot 0.5 \tag{2.2.2-27}$$

From the external mean temperature the internal mean temperatures are calculated using the temperature spread between the external and internal mean temperature which are guessed as parameters of the model as described before. From the internal mean temperatures and the defined efficiency of the solution heat exchanger the Düring parameter B, all internal enthalpies and solution concentrations are calculated the same way as in the absorption chiller model. From the defined cooling capacity of the absorption chiller and the enthalpy difference between the liquid water and the water vapour in the evaporator the amount of evaporated water is calculated:

$$\dot{m}_{H_2O} = \frac{\dot{Q}_e}{h_{10} - h_9} \tag{2.2.2-28}$$

From the water vapour mass flow rate and the difference between the concentration of rich and weak solution the minimum required rich solution flow rate is calculated as follows:

$$\dot{m}_{RS} = \frac{X_{weak}}{X_{weak} - X_{Rich}} \cdot \dot{m}_{H_2O} \tag{2.2.2-29}$$

The characteristic numbers of heat transfer UA are then calculated from the following equations:

$$UA_e = \frac{\dot{Q}_e}{\bar{t}_e - T_e} \tag{2.2.2-30}$$

$$UA_a = \frac{h_3\left(\dot{m}_{RS} - \dot{m}_{H_2O}\right) + h_{10} \cdot \dot{m}_{H_2O} - h_4 \cdot \dot{m}_{RS}}{T_a - \bar{t}_a} \tag{2.2.2-31}$$

$$UA_c = \frac{\left(h_7 - h_8\right) \cdot \dot{m}_{H_2O}}{T_c - \bar{t}_c} \tag{2.2.2-32}$$

$$UA_g = \frac{h_1\left(\dot{m}_{RS} - \dot{m}_{H_2O}\right) + h_7 \cdot \dot{m}_{H_2O} - h_6 \cdot \dot{m}_{RS}}{\bar{t}_g - T_g} \tag{2.2.2-33}$$

In the next step the parameters C_E, G_E and A_E and the heat losses $\dot{Q}_{gx}$ and $\dot{Q}_{ax}$ are calculated with the equations shown in chapter 2.2.2.1. With these values and the cooling capacity of the chiller, rejected heating energy at the absorber and condenser and the supplied heating energy at the generator can be calculated from the equations below:

$$\dot{Q}_c = \dot{Q}_e C_E \tag{2.2.2-34}$$

$$\dot{Q}_a = \dot{Q}_e A_E - \dot{Q}_{ax} \tag{2.2.2-35}$$

$$\dot{Q}_g = \dot{Q}_e G_E - \dot{Q}_{gx} \tag{2.2.2-36}$$

Now the new external absorber outlet temperature is calculated from the calculated UA values, internal temperatures, heat flows and the known external absorber inlet and condenser outlet temperature as follows:

$$t_{a,out} = \frac{UA_a \cdot T_a + UA_c \cdot T_c - \dot{Q}_a - \dot{Q}_c - \frac{UA_a \cdot t_{a,in} - UA_c \cdot t_{c,out}}{2}}{\frac{UA_a + UA_c}{2}} \tag{2.2.2-37}$$

In the last part the mass flow rates are calculated from the heat flows, the external temperature spreads as shown below:

$$\dot{m}_g = \frac{\dot{Q}_g}{c_{H2O} \cdot (t_{g,in} - t_{g,out})} \quad (2.2.2\text{-}38)$$

$$\dot{m}_a = \frac{\dot{Q}_a}{c_{H2O} \cdot (t_{a,out} - t_{a,in})} \quad (2.2.2\text{-}39)$$

$$\dot{m}_c = \frac{\dot{Q}_c}{c_{H2O} \cdot (t_{c,out} - t_{a,out})} \quad (2.2.2\text{-}40)$$

$$\dot{m}_e = \frac{\dot{Q}_e}{c_{H2O} \cdot (t_{e,in} - t_{e,out})} \quad (2.2.2\text{-}41)$$

In an iteration process the external absorber and condenser mean temperature are slightly increased and the whole calculation process is repeated for the new external mean temperatures until the absorber mass flow rate is equal to the condenser mass flow rate.

At the end of the calculations the 13 outputs of the model provide the calculated UA values and the internal mean temperatures of each component together with the Dühring parameter, the rich solution mass flow rate and the three calculated external mass flow rates of the evaporator, generator and absorber/condenser. Now the temperature spreads between the external and internal mean temperatures and the efficiency of the solution heat exchanger need to be adapted until the resulting Dühring parameter is close to or slightly below a typical value of 1.2 and the external mass flow rates fit to the mass flow rates given on the data sheet of the ACM producer. With some experience and knowledge about absorption chillers the parameter identification process can be done quite fast. Of course this is not yet very comfortable and therefore should be improved in the future. The application of computational optimisation tools based on e.g. genetic algorithms could offer here eventually a faster solution. Nevertheless, also with the manual procedure good parameter sets can be produced for the described absorption chiller model. As shown in chapter 3.4.1

and chapter 4.4.2 with the described parameter identification method and the developed ACM model the performance of absorption chillers can be described with high accuracy for a wide operation rang of the absorption chiller.

2.2.2.3 Dynamic Part of the Absorption Chiller Model

The absorption chiller model described in chapter 2.2.2.1 so far does not consider any inertia of the system. However, in chapter 4.5 very detailed analyses are performed for the development and test of control strategies for early chiller startup where the inertia of the chiller plays a major role. On the other hand detailed construction details of the installed 15 kW EAW absorption chiller are not available. Therefore, it was decided to develop a separate model which does only consider an overall inertia of each of the components which can be guessed from the total weight of the system and then further adapted to fit the measured performance data. Additionally, heat losses are considered of the outer chiller casing, with the knowledge that no heat isolation for the installed system was used. Also heat exchanges between the components generator / absorber and evaporator / condenser are considered. Fig. 2-12 shows the construction principle of the EAW chiller.

Since the inertia of the chiller is considered in a separate model the cooling circuit which first cools the absorber and then the condenser is not easy to solve, especially under the consideration that the developed ACM model has only one input for the cooling water. However, the temperature spread of the recooling circuit is quite low with only 6 K under nominal conditions and the absorber and condenser therefore are nearly on the same temperature level. For simplification it was therefore decided to consider the inertia of the absorber and condenser in one unit which is located at the inlet of the absorption chiller. The connection of the two simulation tools is shown in Fig. 2-13.

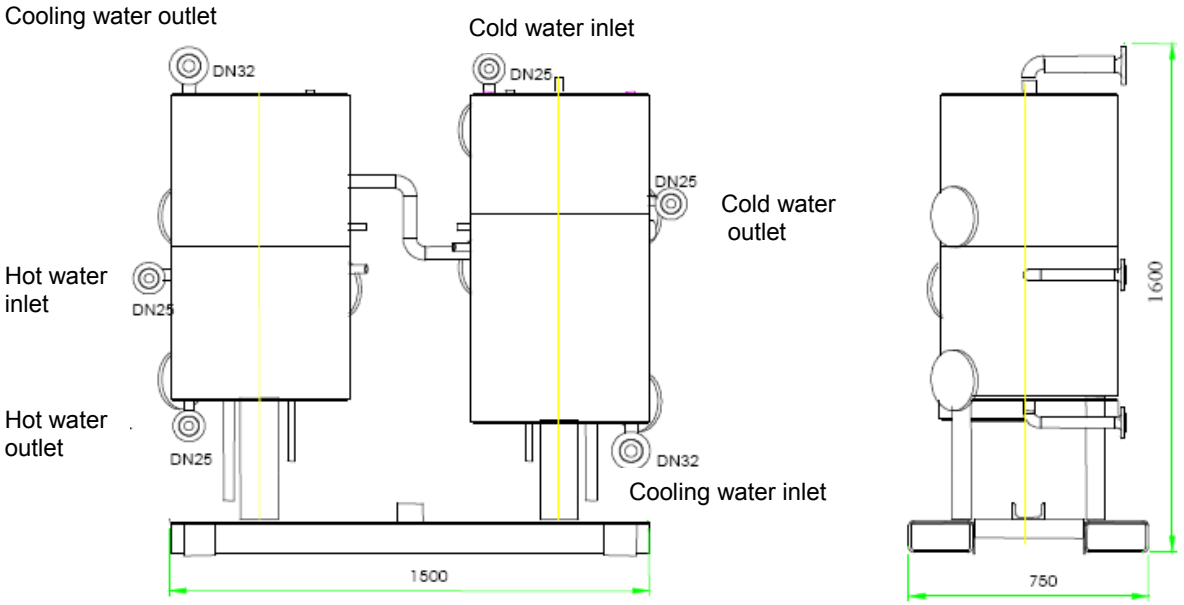

Fig. 2-12: Construction details of the EAW 15 kW absorption chiller

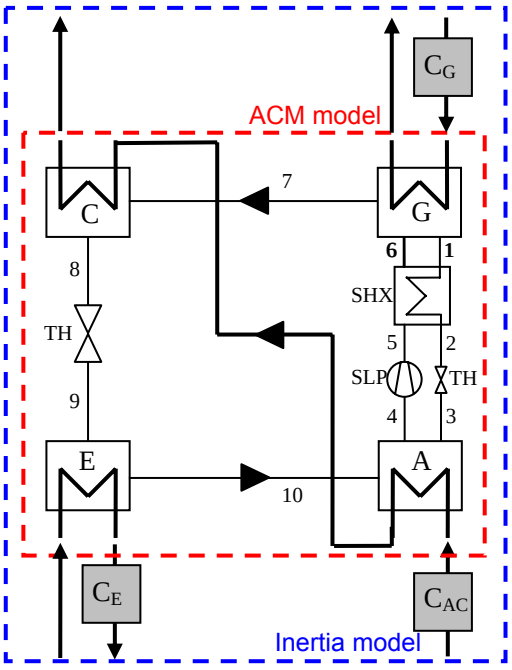

Fig. 2-13: Connection of the ACM and inertia model

The developed equation system with the energy balance for the inertia part of the absorption chiller model is shown below for each component. The solution of the equation system is shown in Appendix A, Paragraph 1.3.

Model for the dynamic parts of the ACM

- Generator

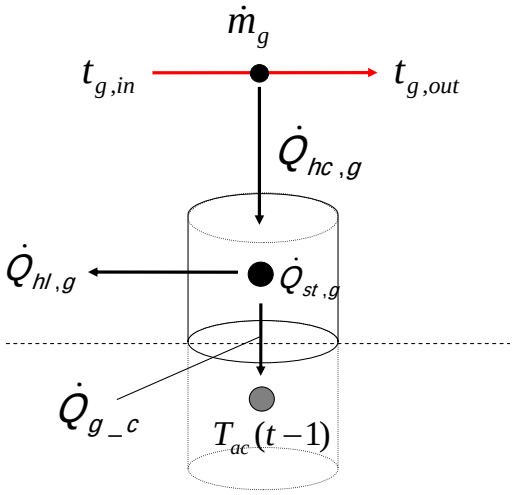

Fig. 2-14: Heat transfer and heat storage of the generator

- Heat balance of the external circuit

$$\dot{Q}_g = \dot{Q}_{hc,g} \tag{2.2.2-42}$$

$$\dot{m}_g \cdot c_{p,g} \cdot \Delta t \cdot \left(t_{g,in} - t_{g,out}\right) = UA_g \cdot \Delta t \cdot \left(\frac{t_{g,in} + t_{g,out}}{2} - \frac{T_g(t-1) + T_g(t)}{2}\right) \tag{2.2.2-43}$$

- Internal heat balance

$$\dot{Q}_{st,g} = \dot{Q}_{hc,g} - \dot{Q}_{hl,g} - \dot{Q}_{g\_c}$$

$$C_g \cdot \left(T_g(t) - T_g(t-1)\right) = UA_g \cdot \Delta t \cdot \left(\frac{t_{g,in} + t_{g,out}}{2} - \frac{T_g(t-1) + T_g(t)}{2}\right) - U_{tot,g} \cdot \Delta t \cdot \left(\frac{T_g(t-1) + T_g(t)}{2} - t_{amb}\right) - U_{g\_c} \cdot \Delta t \cdot \left(T_g(t-1) - T_{ac}(t-1)\right) \tag{2.2.2-44}$$

- Evaporator

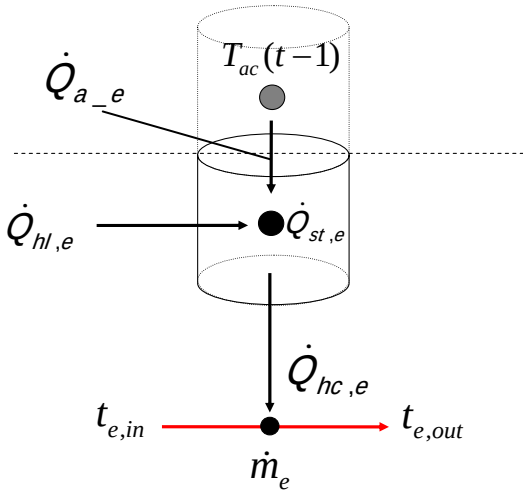

Fig. 2-15: Heat transfer and heat storage of the evaporator

- Heat balance of the external circuit

$$\dot{Q}_e = \dot{Q}_{hc,e}$$

$$\dot{m}_e \cdot c_{p,e} \cdot \Delta t \cdot \left(t_{e,out} - t_{e,in}\right) = UA_e \cdot \Delta t \cdot \left(\frac{T_e(t-1) + T_e(t)}{2} - \frac{t_{e,in} + t_{e,out}}{2}\right) \tag{2.2.2-45}$$

- Internal heat balance

$$\dot{Q}_{st,e} = \dot{Q}_{hc,e} - \dot{Q}_{hl,e} - \dot{Q}_{a\_e}$$

$$C_e \cdot \left(T_e(t) - T_e(t-1)\right) = -UA_e \cdot \Delta t \cdot \left(\frac{T_e(t-1) + T_e(t)}{2} - \frac{t_{e,in} + t_{e,out}}{2}\right) + U_{tot,e} \cdot \Delta t \cdot \left(t_{amb} - \frac{T_e(t-1) + T_e(t)}{2}\right) + U_{a\_e} \cdot \Delta t \cdot \left(T_{ac}(t-1) - T_e(t-1)\right) \tag{2.2.2-46}$$

- Absorber/Condenser

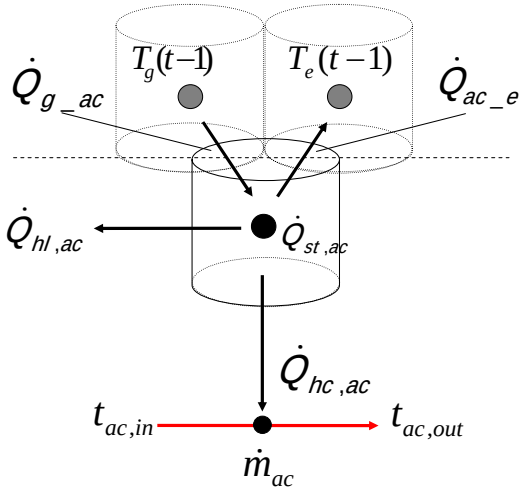

Fig. 2-16: Heat transfer and heat storage of the absorber/condenser

- Heat balance of the external circuit

$$\dot{Q}_{ac} = \dot{Q}_{hc,ac}$$

$$\dot{m}_{ac} \cdot c_{p,ac} \cdot \left(t_{ac,out} - t_{ac,in}\right) = UA_{ac} \cdot \Delta t \cdot \frac{1}{2} \cdot \begin{pmatrix} T_{ac}(t-1) + T_{ac}(t) \\ - t_{ac,in} - t_{ac,out} \end{pmatrix} \qquad (2.2.2\text{-}47)$$

- Internal heat balance

$$\dot{Q}_{st,ac} = -\dot{Q}_{hc,ac} - \dot{Q}_{hl,ac} + \dot{Q}_{g\_ac} - \dot{Q}_{ac\_e}$$

$$\begin{aligned} C_{ac} \cdot \left(T_{ac}(t) - T_{ac}(t-1)\right) = & -UA_{ac} \cdot \Delta t \cdot \frac{1}{2} \cdot \begin{pmatrix} T_{ac}(t-1) + T_{ac}(t) \\ - t_{ac,in} - t_{ac,out} \end{pmatrix} \\ & - U_{tot,ac} \cdot \Delta t \cdot \left(\frac{T_{ac}(t-1) + T_{ac}(t)}{2} - t_{amb} \right) \\ & + U_{g\_ac} \cdot \Delta t \cdot \left(T_g(t-1) - T_{ac}(t-1)\right) \\ & - U_{ac\_e} \cdot \Delta t \cdot \left(T_{ac}(t-1) - T_e(t-1)\right) \end{aligned} \qquad (2.2.2\text{-}48)$$

The solution of the equation system is shown in Appendix A, Paragraph 1.3. In Chapter 4 the developed dynamic model is validated against measured performance data of solar cooling system installed at the office building of the SolarNext AG. A very good agreement between the measured and simulated

performance is reached. The error of the model is only 2% for the generator and evaporator circuit and below 6% for the absorber/condenser circuit. This slightly larger error is an attribute to the simplifications made in the simulation model for this part of the chiller.

2.2.2.4 Cold Water Storage

For the cold water storage exactly the same model with ideal stratification is used as already described in chapter 2.2.1.2 for the hot water storage tank of the solar system.

2.2.3 HEAT REJECTION SYSTEMS

For each cooling system, either electrically driven compression chillers or thermally driven e.g. absorption chillers, an effective heat rejection is essential for the system performance and efficiency. For the development and analysis of new control strategies therefore detailed simulation models of the heat rejection system are required. In this chapter such models are provided for both open wet cooling towers and dry heat rejection systems.

2.2.3.1 Open Wet Cooling Towers

In wet cooling towers mostly latent heat transfer is used to lower the temperature of the cooling fluid. Open cooling towers generally work with water as cooling fluid which is distributed over a fill packing and forced air-cooled by a ventilator. Partial evaporation of approximately 2-3% of the water as well as convective heat transfer between water and ambient air result in the cooling effect. Due to the evaporation of water outlet temperatures of the cooling water below the ambient air temperature can be reached, which are only limited by the wet bulb temperature of the ambient air.

The solar driven absorption cooling system of SolarNext analysed in chapter 4 is equipped with an EWK 036 open wet cooling tower of the German producer AXIMA. The construction details of this cooling tower are displayed in Fig. 2-17. Further technical data are given in Table 1.The left part of Fig. 2-17 shows the

cross section of the EWK cooling tower. The warm water is distributed via spray nozzles at the top of the cooling tower on a fill packing and runs down the fill packing while it is cooled down through evaporation and convective heat transfer effects. After leaving the fill packing the cooled water is collected in the cold water sump from where it leaves the cooling tower again. Air is drawn in counter flow to the water from bottom to the top of the cooling tower by a motor-driven fan. To reduce water spray losses a demister at the top of the cooling tower separates the water droplets from the air stream. A flotation valve (not visible in the figure) controls the water level in the cold water sump and equalizes the water losses due to evaporation, spray losses and water exchange by adding fresh water from the grid.

Fig. 2-17: Construction details of the AXIMA EWK 036 open wet cooling tower (Source: AXIMA)

Table 1: Technical data of the AXIMA EWK 036 cooling tower for design conditions

Total recooling power	35 kW
Water mass flow rate	5 m³/h
Water supply temperature	36 °C
Water return temperature	30 °C
Wet bulb temperature of the ambient air	24 °C
Electrical power of the ventilator motor	0.33 kW
Required power at the ventilator axis	0.17 kW
Engine and ventilator rotation	1430 min^{-1}

a) Model development

- Fundamentals and state of the art

In this thesis detailed simulation models of cooling towers are mainly required for cooling performance predictions, to analysis the influence of the achievable cooling water temperatures on the performance of the whole solar cooling system. However, for the overall energetic and economical performance and for the analysis of the environmental impact also the electricity and water consumption need to be considered. Therefore, a simulation model is required which is able to predict the electricity and water consumption for each operation point of the cooling tower for variable ambient conditions.

In the literature several more or less detailed models for the prediction of the performance of open wet cooling towers can be found. A basic theory of cooling tower operation was originally proposed by (Walker, et al., 1923). However, the first practical use of basic differential equations was first presented by (Merkel, 1925), in which he combined the equations governing heat and mass transfer between water droplets and air in the tower. (Webb, 1984) presented a unified theoretical treatment for thermal analysis of cooling towers, evaporative condensers and evaporative fluid coolers. A very detailed model which separately analyses the cooling effects in the fill packing, in the spray and in the rain zone of a wet cooling tower is presented by (Qureshi and Zubair, 2006). This model also considers fouling effects in the packing material.

However, for most of these models very detailed construction information especially about the implemented fill packing of the cooling tower are required for an accurate prediction of the heat and mass transfer conditions within the packing material. To obtain such specific and detailed information causes the main problem for the application of the mentioned models to available wet cooling towers, since the producers are mostly not willing to provide the required information. Therefore, a model has been developed which only needs the typical information given on the datasheets of the cooling towers for design

conditions like the recooling power, the water mass flow rate, the water supply and return temperature, the wet bulb temperature of the ambient air and the nominal electricity consumption of the ventilator motor. The model described in the following paragraph is mainly based on a method originally used for commissioning measurements on cooling towers described in the German standard DIN 1947 of 1989. This method is based on the work of (Klenke, 1977, Pielke, 1978, 1987, 1989, Schnell, 1978 and Fackelmayer, 1992) and is taken from (Recknagel, Sprenger and Schramek, 1997 pp. 1720-1730).

- Description of the developed model

The process of water cooling in an open wet cooling tower is shown for an ideal cooling tower in Fig. 2-18 . The water is cooled down from tw,in to tw,out while the enthalpy of the air increases due to the increase of water content and temperature from $h_{air,in}$ to $h_{air,out}$. The overall energy balance can be described as follows.

$$\dot{m}_w \cdot c_w \cdot \left(t_{w,in} - t_{w,out}\right) = \dot{m}_a \cdot \left(h_{air,out} - h_{air,in}\right) \qquad (2.2.3\text{-}1)$$

With:

$h_{air,in}$ enthalpy of inlet air / kJ kg^{-1}

$h_{air,out}$ enthalpy of outlet air / kJ kg^{-1}

Due to limited heat and mass transfer coefficients and area in the fill packing the real behaviour of wet cooling towers is not ideal. The green doted lines in Fig. 2-18 show a more realistic behaviour of an open wet cooling tower.

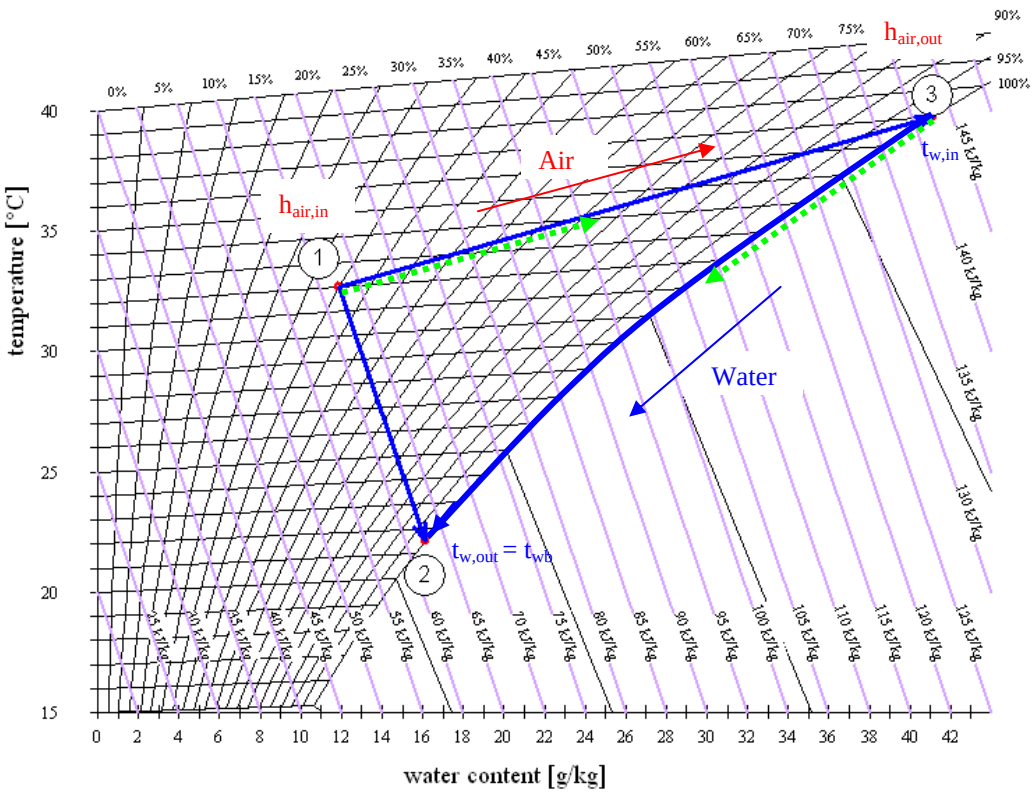

Fig. 2-18: Water cooling in an ideal open wet cooling tower

The recooling quality of a real cooling tower compared to an ideal cooling tower is described by the recooling efficiency η which is the ratio between the difference of the water in- and outlet temperature and the difference between the water inlet temperature and the wet bulb temperature of the ambient air. In an ideal cooling tower, the water outlet temperature is equal to the wet bulb temperature of the ambient air, which results in a recooling efficiency of 1.0 as maximum value. The difference between the water outlet temperature and the wet bulb temperature is called the cooling boundary difference.

$$\eta = \frac{t_{w,in} - t_{w,out}}{t_{w,in} - t_{wb}} \qquad (2.2.3\text{-}2)$$

With:

$t_{w,in}$ Water inlet temperature [°C]

$t_{w,out}$ Water outlet temperature [°C]

t_{wb} Wet bulb temperature [°C]

In case of an ideal cooling tower a minimum air flow rate of $\dot{m}_{a,min}$ is required to cool down a certain water mass flow of $\dot{m}_{w}$ from the inlet temperature $t_{w,in}$ to the wet bulb temperature t_{wb}. The ratio between this minimum air flow rate and the water mass flow l_{min} is called the minimum air to water mass flow ratio. Values of the minimum air to water mass flow ratio are shown in Fig. 2-19 for the typical range of cooling water and wet bulb temperatures (Klenke, 1977).

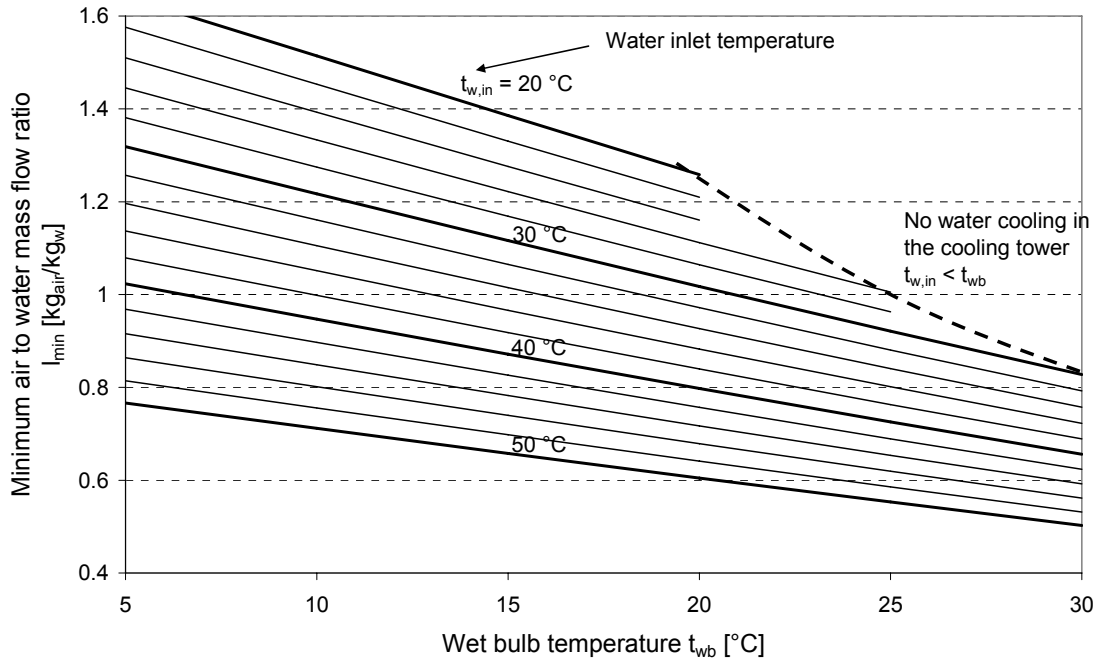

Fig. 2-19: Minimum relative air amount l_{min} of cooling towers

The ratio between the real air flow rate and the water mass flow l_0 is called the effective air to water mass flow ratio. A typical and important parameter of wet cooling towers is the dimensionless air ratio λ, which is defined as the ratio between the effective and the minimum air to water ratio.

$$l_{\min} = \frac{\dot{m}_{a,\min}}{\dot{m}_w} \qquad \left[\frac{kg_{air}}{kg_w}\right]$$

$$l_0 = \frac{\dot{m}_a}{\dot{m}_w} \qquad \left[\frac{kg_{air}}{kg_w}\right] \tag{2.2.3-3}$$

$$\lambda_a = \frac{l_0}{l_{\min}}$$

With:

l_0	effective air to water mass flow ratio
l_{min}	minimum air to water mass flow ratio [kg_{air} / kg_{water}]
$\dot{m}_{a,min}$	minimum air mass flow rate [kg/s]
$\dot{m}_a$	actual air mass flow rate [kg/s]
$\dot{m}_w$	water mass flow rate [kg/s]
λ_a	air ratio

In the developed simulation model the air ratio λ_a is calculated for each operation point of the cooling tower and each ambient condition separately. For the determination of the minimum air to water mass flow ratio l_{min} first the wet bulb temperature is calculated from the following equation:

$$h_1 = h_{wb}$$
$$c_{pl} \cdot t_1 + x_1 \cdot \left(r_{0°C} + c_{pd} \cdot t_1\right) = c_{pl} \cdot t_{wb} + x_{wb} \cdot \left(r_{0°C} + c_{pd} \cdot t_{wb}\right) \tag{2.2.3-4}$$
$$t_{wb} = \frac{c_{pl} \cdot t_1 + x_1 \cdot \left(r_{0°C} + c_{pd} \cdot t_1\right) - r_{0°C} \cdot x_1}{c_{pl} + c_{pd} \cdot x_{wb}}$$

This equation has to be solved iteratively for the water content at wet bulb temperature x_{wb} using the additional condition that no change in the enthalpy of the air occurs. For the ideal cooling tower the outlet air temperature is equal to the water inlet temperature with a relative humidity of 100 % and the outlet water temperature is equal to the wet bulb temperature of the ambient air (see Fig. 2-18). This allows the calculation of the enthalpy of the outlet air $h_{air,out}$. Using Equation (2.2.3-1) the minimum air to water mass flow ratio l_{min} of the cooling tower can be calculated from the enthalpy difference between inlet and outlet air as follows:

$$l_{\min} = \frac{\dot{m}_a}{\dot{m}_w} = \frac{\left(h_{air,out} - h_{air,in}\right)}{c_w \cdot (t_{w,in} - t_{w,out})} \qquad (2.2.3\text{-}5)$$

According to (Klenke, 1977) there is a clear correlation between the heat rejection efficiency η and the air ratio, which can be shown as a curve which is known as the cooling tower characteristic. The characteristic behaviour can be described using the equation:

$$\eta = C_k \left(1 - e^{-\lambda_a}\right) \qquad (2.2.3\text{-}6)$$

C_k is the cooling tower constant, which can be determined for each cooling tower type by performance measurement. If the air flow rate of the cooling tower is given, the data on the data sheet of the cooling tower for the performance under design conditions can be used to calculate the value of C_k.

$$C_k = \frac{\eta}{1 - e^{-\lambda_a}} \qquad (2.2.3\text{-}7)$$

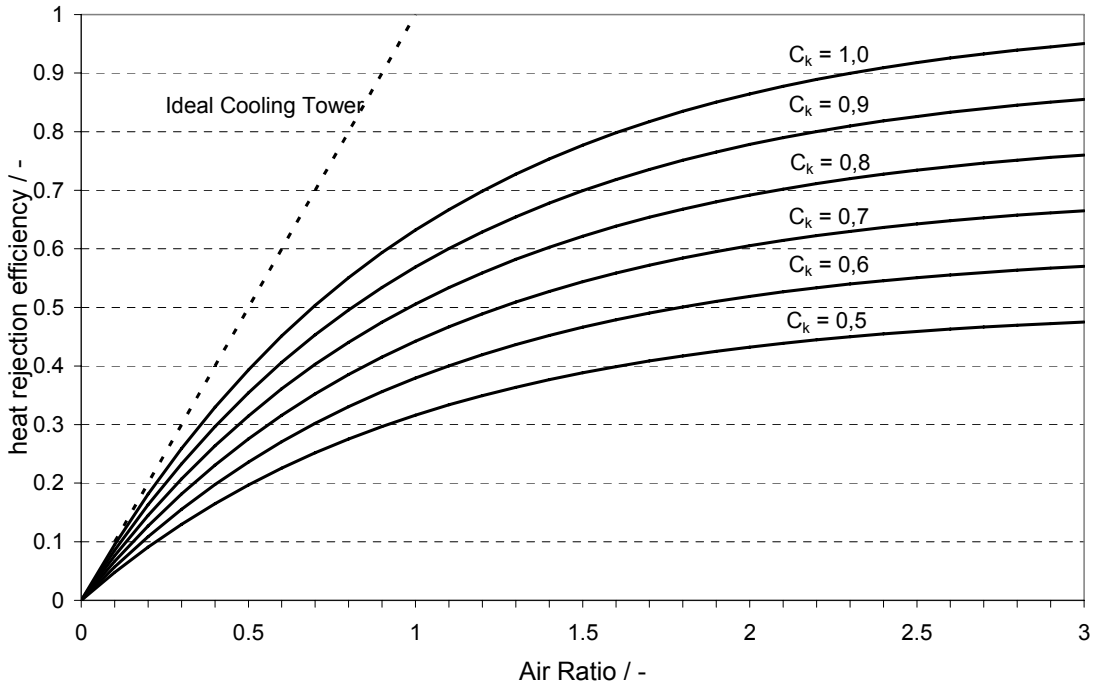

Fig. 2-20: Cooling tower characteristic

However, often only the fan speed and not the air flow rate is given on the data sheets. In this case, typical values of the cooling tower constant C_k given in Table 2 can be used, which have been found for actual open cooling towers with fill packing made of plastic and air to water counter-flow arrangement (source: Recknagel, Sprenger and Schramek, 1995):

Table 2: Typical values of the cooling tower constant C_k

Height of fill packing [m]	0,3	0,5	0,7	0,9
Cooling tower constant C_k	0,65	0,81	0,93	1,0

These values are also shown in Fig. 2-21 together with a polynomial function generated from the values given for the different fill packing heights. This function is used in the simulation model for the determination of the cooling tower constant C_k if no air flow rate is available.

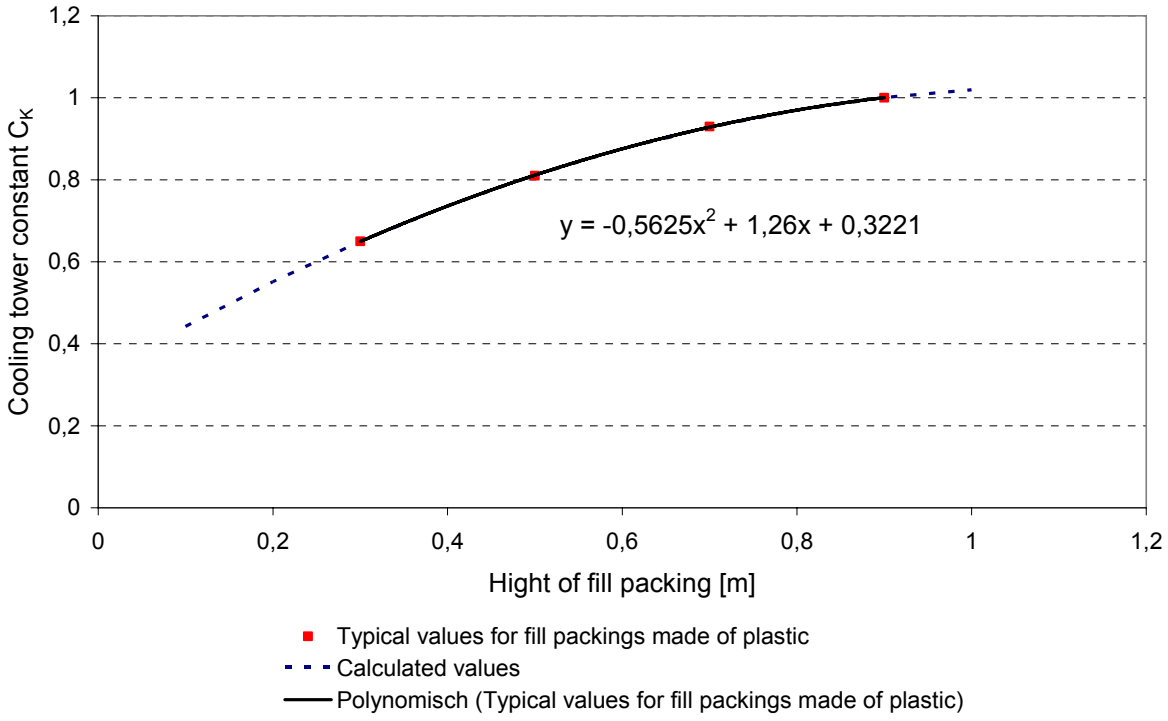

Fig. 2-21: Typical values of the cooling tower constant C_k

If the cooling tower constant C_k has been calculated, the air ratio $\lambda_{a,d}$ and the air flow rate $\dot{m}_{air,d}$ of the cooling tower can be determined for design conditions using the equations:

$$\lambda_d = -\ln\left(1 - \frac{\eta_d}{C_k}\right); \qquad \dot{m}_{air,d} = \lambda_{a,d} \cdot \dot{m}_{w,d} \qquad [kg/s] \tag{2.2.3-8}$$

The required value of the heat rejection efficiency η_d can be calculated for the design conditions from the water inlet and outlet and air wet bulb temperature given on the data sheet of the cooling tower:

$$\eta_d = \frac{t_{w,in,d} - t_{w,out,d}}{t_{w,in,d} - t_{wb,d}} \tag{2.2.3-9}$$

With:

$t_{w,in,d}$	Water inlet temperature for design conditions [°C]
$t_{w,out,d}$	Water outlet temperature for design conditions [°C]
$t_{wb,d}$	Wet bulb temperature for design conditions [°C]

However, for northern Europe climate wet bulb temperatures of 18 to 21°C which result from the design conditions of cooling towers are only given on some days of the year and are much lower on many days of the cooling period. This means that the cooling tower can be operate most of the time in part load conditions by controlling the fan speed in a range of 20 to 100 % according to the water outlet temperature. The reduction of the fan speed is directly correlated to a lower air flow rate. According to the proportional law for axial and radial fans the following general correlation of the mass flow to the fan speed is given:

$$\dot{m}_{air,new} = \dot{m}_{air,d} \cdot \frac{n_{new}}{n_d} \tag{2.2.3-10}$$

With:

$\dot{m}_{air,new}$	Air mass flow rate at n_{new} [kg/s]
$\dot{m}_{air,d}$	Air mass flow rate for design conditions [kg/s]
n_{new}	Fan speed of the cooling tower fan [R/min]
n_d	Fan speed of the cooling tower fan for design conditions [R/min]

This proportional law, which is true for a wide range of Reynolds numbers, can be used with sufficient accuracy for the calculation of flow rates for variable fan speed as long as the differential pressure / volume flow chart of the cooling tower shows a quadratic characteristic.

- Electricity consumption of cooling towers

If the cooling water pump is not considered, the electricity consumption of cooling towers only depends on the electricity consumption of the ventilator. For the electricity consumption of electrically driven ventilators the following general equation can be found.

$$P_{el} = \frac{\dot{V} \cdot \Delta p_t}{\eta_V \cdot \eta_M \cdot \eta_A} \qquad (2.2.3\text{-}11)$$

With:

$\dot{V}$ = Air volume flow rate [m³/s]
Δp_t = Total pressure increase [Pa]
η_V = Ventilator efficiency
η_M = Motor efficiency
η_A = Axis efficiency

In general the electricity consumption for design conditions is given on the data sheet of the cooling tower. If no values are given the following values for the electric power of the ventilator motors of cooling towers for design conditions can be approximately used for the calculation of the electricity consumption (Berliner, 1975).

- Axial ventilators

Electric power of the ventilator motor: 6 … 10 W per kW recooling power

- Radial ventilators

Electric power of the ventilator motor: 10… 20 W per kW recooling power

As already discussed above, for northern Europe climate wet bulb temperatures of 18 to 21°C are only given on some days of the year. This means that the cooling tower can operate most of the time in part load conditions by controlling the ventilator speed in a range of 20 to 100 % according to the water outlet temperature. The reduction of the fan speed is directly correlated to a significant lower electricity consumption. According to the proportional law for axial and radial ventilators the following general correlation of the electricity power consumption to the third power of the fan speed is given:

$$P_{el,new} = P_{el,d} \cdot \left(\frac{n_{new}}{n_d} \right)^3 \qquad (2.2.3\text{-}12)$$

. With:

$P_{el,new}$ Electric power demand at n_{new} [W]
$P_{el,d}$ Electric power demand under design conditions at n_d [W]
n_{new} Fan speed of the cooling tower fan [R/min]
n_d Fan speed of the cooling tower fan under design conditions [R/min]

This proportional law, which is true for a wide range of Reynolds numbers, can be used with sufficient accuracy for the calculation of flow rates under variable fan speed as long as the differential pressure / volume flow chart of the cooling tower shows a quadratic characteristic.

- Water consumption of cooling towers

If no detailed information is available, for the water consumption the following statistically developed hourly values can be approximately used per kW recooling power according to the German standard DIN 4710:

- Water consumption through evaporation 2 kg/h
- Water consumption through spray losses 1 kg/h
- Water consumption through water exchange required to avoid an increase of salt concentration 3 kg/h

The water consumption through evaporation can be calculated from the following equation:

$$\dot{W}_{ev} = \dot{m}_{air,d} \cdot \left(x_{air,in} - x_{air,out} \right) \quad (2.2.3\text{-}13)$$

However, the developed cooling tower model only provides the enthalpy of the outlet air but not the temperature and water content. To calculate the water consumption it is assumed, that the outlet air is humidified to 90 % relative humidity which is quite near to the real value for most of the operation conditions. With the knowledge of the enthalpy and the relative humidity the outlet air temperature and the resulting water content $x_{air,out}$ can be calculated. The water consumption through spray losses strongly depends on construction details of the cooling tower and should be given by the producer. In some cases, wind speed and direction additionally influence this type of water losses. The water consumption through water exchange required to avoid an increase of salt concentration depends on the water consumption through evaporation and on the water hardness.

$$\dot{W}_{ex} = \frac{\dot{W}_{ev}}{\frac{d_z}{d} - 1} \quad (2.2.3\text{-}14)$$

With:

$\dot{W}_{ex}$ Water consumption through water exchange [kg/s]
$\dot{W}_{ev}$ Water consumption through water evaporation [kg/s]
d_z Allowed hardness of the circulated water °dH
d hardness of the fresh water (1°dH = 0.18 mol/m³)

- Validation of the developed model

For the validation of the developed model measured performance data of an open wet cooling tower MITA PMS 4/65 produced by the German company Blacke-Durr is used. The information about the cooling tower and the measured performance data were taken from (Kohlenbach, 2006). For the cooling tower

only very few construction details were available. The following performance data of the cooling tower given for one point of operation was used.

Table 3: Performance date of the MITA PMS 4/65 cooling tower

Total recooling power	40 kW
Water mass flow rate	0.69 kg/s
Water supply temperature	35 °C
Water return temperature	21 °C
Wet bulb temperature of the ambient air	15 °C

Information about the electric power consumption and the air mass flow rate were not available. According to provided photographs the fill packing height was assumed to be 0.6 m. With this little information the cooling performance of the cooling tower has been calculated with the developed model for different wet bulb temperatures of the ambient air and for variable fan speeds. The water inlet temperature and mass flow were kept constant at 35 °C and 0.69 kg/s. The results are shown in Fig. 2-22 and compared to measured performance data. As visible from this figure the simulated performance of the cooling tower fits excellently to measured performance for the whole range of the wet bulb temperature and from medium to maximum fan speed. Only for very low fan speed the performance of the cooling tower is slightly under predicted by the simulation model compared to the measured data. A reason for this could be that the proportional law used to calculate the air volume flow rates at different fan speeds does not fit for very low fan speeds. Altogether, a very efficient model has been developed which accurately predicts the performance over a wide range of operation and needs only very little information which is typically available on the data sheet of the cooling towers. Calculated performance characteristics of the AXIMA EWK 06 open wet cooling tower are shown in Appendix A, Paragraph 1.4.

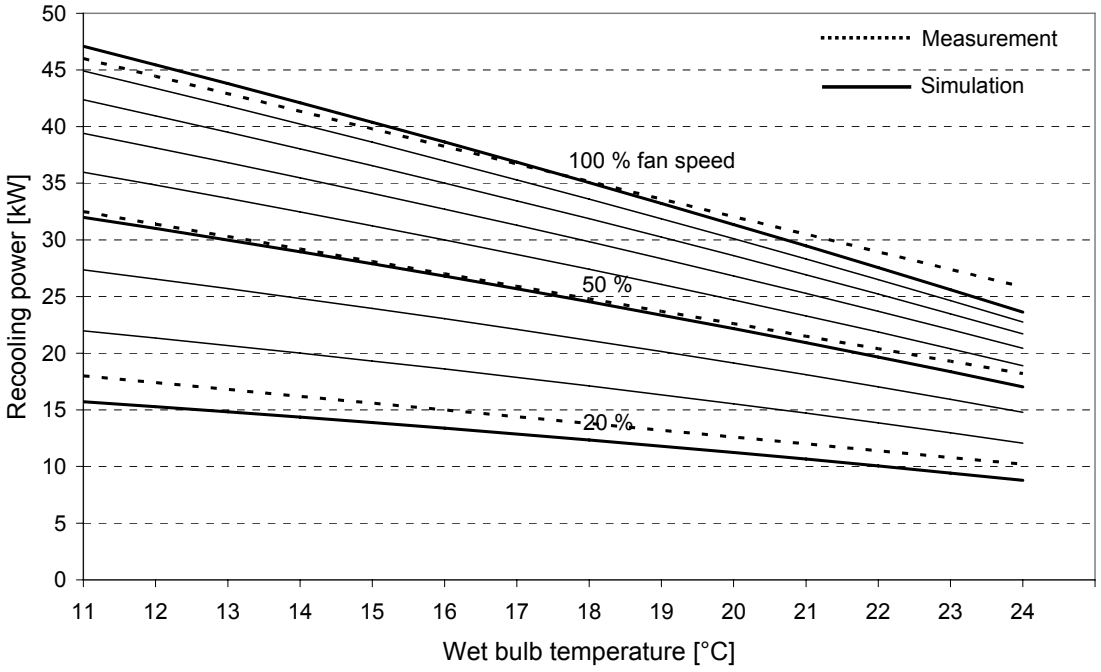

Fig. 2-22: Measured and calculated recooling performance of the MITA PMS 4/65 cooling tower. The inlet water temperature was 35°C and the water mass flow rate was 0.69 kg/s

2.2.3.2 Dry Heat Rejection Systems

Dry heat rejection systems are typically based on an air to liquid heat exchanger, in most cases with forced air flow by a fan. Dry heat rejection systems are not able to cool down the liquid below ambient air temperature. Depending on the flow rate and the size of the heat exchanger the temperature spread between ambient air and liquid outlet temperature is between 3 K for very large heat exchangers compared to the flow rate and 10 K for small heat exchangers. Some of the available dry heat rejection systems operate with constant fan speeds, others offer variable fan speeds to adapt the air flow to the required temperature spread of the liquid in dependence of the ambient air temperature. Two types of fan speed control are available, systems with controllable fan speed stages and systems with e.g. frequency inverters for continuous fan speed control.

The heat rejection system has an important influence on the efficiency of solar cooling systems. The recooling temperature reached significantly influences the efficiency of the absorption chiller and the electricity consumption of the heat

rejection system has a decisive influence on the primary energy efficiency reached. For a detailed analysis of solar driven cooling systems it is therefore important to have a simulation model of dry heat rejection systems, which is able to predict properly the outlet temperature of the cooling water and the electricity consumption of the fan. Very detailed models of the heat exchanger on the other hand require detailed information of the heat rejection system which most of the producers are not willing to provide. Therefore, a simulation model has been developed which requires only the information on the data sheet.

For the model development a dry heat rejection system of the Günthner GmbH type GFH052A/3 is used, which has been installed at the SolarNext AG office building in Rimsting, Germany and is optionally used as dry heat rejection system for their solar cooling plant. The construction details and the technical data of the system as provided on the datasheet are shown in Fig. 2-23, Table 4 and Table 5.

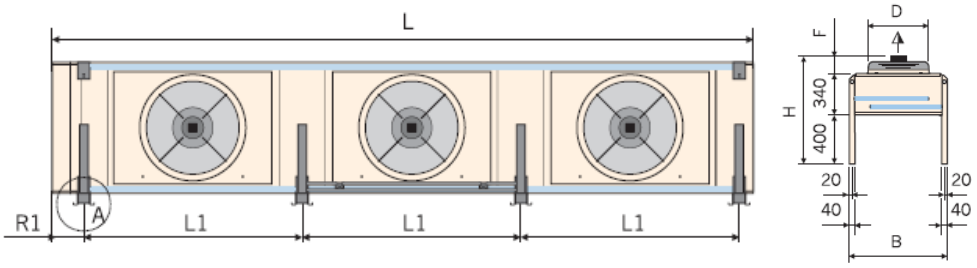

Fig. 2-23: Construction details of the GFH052B/3 dry heat rejection system of the GÜNTHNER GmbH (Source **www.guenthner.de**)

Table 4: Measures of the GFH052B/3 dry heat rejection system

Type	L [mm]	B [mm]	H [mm]	R [mm]	C [mm]
GFH052A/3	3375	895	950	80	875

Table 5: Technical data of the GFH052B/3 dry heat rejection system

Description	Max air flow	Reduced air flow
Nominal cooling power	81.6 kW	65.3 kW
Air volume flow rate	23 200 $m^3 h^{-1}$	17 500 $m^3 h^{-1}$
Ethylene glycol flow rate	13.9 $m^3 h^{-1}$	11.1 $m^3 h^{-1}$
Pressure drop liquid side	0.5 bar	0.4 bar
Consumed electrical power P_{el}	2.1 kW	1.6 kW

All values given in Table 5 are for Ethylene glycol water mixture with 40% Glycol, a water inlet temperature of 40°C and a water outlet temperature of 35°C at 25°C air inlet temperature

- Model development

The behaviour of dry heat rejection systems / air heaters with variable air temperatures and air volume flow rates is typically shown in characteristic diagrams, where the heat transfer efficiency is shown depending on the air volume flow rate for fixed air and fluid inlet temperatures. For fixed air and fluid flow rates, fluid temperatures and air inlet temperature the heat exchanger efficiency of dry heat rejection systems / air heaters is defined as

$$\phi = \frac{\left(T_{air,out} - T_{air,in}\right)}{\left(\frac{T_{fluid,in} + T_{fluid,out}}{2} - T_{air,in}\right)} \qquad (2.2.3\text{-}15)$$

For constant average fluid temperature the heat exchanger efficiency is also given by

$$\phi = 1 - e^{-\frac{UA}{\dot{V}_{air} \cdot \rho_{air} \cdot c_{p,air}}} \qquad (2.2.3\text{-}16)$$

In the developed model the heat exchanger efficiency is calculated for the design conditions using Equation 2.2.3-15. If Equation 2.2.4-16 is solved for heat transfer power UA we get

$$UA = -\ln(1-\phi) \cdot \dot{V}_{air} \cdot \rho_{air} \cdot c_{p,air} \qquad (2.2.3\text{-}17)$$

and the UA value of the heat exchanger can be calculated. The air velocity at design conditions is calculated from the air volume flow rate divided by the heat exchanger inlet area (width of heat exchanger multiplied by the length of the heat exchanger). The air density ρ_{air} and the specific thermal capacity $c_{p,air}$ are calculated from the inlet air temperature and humidity at design conditions. The UA value of water to air heat exchangers follows in general the law

$$UA = C_{HX} \cdot v_{air}^{n} \cdot A \qquad (2.2.3\text{-}18)$$

With C being a characteristic constant of the heat exchanger and n = 0.4 .. 0.6. From Equation 2.2.3-18 the heat exchanger characteristic C_{HX} can be calculated from the design conditions and is assumed to be constant for all operation points. A value of 0.4 is used for n in the simulation model.

Equations 2.2.3-15 to 2.2.3-18 are taken from (Recknagel, Sprenger and Schramek, 1997 Chapter 3, pp. 1098).

For the calculation of the water outlet temperature of other operation points in the model first the new air velocity v_{air} is calculated from the new air flow rate. Then the new UA value is calculated from Equation 2.1.3-18 and the heat exchanger efficiency is calculated from Equation 2.2.3-16. In the model it is assumed, that the water mass flow rate does vary only ±30% and therefore the water based heat transfer coefficient is considered to be constant. For the calculation of the water outlet temperature the energy balance between air and water node is used:

$$\begin{aligned} \dot{Q}_{h,air} &= \dot{Q}_{c,fluid} \\ \dot{m}_{air} \cdot c_{air} \left(T_{air,out} - T_{air,in}\right) &= \dot{m}_{fluid} \cdot c_{fluid} \left(T_{fluid,in} - T_{fluid,out}\right) \end{aligned} \qquad (2.2.3\text{-}19)$$

Equation 2.2.3-15 is solved for the air outlet temperature which is then replaced in Equation 2.2.3-19 and the water outlet temperature can be calculated as follows:

$$T_{fluid,out} = \frac{T_{air,in} - T_{fluid,in} \cdot \left(0.5 - \frac{\dot{m}_{fluid} \cdot c_{fluid}}{\phi \cdot \dot{m}_{air} \cdot c_{air}}\right)}{\left(0.5 + \frac{\dot{m}_{fluid} \cdot c_{fluid}}{\phi \cdot \dot{m}_{air} \cdot c_{air}}\right)} \quad (2.2.3\text{-}20)$$

The electricity consumption of the ventilator is calculated from the proportional law described in Chapter 2.1.3.1 as follows:

$$P_{el,new} = P_{el,d} \cdot \left(\frac{\dot{V}_{new}}{\dot{V}_{max}}\right)^3 \quad (2.2.3\text{-}21)$$

- Model Validation

Unfortunately no measured performance data was available for the installed system. Therefore, the model could only be validated against some operation points provided by the producer on the datasheet for the same heat exchanger but different air flow rates. All data points are for the nominal test conditions mentioned above. The results of the model are shown in Table 6.

Table 6: Model validation for the GFH052B/3 dry heat rejection system

Water flow rate	Air flow rate	Cooling power datasheet	Cooling power model	Error
$m^3\ h^{-1}$	$m^3\ h^{-1}$	kW	kW	%
13.9	23200	81.6	81.6	0.00
11.0	17500	65.3	64.5	1.23
10.4	15600	61.3	58.8	4.01
8.1	11600	47.5	45.3	4.63
6.9	9540	45.0	42.9	4.67
4.1	5420	24.0	22.7	5.54

The results clearly demonstrate that the developed model is able to predict the cooling power of the regarded dry heat rejection system for a wide range of operation with high accuracy. The error between predicted cooling power and the cooling power on the datasheet slightly increases with decreasing air and water flow rate from 1.23 % at 75% air flow rate to 5.5% error at 23 % air flow rate. Since all the thermal results given for the different air flow rates are for

different ventilators and motors, a comparison of the calculated electricity consumption with measured data was not possible.

2.3 OPEN DESICCANT COOLING SYSTEMS

Open desiccant cooling systems are ventilations systems which consist of a sorption based air dehumidification unit with solid or sorbents, a heat exchanger and humidifiers on the supply and return air side. In the present work a system with a solid sorbent dehumidification unit in form of desiccant wheel is regarded. In full desiccant mode the supply air is first dried in the desiccant wheel and afterwards precooled in a heat exchanger by the return air which has been humidified before to the maximum to lower its temperature. The precooled and dry supply air is then humidified to the maximum supply air humidity level to further decrease the temperature which increases the sensible cooling power. The humid return air is preheated in the heat exchanger by the dried supply air and then further heated by e.g. a liquid based solar heating system or by solar air collectors. Within this chapter the models used for the sorption wheel, the rotation heat exchanger, the humidifiers and the solar air collectors are described in detail.

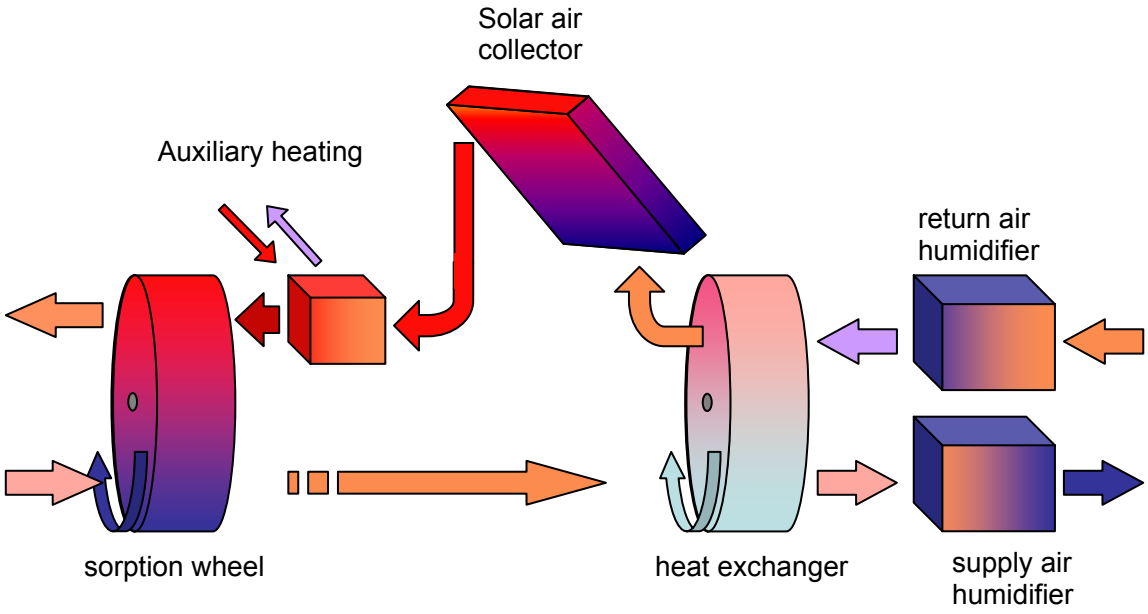

Fig. 2-24: DEC system scheme with solar air collectors and heating coil for additional heating energy supply

2.3.1 SOLID DEHUMIDIFICATION SYSTEMS (ADSORPTION WHEEL)

Since within this work no detailed performance analysis of desiccant wheels is performed, a simple efficiency model already available in INSEL was used for developed simulation model described in Chapter 05. The available efficiency model is based on the model published e.g. in (Eicker, 2001). This model uses the fact that the sorption isotherms are very close together if the stored water fraction is drawn as a function of the relative humidity. Therefore, it can be assumed with sufficient accuracy, that the stored water fraction in the sorption material only depends on the relative humidity of the air. The small temperature dependency is then neglected. In this ideal case the relative humidity of the supply air can be reduced to the relative humidity of the regeneration air. However, due to several irreversible effects, heat losses and heat transfer from the regeneration side to the supply air side, real sorption wheels are not ideal. These non ideal effects are considered by a dehumidification efficiency which is typically in the region of 80%. The dehumidification efficiency is defined as the actual dehumidification divided by the ideal dehumidification:

$$\eta_{dehum} = \frac{x_{amb} - x_{\sup,eff}}{x_{amb} - x_{\sup,ideal}} \qquad \eta_{dehum} \approx 0.8$$
$$x_{\sup,eff} = x_{amb} - \eta_{dehum}\left(x_{au} - x_{zu,ideal}\right) \tag{2.3.1-1}$$

For the calculation of the ideal humidity of the supply air after the sorption process it is considered, that the enthalpy of the supply air does not change during the absorption process and that the supply air at sorption wheel outlet has the same relative humidity as the regeneration air. The relative humidity is defined as:

$$\varphi = \frac{x}{x + 0.622}\frac{p}{p_s(t)} \tag{2.3.1-2}$$

The saturation pressure is given by an empirical equation provided by (Glück, 1991):

$$p_{S,r6} = 611 \cdot \exp\left(\begin{matrix} -1.91275 \cdot 10^{-4} + T \cdot 7.258 \cdot 10^{-2} - T^2 \cdot 2.939 \cdot 10^{-4} \\ + T^3 \cdot 9.841 \cdot 10^{-7} - T^4 \cdot 1.920 \cdot 10^{-9} \end{matrix}\right) \quad (2.3.1\text{-}3)$$

The enthalpy of the air is calculated from equation 2.3.1-4 to 2.3.1-7. The empirical Equations 2.3.1-6 is a 2.3.1-7 are also provided by (Glück, 1991).

$$h = h_L + x \cdot h_V = (c_L + x \cdot c_D)T + x \cdot h_V(T) \quad (2.3.1\text{-}4)$$

$$h_V(T) = h_D(T) - h_{fl}(T) \quad (2.3.1\text{-}5)$$

$$h_D(T) = 2501.482 + 1.789736 \cdot T + 8.957546 \cdot 10^{-4} T^2 - 1.300254 \cdot 10^{-5} \cdot T^3 \quad (2.3.1\text{-}6)$$

$$h_{fl}(T) = -2.25 \cdot 10^{-2} + 4.2063437 \cdot T - 6.014696 \cdot 10^{-4} T^2 + 4.381537 \cdot 10^{-6} T^3 \quad (2.3.1\text{-}7)$$

In the equation 2.3.1-3 to 2.3.1-7 the temperature T is in °C.

It is not possible to solve the implicit equations. Temperature and absolute humidity need to be analytically solved in an iteration process (Regula falsi). The temperature of the supply air at sorption wheel outlet is iteratively calculated from Equation 2.3.1-4 considering the condition that the enthalpy of the supply air does not change during the sorption process. The iteration is performed until the relative humidity of the supply air is equal to the relative humidity of the regeneration air. The resulting absolute humidity and temperature is reached in the ideal case. The real absolute humidity is then calculated from equation 2.3.1-1 for 80% dehumidification efficiency and the outlet temperature of the dried supply air is calculated from equation 2.3.1-4. The relative humidity of the supply air at sorption wheel outlet is then given by equation 2.3.1-2. In Chapter 5.4.1 the model is validated against measured performance data from the DEC test plant installed at the University of Applied Sciences in Stuttgart. A good agreement between measured and predicted values is reached with this quite simple model.

2.3.2 HEAT EXCHANGERS

A simple efficiency model is used for the rotation heat exchanger installed in the DEC system of the University of Applied Sciences in Stuttgart. Since the air volume flow rate of the supply air is equal to that of the return air and the heat exchanger is either turned on or off with one fixed rotation speed, the simple efficiency model reaches a sufficient accuracy. The heat exchanger efficiency with the same mass flow rate on each side of the heat exchanger is defined as follows:

$$\phi = \frac{t_{1,in} - t_{1,out}}{t_{1,in} - t_{2,in}} \qquad (2.3.2\text{-}1)$$

The model is analysed and validated against measured performance data of the installed DEC system in Chapter 5.4.2. The results show a good agreement between the measured and simulated outlet temperatures. The average error found for several hours of operation is below 3%.

2.3.3 HUMIDIFIERS

For the humidifiers in INSEL only a very simple model based on a fixed humidification efficiency was available. This simple model delivers sufficiently accurate results only for annual performance analyses with large time steps. For the development and analysis of new control strategies the consideration of the large inertia of the humidifiers is essential which is not considered in the simple efficiency model. Therefore, a new model has been developed which considers the water storage capacity of the humidifier matrix and startup delays due to the time required for the wetting of the matrix. Fig. 2-25 shows a typical humidifier with a contact matrix produced by MUNTERS as it is installed for return air humidification in the DEC demonstration plant of University of Applied Sciences in Stuttgart.

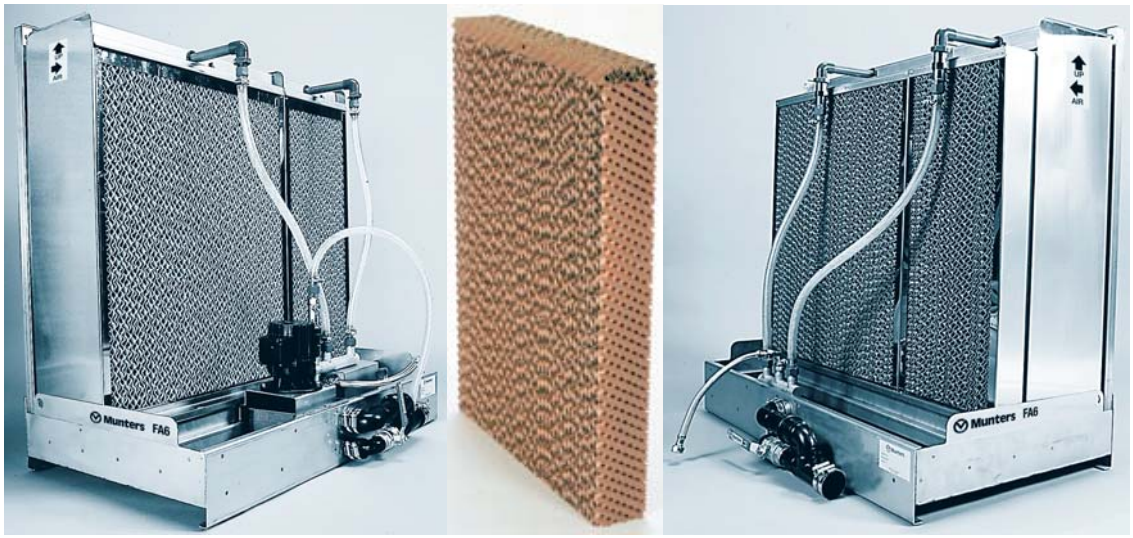

Fig. 2-25: MUNTERS evaporative humidifier FA6™ with GLASdec contact matrix (source: www.munters.de)

- Heat and mass transfer

For the model development the contact matrix is divided into finite elements as shown in Fig. 2-26.

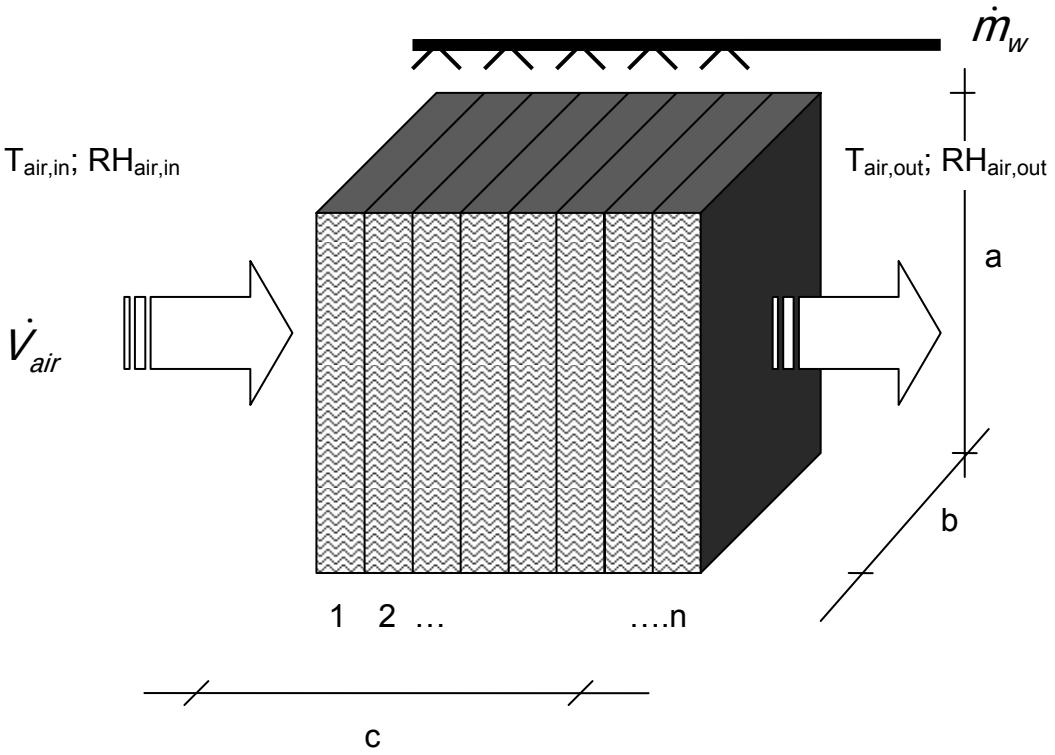

Fig. 2-26: Segmentation of the humidifiers contact matrix

The mass of water stored in the humidifier matrix is normally low compared to the air mass blown through the humidifier. Therefore, it can be assumed for model simplification, that the water temperature is always equal to the temperature of the air which is cooled down by the evaporation of the water. This means the water mass and the heat capacity of the matrix is neglected in the energy balance. With this assumption the energy and mass balance of one segment can be written as:

- Energy balance

$$\dot{Q}_{air,i} = h_{ev,i} \cdot \dot{m}_{w,ev,i}$$

$$\dot{m}_{air,i} \cdot \begin{pmatrix} c_{p,air}\left(T_{air,in,i} - T_{air,out,i}\right) \\ + c_{p,vap}\left(T_{air,in,i} \cdot x_{air,in} - T_{air,out,i} \cdot x_{air,out}\right) \end{pmatrix} = h_{ev} \cdot \dot{m}_{w,ev,i} \quad (2.3.3\text{-}1)$$

- Mass balance

$$\dot{m}_{air,i} \cdot \Delta x_{air,i} = \dot{m}_{w,ev,i}$$

$$\Delta x_{air,i} = x_{air,out} - x_{air,in} \quad (2.3.3\text{-}2)$$

If the evaporated water mass flow $\dot{m}_{w,ev,i}$ is replaced in Equation 2.3.3-1 by Equation 2.3.3-2 we get

$$\begin{pmatrix} c_{p,air}\left(T_{air,in,i} - T_{air,out,i}\right) \\ + c_{p,vap}\left(T_{air,in,i} \cdot x_{air,in,i} - T_{air,out,i} \cdot x_{air,out,i}\right) \end{pmatrix} = h_{ev} \cdot \Delta x_{air,i} \quad (2.3.3\text{-}3)$$

$$T_{air,out,i} = T_{air,in,i}\left(\frac{c_{p,air} + c_{p,vap} \cdot x_{air,in,i}}{c_{p,air} + c_{p,vap} \cdot x_{air,out,i}}\right) + \frac{h_{ev} \cdot \Delta x_{air,i}}{c_{p,air} + c_{p,vap} \cdot x_{air,out,i}} \quad (2.3.3\text{-}4)$$

Following (Kast, 1988) the mass transfer of water vapour from the liquid water film to the adjacent air flow depends on the mass transfer coefficient and on the wetting of the surface. The driving force in the transport process is the

difference in vapour pressure between the air and the water film interface. The mass transfer in flow direction *y* can be calculated from the following equation:

$$\dot{m}_{W,ev} = A\varepsilon \frac{\beta \cdot M}{R_m T}\left[p_{H_2O}(T_{air,in}) - p_{S,H_2O}(T_{water,in})\right] \text{ [kg s}^{-1}\text{]} \quad (2.3.3\text{-}5)$$

The mass transfer coefficient β depends on the flow pattern in the contact matrix channels and can be calculated from the heat transfer coefficient $h_{C,a}$ using the following equation (Kast, 1988):

$$\beta_A = \frac{h_{C,a}}{c_{P,a}\rho_a}\left(\frac{a_a}{\delta_a}\right)^{-(1-n)} \text{ [m s}^{-1}\text{]} \quad (2.3.3\text{-}6)$$

The heat transfer coefficient $h_{c,A}$ can be calculated as a function of the Nusselt number Nu and the characteristic length L. The characteristic length for rectangular channels is two times the distance between the adjacent walls.

$$h_{C,a} = \frac{Nu \cdot \lambda}{L} \quad (2.3.3\text{-}7)$$

If the matrix structure is assumed to be in the form of rectangular air channels the Nusselt number can be calculated from the following correlation.

$$Nu = \left[7{,}541^3 + 1{,}841 \cdot \sqrt[3]{\mathrm{Re}\cdot\mathrm{Pr}\cdot\frac{L}{l}} + \left(\frac{2}{1+22\cdot\mathrm{Pr}}\right)^{1/6} \cdot \left(\mathrm{Re}\cdot\mathrm{Pr}\cdot\frac{L}{l}\right)^{0,5}\right]^{1/3} \quad (2.3.3\text{-}8)$$

With the Prandtl number Pr and the Reynolds Number Re defined as:

$$\mathrm{Pr} = \frac{\upsilon_{Luft} \cdot \rho_{Luft} \cdot c_{P,Luft}}{\lambda_{Luft}} \quad (2.3.3\text{-}9)$$

$$\mathrm{Re} = \frac{v_{Luft} \cdot L}{\upsilon_{Luft}} \quad (2.3.3\text{-}10)$$

- Consideration of water storage effects in the structure of the contact matrix

The inertia of the humidifiers is mainly caused due to water storage in the matrix structure. At system startup it takes some time until the matrix is fully wetted which reduces the humidification efficiency. At system shutdown the water supply is cut off but the matrix structure is still wet and the humidifier operates for a quite long time as if the water supply was turned on. When the matrix structure begins to dry the humidification efficiency decreases slowly. For typical contact matrix humidifiers the drying process takes up to 1 hour until the matrix is completely dry. To consider this effect in the simulation model a water storage capacity of the matrix structure $m_w(t)$ is used together with an effective water flow rate of the fresh or recirculation water. At system startup the matrix is dry ($m_w(t)$ =0) and the water pump is switched on which causes an effective water flow rate $\dot{m}_{w,pump}$ and the matrix structure starts to be wetted as shown in Equation 2.3.3-12 and 2.3.3-12. The stored water $m_w(t)$ is limited to the maximum value defined for the matrix structure. The reduced humidification efficiency is considered by a reduced available matrix surface area for the mass transfer. After shut down of the humidifier pump no water is supplied to the matrix and the matrix structure starts to dry until $m_x(t)$ = 0. The water storage effect is calculated for each segment separately. Thus, a realistic drying process from humidifier inlet to humidifier outlet is reached.

$$A_{eff} = A \cdot \left(\frac{m_w(t)}{m_{w,\max}} \right) \tag{2.3.3-11}$$

$$m_w(t) = m_w(t-1) + \left(\dot{m}_{w,pump} - \dot{m}_{w,ev} \right) \cdot \Delta t \tag{2.3.3-12}$$

In this quite simple model no diffusion effects in the matrix structure are considered, therefore the final drying process is slightly faster than in reality. However, for model simplicity this shortcut is considered to be acceptable. A detailed validation of the developed model is shown in Chapter 5.4.3 and 5.4.2 for different applications. Here an excellent agreement between measured and predicted performance of the humidifiers is reached.

2.3.4 SOLAR AIR COLLECTORS

Standard air collectors typically consist of an absorber plate which is connected to air channels in rectangular shape formed of metal plates for increased heat transfer area. The absorber is covered by a glass cover with high transmittance for solar radiation. To reduce the heat losses the collector case is normally isolated. Fig. 2-27 shows a simplified scheme of a solar air collector.

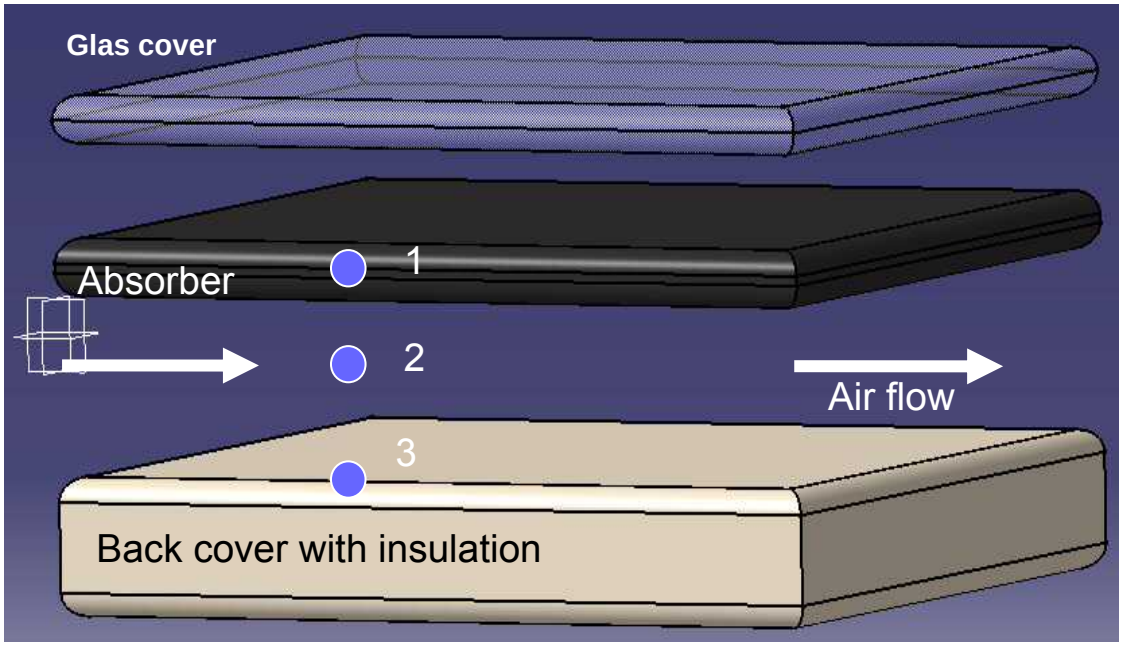

Fig. 2-27: System scheme of a solar air collector

The efficiency of solar air collectors mainly depends on the reflectance and transmittance of the collector glazing, the absorption efficiency of the absorber plate, the overall heat losses of the collector cover and the heat transfer area

offered for the air stream. The collector efficiency decreases with the temperature difference between the collector mean temperature and the ambient air temperature. The efficiency η of solar collectors is defined in the general form as the ratio between the useful heat gained and the total solar radiation on the collector plane:

$$\eta_{col} = \frac{\dot{Q}_h}{G_t} \qquad (2.3.4\text{-}1)$$

For the model development and the solution of the differential equations a simple forward differential method is used which enables the calculation of the temperature at the actual time step from the values of the previous time step. To consider properly the temperature profile of the air and surrounding collector structure between collector inlet and collector outlet the air collector is divided into finite elements in air flow direction as shown in Fig. 2-28.

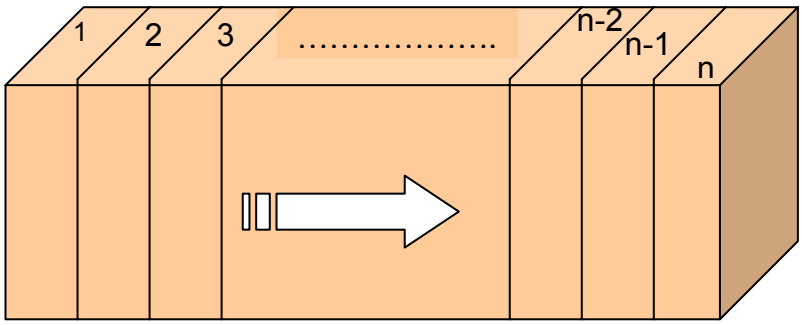

Fig. 2-28: Segmentation of the air collector in finite elements

- Energy balance

For the energy balance of the collector the three temperature nodes (absorber plate, air channel and back cover) shown in Fig. 2-27 are used. With this the energy balance can be written as follows:

- Temperature node 1 (absorber plate):

$$\dot{Q}_a = \dot{Q}_{Gt,a} - \dot{Q}_{hl} - \dot{Q}_{hc,a-f} - \dot{Q}_{r,a-b} \qquad (2.3.4\text{-}2)$$

- Absorbed solar energy

$$\dot{Q}_{Gt,a} = G_t(\tau,\alpha)\cdot A_a \qquad (2.3.4\text{-}3)$$

- Heat losses through the collector glazing

$$\dot{Q}_{hl} = U_{amb}\cdot A_a \cdot \left(T_{A(i,k-1)} - T_{amb}\right) \qquad (2.3.4\text{-}4)$$

- Convective heat exchange between the absorber plate and the air node

$$Q_{hc,a-f} = h_{C,a}\cdot A_a \cdot \left(\frac{T_a(t-1)+T_a(t)}{2} - \frac{T_{air,in}(t)+T_{air,out}(t)}{2}\right) \qquad (2.3.4\text{-}5)$$

- Heat transferred to the air gap back cover by long wave radiation exchange

$$\dot{Q}_{r,a-b} = h_{r,a-b}\cdot A_a \cdot \left(T_a(t-1) - T_b(t-1)\right) \qquad (2.3.4\text{-}6)$$

- Heat stored in the absorber material

$$\dot{Q}_a = \frac{\rho_a \cdot c_a \cdot d_a \cdot A_a}{\Delta t}\cdot\left(T_a(t) - T_a(t-1)\right) \qquad (2.3.4\text{-}7)$$

The absorbed solar energy $\dot{Q}_{Gt,a}$ is given as an external function of the transmission and reflection properties of the glazing and the absorber plate ($G_t(\tau\alpha)$). The calculation of this part is not described here in detail. Interested readers may refer to (Eicker, 2001). For model simplification, the iradiative heat exchange between the absorber plate and the back cover material is calculated from the temperatures of the time step before. For small time steps as used here, this simplification causes no visible error.

- Temperature node 2 (air node):

$$\dot{Q}_{air} = \dot{Q}_{hc,a-f} + \dot{Q}_{hc,b-f} \qquad (2.3.4\text{-}8)$$

- Convective heat exchange between the back cover and the air node

$$\dot{Q}_{hc,b-f} = h_{C,b} \cdot A_b \cdot \left(\frac{T_b(t-1) + T_b(t)}{2} - \frac{T_{air,in}(t) + T_{air,out}(t)}{2} \right) \quad (2.3.4\text{-}9)$$

- Heating energy air node

$$\dot{Q}_{air} = \dot{V}_{air} \cdot \rho_{air} \cdot c_{p,air} \cdot \left(T_{air,out}(t) - T_{air,in}(t) \right) \quad (2.3.4\text{-}10)$$

- Temperature node 3 (back cover):

$$\dot{Q}_b = \dot{Q}_{r,a-b} - \dot{Q}_{hl,b} - \dot{Q}_{hc,b-f} \quad (2.3.4\text{-}11)$$

- Convective heat exchange between the back cover plate and the air node

$$\dot{Q}_{hc,b-f} = h_{C,b} \cdot A_b \cdot \left(\frac{T_b(t-1) + T_b(t)}{2} - \frac{T_{air,in}(t) + T_{air,out}(t)}{2} \right) \quad (2.3.4\text{-}12)$$

- Heat stored in the back cover material

$$\dot{Q}_b = \frac{\rho_b \cdot c_b \cdot d_b \cdot A_b}{\Delta t} \cdot \left(T_b(t) - T_b(t-1) \right) \quad (2.3.4\text{-}13)$$

If this equation system is solved for the temperature of the three temperature nodes we get:

- Temperature of the absorber

$$T_{a(i,k)} = \frac{\begin{pmatrix} G_t(\tau\alpha) \cdot A - C_3\left(T_a(t-1) - T_{amb}\right) \\ -\frac{C_1}{2}\left(T_a(t-1) - T_{air,in}(t) - T_{air,out}(t)\right) \\ +C_2 \cdot T_a(t-1) - R_2\left(T_a(t-1) - T_b(t-1)\right) \end{pmatrix}}{C_2 + \frac{C_1}{2}} \quad (2.3.4\text{-}14)$$

With:

$$C_1 = h_{C,a} \cdot A_a$$

$$C_2 = \frac{\rho_a \cdot c_a \cdot d_a \cdot A_a}{\Delta t}$$

$$C_3 = k_1 \cdot A_a$$

$$R_2 = h_{r,a-b} \cdot A_a$$

- Air outlet temperature

$$T_{air,out}(t) = \frac{\left(\begin{array}{l} \frac{W_1}{2}(T_a(t-1) - T_{air,in}(t) + \frac{W_1}{2 \cdot (C_2 + \frac{C_1}{2})} \left[\begin{array}{l} G_t(\tau\alpha)A_a - C_3(T_a(t-1) - T_{amb}) \\ -\frac{C_1}{2}(T_a(t-1) - T_{air,in}(t)) \\ +C_2(T_a(t-1) - R_2(T_a(t-1) - T_b(t-1)) \end{array} \right] \\ -\frac{W_2}{2}(T_{air,in}(t) - T_b(t-1)) + \frac{W_2}{2(R_1 + \frac{R_3}{2})} \left[\begin{array}{l} \frac{R_3}{2}(T_{air,in}(t) - T_b(t-1)) + R_1 T_b(t-1) \\ +R_2 \cdot T_a(t-1) \\ +R_2(T_a(t-1) - T_b(t-1)) \\ -R_4(T_b(t-1) - T_{amb}) \end{array} \right] \\ +W_3 \cdot T_{air,in}(t) \end{array} \right)}{(W_3 + \frac{W_1}{2} - \frac{W_1 \cdot C_1}{4(C_2 + \frac{C_1}{2})} - \frac{W_2 \cdot R_3}{4(R_1 + \frac{R_3}{2})} + \frac{W_2}{2})}$$

(2.3.4-15)

With:

$$W_1 = h_{C,a} \cdot A_a$$

$$W_2 = h_{C,b} \cdot A_b$$

$$W_3 = \dot{m}_{air} \cdot c_{pair}$$

$$R_1 = \frac{\rho_b \cdot c_b \cdot d_b}{\Delta t} \cdot A_b$$

$$R_3 = h_{C,b} \cdot A_b$$

$$R_4 = U_b \cdot A_b$$

- Temperature of the back cover

$$T_b(t) = \frac{\left(\begin{array}{l}\frac{R_3}{2}\left(T_{air,out}(t) + T_{air,in}(t) - T_b(t-1)\right) + R_1 T_b(t-1) \\ + R_2\left(T_{air,in}(t) - T_b(t-1)\right) - R_4\left(T_b(t-1) - T_{amb}\right.\end{array}\right)}{\left(R_1 + \frac{R_3}{2}\right)} \tag{2.3.4-16}$$

- Consideration of the fins separating the air channels

Within the air collector the air cannels are separated by fins which are connected to the absorber plate and thereby increase the heat transfer area Fig. 2-29. This increase in heat transfer is considered by a heat transfer efficiency factor for the ribs (Altfeld, 1985).

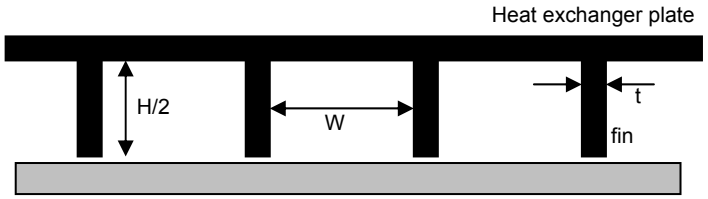

Fig. 2-29: Geometry of an absorber plate with ribs

The heat transfer efficiency factor for fins η_{Rl} is given as:

$$\eta_{Fi} = \frac{\tanh(m \cdot H)}{m \cdot H} \tag{2.3.4-17}$$

With:

$$m = \sqrt{\frac{h_C}{\lambda_{Fi}} \frac{U_{Fi}}{A_q}} \tag{2.3.4-18}$$

$$\frac{U_{Fi}}{A_q} = \frac{2 \cdot (H + t)}{H \cdot t} \tag{2.3.4-19}$$

The area relation of the fin area to the total channel sounding area can be written as:

$$\beta = \frac{A_{Fi}}{A_g} = \frac{2 \cdot H}{2 \cdot (W + H)} \qquad (2.3.4\text{-}20)$$

The ratio γ area of the fins A_w to the separating area between the channels A is:

$$\gamma = \frac{A_W}{A} = \frac{W}{W + t} \qquad (2.3.4\text{-}21)$$

The resulting effective heat transfer coefficient can then be calculated for the absorber surface and the back cover surface as follows:

- Absorber surface:

$$h_{C,a} = \frac{\gamma}{1 - \beta} \cdot (1 + \beta \cdot (2 \cdot \eta_{Fi} - 1)) \cdot h_C \qquad (2.3.4\text{-}22)$$

- Back cover surface:

$$h_{C,b} = \gamma \cdot h_C \qquad (2.3.4\text{-}23)$$

The heat transfer coefficient h_c is calculated in the from Nusselt correlations for air channels with rectangular shape (Eicker, 2001).

A validation of the developed solar air collector model is shown in Chapter 5.4.. Here an excellent agreement between measured and predicted performance of the air collector is reached.

3. DIMENSIONING STRATEGIES FOR SOLAR DRIVEN ABSORPTION COOLING APPLICATIONS IN OFFICE BUILDINGS

3.1 INTRODUCTION

Closed absorption cooling plants operated with solar or waste heat offer the potential to provide cooling energy for buildings at low primary energy consumption. However, these systems need to compete with electrically driven compression chillers which today work at average COPs around 3.0 or higher. Since the most often used single effect absorption cooling machines reach only thermal COPs (ratio of cold production to heat input) of 0.5-0.8, solar or renewable fractions on the heat supply need to be higher than about 50% to start saving primary energy (Mendes, et al., 1998). The exact value of the minimum solar fraction required for energy saving not only depends on the performance of the thermal chiller, but also on the electricity consumption of other components like the cooling tower and all the pumps connected to the system. For example a system with an energy efficient cooling tower performs better than a compression chiller at a solar fraction of 40%, a low efficiency cooling tower increases the required solar fraction to 63%. These values were calculated for a thermal chiller COP of 0.7, a compressor COP of 2.5 and an electricity consumption of the cooling tower between 0.02 or 0.08 kWh_{el} per kWh of cold (Henning, 2004). Much higher thermal COPs of around 1.1 - 1.4 are reached for double effect absorption cycles, but they require significantly higher driving temperatures between 120 and 170°C (Wardono and Nelson, 1996). Therefore, the energetic and economical performance of the solar thermal cooling system is not necessarily better (Grossmann, 2002).

For the design of solar thermal cooling systems so far no standardised methods are available. In the IEA task 25 first attempts were made to compare and evaluated several design methods. In the simplest approach a building load model provides hourly values of cooling loads and the solar fraction is calculated from the hourly produced collector energy at the given irradiance

conditions. Excess energy from the collector can be stored in available buffer volumes without however considering specific temperature levels. Different building types were compared for a range of climatic conditions in Europe with cooling energy demands between 10 and 100 kWh m^{-2} a^{-1}. Collector surfaces between 0.2 - 0.3 m^2 per square meter of conditioned building space combined with 1 - 2 kWh of storage energy gave solar fractions above 70% (Henning, 2004). Within the actual IEA Task 38 attempts are made to provide an accurate simplified design tool for system planers to standardise the design of solar cooling systems. Apart from this different simulation studies most based on TRNSYS simulations have been published which all gave quit big differences in the required collector area for a given solar fraction on the absorption chillers heat demand. The values vary between 0.07 – 0.3 m² per square meter of conditioned space (Henning, et al., 2004; Florides, et al., 2002 and Atmaca, et al., 2003). For real project installations the installed collector area has been related to the installed nominal cooling power of the chillers. The collector areas varied between 0.5 and 5 m² per kW of cooling power with an average of 2.5 m² per kW. To summarise the available solar cooling simulation literature, the main influencing factors for the design of solar driven single effect absorption chillers are the temperature level of the cold distribution, the type and control of the heat rejection system (dry or wet) and the load characteristic, orientation and location of the building. However, so far no structured analysis is available which clearly shows the effect of the different influencing factors on the required dimensions of the solar collector system in order to guarantee a defined solar fraction. For these kind analyses detailed simulation models are required of the whole solar cooling system including precise models of the absorption chiller, the heat rejection system and for the solar system with the solar collectors, the tubing and a stratified storage tank. Such models have been developed within chapter 2 of this work. Within this chapter the component models are combined to integrated system models in the simulation environment INSEL. The simulation work is based on hourly time series of irradiance and temperature data for the two locations Madrid in Spain and Stuttgart in Germany. The internal time step used was 1 minute with linear interpolation of the hourly

values of ambient temperature and solar irradiation. The hourly time series have been generated using long term monthly averages of both global horizontal irradiance and temperature, which are available in the weather database of the INSEL simulation environment. Using the monthly mean values, the well validated algorithms of Gordon and Reddy were used to first statistically generate daily clearness indices, which are not normally distributed around the monthly mean value. The hourly irradiance time series is then obtained by a first order autoregressive procedure, which uses a model from Collares-Pereira to parameterize the hourly clearness index.

3.2 SCOPE AND METHODOLOGY OF THE WORK

This chapter focuses on the analyses of the energetic and economical performance of solar powered absorption chiller systems. The goals are to calculate the solar contribution to the total energy demand of the thermal chiller system and to specify the associated costs. The influence of the building type and different cooling load distributions on dimensioning rules was the main question of the work. To evaluate the influence of chiller and solar thermal system sizing on performance, cooling load files for a small office building with about 450 m^2 floor area were produced to fit a commercially available absorption chiller with 15 kW nominal cooling power of the German company EAW (Wegracal SE 15). The building window surface area and orientation, the shading system and the internal loads were varied to determine the influences of the load distribution on solar fraction. The building construction (insulation standards, orientation, glazing fraction, size, etc.) was chosen so that the chiller power of 15 kW is sufficient to maintain room temperature levels at a given set point of 24°C for at least 90% of all occupation hours. To evaluate the influence of the time dependent building cooling loads on the solar fraction, building load files were calculated with a dominance of internal loads through persons or equipment or with dominating external loads through glazed facades. For the economical analysis, a market survey of thermal chillers up to 200 kW cooling power and for solar thermal collector systems was carried out. The cost annuity

was calculated for different system combinations and cooling energy costs were obtained.

3.3 COOLING LOAD CHARACTERISTICS OF THE ANALYSED BUILDINGS

To evaluate the energetic and economic performance of solar cooling systems under varying conditions, different building cooling load files were produced with the simulation tool TRNSYS. The methodology for choosing the building shell parameters is as follows: for a given chiller power of 15 kW an adequate building size was selected, for example a south orientated office building with 425 m^2 surface area and of rectangular geometry. The orientation of the building was varied to study the influence of daily fluctuations of external loads. The dimensions and window opening of the buildings were adjusted, so that the given chiller power could keep the temperature levels below a set point of 24°C for more than 90% of all operation hours. The air exchange rates were held constant at 0.3 h^{-1} for the office throughout the year. This limited air exchange rate leads to cooling load files, which in some cases contain cooling power demand during winter and transition periods for southern European locations. Only if the air exchange rate can be significantly increased either by natural ventilation or by using a mechanical ventilation system, can such a cooling power demand be reduced by free cooling. In the buildings analysed, heat was always assumed to be removed by a water-based distribution system, which was fed by cold water from the cooling machines. At low ambient temperatures, the cooling tower alone provides the required temperature levels for the cold distribution system. To evaluate the influence of the specific time series of the building cooling load, two cases were simulated:

- Office 1: Cooling load dominated by external loads through solar irradiance for unshaded windows and low internal loads of 4 W per m² conditioned space (see Fig. 3-1 and Table 3-2)
- Office 2: Cooling load dominated by internal loads of 20 W per m² conditioned space with good sun protection of all windows (see Fig. 3-2 and Table 3-3).

In addition, office 1a is an office building with the same geometry, but the main window front to the east instead of south. Office 1b has nearly 40% of the windows facing west.

Table 3-1: Cooled floor area and volume of the office buildings

Building type	Surface (m^2)	Volume (m^3)
Office 1 Madrid	425	1275
Office 1a Madrid	550	1650
Office 1b Madrid	450	1350
Office 2 Madrid	450	1350
Office 3 Stuttgart	500	1500

The peak values of the daily cooling loads are highest for the office with a western window front and lowest for the eastern offices. The phase shift between the curves is about 1 h (see Fig. 3-4). The cooling load file with high internal loads shows less daily fluctuations and is dominated by the external temperature conditions. For the office building, the annual cooling load is between 12 and 14 MWh for low internal loads up to 30 MWh for the same building, but higher internal loads.

Table 3-2: Window size and shading fractions for cooling load calculations

Building case	Window surface fraction (%)				Shading fraction (%)			
	North	South	East	West	North	South	East	West
Office 1 Madrid	39	39	11	11	0	0	0	0
Office 1a Madrid	39	11	39	11	0	0	0	0
Office 1b Madrid	39	11	11	39	0	0	0	0
Office 2 Madrid	39	39	11	11	90	90	90	90
Office 3 Stuttgart	39	39	11	11	0	0	0	0

The same building at a different geographical location (Stuttgart in Germany (Fig. 3-4) instead of Madrid in Spain) has a cooling energy demand of only 4.7 MWh. A wide range of specific cooling energies is covered, ranging from about 10 kWh m^{-2} for an office with low internal loads in a moderate climate up to 70 kWh m^{-2} for the same building in Madrid but with high internal loads (Fig. 3-5).

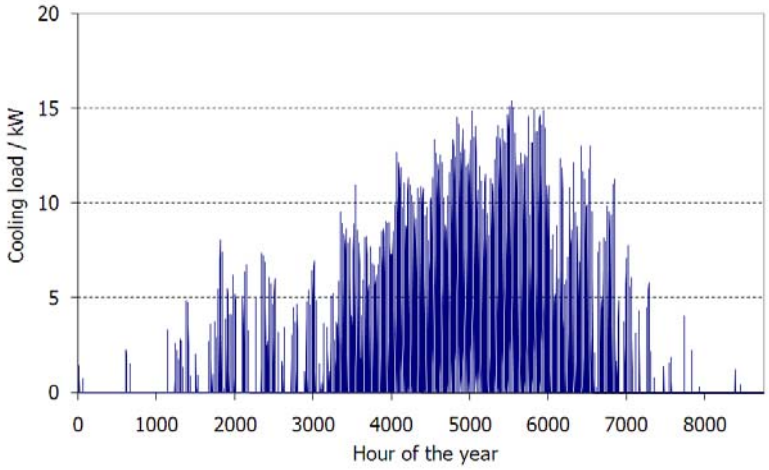

Fig. 3-1: Office building **dominated by external loads** located in **Madrid**, Spain (Office 1)

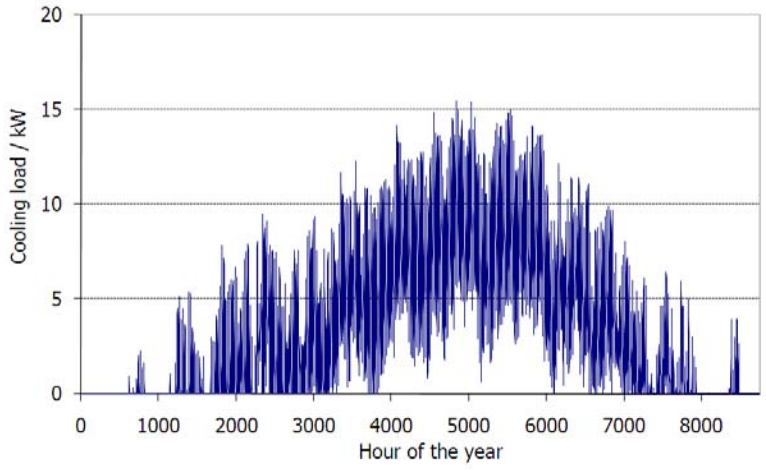

Fig. 3-2: Office building with **high internal loads** and **good sun protection** located in **Madrid**, Spain (Office 2)

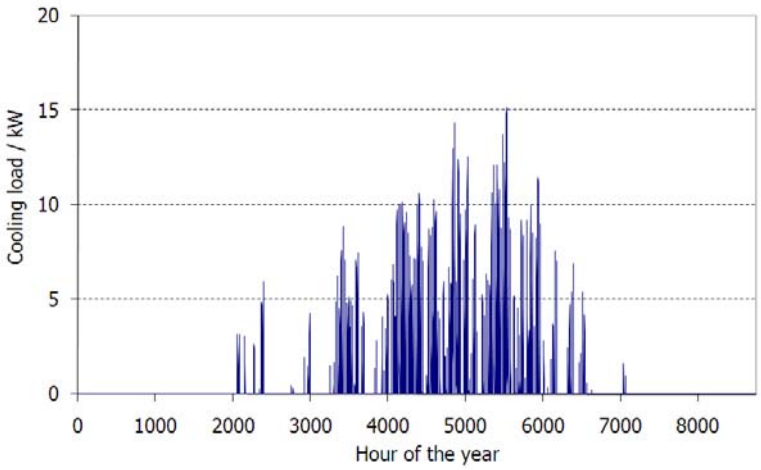

Fig. 3-3: Office building **dominated by external loads** located in **Stuttgart**/Germany (Office 3)

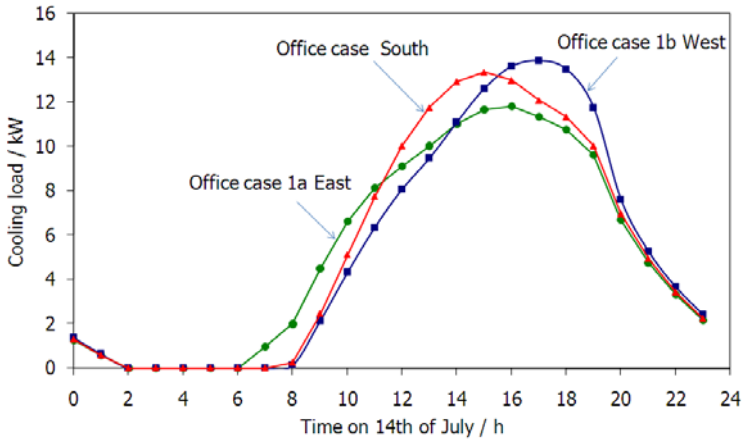

Fig. 3-4: Daily cooling loads of a office building with the main window front facing east, south or west located in Madrid, Spain (Office 1)

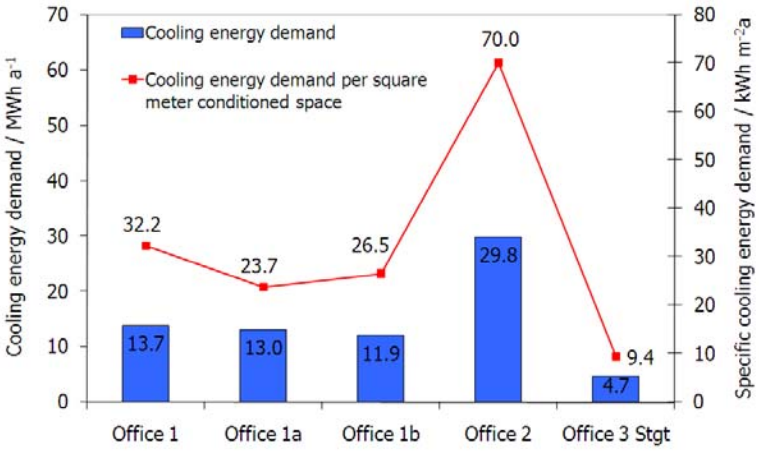

Fig. 3-5: Specific and total annual cooling energy demand for the office building with different orientations and locations and dominated either by external (Office 1 and Office 3) or internal (Office 2) loads

The specifications for the buildings with the different cases are summarized in Table 3-1 and Table 3-2. A crucial factor for the economics of the solar cooling installations is the operation hours of the machines, whereby buildings with higher full load operation have lower cooling costs for the investment part. The load hours for the buildings considered are between 680 h and 2370 h for the location Madrid and only 313 h for an office building in Stuttgart (Table 3-3).

Table 3-3: Internal loads and full load hours for the building in different locations

Building type	Internal load (W m^{-2})	Full load hours (h)
Office 1 Madrid	4	913
Office 1a Madrid	4	866
Office 1b Madrid	4	793
Office 2 Madrid	20	1986
Office 3 Stuttgart	4	313

3.4 COMPONENT AND SYSTEM MODELS

3.4.1 ABSORPTION CHILLER MODEL AND VALIDATION

Most chiller models used in dynamic simulations of whole solar cooling systems are based on measured performance characteristics of absorption chillers. However, the main disadvantage of this simple type of models is that they often do only consider the variation of one or two control variables as the generator inlet temperature and the heat rejection temperature. Variations of the return temperature of the cold water circuit or variations of the mass flow are not considered and therefore are assumed to be constant for all operation conditions even at part load operation. Furthermore, the measured performance of the absorption chillers are mostly based on single operation point measurements under laboratory conditions without consideration of measurement inaccuracies (especially of volume flow sensors) and machine variations. Steady-state absorption chiller models on the other hand are based on the internal mass and energy balances in all components, which depend on

the solution pump flow rate and on the heat transfer between external and internal temperature levels. Several problems are associated with a single characteristic equation, which calculates all internal enthalpies only for the design conditions: if bubble pumps are used, the solution flow rate strongly depends on the generator temperature (Albers, et al., 2003). Also if the external temperature levels differ significantly from design conditions, the internal temperature levels change and consequently the enthalpies. Therefore, in the current work, the quasi stationary model described in Chapter 2.2.2.1 was used with internal energy balances solved for each simulation time step as a function of the external entrance temperatures, so that changing mass flow rates can be considered in the model. For given cold water temperature, the cooling power and the COP mainly depend on the generator and the cooling water temperatures for the absorption and condensation process. As the temperatures deviate significantly from the design point, the variable enthalpy model reproduces the measured results much better than the constant enthalpy equation (see Fig. 2-11 in Chapter 2.2.2.1).

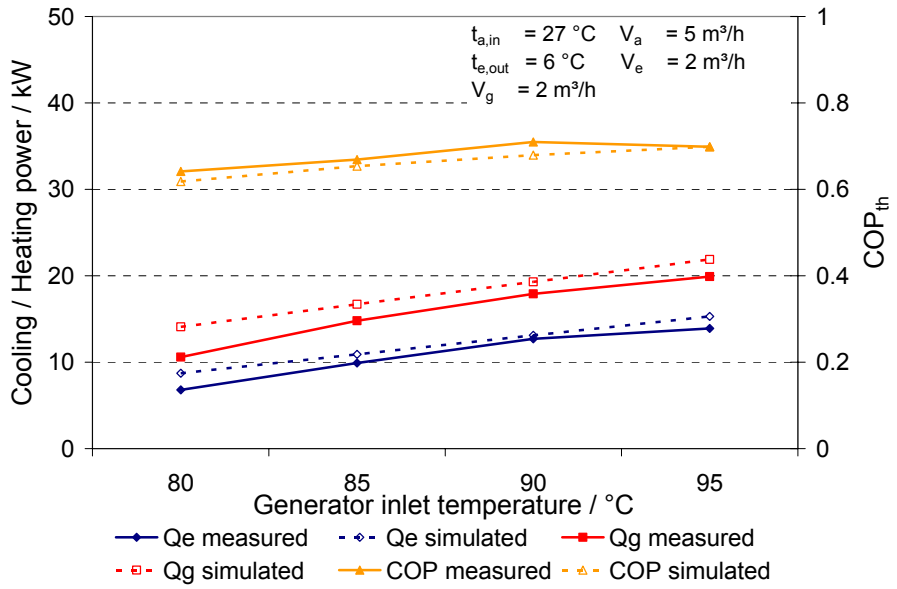

Fig. 3-6: Model validation (EAW, WGRACAL SE 15); cooling power and thermal COP of a 15 kW absorption chiller shown as a function of generator inlet temperature. (**27°C** absorber inlet temperature and **6°C** cold water temperature)

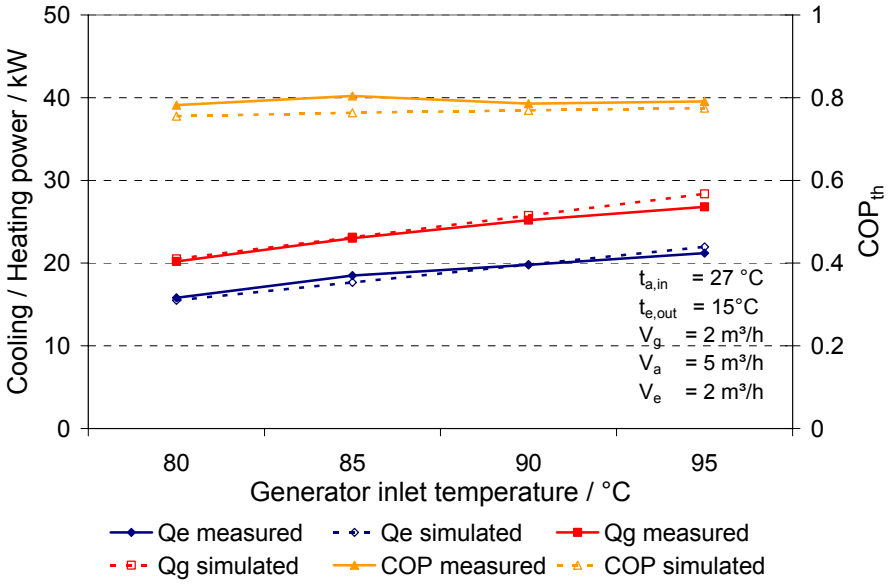

Fig. 3-7: Model validation (EAW, WGRACAL SE 15); cooling power and thermal COP of a 15 kW absorption chiller shown as a function of generator inlet temperature. (**27°C** absorber inlet temperature and **15°C** cold water temperature)

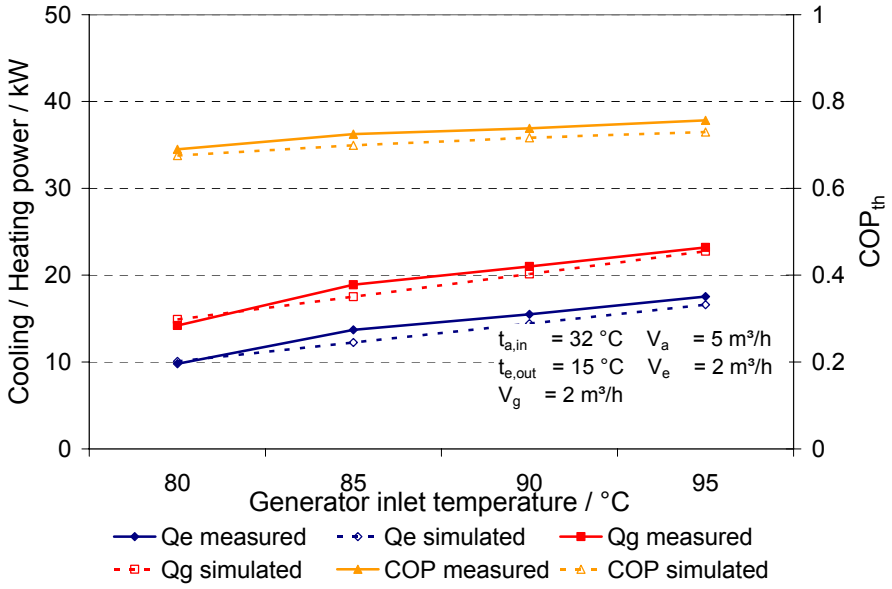

Fig. 3-8: Model validation (EAW, WGRACAL SE 15); cooling power and thermal COP of a 15 kW absorption chiller shown as a function of generator inlet temperature. (**32°C** absorber inlet temperature and **15°C** cold water temperature)

Fig. 3-6 to Fig. 3-8 show the measured and simulated performance data of a 15 kW LiBr–H2O absorption machine produced by the German company EAW in dependence of the generator inlet temperature at different cold water and heat rejection temperatures. The measured performance data was taken from the manufacturer catalogue. Since no exact construction details of the machine

were available, the parameter identification procedure described in Chapter 2.2.2.2 was used to identify the required parameters of the quasi-stationary absorption chiller model. The parameters found are listed in Table 3-4 and the data provided by EAW for the design point of the machine are shown in Table 3-5.

Table 3-4: Parameters of the simulation model derived from the parameter identification method described in chapter 2.2.2

Internal generator mean temperature T_G at design conditions	75.25 °C	UA_G	2.11 kW K^{-1}
Internal condenser mean temperature T_C at design conditions	41.59 °C	UA_C	2.28 kW K^{-1}
Internal absorber mean temperature T_A at design conditions	37.69 °C	UA_A	3.37 kW K^{-1}
Internal evaporator mean temperature T_E at design conditions	10.25 °C	UA_E	3.75 kW K^{-1}
Rich solution mass flow rate	0.33 kg s^{-1}	$C_{p,heating\ fluid}$	4.19 kJ kg^{-1} K^{-1}
Solution heat exchanger efficiency	85 %	$C_{p,\ cooling\ fluid}$	4.19 kJ kg^{-1} K^{-1}
Dühring-Parameter B	1.198686	$C_{p,cold\ water}$	4.19 kJ kg^{-1} K^{-1}

Table 3-5: Technical Data of the EAW WEGRACAL SE 15 Absorption Chiller

Cooling power	15 kW	Thermal COP	0.71
Cold water inlet	17 °C	Cold water outlet	11 °C
Cold water volume flow rate	1.9 m^3 h^{-1}	Nominal pressure loss	350 mbar
Nominal pressure	6 bar	Cold water connection	DN 25
Heating power	21 kW		
Hot water supply	90 °C	Hot water return	80.5 °C
Cold water volume flow rate	2.0 m^3 h^{-1}	Nominal pressure loss	250 mbar
Nominal pressure	6 bar	Cold water connection	DN 25
Heat rejection power	35 kW		
Cooling water supply	30 °C	Cooling water return	36 °C
Cooling water volume flow rate	5.0 m^3 h^{-1}	Nominal pressure loss	900 mbar
Nominal pressure	6 bar	Cold water connection	DN 32
Voltage / Frequency	400 V / 230 V 50 Hz	Electrical power consumption	0,3 kW
Length	1.5 m	Width	0.75 m
Height	1.6 m	Weight	700 kg

As visible from Fig. 3-6 - Fig. 3-8 a good correlation between the performance data predicted by the quasi-stationary model and the measured performance data has been found, although no construction details of the absorption chiller were available.

The simulated cooling power, required heating power and the resulting COP are very close to the measured performance for a wide range of different operation conditions. Larger deviations only occur for low cold water temperatures and low driving temperatures below 85°C. Here the cooling power and required heating power is overestimated by about 30%. The difference in the resulting thermal COP is only 6.5 %. For almost all other operation points the deviation between measured and predicted cooling power and required heating power is clearly below 10% and below 7% for the resulting COP. Since the measured performance data is only based on single operation point measurements, no statistical representative dataset for the operation of the absorption chiller was available. However, if typical measurement inaccuracies especially of mass flow sensors and other sources of error are considered, the deviations between the predicted and measured ACM performance is expected to be quite close to the measurement inaccuracies and machine variations.

A comparison of the measured performance between Fig. 3-6 and Fig. 3-7 clearly shows that a lower evaporator temperature reduces the COP and in consequence a higher generator temperature is required to reach the same cooling power. The cooling water temperature has also a strong influence on the COP and cooling power delivered at a given generator inlet temperature (see Fig. 3-9 and Fig. 3-10). To compare performance of different absorption chillers, it is therefore essential to compare for the same three temperature levels of evaporator, absorber / condenser and generator. As the absorption chiller model is part of a more complex dynamic model including varying meteorological conditions, there is a need to use dynamic system simulation tools anyway. The simplification of the easy to use characteristic equation with

constant slopes is therefore not advantageous and the more exact quasi-stationary model described above has been used throughout this work.

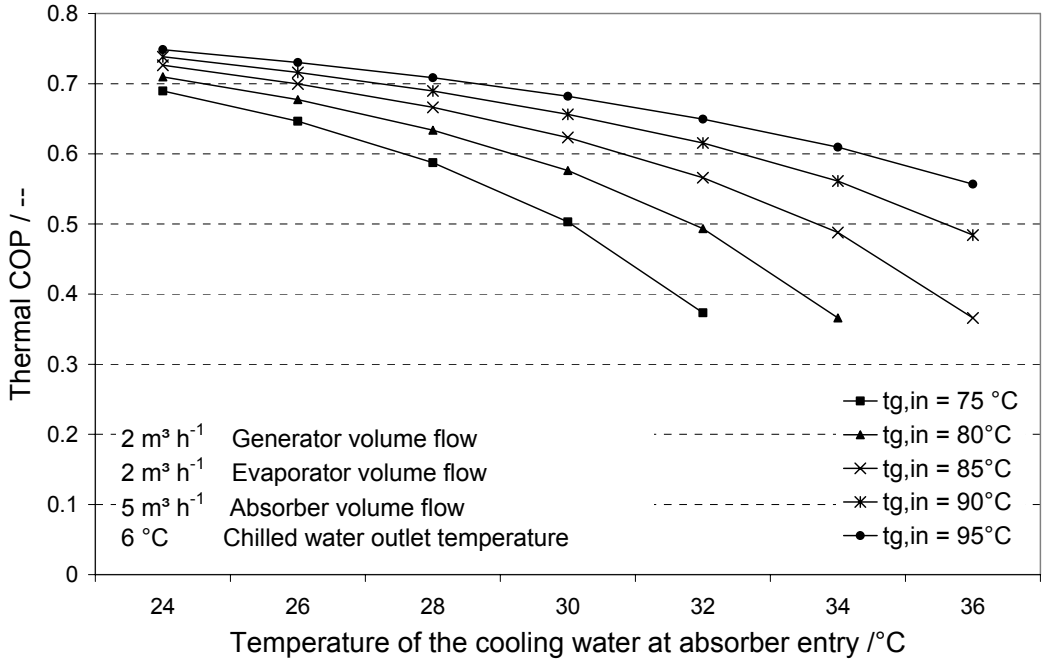

Fig. 3-9: Calculated thermal COP as a function of generator and cooling water inlet temperature for the EAW 15 kW absorption chiller

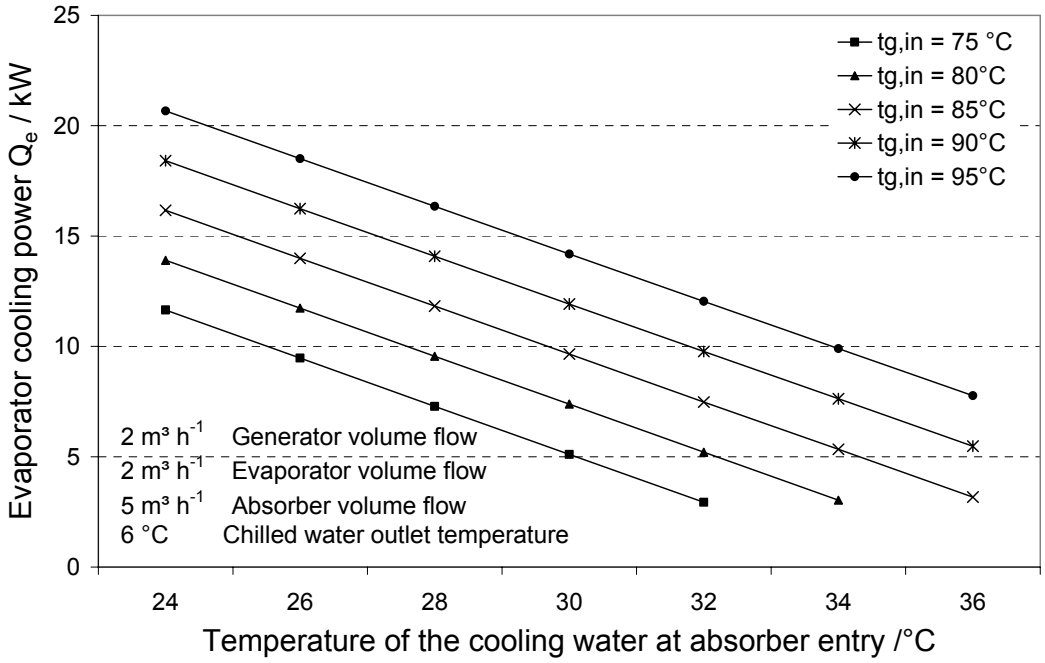

Fig. 3-10: Calculated cooling power as a function of generator and cooling water inlet temperature for the EAW 15 kW absorption chiller.

3.4.2 SOLAR THERMAL SYSTEM MODELS

The solar thermal system model includes a collector, a stratified storage tank, a controller and a back-up heater. The thermal collector is simulated using the steady-state collector equation with an optical efficiency η_0 and the two linear and quadratic heat loss coefficients a_1 and a_2. A vacuum tube collector from the company Schott was used for all simulation runs and has an optical efficiency of 0.775, with a_1 at 1.476 W m^{-2} K^{-1} and a_2 at 0.0075 W m^{-2} K^{-2}. The storage tank has 10 temperature nodes to simulate stratification. The collector injects heat into the storage tank via a plate heat exchanger, if the collector temperature is 5 K above the lowest storage tank temperature. The return to the collector is always taken from the bottom of the tank, the load supply is taken from the top of the tank. The collector outlet and the load return are inserted into the storage tank at the corresponding stratification temperature level. To validate the collector model using experimental data, a dynamic model was also developed, which includes heat capacity effects (see Chapter 2.1.1.1). However, for annual simulations, the steady-state model was considered as sufficiently accurate.

3.5 SYSTEM SIMULATION RESULTS

3.5.1 GENERAL INFLUENCES OF THERMAL SYSTEM DESIGN AND OPERATIONAL CONDITIONS OF THE ABSORPTION CHILLER

Before evaluating the influence of the building cooling load, the thermal cooling system performance was studied in detail for one chosen load file, namely the office building dominated by external loads (office 1). The analysed cases are summarised in Table 3-6.

Table 3-6: Summary of boundary conditions for different simulation runs for office 1

Analysed office cases	Cooling tower type	Cold distribution		Generator inlet temperature	
		6°C / 12°C	15°C / 21°C	90°C constant	70°C – 95°C variable
Case 0	Wet	X		X	
Case 1	Wet	X		X	
Case 2	Wet	X			X
Case 3	Wet		X		X
Case 4	Dry		X		X

Case 0 and Case 1 both operate at constant generator temperature, but in Case 0 the solar thermal system operates at low flow conditions.

The main influences on the cooling system performance are the external temperature levels in the generator, evaporator, absorber and condenser. In case of the evaporator, the temperature level depends on the type of cold distribution system, for example fan coils with 6°C / 12°C (case 0 to case 2) or chilled or activated ceilings with higher temperature levels of 15°C / 21°C (case 3 and case 4). The higher the temperature of the cold distribution, the better is the system performance. In case of the absorber and condenser temperature levels, the type and control of the heat rejection system is decisive for performance. In this work, wet (case 0 – case 3) and dry (case 4) cooling towers have been modelled. The generator temperature level mainly depends on the chosen control strategy. In the simplest case, the inlet temperature to the

generator is fixed (case 0 and case 1), which means high collector temperatures and poorer performance. An improved control strategy allows a temperature reduction in partial load conditions (case 2 to case 4). For an annual cooling energy demand of nearly 14 MWh and an average COP of 0.7 the system requires about 20 MWh of heating energy. To achieve a solar fraction of 80% for the given cooling load profile, a collector aperture area of 48.5 m^2 and a storage tank volume of 2 m^3 is required, if the generator is always operated at an inlet temperature of 85°C. For the constant generator inlet temperature level of 85°C, the specific annual collector energy yield is only 393 kWh per square meter collector aperture area for an annual irradiance of 1746 kWh m^{-2}, i.e. the solar thermal system efficiency is 22% (Case 0).

If the collector field would also be used for warm water heating and heating support the annual yield could be significantly increased (to about 1000 kWh m^{-2} a^{-1}). For such constant high generator inlet temperatures and a low flow collector system with 15 kg m^{-2} h^{-1} mass flow, the temperature levels in the collector are often above 100°C, if the cooling demand is low and the solar thermal energy production high. An increase of mass flow reduces the problem: by doubling the collector mass flow and thus lowering average solar collector temperatures, the solar fraction for the same collector aperture area rises to 90% (see Fig. 3-11). Using the higher mass flow of 30 kg m^{-2} h^{-1} and constant generator temperatures, the collector aperture area can be reduced to 33.1 m^2 and the annual collector energy yield rises to 584 kWh per square meter collector aperture area (33% solar thermal system efficiency) in (Case 1). If the controller allows a reduction of generator temperature for partial load conditions, performance improves due to lower average temperature levels and low flow systems can again be used (see Fig. 3-12). The collector aperture area required to cover 80% of the demand is now reduced to 31 m^2, i.e. only 2 m^2 kW^{-1}. The cold water temperatures were still at 12°C / 6°C and a wet cooling tower was used (Case 2).

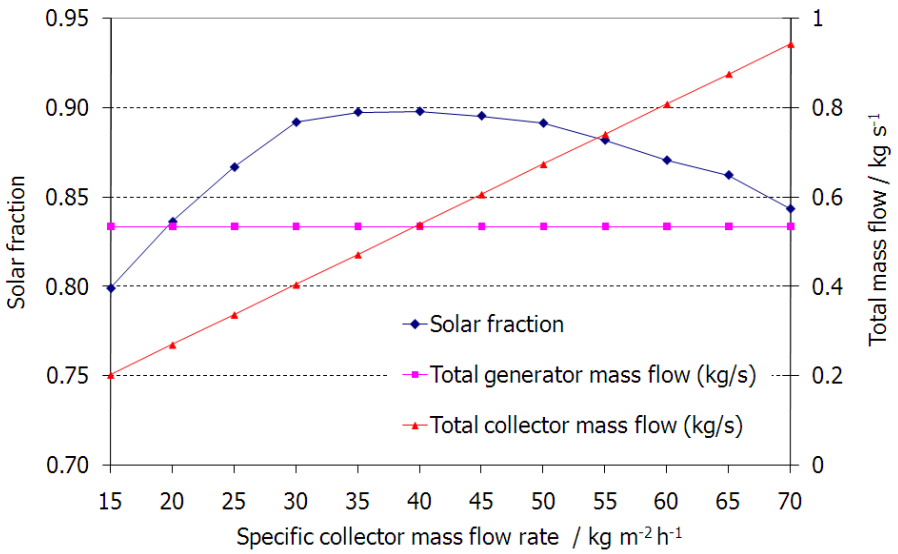

Fig. 3-11: Influence of collector mass flow rate on the solar fraction for a solar driven EAW 15 kW absorption chiller operated at constant generator inlet temperature (Case 0: 48.5 m² collector area)

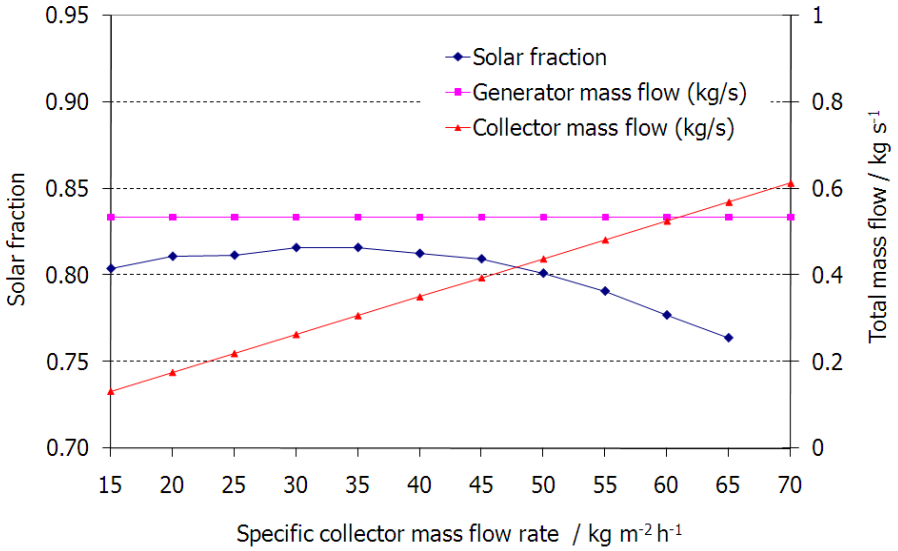

Fig. 3-12: Influence of collector mass flow rate on the solar fraction a solar driven EAW 15 kW absorption chiller operated at variable generator inlet temperatures (Case 2: 31 m² collector area)

If the cold is distributed using chilled ceilings or thermally activated concrete slabs, the temperature levels can be raised and performance improves (Case 3). For cold water temperatures of 21°C/15°C the required collector aperture area is only 27 m^2, i.e. 1.8 $m^2\,kW^{-1}$ (see Fig. 3-13).

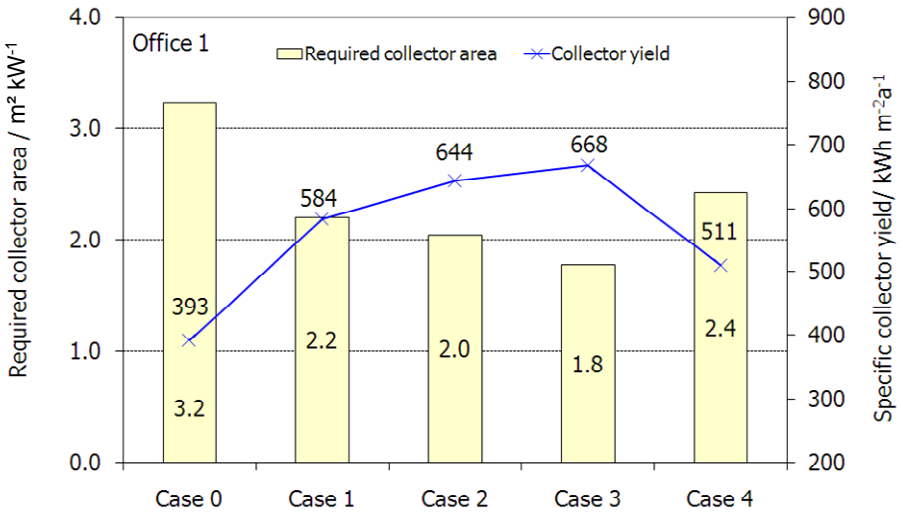

Fig. 3-13: Required collector area per kW cooling power to achieve 80% solar fraction for different generator inlet and evaporator outlet temperatures of the solar driven ACM applied to the office 1

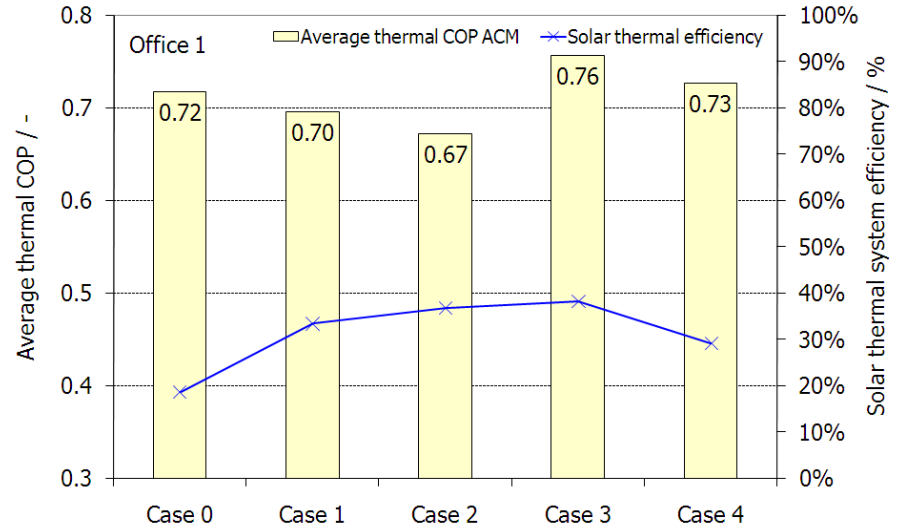

Fig. 3-14: Average annual thermal COP and solar thermal collector efficiency for different generator inlet and evaporator outlet temperatures of the solar driven ACM applied to the office 1

If a dry heat rejection system is used, the heat removal of absorber and condenser occurs above ambient air temperature levels (Case 4). The set point for the absorber inlet temperature is 27°C, which cannot always be reached for the dry heat rejection system. This leads to an increase of required collector aperture area to 36 m^2, i.e. 2.4 m^2 kW^{-1}. For the improved operation strategy, the collector energy delivered to the storage tank reaches annual values

between 511 and 670 kWh m^{-2} depending on the cold and heat rejection water temperature levels. The thermal COP of the absorption chiller is highest (0.76), if the cold water temperature level is high (21°C/15°C) and stays high, even if a dry heat rejection system is used (0.73). Low cold water temperature give COP's of 0.67–0.7 (see Fig. 3-14).

The solar thermal efficiency is calculated from the energy produced and delivered to the hot storage tank divided by the solar irradiance. The storage tank volume only becomes important for solar fractions of 80% and higher. At constant generator temperatures and a collector mass flow of 30 kg m^{-2} h^{-1} the solar fraction drops by a maximum of 10% points, if the specific storage volume is reduced from 50 to 25 l m^{-2}. For specific storage volumes above 0.06 m^3 m^{-2}, the solar fraction hardly changes (see Fig. 3-15). As usual, the annual specific collector yield is highest for low solar fractions, i.e. for small collector aperture areas. For the location Madrid/Spain it varies between 230 and 880 kWh m^{-2} (see Fig. 3-16).

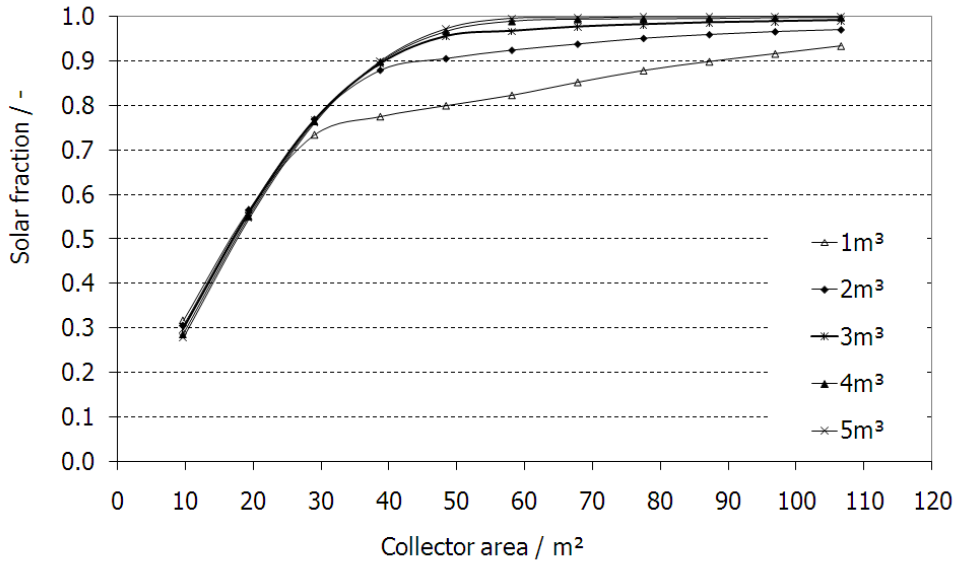

Fig. 3-15: Solar fraction as a function of collector aperture area for a 15 kW solar cooling system operated at constant generator inlet temperatures (Case 1). The storage volume is varied from 1 to 5 m^3.

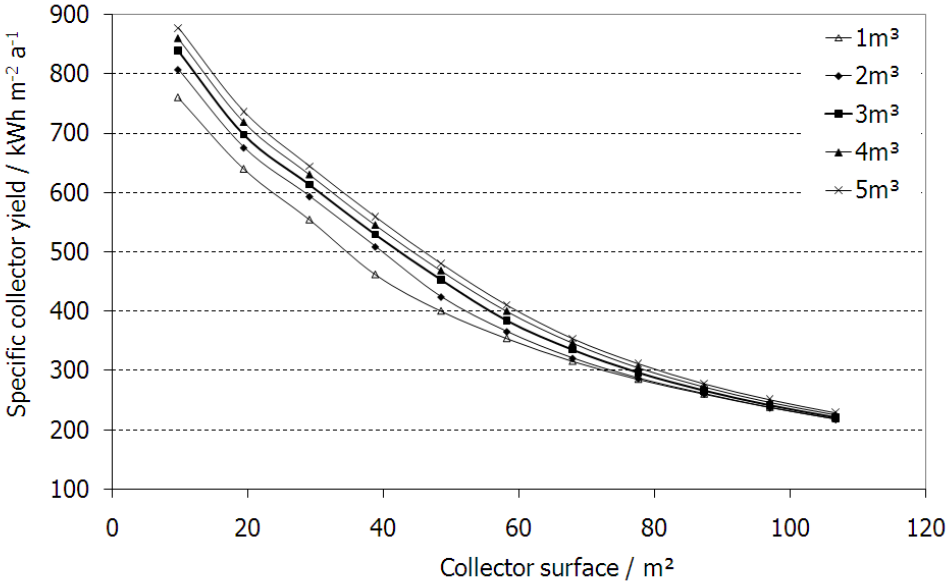

Fig. 3-16: Collector yield as a function of collector aperture area for a 15 kW solar cooling system operated at constant generator inlet temperature (Case 1). The storage volume is varied from 1 to 5 m^3.

In the following, the influence of storage tank volume, insulation thickness and heat exchanger size is evaluated for Case 2 conditions, i.e. improved control with varying generator temperatures. The solar fraction to the total heat demand is reduced by 2% points for a typical insulation thickness of 10 cm compared to an ideal loss free storage tank (see Fig. 15). This corresponds to an additional auxiliary heating demand of 340 kWh or 9% more. Doubling the storage volume increases the solar fraction by 1% point, which corresponds to a reduction of auxiliary heating energy of 200 kWh or 5% less. The larger the storage tank, the more important is a good insulation quality. The specific collector energy delivered to the storage tank even drops if the insulation quality improves, as the storage tank is generally hotter. However, the energy delivered from the storage tank to the absorption chiller increases, so that in total the solar fraction improves. The influence of the solar circuit heat exchanger was analysed by varying the transferred power UA per degree of temperature difference between primary and secondary circuit. The heat exchanger is usually dimensioned for the maximum power of the solar collector field. At a design mean operating temperature of the collectors of 85°C and an ambient air design temperature of

32°C the efficiency of the vacuum tube collectors chosen here is 67.5%, i.e. the collectors produce a maximum of 675 W m^{-2} at full irradiance. For the given collector aperture area of 31 m^2 and a set temperature difference across the heat exchanger of 3 K, this results in a transfer power of 7 kW K^{-1}. A reduction of transferred power from the solar circuit heat exchanger by 50% does not reduce the solar fraction at all.

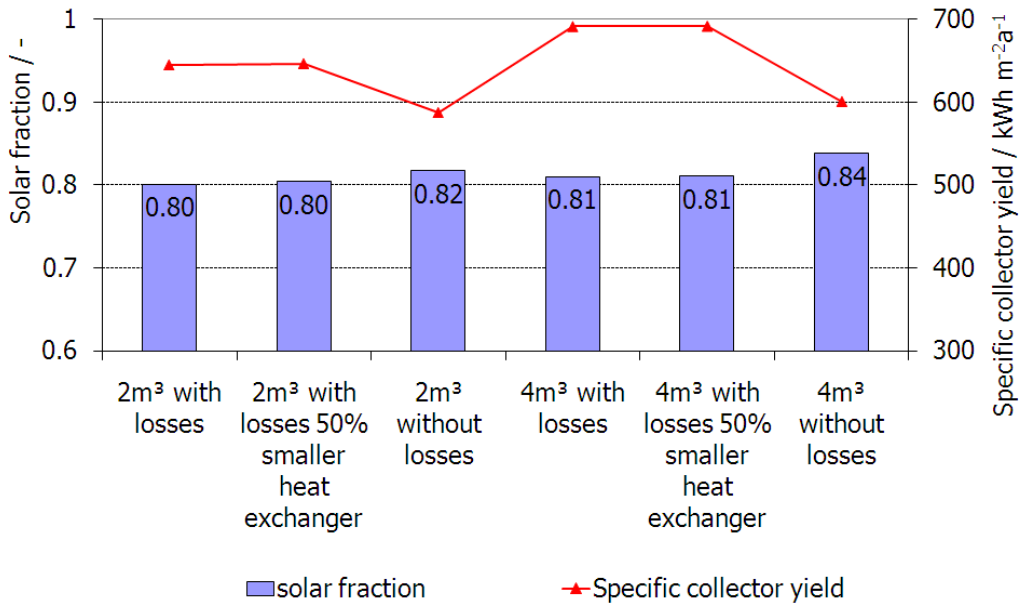

Fig. 3-17: Influence of storage tank insulation and heat exchanger size on the solar fraction and specific collector yield of a 15 kW solar cooling system operated at variable generator inlet temperatures (Case 2)

3.5.2 INFLUENCE OF DYNAMIC BUILDING COOLING LOADS

If a given cooling machine designed to cover the maximum load is used for different cooling load profiles, the influence of the specific load distribution and annual cooling energy demand can be clearly seen. The boundary conditions for the operation strategy were set to Case 2 conditions, i.e. a wet cooling tower, a low cold distribution temperature network of 6°C/12°C and variable generator inlet temperatures. The solar fraction was always at 80%. The office building with low internal loads and the main windows facing south requires 2

m^2 kW^{-1} solar thermal collector aperture area (office 1). The same building with a different orientation to the east can be about 20% bigger in size to fit the 15 kW maximum cooling power. It has a 15% higher collector aperture area and 15% less collector yield. If the building is orientated with the main window front to the west, the building aperture area is only slightly higher than the south orientated building with a lower total cooling energy demand. The collector aperture area is the same as for a south orientated building, which at lower operating hours means higher total costs. The same building now dominated by internal loads (office 2) needs a collector aperture area of 3.6 m^2 kW^{-1}, which is 80% higher than for office 1, although the required maximum power is still only 15 kW. Due to the longer operating hours of the solar thermal cooling system, the specific annual collector yield is 22% higher with 784 kWh m^{-2} at the location Madrid/Spain, so that the solar thermal efficiency is 45% for solar cooling operation alone. If the office building with low internal loads is placed in Stuttgart/Germany with a more moderate climate, the annual collector yield drops to 324 kWh m^{-2} and the required aperture area is 1.7 m^2 kW^{-1} (see Fig. 3-18).

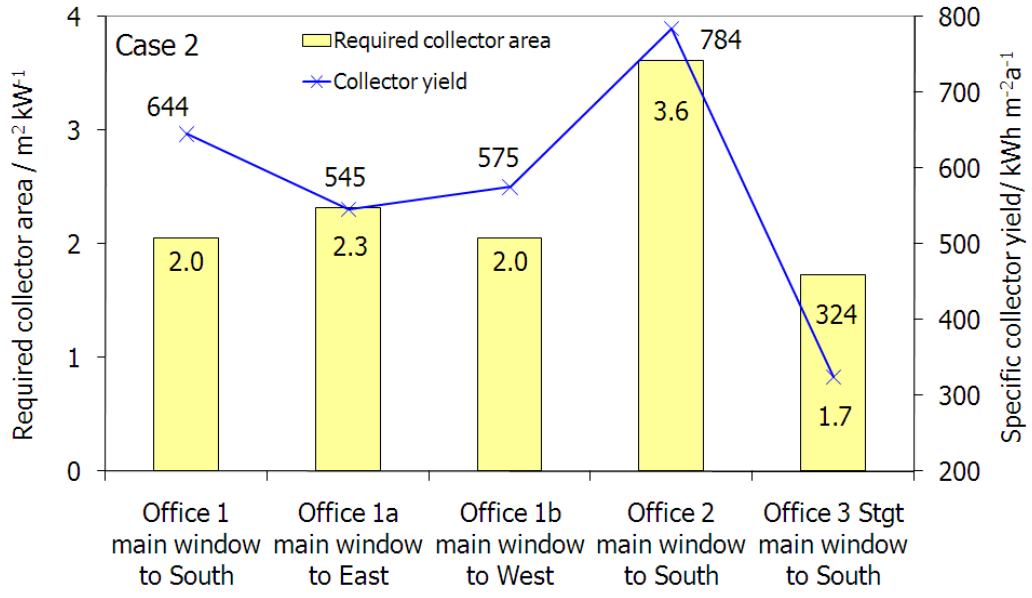

Fig. 3-18: Collector aperture per kW maximum cooling power of the absorption chiller calculated for different office building types and locations

For the location Madrid, the collector aperture area required to cover 1 MWh of cooling energy demand varies between 1.6 and 3.5 m^2 MWh^{-1}, depending on building orientation and operation strategy chosen. The lower the cooling energy demand, the higher the required aperture area per MWh. This is very clear for the building in Stuttgart with a low total energy demand of 4.7 MWh, where between 4.6 and 6.2 m^2 solar thermal collector aperture area per MWh is necessary to cover the energy demand (see Fig. 3-19). The ratios between collector aperture and cooling energy demand vary by about 25% for the same location and operation strategy. In locations with lower annual irradiance such as Stuttgart, the required collector aperture per MWh cooling energy demand is higher. The storage volumes are comparable to typical solar thermal systems for warm water production and heating support and vary between 40 and 110 l/m^2 of collector aperture area, depending on operation strategy and cooling load file. They increase with cooling energy demand for a given location. In moderate climates with only occasional cooling energy demand, the storage volumes are generally higher (see Fig. 3-20).

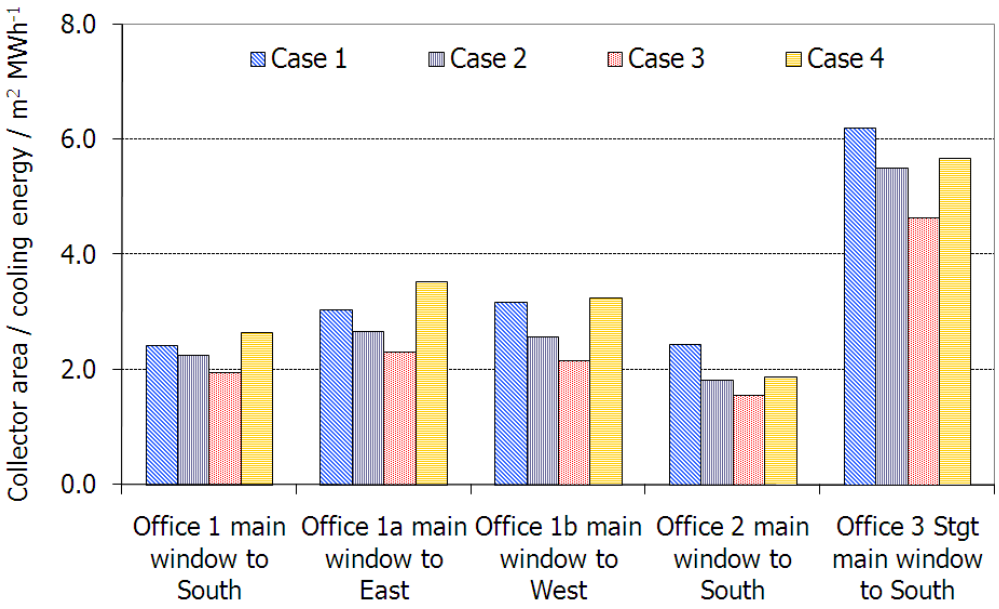

Fig. 3-19: Required collector aperture per MWh cold for different building load characteristics (office 1 to office 3) and different operation strategies and cooling distribution systems (case 1 to case 4)

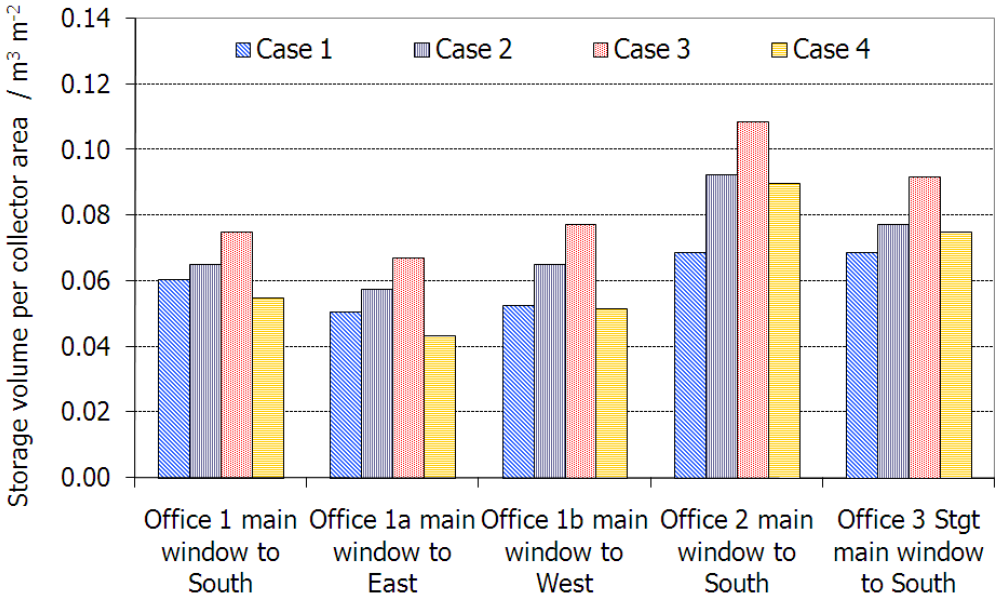

Fig. 3-20: Storage volume per square meter of collector aperture area for different building load characteristics (office 1 to office 3) and different operation strategies and cooling distribution systems (case 1 to case 4)

3.5.3 ECONOMICAL ANALYSIS

To plan and project energy systems such as solar cooling systems, economic considerations form the basis for decision making. The costs in energy economics can be divided in three categories: capital costs, which contain the initial investment including installation, operating costs for maintenance and system operation and the costs for energy and other material inputs into the system. The analysis presented here is based on the annuity method, where all cash flows connected with the solar cooling installation are converted into a series of annual payments of equal amounts. The annuity a is obtained by first calculating the net present value of all costs occurring at different times during the project, i.e. by discounting all costs to the time t = 0, when the investment takes place. The initial investment costs P(t = 0) as well as further investments for component exchange in further years P(t) result in a capital value CV of the investment, which is calculated using the inflation rate f and the discount or

basic interest rate d. The discount rate chosen here was 4% and the inflation rate was set to 1.9%:

$$CV = \sum P(t) \cdot \frac{(1+f)^t}{(1+d)^t} \tag{3-1}$$

Annual expenses for maintenance and plant operation EX, which occur regularly during the lifetime N of the plant, are discounted to the present value by multiplication of the expenses with the present value factor PVF. Thermal chillers today can expect a lifetime of 20 years:

$$PVF(N, f, d) = \frac{1+f}{d-f}\left(1 - \left(\frac{1+f}{1+d}\right)^N\right) \tag{3-2}$$

In the case of solar cooling plants, no annual income is generated, so that the net present value NPV is simply obtained from the sum of discounted investment costs CV and the discounted annual expenses. It is here defined with a positive sign to obtain positive annuity values:

$$NPV = CV + EX \cdot PVF(N, f, d) \tag{3-3}$$

Annual expenses include the maintenance costs and the operating energy and water costs. For maintenance costs, some standards like VDI 2067 use 2% of the investment costs. Some chiller manufacturers calculate maintenance contracts with 1% of the investment costs. For large thermal chillers, some companies offer constant cost maintenance and repair contracts: the costs vary between 0.5% for large machines (up to 700 kW) up to 3% for smaller power. Repair contracts are even more expensive with 2% for larger machines up to 12% for a 100 kW machine. In the calculations shown here, 2% maintenance costs are used. To obtain the annuity a as the annually occurring costs, the NPV is multiplied by a recovery factor r_f, which is calculated from a given discount rate d and the lifetime of the plant N. The cost per kWh of cold is the ratio of the annuity divided by the annual cooling energy produced:

$$a = NPV \cdot r_f(N, d) = NPV \cdot \frac{d(1+d)^N}{(1+d)^N - 1} \qquad (3\text{-}4)$$

The investment costs for the cooling machines were obtained from an own market study (see Fig. 3-21). The costs are from manufacturers based in Germany and from a survey of the International Energy Agency [8,9]. A regression through the data points was used to obtain the costs for the given power used in the calculations. With a discount rate of 4% and 1.9% inflation costs over a service life of 20 years, the annuity for the cooling machine alone was 1518 Euros per year. In addition to the chiller investment costs, the annuity of the solar thermal system was calculated from the surface area dependent collector investment costs, the volume dependent storage costs and a fixed percentage of 12% for system technology and 5% mounting costs. Cost information for the solar thermal collectors and storage volumes were obtained from a German database for small collector systems, from the German funding program Solarthermie 2000 for flat plate collector surface areas above 100 m and for vacuum tube collectors from different German distributors (see Fig. 3-22 and Fig. 3-23).

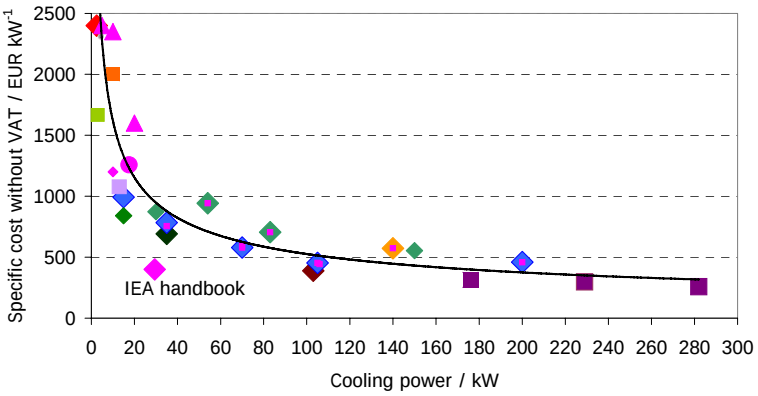

Fig. 3-21: Specific absorption chiller costs without VAT as a function of cooling power

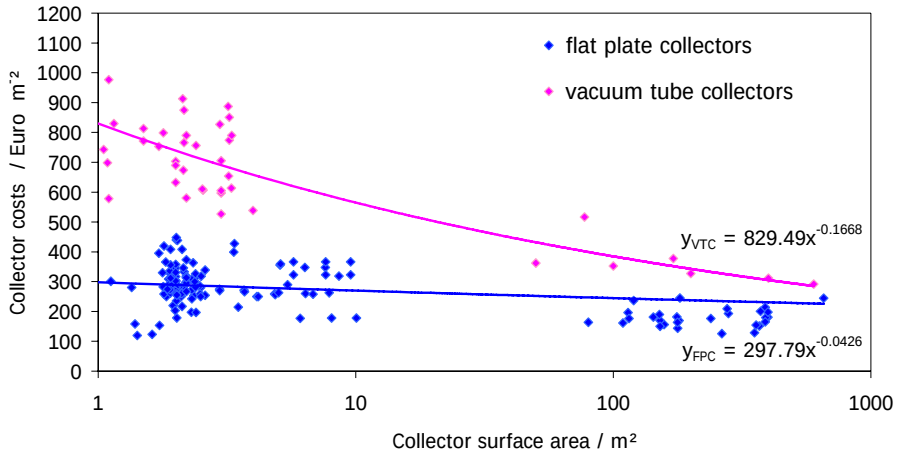

Fig. 3-22: Specific collector costs without VAT as a function of size of the installation.

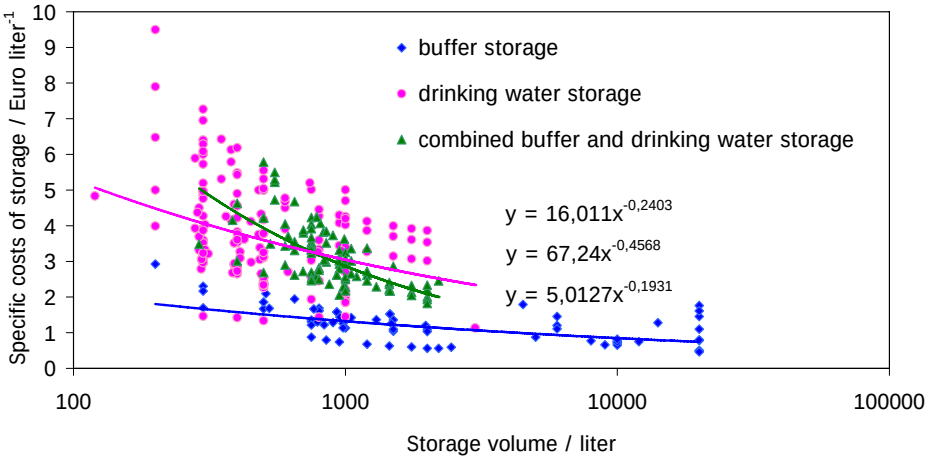

Fig. 3-23: Costs for different storage tank systems without VAT

Maintenance costs and the operating costs for electrical pumps were set to 2%. Major unknowns are the system integration and installation costs, which depend a lot on the building situation, the connection to the auxiliary heating or cooling system, the type of cooling distribution system and so on. Due to the small number of installations, it is difficult to obtain reliable information about installation and system integration costs. Therefore, two simulation runs were done with different cost assumptions for installation and integration. The first simulations were done with very low installation costs of 5% of total investment plus 12% for system integration. A second round of simulations is based on 25% installation and 20% system integration costs. The total costs per MWh of cold produced C_{total} are obtained by summing the chiller cost $C_{chiller}$ to the solar

costs C_{solar}, the auxiliary heating costs C_{aux} and the costs for the cooling water production $C_{cooling}$. The costs for heating have to be divided by the average COP of the system to refer the cost per MWh heat to the cold production and multiplied by the solar fraction s_f for the respective contributions of solar and auxiliary heating. For the cooling water, the costs per MWh of cooling water were taken from literature [6] and referred to the MWh of cold by multiplication with (1 + 1 / COP) for removing the evaporator heat (factor 1) and the generator heat with a factor 1 / COP:

$$C_{total} = C_{chiller} + \frac{s_f \cdot C_{solar}}{COP} + \frac{(1 - s_f) \cdot C_{aux}}{COP} + C_{cooling}\left(1 + \frac{1}{COP}\right) \qquad (3\text{-}5)$$

For heat rejection costs $C_{cooling}$ a value of 9 € MWh^{-1} was used and the auxiliary heating costs $C_{heating}$ were set to 50 € MWh^{-1} heat. The chosen system technology (dry or wet chiller, low or high temperature distribution system, control strategy) influences the costs only slightly (7% difference between the options), if the operating hours are low (such as in the office 1 example with low internal loads, see Fig. 22). If the operating hours increase, the advantage of improving the operation strategy (Case 2) or increasing the temperature levels of the cooling distribution system (Case 3) become more pronounced (16% difference between the different cases, see Fig. 23). For very low operating hours such as the office building in the Stuttgart climate with only 313 full load hours, the costs are between 640 and 700 € MWh^{-1}, 60% of which are due to the chiller investment costs only (see Fig. 24). The calculated solar thermal system costs were between 85 and 258 € MWh^{-1} for solar cooling applications, depending on the operating hours and the location. They go down as far as 76 € MWh^{-1} for the office in Madrid with high internal loads and a high temperature cooling distribution system. These costs are getting close to economic operation compared with fossil fuel heating supply.

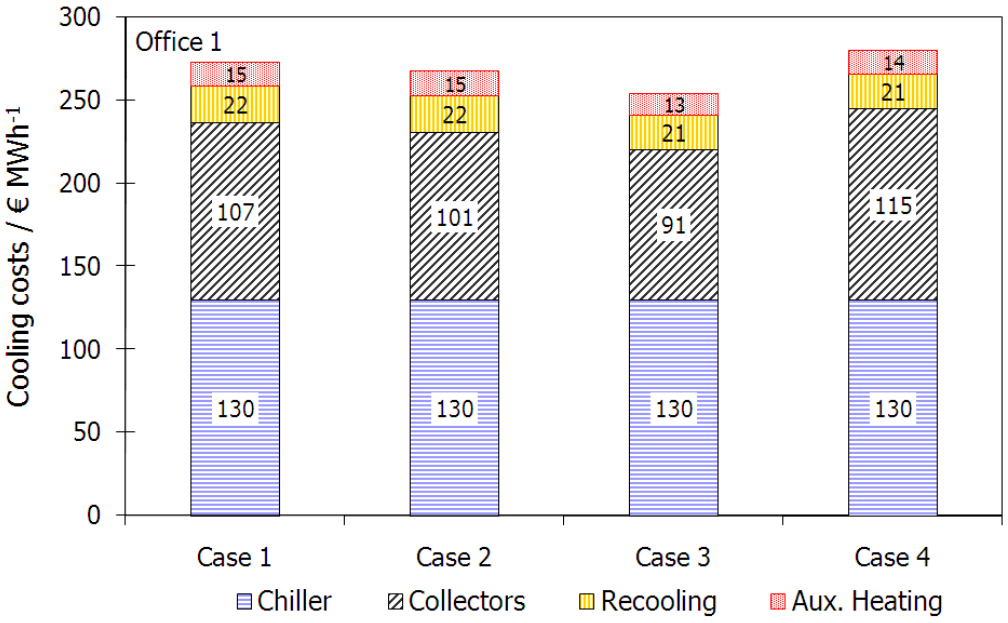

Fig. 3-24: Cooling costs per MWh of cold for different operation strategies and cold distribution systems for office 1 with **high external loads**

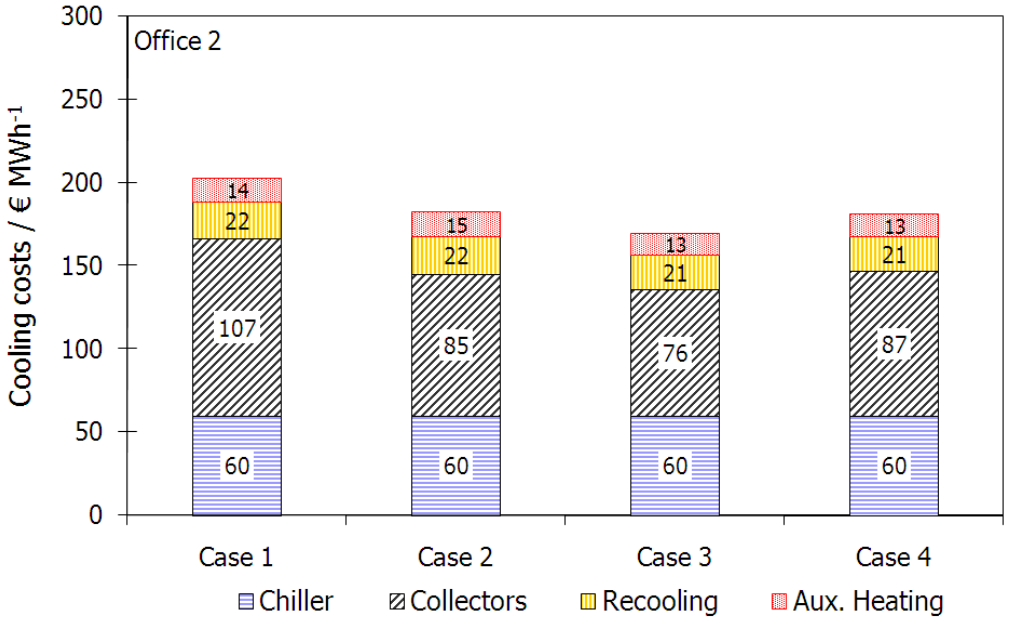

Fig. 3-25: Cooling costs per MWh cold for different operation strategies and cold distribution systems for office 2 with **high internal loads**

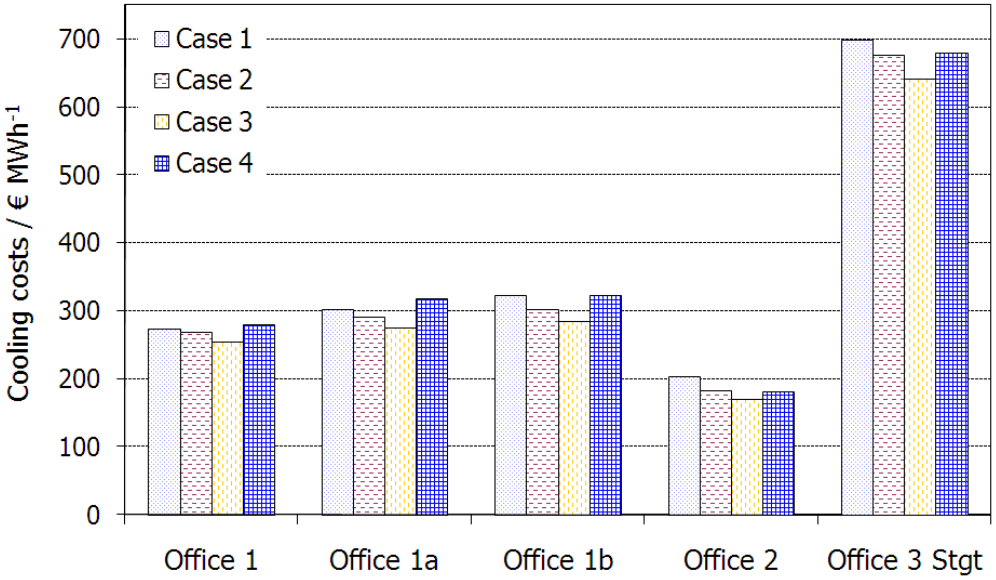

Fig. 3-26: Cooling costs per MWh of cold for different load situations of office buildings in Madrid and Stuttgart (office 1 to office 3) and for different operation strategies and cold distribution systems (case 1 to case 4)

The main dimensioning results for the buildings with a good operation strategy and a low temperature fan coil distribution system (Case 2) are summarized in Table 3-7 and Table 3-8.

Table 3-7: Summary of design values for the office with variable control strategy

Cooling load file (Case 2)	ACM power (kW)	Collector area (m²)	Storage volume (m³)	Solar yield (kWh m $^{-2}$)	Average COP
Office 1	15	31	2	644	0.67
Office 2	15	54	5	784	0.67
Office 3	15	25	2	324	0.64

Offices 1 and 2 are located in Madrid, office 3 in Stuttgart.

Table 3-8: Summary of energy performance data

Cooling load file (Case 2)	Cooling energy demand (MWh)	Collector aperture area per MWh cold (m^2 MWh^{-1})	Collector aperture area per kW cooling power (m^2 kW^{-1})	Storage volume per collector aperture area (m^3 m^{-2})	Solar thermal system efficiency (%)
Office 1	13.7	2.2	2.0	0.07	37
Office 2	28.8	1.8	3.6	0.09	45
Office 3	4.7	5.5	1.7	0.08	26

The total costs per MWh of cold produced by the thermal chillers are given in Table 3-9. If the system integration and installation costs are assumed to be 45% of total investment costs instead of 17%, the costs per MWh of cold are in the range of 300–390 € MWh^{-1} for the office in Madrid with low internal loads and 200 € MWh^{-1} for the best case of the office with longer operating hours (see Fig. 3-27).

Table 3-9: Costs for solar thermal cooling systems

Cooling load file (Case 2)	Solar investment (€)	Total investment (€)	Chiller cost, $C_{chiller}$ (€ MWh_{cold}^{-1})	Solar cost, C_{solar} (€ MWh_{heat}^{-1})	Total cost, C_{total} (€ MWh_{cold}^{-1})
Office 1	14 260	32 490	130	101	268
Office 2	22 400	40 630	60	85	183
Office 3	12 140	30 370	378	258	676

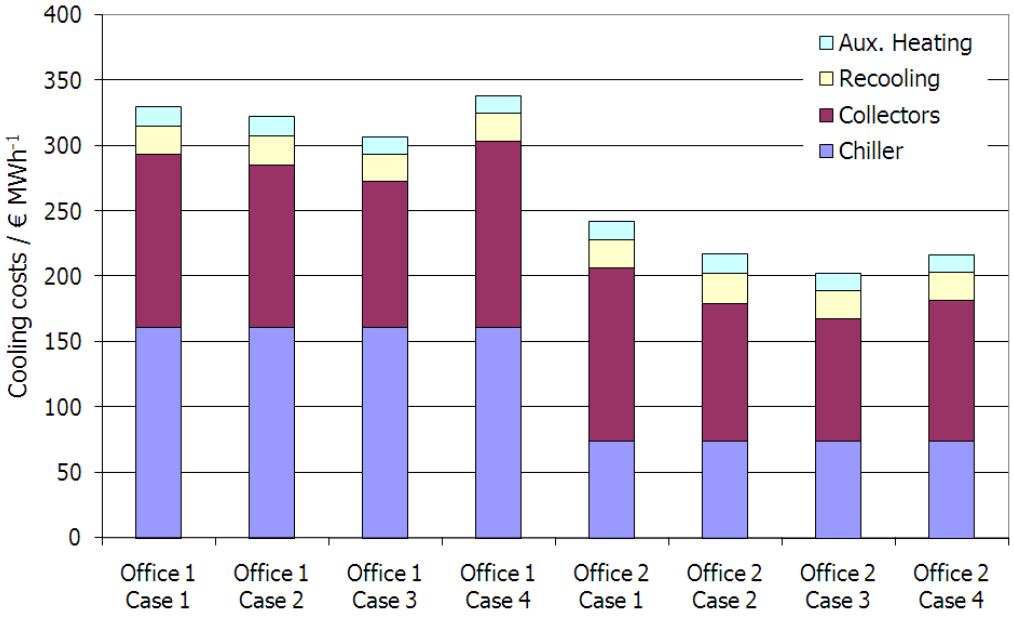

Fig. 3-27: Cost distribution for a solar thermal absorption chiller system with mounting and integration costs of 45% of total investment cost

By comparison, Schoelkopf calculated the cost of conventional cooling systems for an energy efficient office building in Germany with 180 € MWh^{-1} (Schoelkopf, et al., 2004). 17% of the costs were for the electricity consumption of the chiller.

The total annual cooling energy demand for the 1094 m^2 building was 1 kWh m^{-2} a^{-1}. Own comparative calculations for a 100 kW thermal cooling project showed that the compression chiller system costs without cold distribution in the building were between 110 and 140 € MWh^{-1}. Henning also investigated the costs of solar cooling systems compared to conventional technology (Henning, 2004). The additional costs for the solar cooling system per MWh of saved primary energy were between 44 € MWh^{-1} in Madrid and 77 € MWh^{-1} in Freiburg for large hotels. It is clear that solar cooling systems can only become economically viable, if both the solar thermal and the absorption chiller costs decrease. This can be partly achieved by increasing the operation hours of the solar thermal system and thus the solar thermal efficiency by using the collectors also for warm water production or heating support.

3.6 CONCLUSIONS

In chapter 3 the design, performance and economics of solar thermal absorption chiller systems were analysed. Absorption chillers were modelled under partial load conditions by solving the steady-state energy and mass balance equations for each time step. The calculated cooling power and coefficient of performance fit the experimental data better than a constant characteristic equation. The chiller model was integrated into a complete simulation model of a solar thermal plant with storage, chiller and auxiliary heating system. Different cooling load files with a dominance on either external or internal loads for different building orientations and locations were created to evaluate the influence of the special load time series for a given cooling power. The investigation showed that to achieve a given solar fraction of the total heat demand requires very different collector surfaces and storage volumes, depending on the characteristics of the building load file and the chosen system technology and operation strategy. To achieve a solar fraction of 80% at the location Madrid, the required collector surface area is above 3 m^2 kW^{-1}, if the generator is operated at constant high temperature of 90°C and the solar thermal system operates under low flow conditions. In this case, it is recommended to increase the collector field mass flow rate, so that temperature

levels cannot rise too much. Doubling of mass flow rate decreases the required collector surface area and thus solar thermal system costs by 30%. For buildings with the same maximum cooling load, but different load time series, the required surface area varies by a factor 2 to obtain the same solar fraction. The influence of building orientation with the same internal load structure is about 15%. More important are different internal loads, which can increase the required collector surface area by nearly a factor 2. The best solar thermal efficiency was 45% for high full load hours of nearly 2000 h. For the location Madrid, 80% solar fraction are possible for surface areas between 2 and 4 m^2 kW^{-1} cooling power, the high values occurring for larger full load hours. For each MWh of cooling energy demand, between 1.6 and 3.5 m^2 collector aperture area are required for the Spanish site and between 4.6 and 6.2 m^2 for the German installation. The total system costs for commercially available solar cooling systems are between 180 and 270 € MWh^{-1} cooling energy, again depending on the cooling load file and the chosen operation strategy. The total costs are dominated by the costs for the solar thermal system and the chiller itself. For a more moderate climate with low cooling energy demand, the costs can rise as high as 680 € MWh^{-1} cold. The work shows that dynamic system simulations are very useful to determine the correct solar thermal system size and to reach a given solar fraction of the total energy requirement.

4. Model Based Control Strategy Optimisation of Solar Driven Absorption Cooling Systems

4.1 INTRODUCTION

The performance of solar driven cooling systems strongly depends on the implemented control strategies of the absorption cooling system including the chiller, the cooling tower, the installed cold distribution system and the solar collector field (Kohlenbach, 2006; Sumath, 2003). High electricity consumptions caused by suboptimal control in combination with low solar fractions through insufficient system design are critical for the environmental and economical performance of installed absorption cooling systems (ACM), especially if they are compared to highly efficient electrical driven compression chillers (Henning, 2004). To evaluate the overall efficiency of real installed solar cooling systems within the IEA TASK 38 (International Energy Agency Solar Heating and Cooling Programme) several solar cooling systems are monitored in detail. The results clearly demonstrate, that the electrical COP are still low with values of up to 6 in the best case and values of below 3 in the worst case. For the primary energy ratio values obtained are 1.7 in the best case and values clearly below 1.0 in the worst case (Sparber, et al., 2009; Núnez, et al., 2009). Good systems with compression chillers in the same power range with dry heat rejection typically reach average electrical system COP of 3.0 and primary energy ratios which are slightly above 1.0 (Yu, et al., 2004). The main reasons for the low system efficiencies of solar cooling systems found by Sparber, et al. (2009) and Núnez, et al. (2009) are low solar fractions caused by insufficient system design and high electricity consumptions resulting from a suboptimal control of the cooling tower fan speed and oversized system pumps. This demonstrates, that apart from a good system design improved control strategies are required, to ensure high overall system efficiencies of solar driven absorption chillers. However, for the control of the complex solar cooling systems, up to now the implementation of independently operating component controllers is still standard. Such local controllers do not allow the implementation of improved

control strategies with interactions between the system components. In consequence this often leads to suboptimal control of the systems in terms of energy efficiency. Examples for possible improved control strategies are:

- Decrease fan speed of cooling tower for cooling power reduction at part load conditions only if no additional heating is used (→Electricity savings and reduction of on/off cycles of the absorption chiller)
- Start the absorption chiller if the solar system is about to go into stagnation and operate the chiller until the evaporator outlet temperature drops below the lower temperature limit (→ Avoid stagnation of collector field → sufficient heat supply in the afternoon and reduction of additional heating)
- Decrease the heat rejection temperature setpoint instead of additional heating if the chiller operates at pure solar operation, the solar system still provides heating energy and further cooling power required (→ Avoid additional heating and increase of solar fraction)

To allow the implementation of such advanced control strategies, the development of combined system controllers are required, which are able to control all components of a solar cooling and heating system. The present work aims to support the development process of such combined controllers by a detailed analysis of the effect of different control options and system configurations on the overall system performance and energy efficiency of solar driven absorption cooling systems.

4.2 SCOPE AND METHODOLOGY OF WORK

For an energy efficient operation of solar cooling systems, the SolarNext AG started the development of an integrated system controller which is able to control all components of solar driven absorption or adsorption cooling systems. For the development of improved control strategies detailed analyses on the effect of different control options on the primary energy efficiency are performed in this chapter on the example of a 15 kW chilii® solar driven absorption cooling system installed at the office building of the SolarNext AG in Rimsting,

Germany. Detailed dynamic simulation models of the whole solar cooling system are developed and validated against measured performance data within this work. The measured performance data of the installed system was provided by the SolarNext AG who planned and installed the whole system including the monitoring devices. The developed system models not only describe the thermodynamic processes but also include the electricity consumption of the ACM, all pumps and of the heat rejection system. These models are used to analyse the effect of different control options of the solar cooling system on the overall system performance and the primary energy efficiency reached. For early system startup and stable system operation of purely solar driven absorption cooling systems the effect of different storage charge and discharge strategies with and without storage bypass are developed and analysed in the simulation environment for different typical summer weather conditions. Clear recommendations for an improved control of solar driven absorption cooling systems are derived from all results obtained.

4.3 DESCRIPTION OF THE ANALYSED SOLAR COOLING SYSTEM

4.3.1 GENERAL SYSTEM DESCRIPTION

The analysed chillii® solar driven absorption cooling system has been set up and installed as a test facility by the SolarNext AG to cool and to heat their office building in Rimsting, Germany. Rimsting is located in the south part of Germany at a latitude of 47.88 degrees north and a longitude of 12.33 East and an altitude of 564 m above sea level. The system includes a market available 15 kW chillii® ESC15 (EAW WGRACAL SE 15 LiBr absorption chiller, see chapter 3.4.1), two 1 m³ hot water storage tanks, one 1 m³ cold storage tank, 37 m² CS-100F flat plate collectors and 34 m² TH SLU1500/16 solar vacuum tube collectors all facing south with an inclination of 30°, a 35 kW EWK wet cooling tower and an additional dry heat rejection system. For the distribution of the cooling energy chilled ceilings and fan coils are used with 16°C supply and

18°C return temperature and an automated supply temperature increase for dew point protection.

The cooling load of the single story office building with 566 m² of conditioned space has been analysed by the SolarNext AG for different internal load options during the design phase using dynamic building simulations with TRNSYS. The resulting cooling load of the most realistic option with a total annual cooling energy demand of 8.9 MWh per annum (16 kWh per square meter conditioned space and annum) and a maximum cooling load of 18 kW is shown in Fig. 4-1. In addition Fig. 4-2 shows the dependency between the ambient temperature and the simulated hourly cooling and heating load.

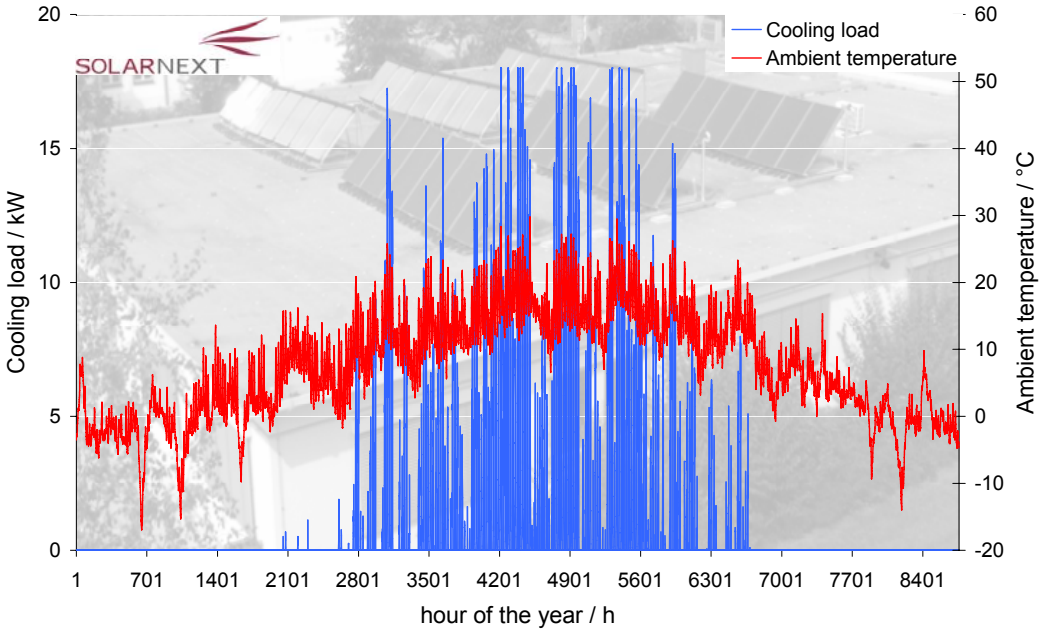

Fig. 4-1: Annual cooling load and ambient temperature distribution, SolarNext office building in Rimsting, Germany (Source: SolarNext)

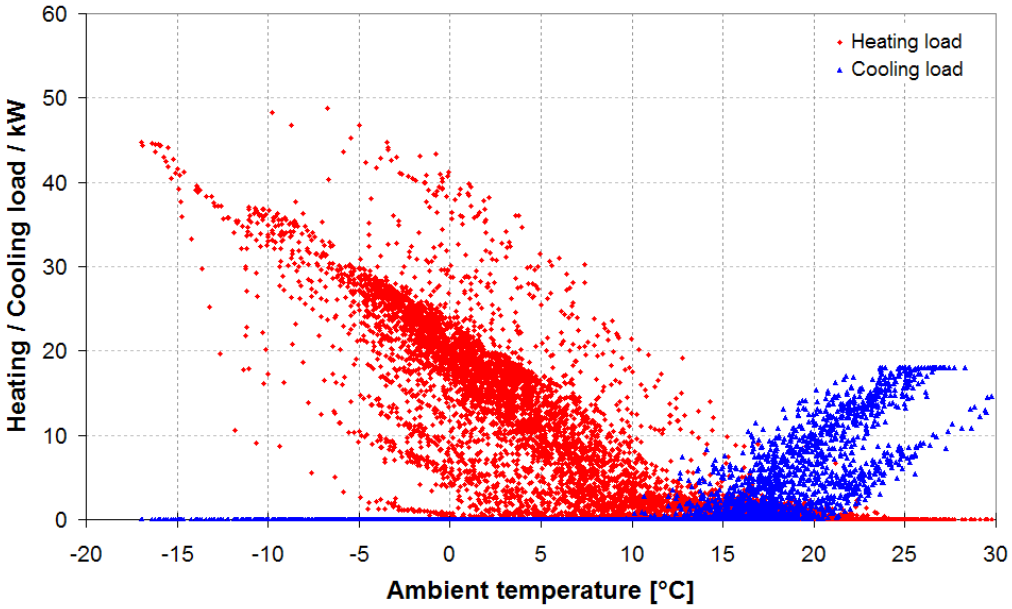

Fig. 4-2: Ambient temperature dependent cooling and heating load distribution, SolarNext office building in Rimsting, Germany (Source: SolarNext)

The installed absorption chiller is able to provide the required cooling power of 18 kW if the set point of the heat rejection temperature is reduced by 3 K from 30°C at design conditions to 27°C. To avoid stagnation in the collector circuit during periods of chiller shut down, a water to air cooler (KAMPMANN air heater TOP 474136) has been implemented in the system, which rejects the solar heat to the environment if the temperature in the collector return increases above 100 °C. After activation the solar circuit cooler remains in operation until the temperature in the collector return decreases below 90°C.

Table 4-1 shows the installed pumps and their electricity consumption which are used to calculate the electrical COP and the primary energy consumption of the system.

Table 4-1: Implemented pumps, pressure drop and electrical power demand

Description of pump	Type of pump	Nominal volume flow [m³/h]	Pressure drop [mbar]	Electrical power demand [W]
Absorber / Condenser pump	Wilo-IP-E 40/115-0,55/2 3~ PN10 Wilo-VeroLine-IP-E	5.0	1200	550
Generator pump	High efficiency pump Wilo-Stratos ECO 25/1-5 PN10	2.0	250	56
Evaporator pump	High efficiency pump Wilo-Stratos 25/1-6 PN 10	1.9	350	52
Primary solar pump	WILO Stratos 30/1-12 PN 10	1.39	900	120
Secondary solar pump	WILO TOP-S 30/7	1.39	450	100

More detailed information about the installed main system components are given in Appendix B.

4.3.2 SYSTEM DIAGRAM WITH COMPONENTS OF THE SYSTEM CONTROL

Fig. 4-3 shows some pictures and a schematic diagram with the main control parameters of the chillii® solar cooling system installed at the office building of the SolarNext AG in Rimsting, Germany. A detailed list of all sensors and actuators implemented in the chillii® solar cooling system of the SolarNext AG is shown in Appendix B.

Source of pictures: SolarNext AG in Rimsting, Germany

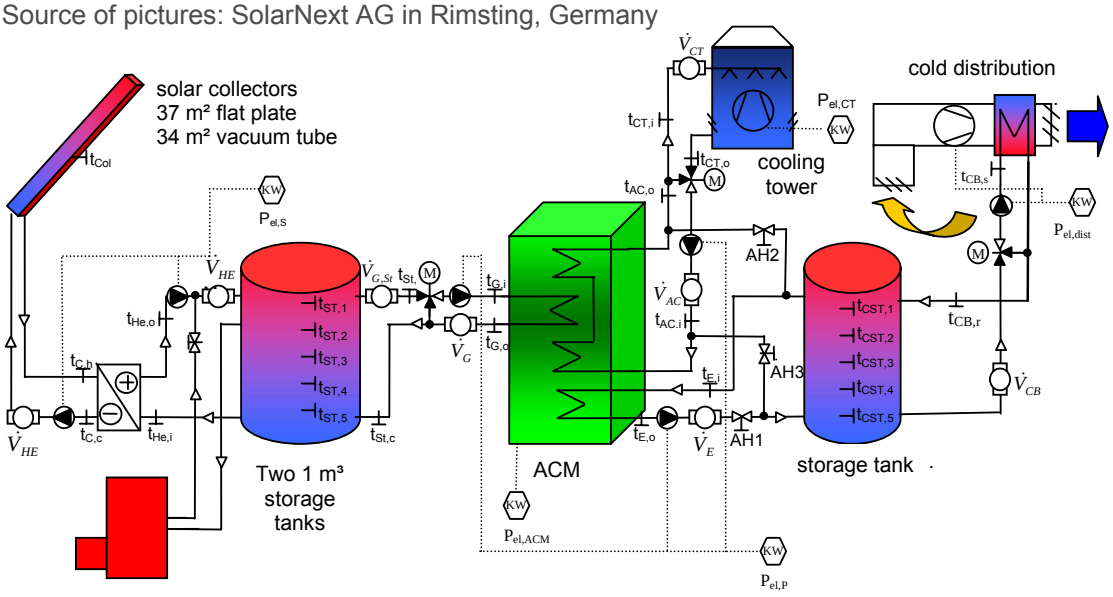

Fig. 4-3: Schematic diagram of the chillii® solar cooling system

4.3.3 GENERAL DISCUSSION OF POSSIBLE CONTROL OPTIONS

Solar driven or solar assisted absorption cooling systems include a number of components, which need to be controlled efficiently in order to cover the cooling load and to meet the expectations of the overall system performance and efficiency. On the other hand the implementation of control features increases the system complexity and costs and therefore has a significant influence on the economic efficiency of the system. Considering these facts, the control devices should be selected in order to meet the highest possible system efficiency with the lowest possible control effort. However, there are often different control options to meet the same control task, but with different effect on the overall system performance.

a) Solar Thermal System Control

The solar system is controlled via the mass flow caused by the operation of the solar pumps. In the simplest case an On/Off control is used depending on the collector outlet temperatures. In this case at low solar irradiation the collectors are used as a kind of additional storage. The collector pump is switched ON as soon as the collector temperature is e.g. 10 K above the lowest temperature in the hot storage temperature and switched off again as soon as the collector outlet temperature is lower than e.g. 5 K above the collector inlet temperature. More sophisticated solar controllers use a mass flow control for a constant collector outlet temperature or a constant temperature difference between collector inlet and outlet. However for systems with hot water storage the main difference between the simple On- / Off control and the mass flow control result from the collector losses, which are slightly higher for the simple On/Off control. For solar cooling applications during the summer months the difference between the solar system efficiency is in the range of only one to two percent (Kohlenbach, 2006). A significant advantage of an On/Off control of the solar pump is the high mass flow rate which ensures a uniform flow rate in large collector fields. For systems with large collector fields as usual for solar cooling applications, a mass flow control of the solar pump can lead to large

temperature differences in the collector field at the lower mass flow limit. The main reason for this is that the pressure drop in the collector field is often not as uniform as expected. In extreme cases, this leads to partial evaporation of the collector fluid.

b) Absorption Chiller Control

In standard solar driven absorption cooling systems the absorption chiller is often operated at constant generator inlet temperature. In this case the required cold water outlet temperature is controlled by a control of the evaporator mass flow rate. In solar cooling systems with more advanced control strategy the cold water outlet temperature of the ACM is controlled by the generator inlet temperature which is varied in a range of 70 to 95°C and adjusted by a three way valve control. This reduces the temperature level in the hot storage tank at part load conditions and therefore improves the efficiency of the solar system. Furthermore, the number of on/off cycles of the chiller are reduced which significantly improves the thermal COP and thereby the overall system efficiency. A further possibility to control cold water outlet temperature of the absorption chiller is the control of the cooling water supply temperature (Kühn, et al., 2008 and Albers, et al., 2009). This control is able to assure a stable cold water temperature at variable generator inlet temperatures through an increase or decrease of the thermal COP of the chiller. It has the potential to significantly improve the electrical COP of the system if a fan speed control of the cooling tower used. However, due to the reduced thermal COP the increase of cooling water temperature only increases the overall system efficiency, if no backup system is used for heat supply. A control of the cooling water temperature through a simple three way valve and fixed fan speed of the cooling tower decreases the system efficiency in any case and should therefore not be used.

For systems with cold distribution at high cold water temperature like chilled ceilings (e.g. 16°C supply temperature), the cold storage offers a higher storage capacity, if the produced cold water temperature is allowed to drop significantly below the cold water supply temperature setpoint (e.g. 6°C) at part load

conditions. In this case a control for the cold water outlet temperature is not really required. If flexible generator inlet temperatures according to the temperature level in the hot storage tank are allowed, the backup system should only be set in operation, if the cold water temperature in the cold storage tank increases the required cold water supply temperature.

For high system efficiency the backup heating system should always provide hot water on a high temperature level (e.g. ≥ 80°C) if set in operation.

4.3.4 CONTROLLABLE PARAMETERS OF THE CHILLII® SOLAR COOLING SYSTEM

The installed solar cooling system was designed by the SolarNext AG as a test plant. Therefore, different control options have been implemented to analyse the effect of different control strategies on the overall system performance. The controllable parameters are listed in Table 4-2 for the different components. As mentioned above, for standard installations the control effort should be kept as low as possible according to the requirements of the system configuration.

Table 4-2: Controllable parameters of the chillii® solar cooling system

System part	Control task	Required control equipment
1. Generator	I. Variable supply temperature according to temperature in hot storage tank	a) Relay for On/Off control of generator pump
	II. Supply temperature control	a) Relay for On/Off pump control b) 3-way mixing valve with electrical motor c) PID-controller (0…10 VDC)
2. Absorber / Condenser	I. Simple cooling water temperature control	a) Two relay for On/Off control of pump and cooling tower ventilator b) 3-way mixing valve with electrical motor c) PID-controller (0…10 VDC)

System part	Control task	Required control equipment
	I. Advanced control of cooling tower	a) Two Relay for On/Off control of pump and cooling tower ventilator b) Ventilator with variable speed c) PI-controller (0…10 VDC) for ventilator d) 3-way mixing valve with electrical motor e) PID-controller (0…10 VDC)
3. Evaporator	I. Cold water temperature flexible (fixed mass flow) (only possible for high temperature cold distribution)	a) Relay for On/Off pump control
€	II. Cold water control (alternative to (1.II.))	a) Pump with variable mass flow b) Relay for On/Off control c) PID-controller (0…10 VDC)
4. Cold water distribution	I. Mass flow control (control of return temperature) (Supply temperature is controlled by generator inlet temperature and / or absorber inlet temperature).	a) Pump with variable mass flow through frequency inverter b) Relay for On/Off control c) PID-controller (0…10 VDC)
5. Free cooling mode	I. Valve control AH1, AH2 and AH3	a) Relay for On/Off control
6. Solar system	I. On-/Off-control (Temperature difference storage/collector)	a) Relay for On/Off pump control
	II. Advanced mass flow control	a) Pump with variable mass flow for e.g. $\Delta T = 10$ K b) Relay for On/Off control

4.4 ANALYSIS OF THE OVERALL SYSTEM EFFICIENCY FOR DIFFERENT CONTROL STRATEGIES

4.4.1 INTRODUCTION

Up to now nearly all installed small and medium size solar cooling systems are operated with separate controllers for the solar circuit, for the absorption chiller and the heat rejection system. In some cases also the additional heater or additional cooling devices have their own controllers. The consequence is that these components operate independently, although they are influencing each other significantly. This typically results in a less efficient operation of the solar cooling system. The heat rejection temperature for example has a very strong effect on the cooling power and electricity consumption of the chiller. Especially at part load conditions it could be preferable to increase the heat rejection temperature to limit the cooling power of the absorption chiller in order to reduce the electricity consumption and the on/off cycles of the absorption chiller (Albers, et al., 2009). Since an increase in heat rejection temperature also decreases the thermal COP, this control only increases the primary energy efficiency of the system if the heating energy demand is covered by the solar collector system and no backup heating is used. If independent controllers are used, the single controllers have no information about the performance of the other systems and of the actual cooling load of the building. Therefore, common problems observed for systems with independent component controllers are very low electrical COP and low solar fractions of the overall heating energy demand of the absorption chillers. Both results in low primary energy ratios (PER) which are in some cases even lower than for good standard systems with electrically driven compression chillers (Sparber, et al., 2009). This clearly emphasises the necessity to develop integrated system controllers, which are able to exchange information about the status and performance of the single system components and therefore are able to control the solar cooling system more efficiently. The SolarNext AG was the first company who started the development of such an integrated system controller for their solar cooling kits. For the development of new integrated control strategies detailed simulation based analyses on the effect of different control options on the overall

performance and primary energy efficiency of solar driven absorption cooling systems are carried out within this part of the work. The chillii® solar cooling system of the SolarNext AG described in chapter 4.3 is used as reference system for this analysis.

4.4.2 DYNAMIC SIMULATION MODEL AND VALIDATION

For the development and analysis of new innovative control strategies, a detailed dynamic simulation model of the installed system which also considers the electricity consumption of all installed components (fans, pumps, etc.) has been developed in the simulation environment INSEL (Schumacher, 1991). The component models used are described in chapter 2.2, with dynamic models for the solar collectors and the hot and cold storage tank. Since annual simulations are performed no inertia is considered for the absorption chiller, the piping, the wet cooling tower and the dry recooler in this case. For the installed 15 kW chillii® ESC15, which is identical to the EAW WEGRACAL SE 15 LiBr absorption chiller, the same model with the same parameters as described and validated in chapter 3.4.1 are used. The dynamic model of the whole chillii® solar cooling system is shown in Fig. 4-4.

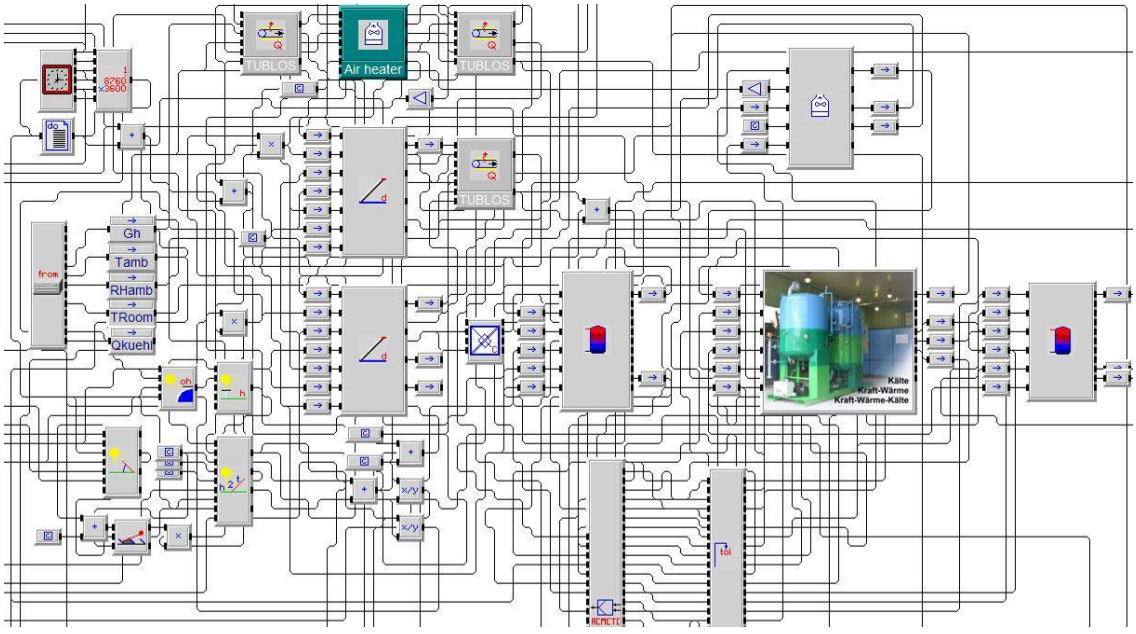

Fig. 4-4: Developed simulation model of the chillii® solar cooling system in INSEL

Measurement data of the solar driven absorption chiller obtained from the preliminary testing phase in summer 2007 was used to validate the developed simulation model of the installed system. As an example Fig. 4-5 shows the measured performance of the solar cooling system together with the simulation results for one day in August 2007. A comparison of the simulated and measured outlet temperatures of the generator, condenser and evaporator of the ACM and of the collector field clearly visualise that the performance of the installed system is well described by the developed simulation model. The deviation between the predicted and measured solar heating power of the collector circuit (dynamic model) is below 1% for the analysed day. For the absorption chiller larger differences only occur at system startup and system shutdown, which is attributable to the omitted inertia of the absorption chiller in the model. If the region of inertia influence is omitted, the deviation between simulated and measured generator and evaporator power is below 4% and below 3% for the heat rejection power. If the region of inertia influence is considered the deviation between measured and predicted performance increases to 16% for the generator, 12% for the evaporator and 10% for the heat rejection circuit of the absorber and condenser. These quite large deviations can be partly attributed to the large fluctuations of the generator inlet temperature for the combined operation mode with auxiliary heating. These fluctuations result from a bad hydraulic integration of the auxiliary heater (very long distance between chiller and boiler) and a poorly controlled three way mixing valve in the original system setup (optimised during the heating period 2008 / 2009). If only the purely solar driven part is considered, the deviations between measurement and simulation are reduced to 12% for the generator, 10% for the evaporator and 6% for the heat rejection circuit of the absorber and condenser. As an attribute to feasible durations of simulation runs, the error resulting from the omitted inertia is considered to be acceptable for the analysis of different control options on an annual basis. For the more elaborated analysis of storage charge and discharge strategies in chapter 4.5 an advanced chiller model which includes the inertia of all components is used.

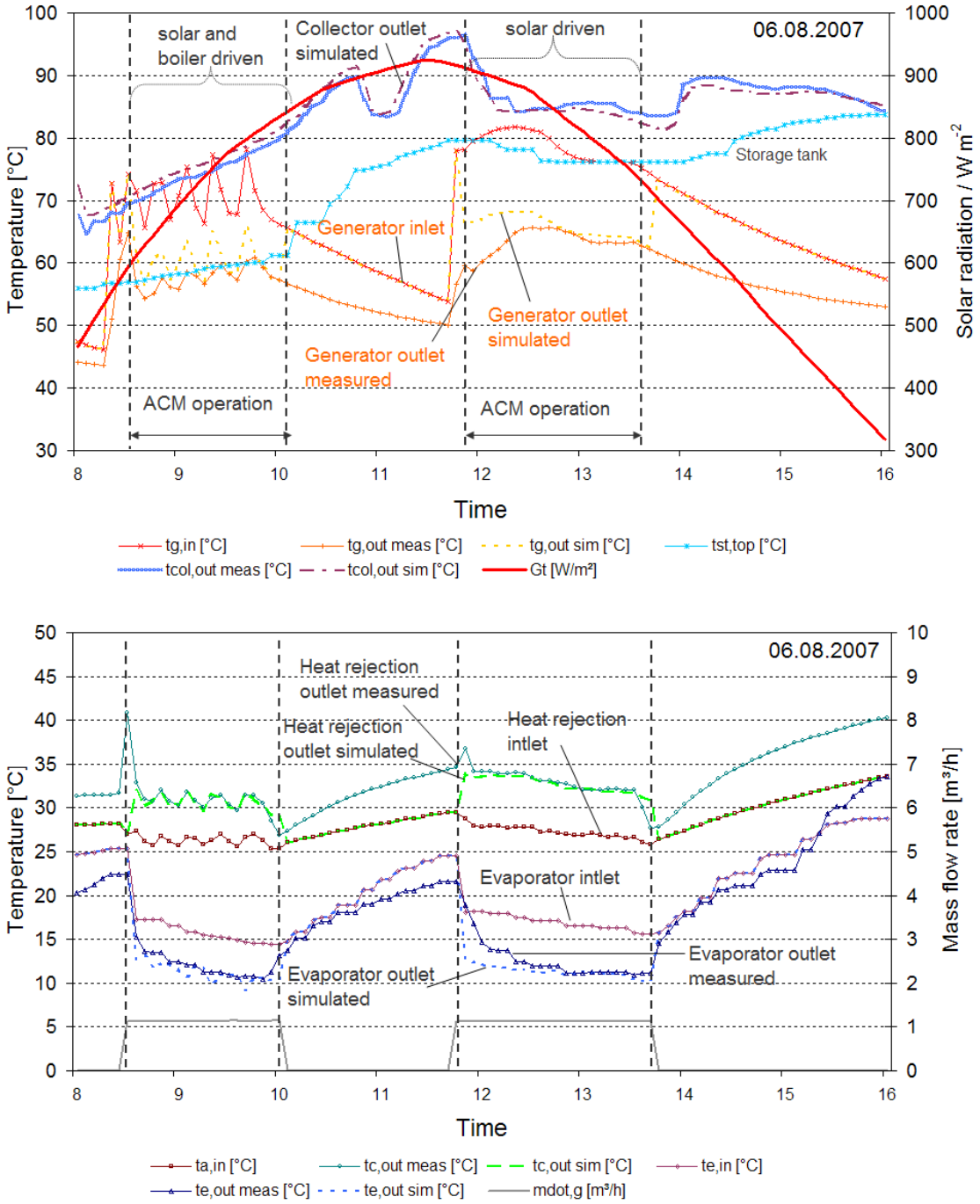

Fig. 4-5: Measured and simulated performance of the solar cooling system

4.4.3 Analysed Control Strategies

The simulation model described in the previous chapter is used to analyse the effect of different control strategies for the installed ACM, the solar thermal system and the cold distribution on the overall performance of the chillii® solar cooling system. The pumps of the solar collectors are considered as On/Off controlled in all cases. The collector pump is set in operation as soon as the collector temperature is 10 K above the temperature at hot storage bottom and is switched off again if the collector outlet temperature is 5 K above the temperature at hot storage bottom or if the temperature in the upper part of the hot storage increases above 95°C. The minimum operation time of the collector pump is set to two minutes. According to the system design the cold supply temperature was set to 16°C. For simple control, the cases with variable generator inlet temperature are without temperature control at generator inlet and constant evaporator mass flow rate. The ACM is turned off if the generator inlet temperature drops below 65°C or the evaporator outlet temperature decreases below 6°C. The analysed cases with different control options for either constant or variable generator supply temperature, with and without fan speed control of the cooling tower etc. are described in Table 4-3.

The idea behind the described cases is to show how different control options influence the primary energy efficiency of the system. It starts in case 1 with the expected worst case of control which is then successively improved from case 2 to case 3.2 by different control measures (e.g. fan speed control of the cooling tower, mass flow control of the cold distribution pump, flexible generator inlet temperature and lower temperature setpoints for the cooling tower). Case 4 and case 5 analyse the effect of a dry heat rejection system instead of a wet cooling tower with and without fan speed control at flexible generator inlet temperatures.

An additional Case 6 has been defined and analysed as reference system for a compression chiller with a quite high electrical COP of 4.0 at 27 °C heat rejection temperature and high cold water supply temperatures. In the electrical COP only the electricity consumption of the chiller is considered. The electricity consumption for heat rejection and cold distribution is considered separately. The compression chiller is combined with a dry recooler with constant fan speed.

Table 4-3: Analysed control options of the absorption cooling system

Analysed cases	Control options										
	Cooling tower			$t_{a,in}$			$t_{g,in}$			Cold dist. pump	
	Typ	3-way-valve	fan speed	27°C	24°C	21°C	90°C	70-90°C variable	70-95°C variable	ΔT-control	
										yes	no
Case 1	wet	X		X			X				X
Case 2	wet		X	X			X			X	
Case 3	wet		X	X				X		X	
Case 3.1	wet		X		X			X		X	
Case 3.2	wet		X			X		X		X	
Case 4	Dry	X		X					X	X	
Case 5	dry		X	X					X	X	

$t_{a,in}$ Absorber inlet temperature, either controlled by a 3-way-valve or by fan speed control of the cooling tower. Values below 27°C (30°C for dry cooling tower) are only provided as long as reachable at the given ambient conditions.

$t_{g,in}$ Generator inlet temperature, either constant or variable according to the temperature in the hot and cold storage tank.

Annual simulations were carried out to analyse the effect of the described control options on the overall system performance of the installed solar cooling system. For the meteorological conditions Meteonorm weather data of the location Rimsting in Germany was used with an hourly time step. The cooling load of the building was assumed to be equal to the cooling load calculated by TRNSYS simulations as shown and described in chapter 4.2.1. For a correct consideration of the inertia in the solar thermal system and the storage capacity

of the hot and cold water storage tanks, the internal simulation time step used was 1 min. A linear interpolation was used for the hourly values of the meteorological conditions and the cooling load of the building.

4.4.4 SIMULATION RESULTS AND DISCUSSION

The main results are summarised in the graphs shown in Fig. 4-6 to Fig. 4-8. To compare the efficiency of the system with varied control strategies three different COP are used: 1. The standard thermal COP_{th}; 2. The electrical COP_{el} which considers the electricity consumption of the ACM, the cooling tower and all pumps including the cold distribution pump; 3. The total primary energy ratio (PER) which is defined as the provided cooling energy divided by the sum of consumed electricity and additional thermal energy multiplied by the PEF factors of 2.7 for electricity in Germany (GEMIS) and 1.1 for the gas boiler:

$$PER = \frac{Q_{cool}}{Q_{el} \cdot PEF_{el} + Q_{h,add} \cdot PEF_{gas}} \qquad (4\text{-}1)$$

As visible from Fig. 4-6, the electrical performance of the system strongly depends on the fact whether the cold water distribution pump of the building and the ventilator of the cooling tower are controlled according to the load or not. The electrical COPs vary between 6 and 11.5 for the cases with wet cooling tower and between 4 and 8 for the cases with dry recooler. The compression chiller system reaches an electrical COP of 3.2.

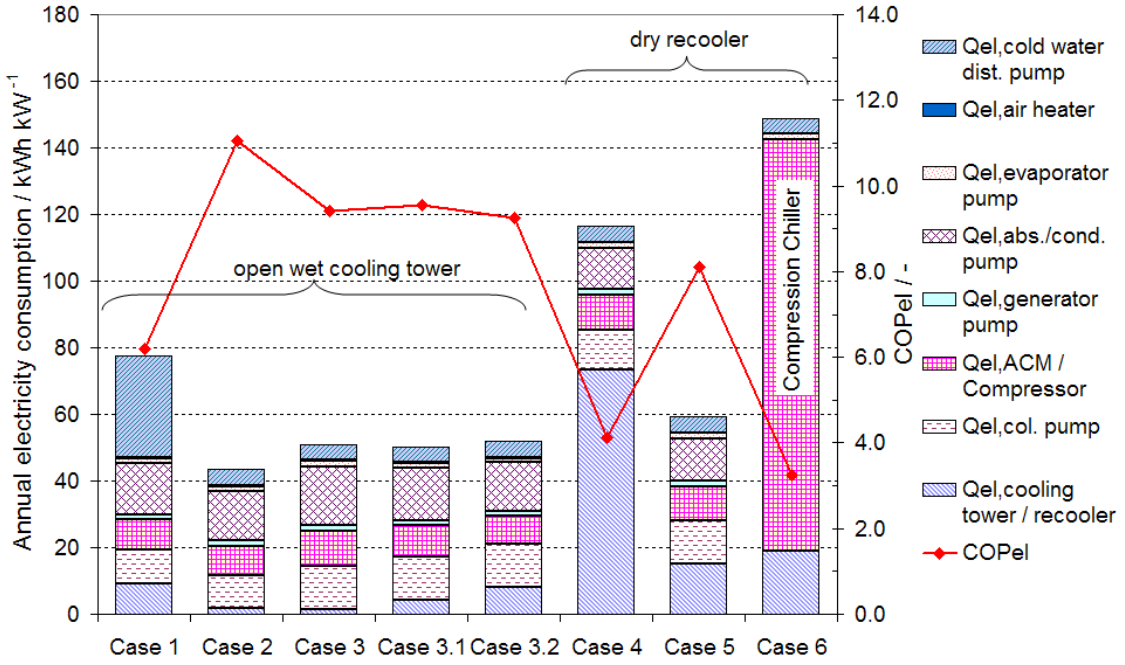

Fig. 4-6: Annual electricity consumption and electrical COP

The lowest electricity consumption of 42 kWh per kW of installed cooling power and therefore the highest electrical COP of slightly above 11 is obtained for Case 2 with a controlled cold water distribution pump and cooling tower fan but with the absorption chiller operated at constant generator inlet temperature. If the generator inlet temperature is allowed to vary between 70°C and 90°C according to the temperature in the hot and cold storage tank (Case 3) the thermal COP decreases only slightly from 0.75 in case 2 to 0.74 (Fig. 4-7). The lower generator temperatures lead to longer operating hours of the solar system and of the chiller to provide the same cooling energy and therefore increases the electricity consumption. However, at the same time the solar fraction is significantly increased from around 70% in case 1 and 2 to 83% in case 3.

A further increase of the solar fraction up to 88% can be achieved, if the heat rejection temperature set point is decreased from 27°C to 24°C in case 3.1 and 21°C in case 3.2. The reduced heat rejection temperature set points lead to an increase in the electricity demand of the cooling tower due to higher fan speeds but at the same time reduce the operating hours of the whole cooling system

due to the increased thermal COP and cooling capacity, which equalises the additional electricity demand.

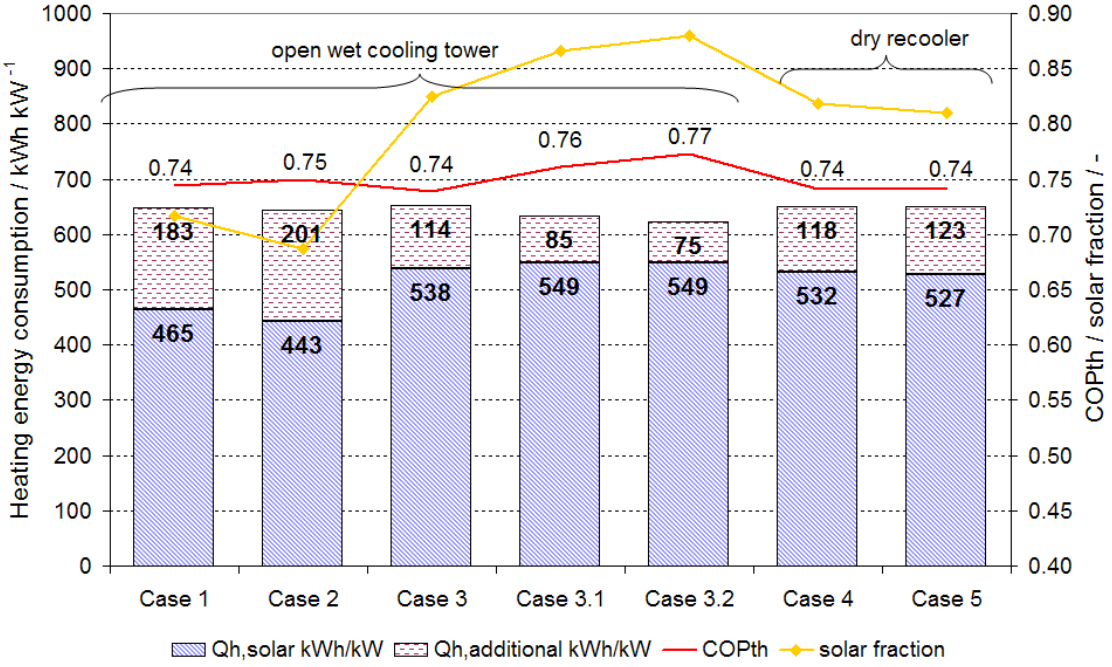

Fig. 4-7: Heating energy consumption and solar fraction

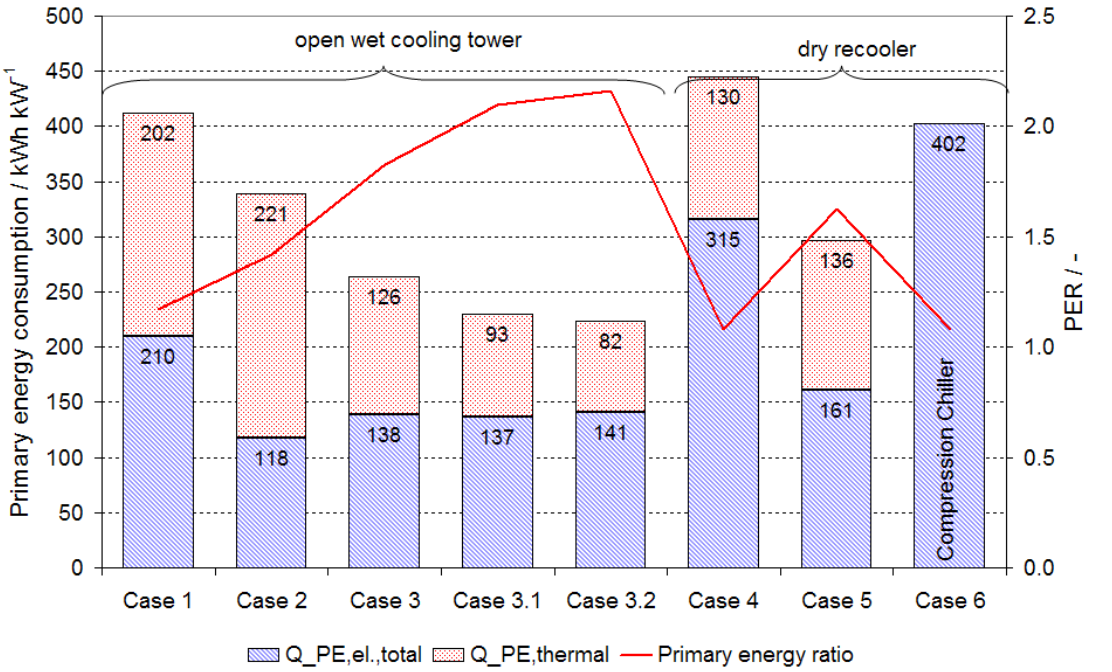

Fig. 4-8: Primary energy consumption and primary energy ratio

The values of the primary energy ratio (Fig. 4-8), which consider the electricity and additional heating energy consumption, vary between 1.1 and 2.2, with the lowest value for case 4 with dry recooler and without fan speed control and the highest value for case 3.2 with the lowest set point for the heat rejection temperature including fan speed control and a variable generator inlet temperature. The reference system with the compression chiller reaches a primary energy ratio of 1.1 which is nearly half of the value of the best absorption chiller case (Case 3.2) but equal to the worst absorption chiller case with dry recooler with constant fan speed (Case 4). This clearly indicates the importance of an energy efficient control and design of solar cooling systems and the requirement of further optimised hydraulic systems with reduced pressure drops and the utilisation of highly energy efficient pumps.

4.4.5 FURTHER OPTIMISATION POTENTIALS

If the electricity consumption of e.g. case 3 with optimised control is regarded (Fig. 4-9) it becomes obvious, that the remaining main electricity consumers are the absorber and condenser pump 37%, the collector pumps 28%, and the absorption machine itself 23% (mainly solution pumps). In order to further improve the overall efficiency of the solar cooling system the electricity consumption of these three components needs to be reduced significantly. For the cooling circuit of the absorber and condenser attempts need to be made to further reduce the pressure drop of the heat exchangers and of the spray nozzles (alternative distribution system) of the open wet cooling tower. A reduction in electricity consumption of at least 30% could be reached by these measures.

For the solar system the electricity consumption could be significantly reduced by up to 50% and more, if the solar system would be operated with pure water. The electricity savings result from the fact, that for pure water systems no solar exchanger and no secondary solar pump are required. Such a system is e.g. provided by Paradigma in Germany. In this case the pressure drop and heat losses of the heat exchanger and the secondary collector pump could be

avoided completely. However, in regions with danger of frost a special frost protection control and additional temperature sensors need to be implemented in the system. If danger of freezing is detected by the control system from the temperature sensors, the control system switches the collector pump ON for a short time in order to pump warm water from hot storage bottom into the collector field. According to recent analyses on a large solar cooling installation at the FESTO AG in Esslingen (Pietruschka, et al., 2009) the heating energy losses caused by frost protection of the annual solar energy production of the collector field are only about 3% in the best case and can increase up to 8% if wrongly dimensioned hydraulic valves (gravity brakes) are implemented and the hot storage is not charged efficiently. However, these additional losses are partly equalised by the higher efficiency of the pure water system, which does not require a heat exchanger between collector circuit and hot water storage tank.

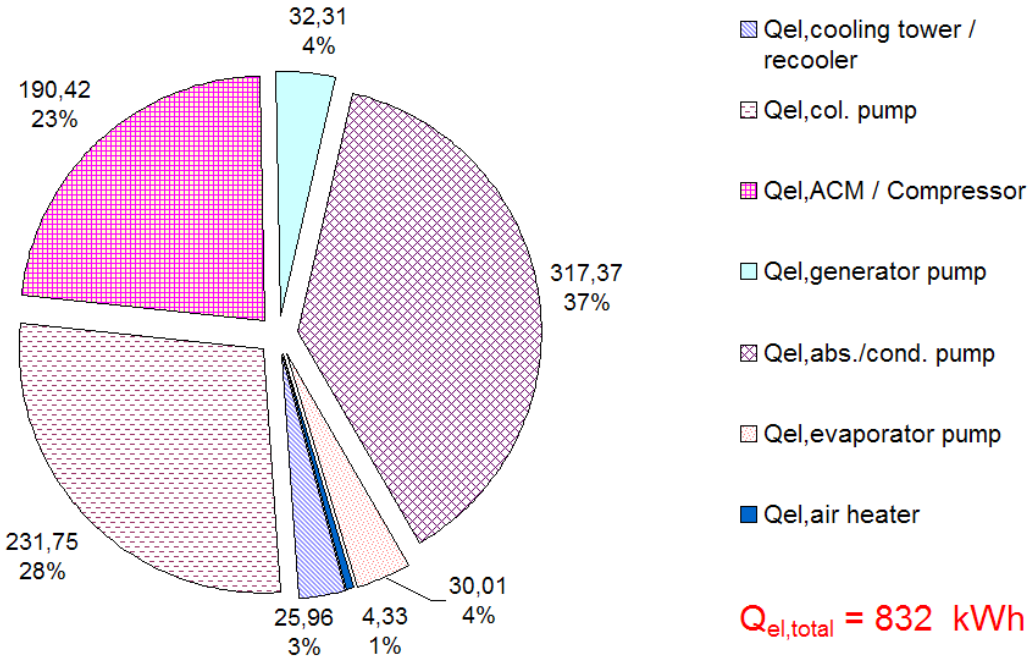

Fig. 4-9: Electricity consumption of Case 3

For the absorption chiller, the electricity consumption is mainly caused by the integrated water and solution pumps. Due to the actual system design of the

EAW WERACAL SE 15 with two containers, the absorber and generator are mounted at the same level. Therefore, two solution pumps are required, one for the concentrated and one for the diluted solution. Currently a new system design is developed by EAW (Energieanlagenbau GmbH Westenfeld) in cooperation with the ILK in Dresden (Institute of Air Handling and Refrigeration in Dresden) which integrates all components in one container with the generator and absorber mounted on different height levels (Weidner, 2009). For this new design only one solution pump is required, which will reduce the electricity consumption of the absorption chiller by at least 30%. Considering all these reduction potentials the electrical COP of case 3 could be improved by 40% to a value of 13. This would result in an increase of the primary energy ratio of 18 % to a value of 2.2.

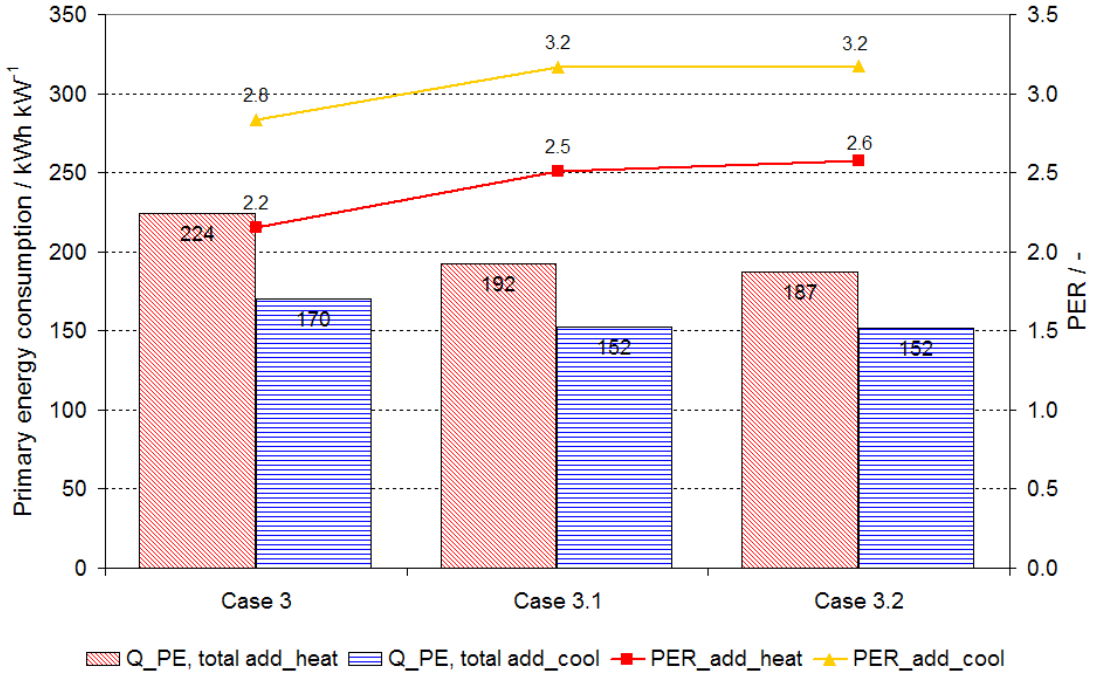

Fig. 4-10: Reachable specific primary energy consumptions and primary energy ratios for the electricity optimised solar cooling system. Comparison between additional heating and additional cooling in case of insufficient solar heat supply

As visible from Fig. 4-8 the additional heating energy consumption significantly increases the primary energy consumption although a high solar fraction of 70% and above is reached. This is an attribute to the relatively low thermal COP of

single effect absorption chillers. If the additional heating energy would be replaced by additional cooling provided by a highly efficient electrically driven compression chiller with an average overall electrical COP of 3.0 (including electricity energy consumption of pumps and heat rejection system) higher primary energy ratios can be reached. In this case the absorption chiller only provides cooling energy as long as sufficient heating energy is provided by the solar system and the remaining cooling energy is provided by the compression chiller. The effect of additional cooling instead of additional heating has been analysed in further simulations. Here the optimisation potential described above for reduced electricity consumption of the solar cooling system is already considered. The results are shown in Fig. 4-10 for case 3, case 3.1 and case 3.2. In case of additional heating the primary energy ratio of the electricity improved system can be increased by around 18% as mentioned above and primary energy ratios between 2.2 and 2.6 can be reached. If additional cooling is used instead of additional heating the primary energy ratio increases by further 23% to 29% to values between 2.8 and 3.2. Compared to the original system setup show in Fig. 4-8 the overall reachable improvement in primary energy ratio is more than 50%, e.g. in case 3 from a value of 1.8 to value of 2.8. The highest primary energy ratio of 3.2 is reached for the cases with reduced temperature setpoint of the heat rejection system (case 3.1 and 3.2). These results clearly demonstrate that additional cooling instead of additional heating significantly improves the primary energy efficiency of solar driven absorption cooling systems. Altogether, it can be concluded that there is still a significant potential for further improvements of the system efficiency of solar driven absorption cooling systems. If all these potentials are used, solar driven absorption cooling systems can be better than conventional cooling systems with efficient compression chillers by a factor of three.

4.4.6 CONCLUSIONS

The results obtained clearly demonstrate that solar cooling systems are not necessarily better than standard systems with compression chillers. A good system design with high solar fraction, low pressure losses, highly efficient pumps and optimal control strategies are essential for a high overall efficiency. Considering all results it can be concluded, that a proper fan speed control of the cooling tower / dry heat rejection ventilator as well as a ΔT mass flow control of the cold distribution pump are necessary to obtaining a high electrical COP of the system of above 8. The highest total primary energy ratio of 2.0 and therefore the best overall efficiency is obtained if additionally the generator temperature is allowed to vary between 70°C and 90(95)°C and if the lowest possible set point for the absorber/condenser inlet temperature is used. For optimised control the remaining main electricity consumers are the absorber and condenser pump 37%, the collector pumps 28%, and the absorption machine itself 23% (mainly solution pumps). For a further improvement of the primary energy efficiency therefore the electricity consumption of these three components needs to be reduced. For the absorber and condenser cooling water pump this requires despite of the utilisation of highly efficient pumps structural changes in the heat exchangers (e.g. larger diameters) of the ACM and on the spray nozzles in the cooling tower (alternative distribution systems) in order to reduce the quite high pressure drops. A reduction potential of 30% can be expected. If the heat exchanger between solar circuit and hot water storage is omitted and the solar system is operated as pure water system, the electricity consumption of the solar circuit can be reduced by up to 50%. However, a special frost protection control is required which pumps warm water into the collector field in case of frost risk. This of course reduces the thermal efficiency of the collector field, but the omission of the heat exchanger partly equalises these additional heat losses. The remaining heating energy losses are in the region of 3% for well controlled systems. The quite high electricity consumption of the absorption chiller results from the design of the EAW chiller with two separate tanks and the absorber and generator on the same height.

Therefore, two solution pumps are required which is very special for EAW chillers. For the new generation of EAW chillers this problem will be solved by a new integrated system design. A reduction of electricity consumption by 30% is expected. Considering all mentioned reduction potentials the electrical COP could be improved by 35% to 41% and values of 12.4 to 13.3 are reached (case 3 to case 3.2). This would result in an increase of the primary energy ratio between 18% and 20% to values of between 2.2 and 2.6. A further significant improvement of the primary energy ratio can be reached, if additional cooling instead of additional heating is used. Together with the reduced electricity consumption the primary energy ration can then be improved by 50% to values between 2.8 and 3.2 for the same system. For comparison, conventional cooling systems with highly efficient compression chillers reach a primary energy ratio of slightly above 1. This means that improved solar cooling systems based on single effect absorption chillers can be by a factor of three better than conventional systems with a compression chiller.

4.5 Analysis and Development of Control Strategies for Early System Start-up of Purely Solar Driven Absorption Chillers

4.5.1 INTRODUCTION

One essential weak point especially of purely solar driven absorption chillers is a quite late system startup in the morning. This mainly results from the inertia in the collector field and of the water in the hot storage tank, which first needs to be heated up to the temperature limit required for the startup of the absorption chiller. The required temperature limit is typically in the region between 75°C and 85°C. This high temperature level is required in order to heat up the thermal mass of the absorption chiller and for a fast regeneration of the diluted LiBr-solution. If lower temperatures are used after a longer standstill of the machine the chiller needs a quite long time to reach the nominal performance at the given external temperature conditions. This results in low thermal COPs and a bad overall performance of the solar cooling system (Safarik, 2008; Knapp, 2008). A further disadvantage of low startup temperatures is that fluctuations in the solar irradiation can lead to a shutdown of the absorption chiller shortly after the system startup, a condition which in extreme cases can occur several times over a period of several hours.

To overcome the late system startup several attempts have been made in the development of direct solar driven absorption chillers without any hot water storage in some cases even without cold water storage (Kühn, et al., 2008, Safarik, 2008). However, these systems operate very well on cloudless or only slightly clouded days. Since there is no real storage capacity, the direct solar driven systems only operate stably if the cooling load of the building is always equal or higher than the actual cooling power of the chiller. Otherwise, too low evaporator temperatures occur which lead to chiller shutdowns to avoid freezing in the evaporator. During these non operating periods the heat produced by the solar system needs to be released to the environment by a ventilator driven air cooler to avoid stagnation in the collector field. New system concepts therefore

try to reduce the chiller performance of direct solar driven absorption chillers by increasing the heat rejection temperature at part load conditions (Kühn, et al., 2008; Albers, et al., 2009). This means that the thermal COP is significantly reduced to meet the actual cooling demand. However, considering the overall primary energy efficiency this is only recommendable if at the same time the electricity consumption of the cooling tower is significantly reduced through fan speed control. A further disadvantage of direct solar driven absorption chillers results from the missing storage capacity in the solar thermal system. Therefore, a stable operation of the absorption chiller is only guaranteed for short periods of reduced solar irradiation (caused by single clouds) which is then covered by the inertia in the collector field and in the absorption chiller. Longer periods of reduced solar irradiation (> 5 minutes) lead to a chiller shutdown, although cooling energy is still required. To overcome these shortcuts of direct solar driven absorption chillers, hot water storages with storage bypass can be implemented in the systems. However, intelligent storage charge and discharge strategies are required to ensure an early system startup and a stable operation of the absorption chiller on partly cloudy days. The development of such intelligent storage charge and discharge control strategies is the focus of this work. To ensure optimal system operation the developed advanced control strategies have been implemented and tested in the dynamic simulation environment. This method is demonstrated for the optimisation of the start-up process through improved storage charge management of the chillii® solar cooling system installed at the office building of the SolarNext AG in Rimsting, Germany (See chapter 4.2). The design methods used for the developed control strategies, the controller algorithms found and the results of the controller tests in the simulation environment are presented and discussed in detail.

4.5.2 SIMULATION MODEL AND VALIDATION

For the analysis of different storage charge and discharge strategies a detailed fully dynamic simulation model of the installed chillii® solar cooling system has been developed in the simulation environment INSEL. In addition to the model described in chapter 4.3.2 this model also considers the inertia of the absorption chiller and of all connected tubes. The dynamic chiller model is described in chapter 2.1.2.3. Similar to the static ACM model the electricity consumptions of all installed components (fans, pumps, etc.) are considered. The complete system simulation model (Fig. 4-11) is used to analyse the effect of different storage charge and discharge options. A small time step of 10 seconds is used for an accurate consideration of all thermal capacities in the complex system.

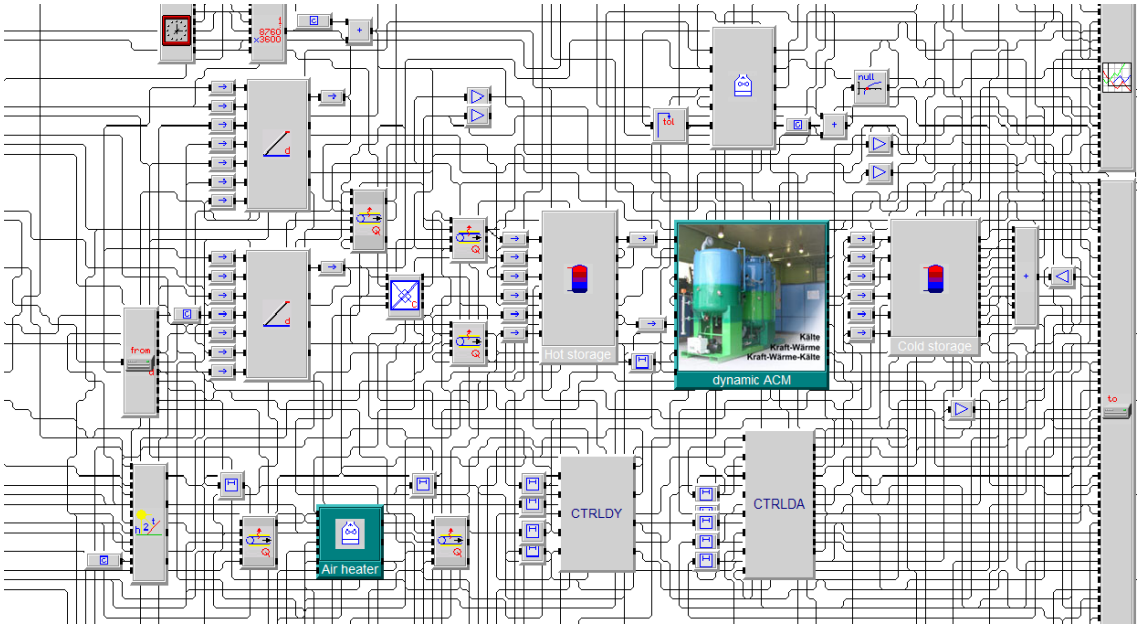

Fig. 4-11: Developed fully dynamic simulation model of the chillii® solar cooling system in INSEL

The complete model has been validated against measured data of the installed system. Fig. 4-12 shows the measured performance of the solar cooling system together with the simulation results for one day in August 2007.

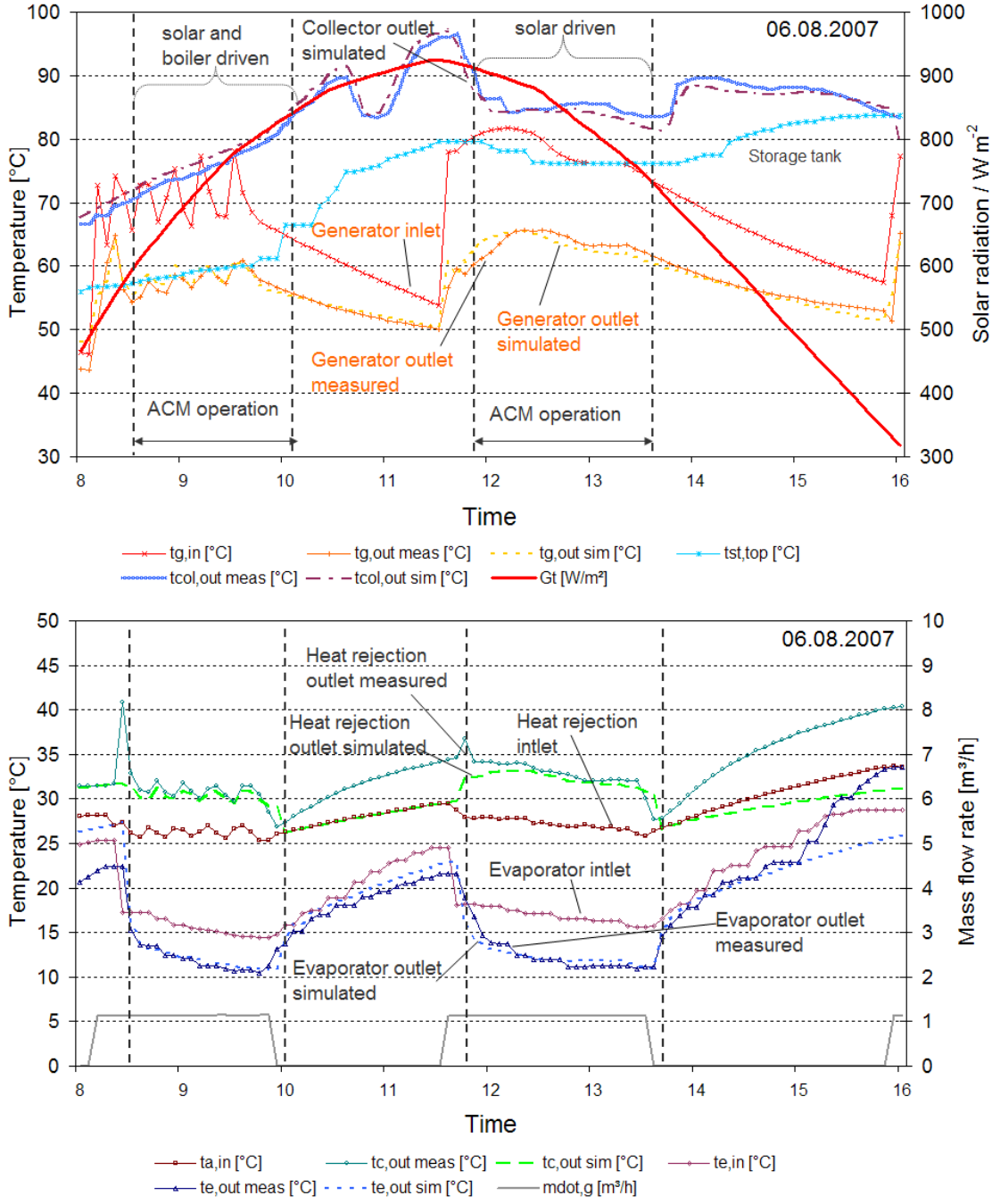

Fig. 4-12: Measured and simulated performance of the solar cooling system. The simulations are based on the fully dynamic model including the dynamic ACM model. **(Same day as in Fig. 4-5; differences visible at system startup and shutdown)**

A comparison of the simulated and measured outlet temperatures of the generator, condenser and evaporator of the ACM and of the collector field shows that the performance of the installed system is well described by the developed simulation model. Due to the consideration of the chillers inertia even

the start up process and fluctuating operation conditions are precisely described, which was not the case with the static chiller model (see chapter 4.4.2). For the regarded day the deviation between the predicted and measured solar heating energy of the collector circuit (dynamic model) is below 1%. The deviation between simulated and measured performance of the absorption chiller is below 2% for the generator and evaporator energy. For the heat rejection circuit slightly larger deviations between measured and predicted heat removal of slightly below 6% occur. Altogether the developed fully dynamic simulation model reaches a very high accuracy, which is more than sufficient for the analysis of the different storage charge and discharge strategies.

4.5.3 CONTROL CODE DEVELOPMENT AND TEST

The fully dynamic simulation model of the solar driven absorption cooling system was used during the development phase of the control strategies for different storage charge and discharge strategies to test and optimise the behaviour of the developed control algorithms. With this method several not obvious control errors could be detected and directly eliminated in the controller code without the necessity of time consuming on site or laboratory tests. Fig. 4-13 illustrates the control code development process in the simulation environment.

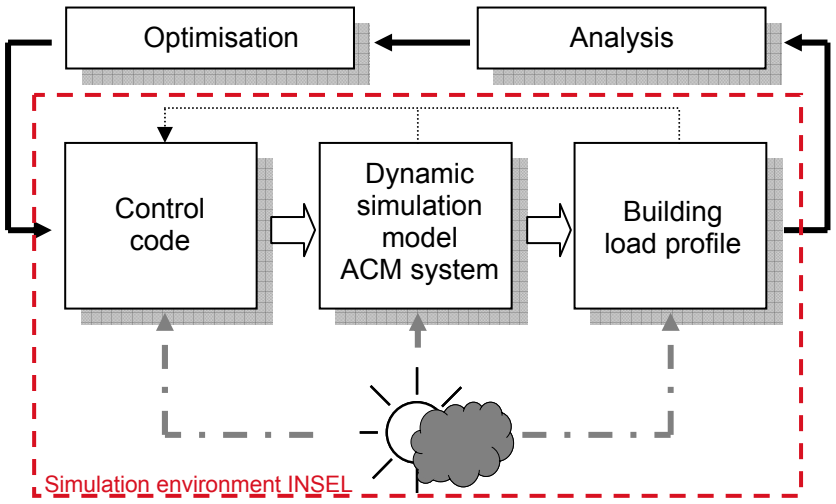

Fig. 4-13: Development and test of control algorithms in the simulation environment

Apart from a sufficient sizing of the solar system, the start-up time of solar driven cooling systems in the morning and a sufficient heat supply during operation strongly depends on the charge control of the hot water storage tank. Four different cases (Table 4-4) with improved storage charge and discharge control strategies reaching from full storage (case 1), bypass (case 2) and partitioned storage (case 3) to a combination of both (case 4) have been developed, analysed and optimised in the dynamic simulation environment. The optimised control sequences for the four analysed storage charge and discharge cases are shown in Appendix C.

Table 4-4: Analysed storage charge and discharge cases

Case 1	Case 2	Case 3	Case 4
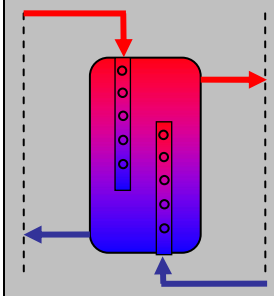	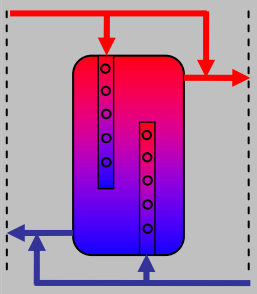	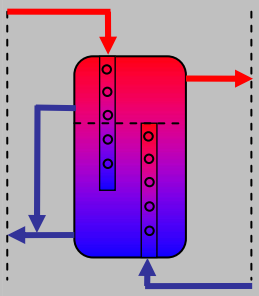	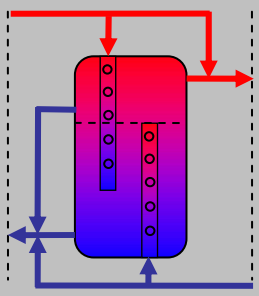
Control mode description			
2000 l hot water storage, full volume always used	2000 l hot water storage with bypass Control modes: 1. Bypass storage completely; 2. Bypass hot water supply, feed in generator return; 3. Use full storage volume; 4. Charge storage in case of ACM shut down	Partitioned 2000 l hot water storage for early system start-up, with 300 l on top and 1700 l below Control modes: 1. Use upper storage part only 2. Use full storage volume	Combination of case 2 and 3: Partitioned 2000 l storage with bypass Control modes: First control modes of bypass applied to upper storage part, then control modes of partitioned storage used

4.5.4 ANALYSED WEATHER CONDITIONS

For testing the developed control strategies and control codes, three typical summer days and the corresponding cooling loads of the building have been analysed. The ambient temperature, relative humidity, solar radiation and the cooling load of the analysed days are based on onsite measurements and are shown in Table 4-4 (21st June 2008 - hot summer day with single clouds, 10th July 2008 - hot summer day with almost clear sky and 11th July 2008 - hot summer day with some clouds in the early morning and thunderstorm in the early afternoon). For all analysed cases it has been assumed, that the starting temperature is 55°C on storage top and 50°C on storage bottom, which e.g. corresponds to a hot summer day after a period with heavy clouds.

Table 4-5: Analysed typical hot summer days

21st June 2008 Hot summer Day with single clouds		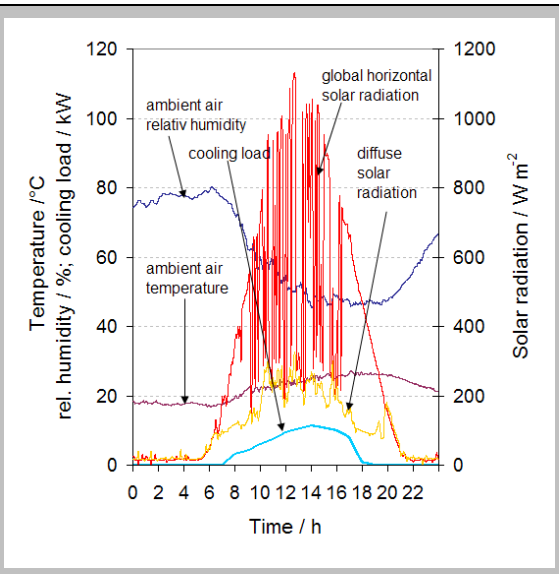
Average ambient temperature	22.1°C	
Average ambient humidity	60.9%rH	
Total solar radiation	7 016.9 Wh/m²	
Total cooling energy demand	81.5 kWh	
10th July 2008 Hot summer day with almost clear sky		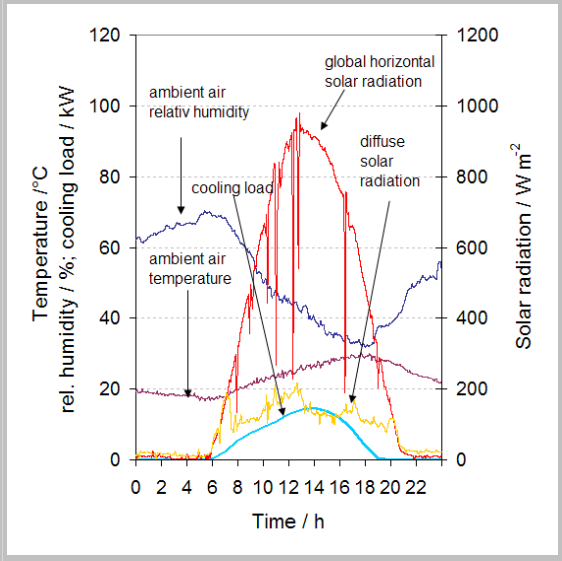
Average ambient temperature	23.3 °C	
Average ambient humidity	50.7%rH	
Total solar radiation	8 235.1 Wh/m²	
Total cooling energy demand	115.1 kWh	
11th July 2008 Hot summer day, some clouds in the early morning and thunderstorm in the afternoon		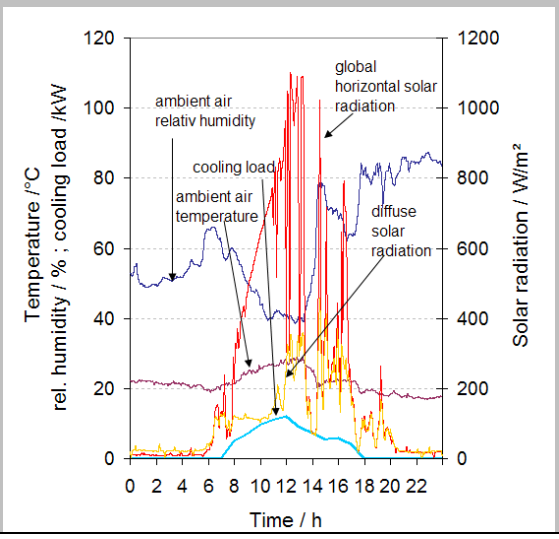
Average ambient temperature	21.7°C	
Average ambient humidity	61.9%rH	
Total solar radiation	5 461.4 Wh/m²	
Total cooling energy demand	75.9 kWh	

4.5.5 RESULTS AND DISCUSSION

4.5.5.1 DETAILED SIMULATION RESULTS

For the discussion of the behaviour of the developed control algorithms, the simulation results for the day with single clouds (21st June 2008) is selected. For this day the differences in the control algorithms analysed become clearly visible. The simulation results of the four analysed cases are shown in Fig. 4-14 to Fig. 4-17. Further detailed results of the other analysed days are shown in Appendix D.

- **Case 1: 2000 l hot water storage**

For case 1 (Fig. 4-14) with the simplest control and the full hot storage volume always used, the collector field first needs to heat up the hot water storage to the minimum start-up temperature of 75°C before the controller sets the ACM in operation. As soon as the collector temperature is 10 K above the temperature at the hot storage bottom the primary collector pump is set in operation to heat up the water in the collector circuit (4 minutes minimum operation time). Due to the cold water in the collector tubing, the temperature at heat exchanger inlet first increases very fast and then decreases again below the temperature at hot storage bottom. In consequence, the primary collector pump is switched off again. At second start-up of the primary collector pump the temperature at heat exchanger inlet again drops below the temperature at hot storage bottom with the same consequence. At third start-up of the collector pump the temperature does not drop below the temperature at hot storage bottom and the secondary collector pump is set in operation in order to charge the hot storage. The time delay for the startup of the secondary collector pump is 5 minutes to the startup of the primary collector pump. Due to fluctuations of the solar irradiation caused by single clouds, the collector outlet temperature varies but doesn't drop below the hot storage bottom temperature. At 11:30am the temperature at hot storage top reaches the minimum start-up temperature of 75°C and the generator pump of the ACM is set in operation to heat up the generator and to concentrate the diluted LiBr solution. As soon as the generator outlet temperature increases

above 65°C (lower limit for full ACM operation) at 11:38am the absorber/condenser and evaporator pump of the ACM are set in operation in order to cool down the cold water storage.

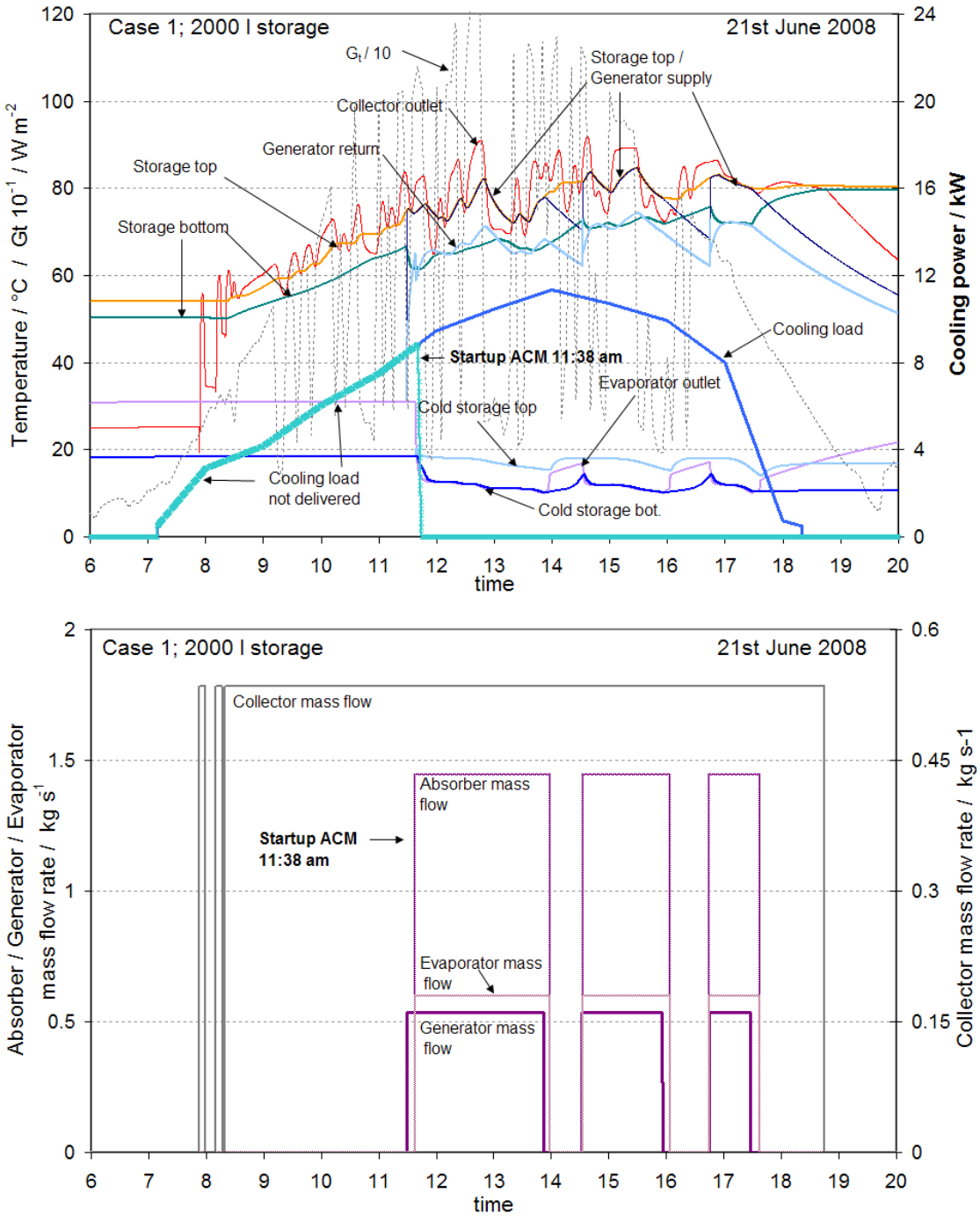

Fig. 4-14: Detailed simulation results for case 1 on 21st June 2008

Although cooling energy is delivered to the building, the temperature in the cold storage drops slowly. As soon as the evaporator outlet temperature reaches the lower limit of 10°C, the generator pump of the ACM is switched off. The absorber/condenser and evaporator pump remain in operation to dilute the LiBr-solution in order to prevent crystallisation. Meanwhile further cooling energy is delivered to the cold storage tank for another 6 minutes. The evaporator and absorber/condenser pumps are switched off as soon as the evaporator outlet temperature is only 1 K below the temperature at cold storage top. As soon as the temperature in the middle of the cold storage increases above the required supply temperature of the cold water circuit of 15°C, the generator pump is set in operation again to concentrate the diluted LiBr solution. As soon as the generator outlet temperature increases above 65°C the absorber/condenser and evaporator pump of the ACM are set in operation and cooling energy is provided to the cold water storage.

- Case 2: 2000 l hot water storage with bypass

For case 2 with bypass of the hot storage tank (Fig. 4-15) the decision whether the system is operated in full storage or bypass mode depends on the temperature available in the hot storage tank. If the temperature at top of the hot storage tank is below the minimum startup temperature of the generator of 75°C the system starts the operation in bypass mode. For the analysed day the temperature at top of the hot storage tank is only 55°C therefore the system starts in bypass mode. In bypass mode the primary collector pump is switched on as soon as the collector temperature reaches 80°C. Due to the cold water in the collector tubing, the temperature at heat exchanger inlet first increases very fast and then decreases again below the minimum generator inlet temperature of 65°C. In consequence, the primary collector pump is switched off again after a minimum operation time of 4 minutes. At second start-up of the primary collector pump at 08:40am the temperature at the heat exchanger inlet reaches the required temperature level of 75°C required for ACM startup and the primary collector and generator pump are set in operation to heat up the generator and to concentrate the diluted LiBr solution. In consequence of the relatively cold

water at generator outlet, the collector temperature at heat exchanger inlet decreases very fast below the minimum generator inlet temperature of 65°C and the secondary collector and generator pump are switched off again.

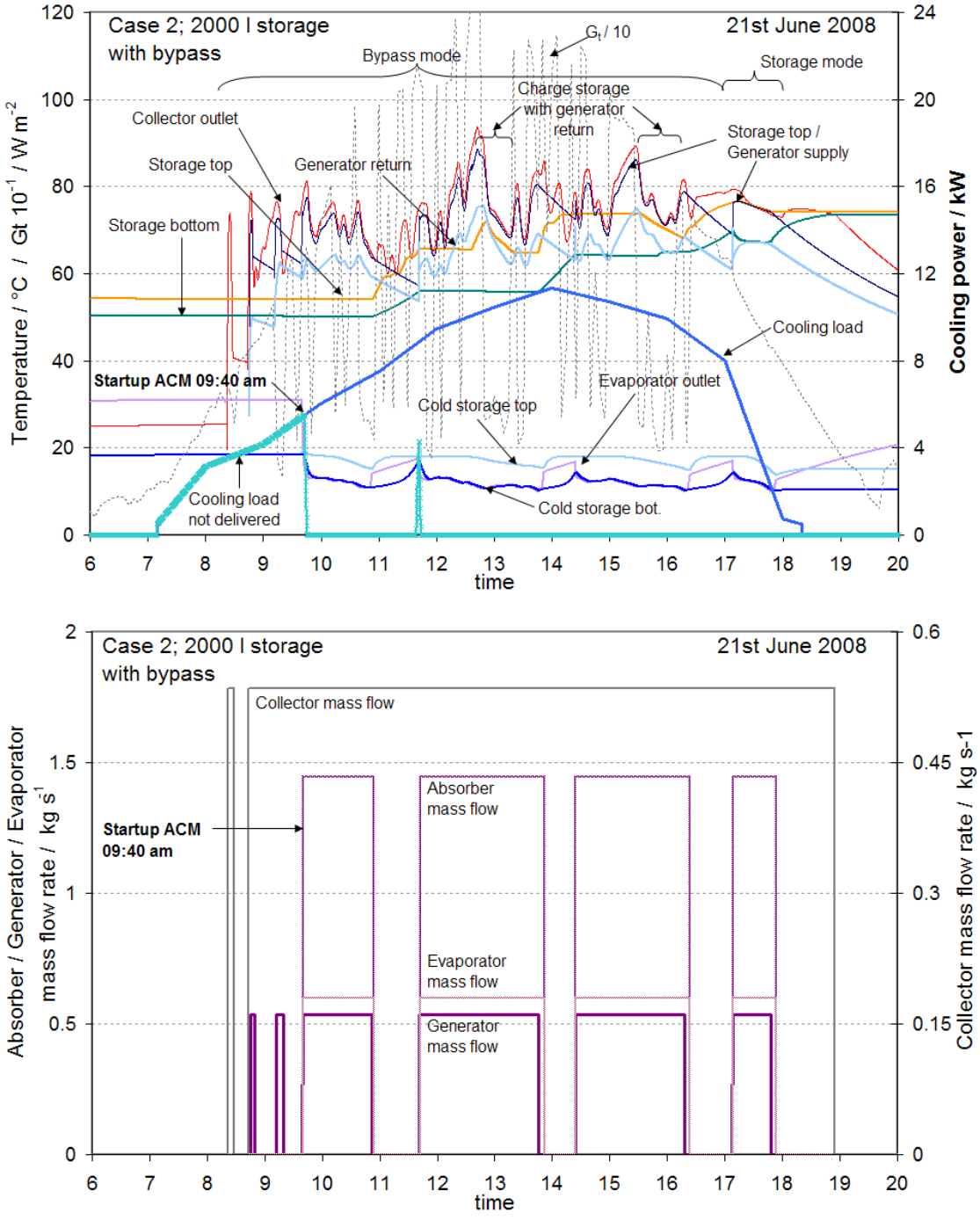

Fig. 4-15: Detailed simulation results for case 2 on 21st June 2008

At 09:10am the temperature of the collector circuit again reaches 75°C at heat exchanger inlet and the secondary collector and generator pump are switched on with the same consequence. At third startup of the generator pump at 09:40am the generator outlet temperature increases very fast above 65°C and the absorber/condenser and evaporator pump of the ACM are set in operation and provide cooling energy to the cold water storage (two hours earlier than for case 1). Although cooling energy is delivered to the building, the temperature in the cold storage drops slowly. Due to low solar irradiation the collector outlet temperature drops below the minimum generator inlet temperature of 65°C at 10:55am and the generator pump is switched off and the storage bypass is closed. The absorber/condenser and evaporator pump remain in operation until the outlet temperature is only 1 K below the temperature at cold storage top. Since the temperature at hot storage bottom is still below the collector outlet temperature the primary and secondary collector pumps stay in operation and the hot storage tank is charged. Due to the low cold water temperature in the cold water storage of 11°C the cooling load can be covered for nearly the whole stand still period of the absorption chiller. At 11:40am the temperature of the collector circuit at heat exchanger inlet again reaches the required generator startup temperature of 75°C and the bypass is opened and the generator pump is switched on. Shortly after this also the absorber/condenser and the evaporator pump are switched on and cooling energy is delivered to the cold storage. At 12:40am the collector outlet temperature increases above 95°C. In consequence the bypass at storage bottom is closed and the hot generator return water is used to charge the hot storage while cold water from the storage bottom is pumped to the solar heat exchanger. This leads to a fast drop of the collector outlet temperature to a value below 70°C and the lower storage bypass is opened again. Since the cooling energy provided by the absorption chiller is higher than the cooling load of the building, the temperature in the cold storage drops slowly until the evaporator outlet temperature reaches the lower temperature limit of 10°C and the generator pump of the ACM is switched off. The absorber/condenser and evaporator pump remain in operation for another 4 minutes. During the standstill phase of the ACM the hot storage tank is

charged again by the solar system but does not reach the required temperature of 75°C before the third ACM startup. Therefore the system is still operated in bypass mode with exactly the same procedure as described before. During the third standstill phase the hot storage tank temperature increases above 75°C. Therefore at fourth ACM startup the system is operated in storage mode.

- Case 3: Partitioned 2000 l hot water storage

As visible from Fig. 4-16 the partitioned storage tank with 300 l top storage volume of case 3 performs similar to case 1 with two startups of the primary collector pump before at the third startup the upper part of the hot water storage is charged. Due to the lower active volume of the storage partition the temperature increases much faster and reaches the required startup temperature of the ACM already at 09:52am. This is 1 hour 46 minutes earlier compared to case 1 with full storage but 12 minutes later than in case 2 with storage bypass. During the non operating phases of the ACM the partitioned upper part is further charged by the solar system. At 13:15 the collector outlet temperature increases above 95°C and the full storage mode is activated. Due to the low cold water at hot storage bottom the collector outlet temperature drops very fast. Since the ACM is in operation at the same time also the temperature at hot storage top and generator supply decreases but does not drop below 65°C. Therefore the ACM remains in operation and provides cooling energy to the cold storage tank. At 16:35am the evaporator outlet temperature decreases below the lower temperature limit at evaporator outlet of 10°C and the generator pump of the ACM is switched off. The absorber/condenser and evaporator pumps remain in operation and provide cooling energy to the cold storage tank while diluting the LiBr-Solution for another 3 minutes.

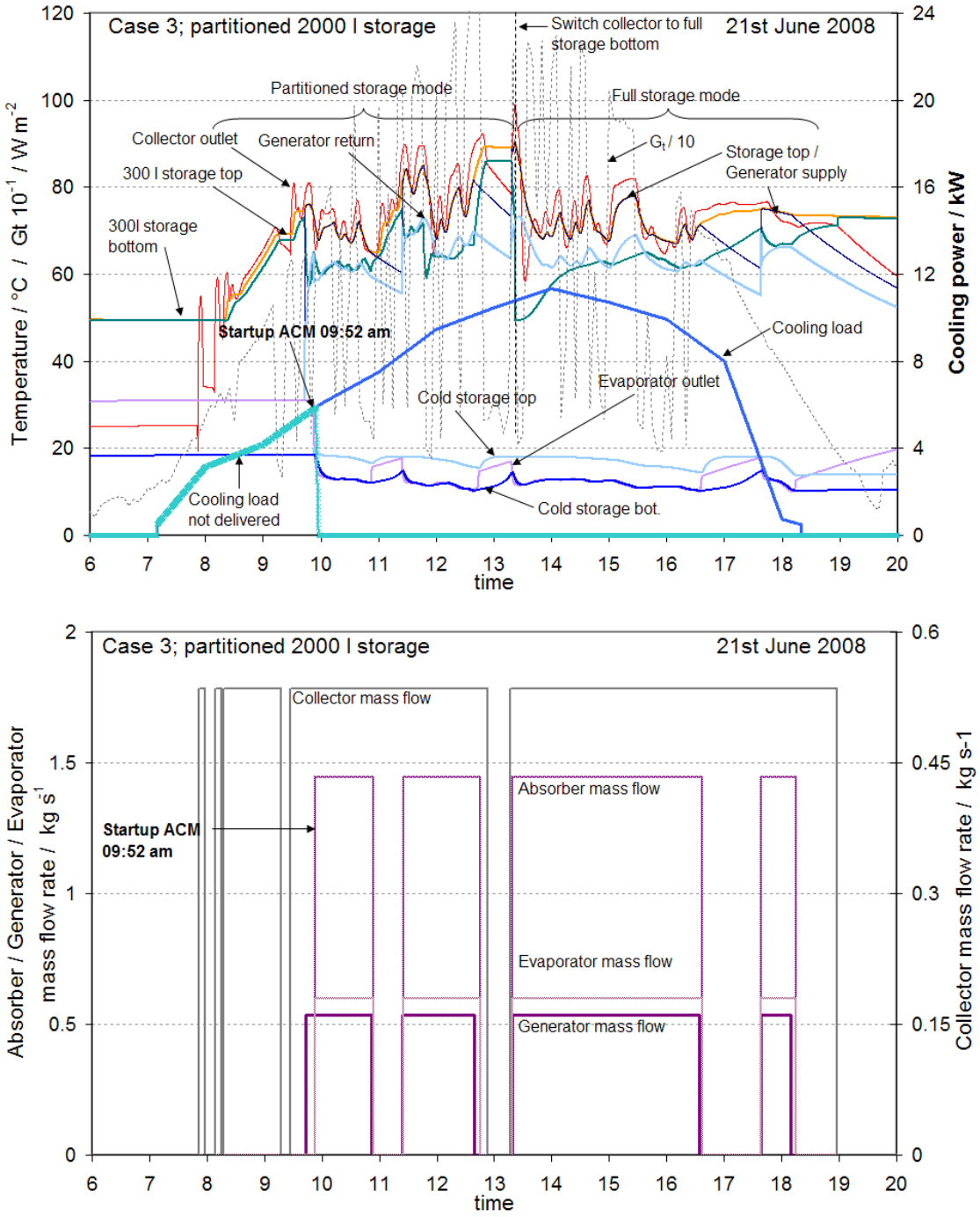

Fig. 4-16: Detailed simulation results for case 3 on 21st June 2008

- Case 4: Partitioned 2000 l hot water storage with bypass

The partitioned storage tank with 300 l top volume and bypass operates during the first part of the day until 10:55am in bypass mode with exactly the same behaviour as already described for case 2 with full storage volume and bypass. At 10:55am the evaporator temperature drops below 10°C and the generator pump is switched off.

During the stand still phase of the ACM the bypass is closed and the upper partitioned part of the hot storage tank is charged by the solar system. Due to the small volume the temperature in the partitioned hot storage part increases very fast above 75°C. Therefore at second startup at 11:35am the ACM system is operated in partitioned storage mode. Then the temperature in the cold storage slowly decreases which results in an evaporator outlet temperature below 10°C at 12:40am and the generator pump is switched off. Since further heating energy is delivered by the solar system the temperature in the partitioned storage volume increases above 90°C. In consequence the collector circuit switches from partitioned to full storage mode.

Due to the cold water at hot storage bottom combined with a period of low solar radiation the collector outlet temperature drops quite fast below 60°C but remains above the temperature at hot storage bottom. Therefore the collector pumps remain in operation. At third and fourth startup of the ACM the system is operated in full storage mode with stable heat supply from the solar system.

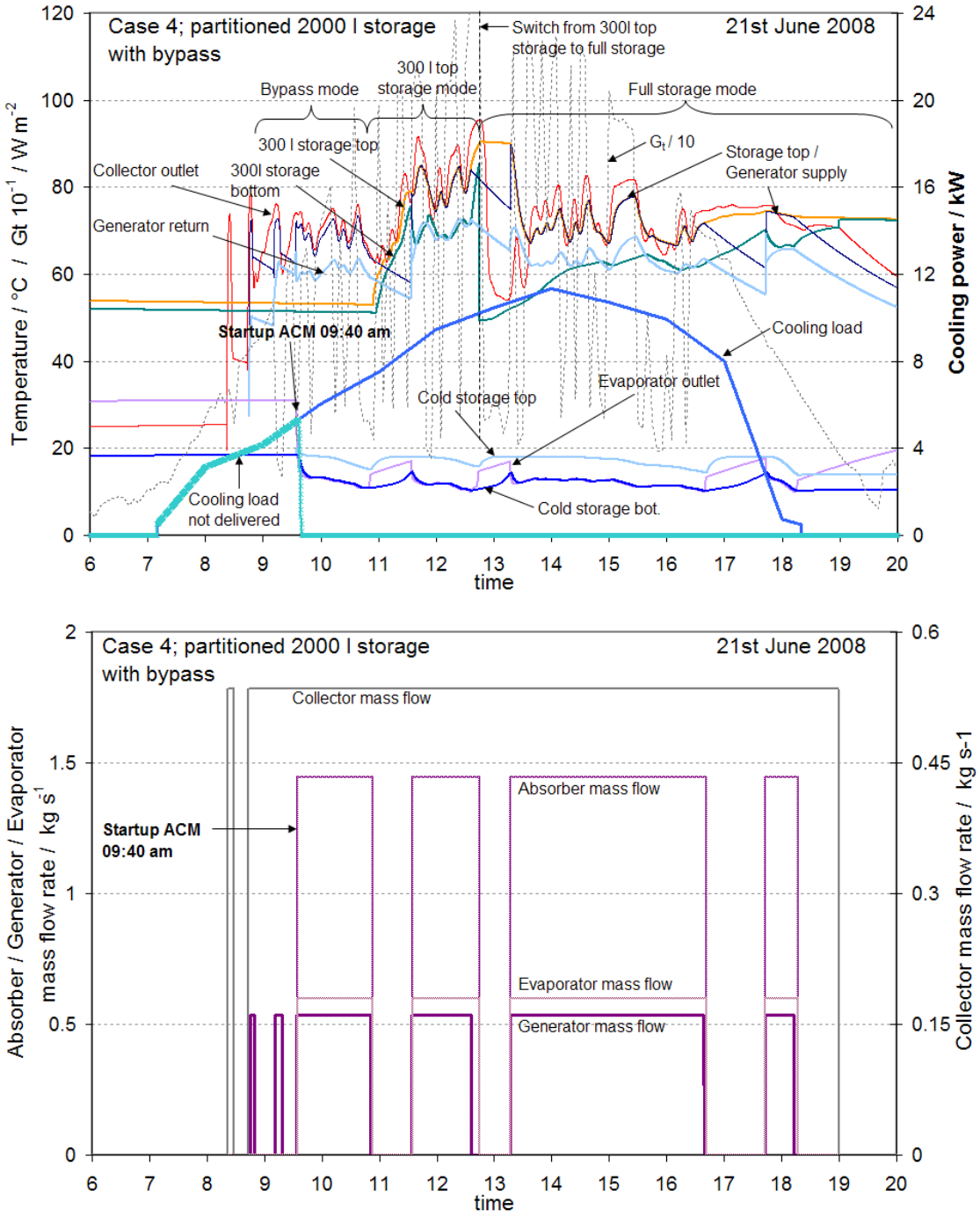

Fig. 4-17: Detailed simulation results for case 4 on 21st June 2008

4.5.5.2 DAILY SIMULATION RESULTS

The results for all analysed storage charge and discharge cases (case 1-4) and daily weather conditions are summarised as daily sum / average values in Table 4-6 to 4-8. If always the full storage volume is used (case 1) the start-up time of the absorption chiller varies between 11:03 and 11:38am depending on the summer day regarded. This perfectly corresponds with the commonly expected performance of solar driven absorption cooling systems. However, as a result of the late start-up 27 to 39% of the cooling load of the building can't be covered by the system. As expected for case 1, the best results are obtained for the 10th July (cloudless day) and the worst result for the 11th July (some clouds in the early morning and thunderstorm in the early afternoon).

In case 2 with bypass of the hot storage, the start-up times can be significantly reduced by more than 1h 40 min for all of the three analysed days. The earliest start-up time of 9:23am is obtained on 10th July followed by 9:26am on 11th July and 9:40am on 21st June (single clouds). Due to the early system start-up, the cooling load which can't be covered is also significantly reduced and varies between 11% and 14%.

The partition of the storage tank in case 3 leads also to much earlier system start-up times but does not reach a higher coverage of the cooling load compared to case 2 on any of the analysed days.

The best overall performance is reached for case 4 with combined bypass and partitioned storage control. Compared to case 1 the part of the cooling load which can't be covered is reduced to 14% (10th June), 10% (21st June) and 16% (11th July) with almost the same start-up times as in case 2. If the produced cooling energy is regarded, the advantage of the improved storage charge and discharge control in case 4 compared to case 1 becomes even more visible with 18% more cooling energy production on 21st June, 23% more cooling energy production on 10th July and 33% more cooling energy production on 11th July.

The thermal and electrical COP is very slightly influenced by the analysed storage charge and discharge control cases but is significantly influenced by the type of summer day. The highest thermal COP of the absorption chiller of 0.69 and the highest electrical COP of the complete solar cooling system of 8.5 are reached on 10th July with almost clear sky due to the highest driving temperatures.

For 21st June and 11th July significantly lower thermal COP of 0.64 to 0.66 and electrical COP of 7.1 to 7.7 are reached, which is mainly caused by the overall lower driving temperatures at generator inlet. The electrical COP of the solar cooling system includes the electricity consumption of all components and pumps (ACM, cooling tower (fan speed control) and all pumps (generator, evaporator, absorber/condenser and primary and secondary collector pump), only the distribution pump and fan coils are not considered.

Table 4-6: Overview of main results

Storage charge and discharge control options	Case1		Case 2		Case 3		Case 4	
	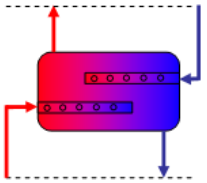 Full storage always used		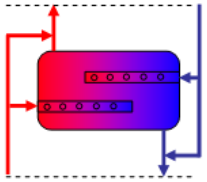 Full storage with bypass		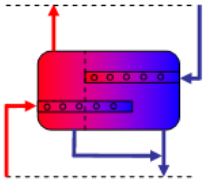 Partitioned storage with 300 l top volume		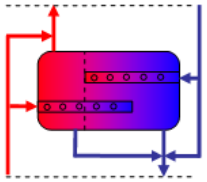 Partitioned storage with 300 l top volume and bypass	
Analysed day	21st June	10th July	21st June	10th July	21st June	10th July	21st June	10th July
Start up time of ACM	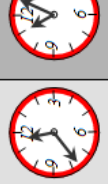		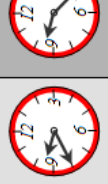				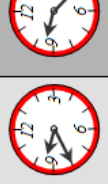	
Coverage of cooling load	72%	73%	89%	86%	88%	84%	90%	86%
COP_{th} [-]	0.66	0.68	0.66	0.68	0.66	0.68	0.66	0.69
COP_{el} [-]	7.07	8.51	7.26	8.49	7.07	8.47	7.06	8.39

	11th July	11th July	11th July	11th July
Start up time of ACM				
Coverage of cooling load	61%	83%	80%	84%
COP_{th} [-]	0.64	0.65	0.65	0.65
COP_{el} [-]	7.50	7.69	7.42	7.18

Table 4-7: Results related to heating energy consumption and cooling energy production

Case	Start-up time ACM	Q_S	Q_{h,st_in}	η_S	$Q_{h,ACM}$	$Q_{h,stored}$	$Q_{c,req}$	$Q_{c,ACM}$	$Q_{c,stored}$	Cooling energy not covered	
	[h:min]	[kWh]	[kWh]	[%]	[kWh]	[kWh]	[kWh]	[kWh]	[kWh]	[kWh]	[%]
10th July, hot summer day with almost clear sky											
1.1	11:04 AM	592.7	223.4	38%	135.7	77.8	114.7	92.1	7.7	31.2	27%
2.1	9:23 AM	592.7	228.8	39%	148.0	70.8	114.7	101.4	1.4	15.5	14%
3.1	9:43 AM	592.7	233.0	39%	154.9	70.9	114.7	105.4	7.6	17.9	16%
4.1	9:23 AM	592.7	232.5	39%	150.3	73.2	114.7	103.1	3.0	15.5	14%
21st June, hot summer day with single clouds											
1.2	11:38 AM	481.5	166.6	35%	99.8	57.3	81.3	65.6	6.3	22.9	28%
2.2	9:40 AM	481.5	172.2	36%	120.3	43.3	81.3	79.9	6.7	9.0	11%
3.2	9:52 AM	481.5	174.0	36%	119.3	48.3	81.3	79.2	6.9	10.0	12%
4.2	9:40 AM	481.5	177.6	37%	121.9	47.3	81.3	80.8	6.9	8.3	10%
11th July, hot summer day, some clouds in the early morning and thunderstorm in the early afternoon											
1.3	11:07 AM	399.3	134.9	34%	80.5	45.2	75.9	51.1	3.6	29.2	39%
2.3	9:26 AM	399.3	138.8	35%	102.3	28.4	75.9	67.0	2.9	12.6	17%
3.3	9:45 AM	399.3	141.6	35%	95.6	36.5	75.9	62.2	3.1	15.2	20%
4.3	9:26 AM	399.3	136.0	34%	103.9	22.4	75.9	68.0	3.6	12.4	16%

Legend:

Q_s	Solar irradiation on the collector plane (gross area)	Q_{h,st_in}	Solar heating energy storage input
Q_{h,st_in}	Heating energy stored in the hot storage at the end of the day	η_s	Efficiency of the solar system
$Q_{c,ACM}$	Cooling energy produced by the ACM	$Q_{c,req}$	Required cooling energy
$Q_{c,stored}$	Cooling energy stored in the cold storage at the end of the day	$Q_{h,ACM}$	heating energy used by the ACM

Table 4-8: Results related to ACM operation

Case	ACM operation time [h:min]	Q_h [kWh]	Q_{el} [kWh]	Q_c [kWh]	$\overline{\dot{Q}_h}$ [kW]	$\overline{\dot{Q}_c}$ [kW]	COP_{th} [-]	COP_{el} [-]	$t_{g,in}$ [°C]	$t_{g,out}$ [°C]	$t_{e,in}$ [°C]	$t_{e,out}$ [°C]	$t_{a,in}$ [°C]	$t_{c,out}$ [°C]
10th July, hot summer day with almost clear sky														
1.1	5:54 AM	135.7	10.8	92.1	85.2	15.6	0.68	8.51	86.4	74.6	17.6	11.4	25.9	32.1
2.1	7:30 AM	148.0	11.9	101.4	22.6	14.8	0.68	8.49	79.4	69.4	17.6	11.7	25.4	31.2
3.1	7:10 AM	154.9	12.4	105.4	23.5	14.8	0.68	8.47	80.4	70.0	17.5	11.6	25.5	31.3
4.1	7:48 AM	150.3	12.3	103.1	21.9	14.5	0.69	8.39	78.2	68.5	17.6	11.8	25.3	31.0
21st June, hot summer day with single clouds														
1.2	4:44 AM	99.8	9.3	65.6	22.1	13.7	0.66	7.07	78.3	68.5	17.1	11.6	25.5	31.0
2.2	6:07 AM	120.3	11.0	79.9	20.0	13.1	0.66	7.26	74.4	65.5	17.1	11.9	25.1	30.2
3.2	6:18 AM	119.3	11.2	79.2	19.3	12.6	0.66	7.07	73.0	64.4	17.0	12.0	24.9	29.9
4.2	6:26 AM	121.9	11.4	80.8	19.1	12.6	0.66	7.06	72.5	64.0	17.0	12.0	24.9	29.9
11th July, hot summer day, some clouds in the early morning and thunderstorm in the early afternoon														
1.3	3:43 AM	80.5	6.8	51.1	23.6	13.8	0.64	7.50	79.7	69.3	17.4	11.8	25.9	31.4
2.3	5:11 AM	102.3	8.7	67.0	20.1	13.0	0.65	7.69	75.0	66.0	17.1	11.9	25.4	30.6
3.3	5:03 AM	95.6	8.4	62.2	19.8	12.9	0.65	7.42	74.7	65.9	17.0	11.9	25.4	30.5
4.3	5:28 AM	103.9	9.5	68.0	19.3	12.5	0.65	7.18	72.8	64.2	17.2	12.2	25.2	30.1

Legend:

Q_{el}	Electricity used by the whole solar cooling system, including the ACM, cooling tower and all pumps	Q_h /Q_c	heating energy used / cooling energy produced by the ACM
COP_{el}	Electrical coefficient of performance of the whole solar cooling system	COP_{th}	Thermal coefficient of performance of the ACM
$t_{g,in}$/$t_{g,out}$	Average Generator inlet / outlet temperature	$t_{e,in}$/$t_{e,out}$	Average Evaporator inlet / outlet temperature
$t_{a,in}$/$t_{c,out}$	Average Absorber inlet / condenser outlet temperature	$\overline{\dot{Q}_h}$ / $\overline{\dot{Q}_c}$	Average heating / cooling power

4.5.6 CONCLUSIONS

The focus of the presented work is on the optimised control of solar driven absorption cooling systems for early system start-up in the morning and sufficient heat supply during operation. For the analysis of the behaviour of the developed control algorithms and their effect on the overall performance of the solar cooling system a detailed full dynamic simulation model developed in INSEL has been used. Four different control options for the storage charge and discharge control of a 15 kW chillii® Solar Cooling System installed in an office building of the SolarNext AG in Rimsting Germany have been analysed for three different typical summer days. In case 1 always the full hot water storage volume is used for the solar system, in case 2 a storage bypass is integrated for an early system start-up. In case 3 the storage is partitioned in an upper 300 l part and a lower 1700 l part and in case 4 the storage bypass is combined with a partitioned storage tank. The developed control algorithms have been tested and improved in the dynamic simulation environment for different weather conditions. Several not obvious control errors could be detected and removed from the control sequences shown in Appendix C without the necessity of time consuming on site or laboratory tests. The validated control sequences of the four cases mentioned above were then used to analyse the overall performance of the solar cooling system for three different typical hot summer days. It could be shown, that through the implementation of a storage bypass the start up time can be significantly reduced by 1h 40 min in the worst and nearly 2 h in the best case. For the partitioned storage case, the start-up time is between 12 and 20 minutes later. On a cloudless summer day the start-up of the solar cooling system is at 9:23am (Bypass), 9:43am (partitioned storage) instead of 11:04am (full storage). The best performance is reached for case 4 with the combined bypass and partitioned storage control. If the produced cooling energy is regarded, the advantage of the improved storage charge and discharge control in case 4 compared to case 1 becomes clearly visible with 19% more cooling energy production on 21st June 2008 (day with some clouds) and 10th July 2008 (cloudless day) and 33% more cooling energy production on 11th July 2008

(some clouds in the early morning and thunderstorm in the early afternoon). The thermal and electrical COP of the solar cooling system is only very slightly influenced by the different control modes but strongly depends on the analysed type of summer day. For a hot cloudless summer day (10th July) the thermal COP is 0.69 and the overall electrical COP is 8.5 in the best case. Due to the lower available driving temperatures, the thermal COP is reduced on cloudy days (21st June and 11th July) to 0.64 in the worst case. The lower thermal COP results in longer operational hours at low cooling capacity and thereby reduces also the electrical COP which is 7.06 in the worst case.

4.6 RECOMMENDATIONS

Considering all results it can be concluded, that a high solar fraction on the heating energy demand of the ACM and low electricity consumptions of all components of the solar cooling system are required for a high overall efficiency of solar cooling systems. To achieve a primary energy efficiency which is nearly a factor two better compared to standard compression chillers it is essential, that the fan speed of the cooling tower ventilator or the ventilator of dry heat rejection system is controlled according to the ambient conditions and the required cooling power. The highest total primary energy ratio (PER) and therefore the best overall efficiency is obtained if additionally the generator temperature is allowed to vary between 65°C and 90(95)°C according to the temperature in the hot water storage tank and if a low set point for the absorber inlet temperature (e.g. 22°C) is used for the cooling tower control. A further significant improvement of the primary energy efficiency of 25% is reached if the additional heating is replaced by additional cooling. A solar driven absorption cooling system with further reduced electricity consumption and additional cooling instead of additional heating reaches primary energy ratios between 2.8 and 3.2. This is up to a factor of three better than conventional systems with compression chillers. The results of chapter 3 clearly demonstrated that, from the economical point of view, long fulload hour of the solar cooling system significantly improves the economic feasibility of the system. If it is also

considered that an operation at partload conditions can significantly reduce the thermal COP of the system, a design of the solar cooling systems for 40 to 60% of the maximum required cooling power results in a much better system performance.

For purely solar driven absorption chillers it is important to achieve an early system startup in the morning and a stable system operation during the day. A bypass of the hot water storage tank or a partitioned small upper storage part can significantly reduce the startup time by up to two hours but requires an intelligent storage charge control for a stable system operation on partly clouded days. A partitioned storage tank with a small upper volume needs a slightly longer time period (around 15 minutes) to reach the required startup temperature but offers a more stable system operation especially on days with partly cloudy periods during the morning. The overall best performance is reached for the storage tank with bypass and partitioned upper part. However, the additional effect compared to the bypass or partitioned storage case is low and therefore does not pay for the additional control effort. The do's and don'ts listed below summarise the results found and give recommendations for a highly energy efficient control of solar driven absorption chillers:

Do's:

- Fan speed control of the cooling tower / dry heat rejection according to the ambient conditions and cooling load. The lowest possible cooling water temperature setpoint (e.g, 22°C) should be used as setpoint for the outlet temperature of the heat rejection system
- ΔT- mass flow control of the cold water distribution pump
- Use high energy efficient pumps only and ensure a good hydraulic design with low pressure drops in the system
- Intelligent hot storage control with bypass or partitioned upper storage part, especially for purely solar driven cooling systems
- Use preferably cold distribution systems with high supply temperatures (e.g. 16°C / 18°C) and cold water storage:
    - Allow variable generator inlet temperatures according to the

temperature in solar hot water storage tank
    - Use backup heating system only if solar heat supply is not sufficient to reach the cold water temperature setpoint
    - Chose supply temperature from the backup heating-system as high as possible for a high thermal COP of the ACM.
- For cold distribution systems with low supply temperatures in case of dehumidification requirements (e.g. 7°C / 12°C):
    - Control of the generator inlet temperature for a constant cold water outlet temperature of the ACM
    - Use backup heating system only if solar heat supply is not sufficient to reach the cold water temperature setpoint.
- If any possible, use additional cooling with efficient compression chillers instead of additional heating and design the solar cooling system to cover not more than 40 to 60% of the maximum cooling load.

Don’ts

- Control with constant generator inlet temperature
- Cooling tower / dry heat rejection system with three-way valve control instead of fan speed control of the cooling water temperature
- Over dimensioning of pumps with constant volume flow
- Hydraulic design with too small tube cross sections, high tube length and rambling tubing resulting in high pressure drops
- Cold distribution pump without ΔT- mass flow control
- Solar system with only one big hot water storage tank without bypass or partitioned upper storage part.

5. MODEL BASED DEVELOPMENT OF PRIMARY ENERGY OPTIMISED CONTROL STRATEGIES FOR OPEN DESICCANT EVAPORATIVE COOLING SYSTEMS

5.1 INTRODUCTION

Conventional control strategies of open desiccant evaporative cooling systems (DEC) try to cover the required cooling load through a control cascade which switches on or off single components of the DEC system in dependence of the deviation between the setpoint and the actual measured room temperature. In the simplest case with cool and dry ambient air conditions first the air volume flow is increased, afterwards the return air humidifier and the heat exchanger between supply and return air are activated before the supply air humidifier is switched on for combined humidification. The sorption mode with startup of the sorption wheel and return air heater is very often considered as last control option in the control sequence if the maximum room air humidity is exceeded or if the supply air humidifier operates at full load and still more cooling energy is required to keep the room air below the upper threshold. The performance analysis of monitoring data of installed DEC systems showed very low solar system efficiencies of the installed collector fields (Eicker, et al., 2006) and moderate primary energy efficiencies with values between 1.2 and 1.7 (Henning, et al., 2002; Vitte, et al., 2008). Comparable systems with compression chillers with electricity supply from the local electricity grid reach primary energy efficiencies in the region of one or slightly below one (Vitte, et al., 2008). At dry and moderate climatic conditions the main reason for the low solar efficiency of the collector fields of DEC systems can be attributed to the fact that indirect or combined humidification is often sufficient to cover the required cooling load, especially if the system is operated at maximum air flow rate. Therefore, the sorption wheel is very seldom in operation. Additional reductions of the solar system efficiency result from constant regeneration temperatures implemented in some control strategies, although often much

lower regeneration temperatures would be sufficient to cover the required cooling load (Schürger, et al., 2006). Control optimised systems therefore operate at variable regeneration temperatures between 45°C and 90°C. Recent published analyses show that an early increase of the air volume flow rate is only favourable from the energy point of view, if the required regeneration heat cannot be provided by the solar system (Ginestet, et al., 2002 and 2003; Vitte, et al., 2008). Therefore, the regeneration mode should be activated with priority to the increase of the air flow rate if sufficient solar energy is available and the cooling load cannot be covered with combined humidification at the lowest possible air flow rate. .

5.2 SCOPE AND METHODOLOGY OF WORK

In the present work a primary energy optimised controller is developed for a DEC demonstration plant installed at the University of Applied Science in Stuttgart which has been newly set up in 2007 and 2008. This system is supposed to supply in future two smaller lecture rooms with fresh and cold air. The main idea of the new controller is to operate the DEC system at the lowest possible primary energy consumption. Therefore, the controller aims to cover the cooling load with preferably low supply air. The architecture of the new controller consists of a simple sequence controller which switches on or off the components of the DEC system depending on the room air temperature and room air humidity. Additionally, this sequence controller is supported by a primary energy optimiser, which evaluates continuously the optimum operation mode of the DEC system. The primary energy optimiser is an online simulation tool which consists of simplified simulation models of the relevant DEC components. For the development and test of the new controller a detailed dynamic simulation model of the installed DEC system including the collectors and the connected rooms has been developed in the dynamic simulation environment INSEL (Schumacher, 1991). Measured performance data of the system and the components were carried out in summer 2009 within this work, which are used for the validation of the developed simulation model. To demonstrate the efficiency of the new controller compared to simple and

optimised standard control strategies, simulations over a whole cooling period are performed for the DEC system. Finally the efficiency of the DEC system is compared to an efficient reference ventilation system with a cooling coil supplied by a compression chiller.

5.3 DESCRIPTION OF THE DESICCANT EVAPORATIVE COOLING SYSTEM

5.3.1 GENERAL SYSTEM DESCRIPTION AND COMPONENTS

The analysed DEC system is installed beneath the roof on the fourth floor of one of the buildings of the University of Applied Sciences in Stuttgart. The system was originally used as a test plant for tests of the efficiency of different desiccant wheels (Schürger, 2007). Apart from the desiccant wheel it consisted of a Rototherm rotary heat exchanger and two Munters contact matrix humidifiers, one for the return air and one for the supply air side. For the regeneration of the sorption wheels a 20 m² solar air collector field and a 18 m² vacuum tube collector field can be used. The vacuum tube collector field is connected to two 1000 l hot water storage tanks. When the solar air collectors are used, a water to air heat exchanger can supply additional heating to the regeneration air from the vacuum tube collectors. Before entering the sorption wheel an additional electrical air heater and a vapour humidifier were integrated in the system on the return and supply air side to enable system tests independent of the ambient conditions. At present the system is connected to a large presentation room in the fourth floor. It has been newly set up in 2007 and 2008 and some of the components have been exchanged or removed. New fans with Hitachi frequency inverters for variable air flow have been integrated in the system. Due to the higher power of the fans the maximum air flow rate on the supply and return air side is now increased to 3000 m³ per hour. On the supply air side the contact matrix humidifier has been removed by a new hybrid spray humidifier including a water treatment system. This system offers much higher hygienic security and a better control of the supply air humidity.

Furthermore, all temperature and humidity sensors have been replaced and connected to the Siemens Desigo control system to ensure a more accurate measurement. On the supply air side an additional water to air heat exchanger has been integrated in the system for solar heating in winter operation. The new system setup is shown in Fig. 5-1. A more detailed description of the installed components is shown in Table 5-1 to Table 5-4. Within this work the whole cabling of the system components, the sensors and actuators was done and connected to the Siemens Desigo control unit. Furthermore, the control in the Siemens Desigo control unit was newly programmed together with a programmer from Siemens.

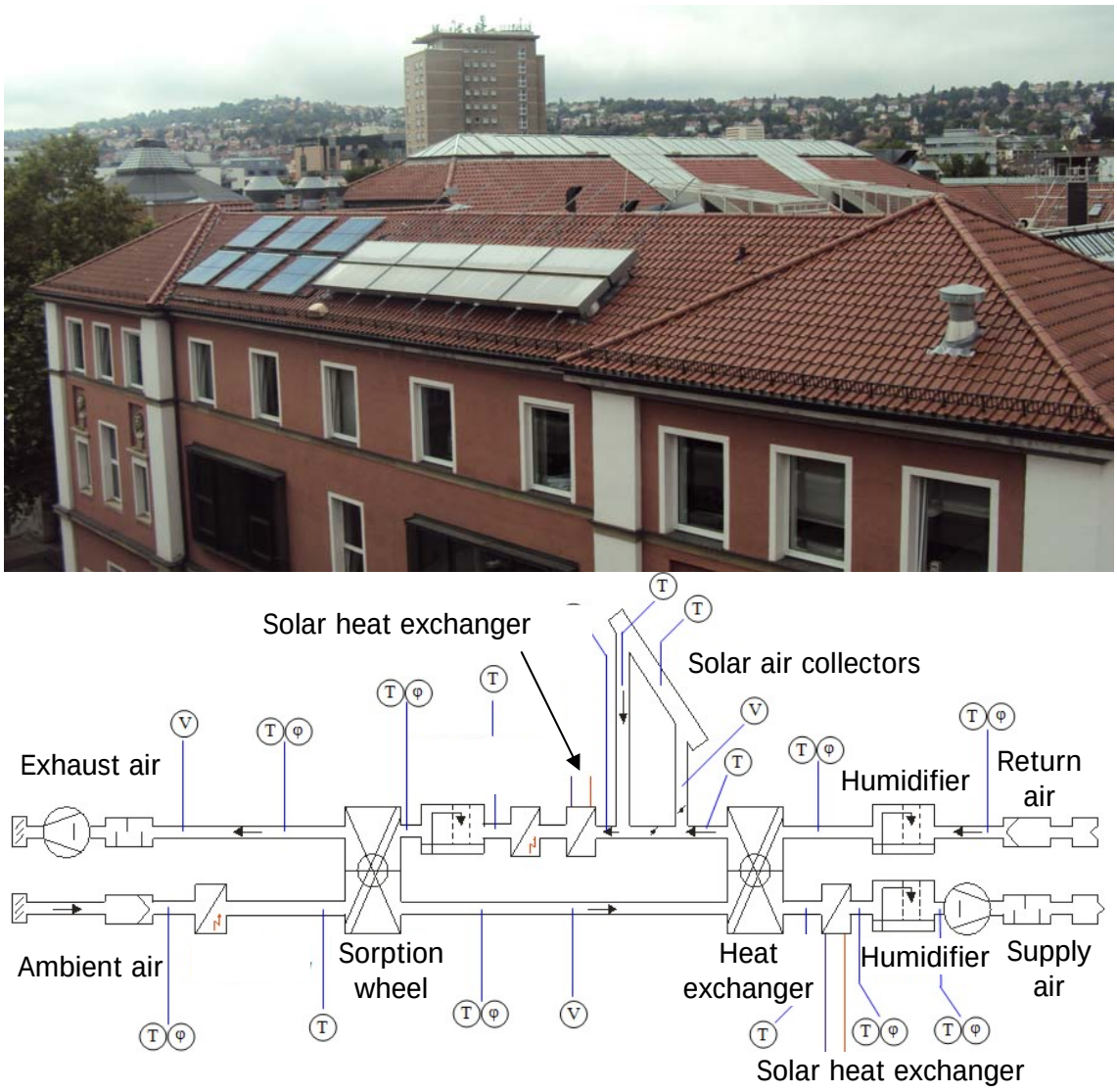

Fig. 5-1: Picture and schematic diagram of the installed DEC system

The electricity consumption of the system is mainly caused by the fans which need to overcome the pressure drop of the system. The technical data of the installed ventilator types are described in Table 5-1 together with the measured total pressure rise and the resulting electrical power demand at a nominal air flow rate of 3000 m³/h for the supply air fan and 3200 m³/h for the return air fan. For the return air fan the values are given for both the regeneration mode with the return air drawn through the air collectors and the standard mode with opened collector bypass. The technical data of the other main components of the installed DEC system are summarised in Table 5-2.

Table 5-1: Ventilators installed, pressure drop and electrical power demand

Ventilators	Type	Air volume flow rate [$m^3 h^{-1}$]	Total measured preassure drop [Pa]	Efficiency [%]	Electrical power [kW]
Supply air ventilator	Gebhard radial ventilator PLT-Compact Type P2M-H3F2J-RRB	3000	2200	70	2.62
Return air ventilator, with air collectors connected	Gebhard radial ventilator PLT-Compact Type P2M-J6B2K-RRB	3200	2670	70	3.39
Return air ventilator, without air collectors		3200	2070	70	2.63

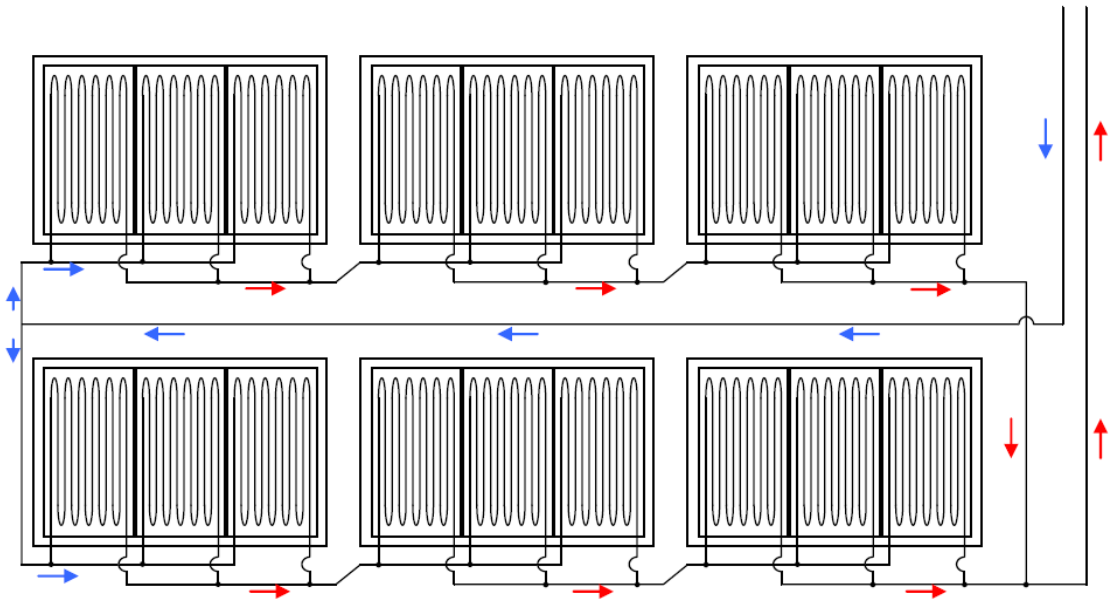

Fig. 5-2: Connection of the 18 Tubo CPC 12 collectors

The liquid solar collector field consists of 18 TUBO CPC 12 vacuum tube collectors produced by CONSOLAR. Three modules are interconnected in parallel to one big module. The resulting 6 big modules are connected in two rows with three big modules connected in series. The two collector rows are connected in parallel according to the Tichelmann principle. The connection of the installed collectors is shown in Fig. 5-2 and the technical data is presented in Table 5-3. The collector field is connected to two 1000 l hot water storage tanks with 10 cm thermal isolation. The two storage tanks are connected in parallel.

The installed solar air collector field consists of 8 Grammer GLK 3 air collectors connected in series with 2.51 m² gross collector area and 2.3 m² aperture area per collector. The total gross collector area is 20 m². The maximum recommended air volume flow rate of the collectors is 2300 $m^3\ h^{-1}$. At the maximum return air flow rate of the installed DEC system of 3200 $m^3\ h^{-1}$ the pressure drop of the collector field increases to 660 Pa, which clearly demonstrates that such high air flow rates should be avoided in any case. In order to significantly reduce the pressure drop of the collector field and to avoid too high temperature peaks at collector startup, only 50 % of the actual return air flow rate (max. 3000 $m^3\ h^{-1}$) is passed through the air collector field and mixed afterwards with the remaining part of the return air. This control increases the heat losses in the collector field due to higher temperatures by max. 9 % at maximum solar irradiation, but at the same time significantly decreases the electricity consumption of the return air ventilator by more than 15 %. The higher heat losses of 9 % reduce the regeneration temperature obtained from the solar air collector only by 3 K at 1500 $m^3\ h^{-1}$ air flow rate. This small temperature difference has nearly no influence on the cooling power reached and therefore is negligible in terms of the overall system efficiency. The reduced electricity consumption on the other hand improves the primary energy efficiency of the system remarkably. The technical data of the installed GLK 3 collectors is summarised in Table 5-4.

Table 5-2: Technical data of the main components of the installed DEC system

1. Engelhard HexCore desiccant wheel			
Matrix material	HexCore Nomex™	Wheel depth	320 mm
Desiccant type	HexCore ETS™ (titanium silicate)	Wheel diameter	950 mm
Matrix structure	Honeycomb	Nominal heat recovery efficiency	80 %
Wheel depth	140 mm	Pressure drop at 3000 m³/h air flow rate	90 Pa
Wheel diameter	870 mm	Average electrical power demand	90 W
revolutions per hour	15-100 (winter)		
face velocity	2 – 2.6 m/s	**4. CONDAIR hybrid supply air humidifier**	
Regeneration temperature	55°C to 85°C (max. 120°C)	Hybrid supply air humidifier	CONDAIR DUAL
Average electrical power demand	50 W	Number of spray nozzles	9
2. Rototherm rotating heat exchanger		Controllable stages	7
Type	PT 10W 950 320 V70	Humidifier matrix for additional humidification	Control accuracy
Wheel depth	320 mm	Water disinfection system	Silver ion cartridge
Wheel diameter	950 mm	Humidification efficiency	88%
Nominal heat recovery efficiency	80 %	Average electrical power	65 W
Pressure drop at 1500 m³/h air flow rate	90 Pa	Water softening system	CONDAIR Soft PEH
Average electrical power demand	80 W	Reverse osmosis system	CONDAIR AT
3. Munters contact matrix return air humidifier		**4. Solar water to air heat exchanger**	
Type	FA4-95-090-060-C1-0-R/L	Helios High Vent	WHR 4/60/35-30
Contact matrix	GLASdek	Heating power at 0°C air temperature and 90/70°C fluid temperature	51 kW
Matrix height	675 mm	Width / height / depth [m]	0.650/0.40/0.30
Matrix length	900 mm	Nominal air flow rate	4 500 $m^3 h^{-1}$
Matrix width	350 mm	Electrical power demand heat exchanger pump	50 W
Nominal humidification efficiency	95 %	Pressure drop air side, at 3000 m³/h	150 Pa

Table 5-3: Technical Data of the vacuum tube collector field TUBO CPC 12

Collector type	TUBO CPC 12	Number of collector	18
Collector aperture area	0.980 m²	Collector mass flow rate	15 l m^{-2} h^{-1}
Collector efficiency related to the collector aperture area			
Maximum efficiency η_0	0.62	Linear heat loss coefficient a_1	0.395 W m^{-2} K^{-1}
Quadratic heat loss coefficient a_2	0.02 W m^{-2} K^{-2}	Area related heat capacity	6.73 kJ m^{-2} K^{-1}

Table 5-4: Technical Data of the Grammer Solar GLK 3 solar air collectors

Collector type	GLK 3	Number of collectors	8
Collector gross area	2.51 m²	Collector aperture area	2.30 m²
Collector efficiency related to the collector aperture area			
Maximum efficiency η_0	0.82	Linear heat loss coefficient a_1	4.2 W m^{-2} K^{-1}
Quadratic heat loss coefficient a_2	0.034 W m^{-2} K^{-2}	Collector length	2500 mm
Collector width	1003 mm	Collector height	175 mm

5.3.2 DESCRIPTION OF THE CONTROL SYSTEM

For the control of the DEC system a Siemens control unit has been implemented. This unit consist of a Building Process Station (BPS) with Visonik control software for PC independent plant operation. The programming language used is COLBAS, a special Siemens language which is quite close to BASIC. The BPS consists of a micro controller which is connected to I/O elements for plant observation and control. A system scheme and a table in Appendix D give an overview of the connected I/O elements and their sensor connection or control tasks.

For visual plant observation and manual control the BPS is connected via TCPIP (Ethernet) with a master PC. On this PC a Siemens DESIGO Insight BMS software is installed, which enables the direct communication with the BPS and offers a system scheme for graphical visualisation of the actual plant performance.

Fig. 5-3 shows a screen shot of this graphical surface where parts of the plant can be either operated automatically or set to manual operation. For automatic operation the system performs according to the program code with different control sequences. For more detailed performance observation and storage of time series the so called trend viewer can be used. Within this tool several datapoints of the DEC system can be selected and are visualised on simple line graphs.

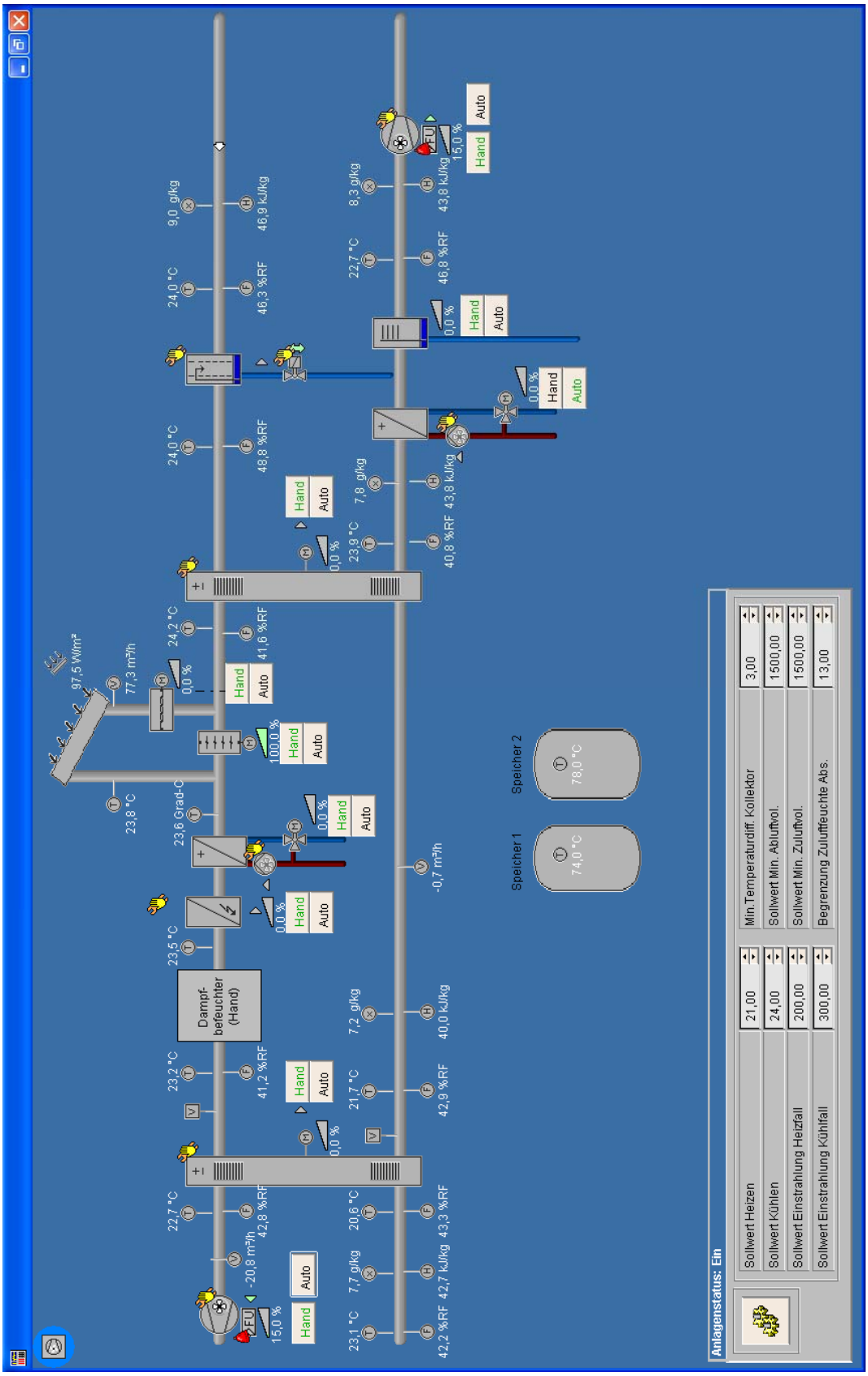

Fig. 5-3: Screen shot of the DESIGO Plant Viewer of the installed DEC System

The time series of the different datapoints shown here are permanently stored in an internal database. If required for further analysis these datasets can be transferred to either CSV of Excel files. For online data exchange with external tools (e.g. simulation tools) the Siemens DESIGO Insight software offers an OPC client. The structure of the Siemens Desigo Insight BMS system and the possibilities for external data exchange are shown in Fig. 5-4.

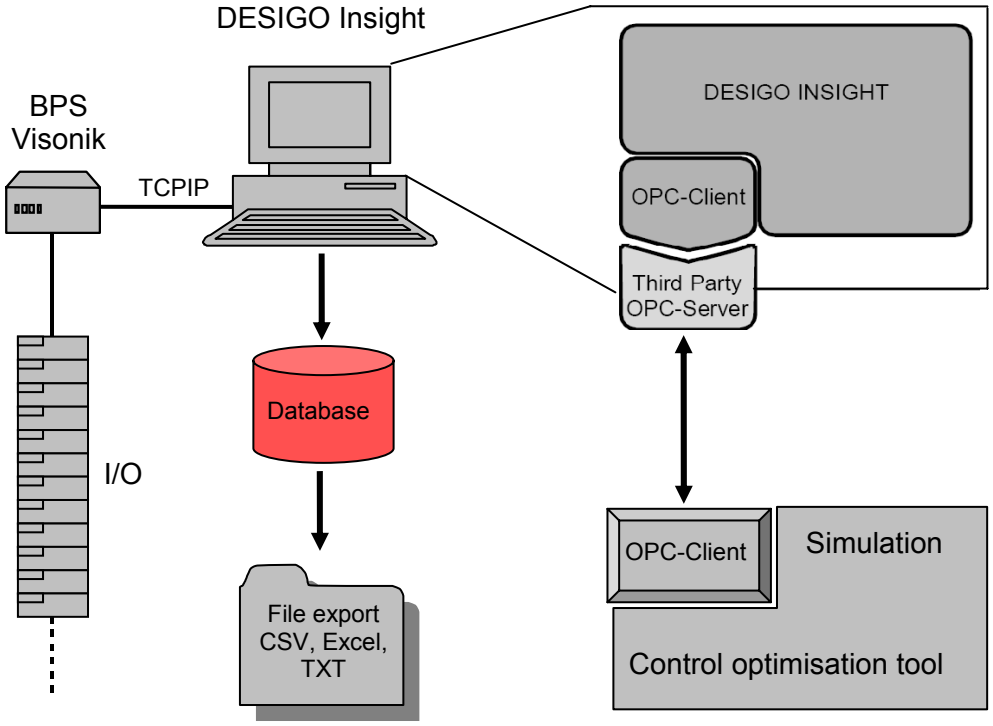

Fig. 5-4: Data communication structure of Siemens DESIGO Insight system

5.3.3 CONNECTED ROOMS, PRESENT AND FUTURE SITUATION

At present the DEC-system is connected to a large presentation room on the fourth floor directly below the roof. This room has a floor area of several hundred square metres and a huge glazing integrated in the top of the roof without sun protection. Due to the large cooling load in this room, the maximum sensible cooling power provided by the installed DEC system of 10 kW is far too low and has nearly no influence on the room temperature. To overcome this unsatisfactory situation, it is planned to connect the DEC system to two smaller seminar rooms in the third floor below the presentation room. The seminar

rooms offer a floor area of 71 m² and 79 m² each for around 25 students. The maximum sensible cooling load of the two rooms together is 10 kW which gives 67 W per square metre conditioned floor area. A ground floor plan and some pictures of the façade and of the seminar rooms are shown in Fig. 5-5.

Fig. 5-5: Floor plan and pictures of the two seminar rooms to be conditioned by the DEC system

The material and thermal properties of the rooms surrounding structure are shown in Table 5-5. All room walls including the external wall are made of brickwork with plaster finishing on the room facing surfaces. The room is equipped with a suspended acoustic ceiling and has a hard wooden floorage. The windows in the southwest facing façade are double glazed but without external sun shading system.

Table 5-5: Material and thermal properties of the room surrounding structure

Description	d [m]	λ [W $m^{-1}K^{-1}$]	d/λ [m^2 K W^{-1}]	$1/h_{c+i}$ [m^2K W^{-1}]	ρ kg m^{-3}	C J kg^{-1} K^{-1}
External wall						
Heat transfer coefficient inside				0.13		
Plaster	0.015	0.87	0.02		1800	1050
Brickwork	0.6	1.18	0.51		1600	1050
Plaster	0.015	0.87	0.02		1800	1050
Heat transfer coefficient outside				0.04		
U-Value	**1.39**	W m^{-2} K^{-1}				
Internal walls						
Heat transfer coefficient inside				0.13		
Plaster	0.015	1	0.02		1800	1050
Brickwork	0.24	0.56	0.43		1300	1050
Plaster	0.015	0.87	0.02		1800	1050
Heat transfer coefficient outside				0.13		
U-Value	**1.37**	W m^{-2} K^{-1}				
Floor						
Heat transfer coefficient inside				0.17		
Hard wooden floorage	0.022	0.13	0.16		600	1160
Floating floor	0.045	1.4	0.032		2200	1050
Insulation	0.025	0.04	0.625		50	1050
Concrete ceiling	0.25	2.1	0.12		2300	1050
Insulation	0.025	0.04	0.625		50	1050
Gypsum plaster board	0.0125	0.9	0.016		1200	1050
Heat transfer coefficient outside				0.13		
U-Value	**0.49**	W m^{-2} K^{-1}				
Ceiling						
Heat transfer coefficient inside				0.13		
Gypsum board	0.0125	0.9	0.016		1200	1050
Isolation	0.025	0.04	0.625		50	1050
Concrete ceiling	0.25	2.1	0.12		2300	1050
Isolation	0.025	0.04	0.625		50	1050
Floating floor	0.045	1.4	0.032		2200	1050
Hard wooden floorage	0.022	0.13	0.16		900	1050
Heat transfer coefficient outside				0.17		
U-Value	**0.49**	W m^{-2} K^{-1}				

The minimum air volume flow at full occupation is calculated according to the humidity and CO_2 emissions of the persons in the room and the upper comfort limit for the room air humidity of 12 g/kg and the upper limit of CO_2 concentration of 1000 ppm according to the ASHRAE standard (ASHRAE 1989). If a humidity exposure of 50 g per hour and a CO_2 exposure of 18 l per hour are considered for each person at low degree of activity, a minimum fresh air flow rate of 30 m³ per person and hour is required to keep both the humidity ratio and the CO_2-concentration of the room air within the comfort limit. This minimum air flow rate is calculated for supply air with a maximum absolute humidity of 10 g per kg and a maximum outdoor CO_2-concentration of 300 ppm. The resulting minimum air flow rate of 30 m³ per person and hour is exactly equal to the recommended minimum air flow rate defined in the national standard DIN 1946-2 (2005 replaced by DIN EN 13779).

If the two rooms are fully occupied with 25 persons a minimum air volume flow rate of 750 m^3h^{-1} is required per room which is equal to around three air changes per hour and gives a minimum air flow rate of the DEC system of 1500 m^3/h^{-1} when both rooms are occupied and 750m^3 h^{-1} when only one room is occupied. To increase the cooling power this minimum air flow rate can be increased to 3000 m^3 h^{-1} which gives a maximum air change rate in the two rooms of around 6 air changes per hour.

Without finance support it was not possible to really connect the DEC system to the two seminar rooms within this work. Therefore, the present work focuses only on the theoretical analysis of the new situation in the simulation environment.

5.3.4 ROOM UTILISATION

The two seminar rooms described in section 5.3.3 will be the only actively cooled seminar rooms at the University of Applied Sciences in Stuttgart if connected to the DEC system. Therefore, it is expected that these two rooms are not only used during semester but also during the summer break for summer school and additional course offers. The utilisation profiles shown in Table 5-6 have been developed for the two seminar rooms and are considered in the simulation based control analysis of the DEC system. The rooms are named as Seminar Room 1 (S1: bigger room) and Seminar Room 2 (S2: smaller room).

Table 5-6: Utilisation profile of the two seminar rooms

Time of day	Monday		Tuesday		Wednesday		Thursday		Friday	
	S1	S2	S1	S2	S1	S2	S1	S2	S1	S2
08:00 – 09:30	25	0	25	25	0	25	25	0	25	0
09:30 – 09:45	10	0	10	10	0	10	0	0	10	0
09:45 – 11:15	25	25	25	0	25	25	0	25	25	25
11:15 – 11:30	0	0	10	0	10	10	10	10	10	10
11:30 – 13:00	0	0	25	25	25	25	25	25	25	25
13:00 – 14:00	0	0	5	5	5	5	5	5	0	0
14:00 – 15:30	25	25	25	25	25	25	25	25	0	0
15:30 – 15:45	10	10	10	10	10	10	10	10	0	0
15:45 – 17:15	25	25	25	25	25	25	25	25	0	0

5.4 SIMULATION MODELS AND VALIDATION

A complete model of the installed solar driven desiccant cooling system has been developed in INSEL. The model includes the solar air collector field, the vacuum tube collectors with heat exchanger and the two 1000 l hot water storage tanks, the DEC system with sorption wheel, heat exchanger and the two humidifiers and the system controller with a primary energy optimisation tool which is described in detail in section 6.5.2. Apart from the thermal part the model also considers the electricity consumption of all components like the return and supply air fan, the primary and secondary pumps of the solar system, the pumps of the humidifiers and the motors of the desiccant and heat exchanger wheel. The electricity consumption of the ventilators at nominal air flow rate given in Table 5-1 (3200 $m^3\ h^{-1}$ return air and 3000 $m^3\ h^{-1}$ supply air) is used to calculate the electricity consumption in dependence of the actual air volume flow rate. It can be assumed with sufficient accuracy that the electricity consumption of the fans decreases with the third power of the ratio between the actual air volume flow rate and the nominal air volume flow rate (equation 5-1).

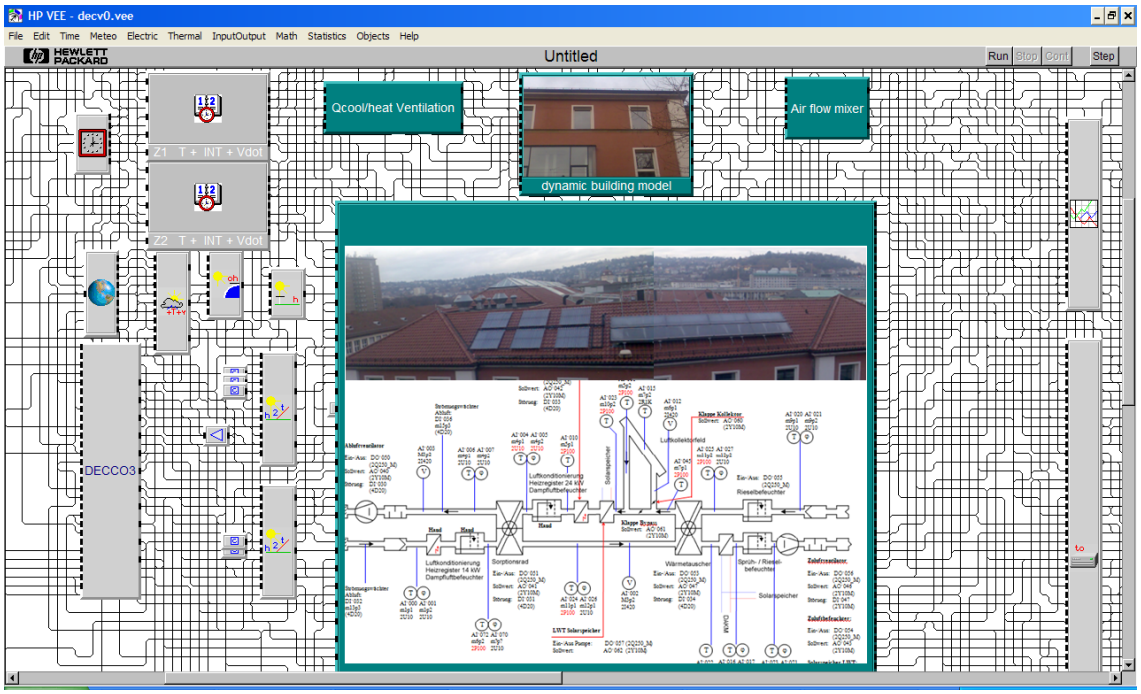

Fig. 5-6: Complete model of the DEC system with connected seminar rooms

$$P_2 = P_1\left(\frac{n_2}{n_1}\right)^3 = P_1\left(\frac{\dot{V}_2}{\dot{V}_1}\right)^3 \quad (5\text{-}1)$$

The temperature increase of the supply and return air through the ventilators mainly depends on the total pressure increase and the efficiency of the fan and can be calculated by the empirical approximation shown in Equation (5-2).

$$\Delta T_{air} = \frac{\Delta p_{fan}}{1200 \cdot \eta_{fan}} \quad (5\text{-}2)$$

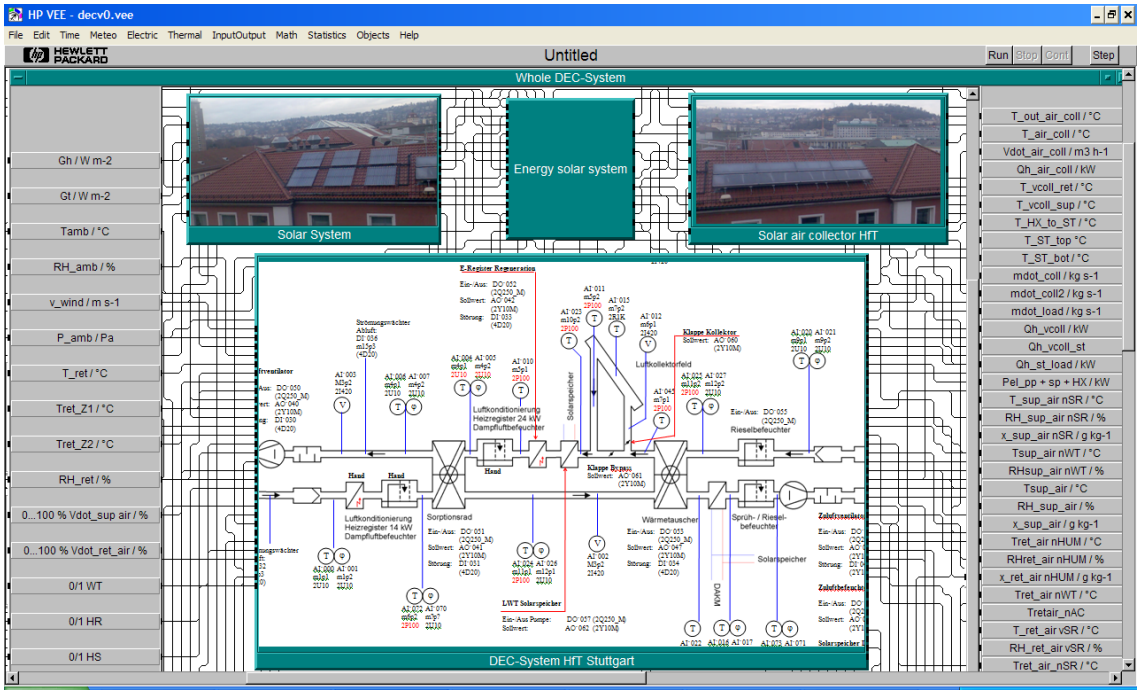

Fig. 5-7: More detailed view into the DEC system with solar collectors

Due to the high complexity of the model it is not possible to show the whole developed model in one graph. Therefore only a model overview of the main components is shown in Fig. 5-6 and Fig. 5-7. The green coloured boxes with pictures are user blocks with the detailed model of the components behind. For a more detailed view these boxes can be opened by double click with the left mouse button on the box. Fig. 5-8 represents the detailed view of the model of the DEC system. For model validation measured performance data of the installed DEC system obtained from preliminary tests during the summer of 2009 are used. The validation results are shown in the following paragraphs

component by component. For the evaluation of the accuracy of the developed model a relative error is used which is defined as the difference between measured and simulated value divided by the measured value. The results are given in %. Additionally, the absolute error is shown in brackets.

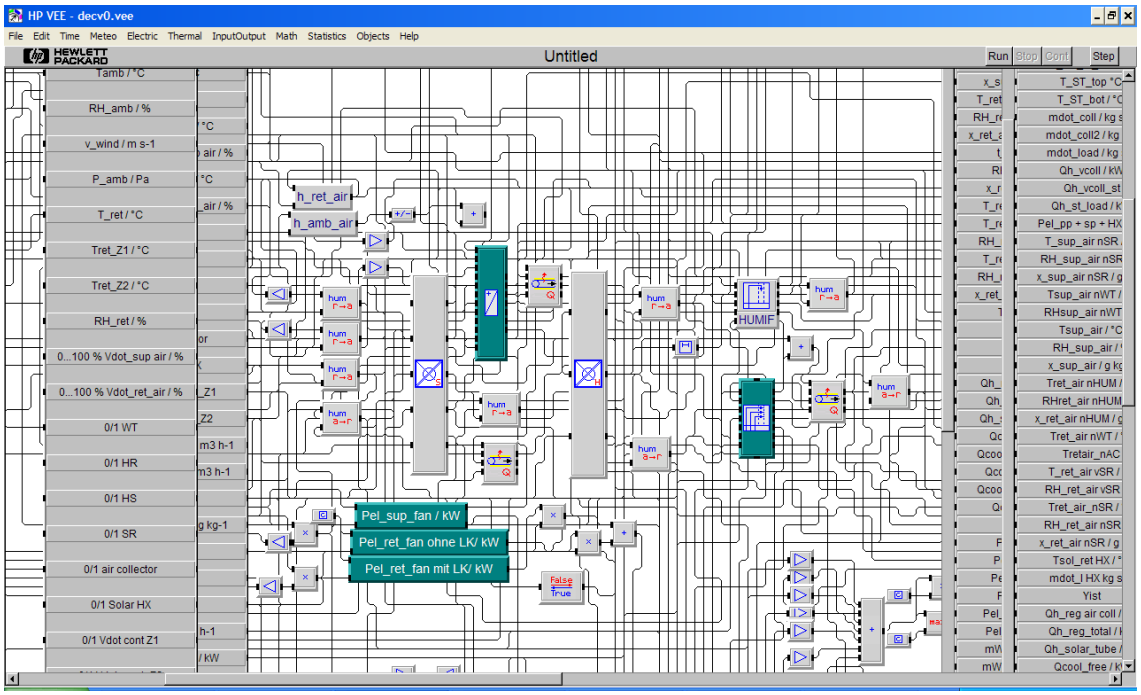

Fig. 5-8: Detailed view into the DEC system model

5.4.1 DESICCANT WHEEL

The model used for the sorption wheel is based on the simple dehumidification efficiency model described in section 2.3.1. This model calculates the maximum possible dehumidification using the assumption that the supply air at sorption wheel outlet can be dried at maximum to the relative humidity of the regeneration air. Using this condition the supply air temperature after the sorption wheel is calculated iteratively from the enthalpy equation and the condition that the enthalpy of the supply air does not change during the adsorption process (isenthalpic dehumidification). From the given relative humidity and temperature after the sorption wheel the absolute humidity of the ideally dried supply air can be calculated. The dehumidification efficiency considers the fact that the ideal dehumidification is not reached by real desiccant wheels due to irreversibility, binding enthalpy etc.. The

dehumidification efficiency is typically 0.8 for most market available silicagel wheels. Therefore, this value is also used in the model for the installed HEXCORE wheel. Further influences like variable air flow rates, rotation speed and the ratio between the supply air and regeneration air volume flow rate are not considered in the model, since the rotation speed and air flow ratio are constant and the system is operated most of the time at 1500 m^3h^{-1} on supply and return air side. The ideally reached dehumidification (difference between the absolute humidity at sorption wheel inlet and at sorption wheel outlet) is multiplied by the dehumidification efficiency of the wheel and then added to the absolute humidity of the supply air at sorption wheel inlet. With this absolute humidity the outlet temperature of the supply air at sorption wheel outlet is calculated by iteration assuming isenthalpic dehumidification. From the resulting temperature and absolute humidity the relative humidity of the supply air is calculated. For validation of the sorption wheel model measured performance data of the installed DEC system of a dehumidification process with decreasing regeneration temperature was used. The results are shown in Fig. 5-9 for the supply air side and in Fig. 5-10 for the return air side.

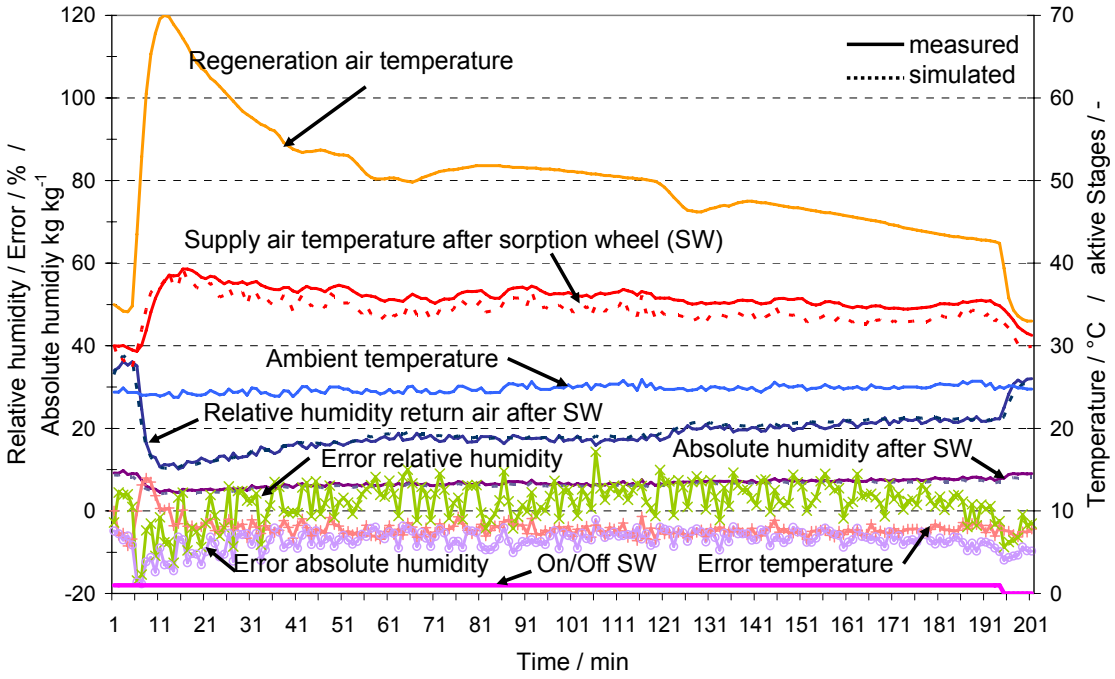

Fig. 5-9: Comparison of measured and simulated performance of the desiccant wheel for the supply air side at 1500 m^3h^{-1} air volume flow on the return and supply air side

As visible from the graphs, a good correlation between the measured and simulated performance of the sorption wheel is reached. The relative error for the predicted outlet temperatures vary between 10% (~3.8 K) at system startup and around – 4% (~1.5 K) during operation for the supply air and between 10% (~3.5 K) at system startup and -10% (~3.0 K) at shut down and -2% (~0.7 K) during operation for the return air. The larger relative errors at system startup and shut down are attributed to the omitted inertia of the sorption wheel. However, over the whole period the average relative error for the predicted outlet temperatures is only 4.2% (1.5 K) on the supply air side and 1.4% (0.6 K) on the return air side.

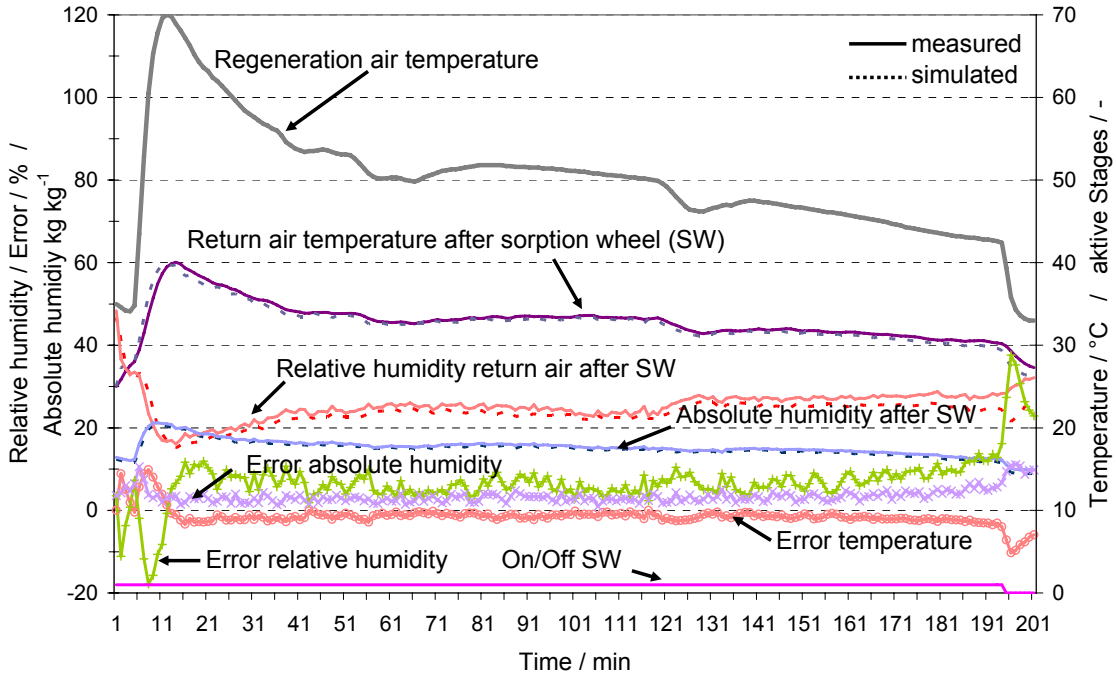

Fig. 5-10: Comparison of measured and simulated performance of the desiccant wheel for the return air side at 1500 m^3h^{-1} air volume flow on the return and supply air side

Larger absolute errors occur between the predicted and measured relative humidity, which is partly caused by the error in predicted temperature but can also be attributed to larger measurement errors of the humidity sensors at low relative humidity. As visible from the graphs the relative error in relative humidity of the return air after sorption wheel varies between 2% (~0.5 %RH) and 10% (~2.5 %RH) during wheel operation and rises up to – 18% (~5.0 %RH) at system startup and very shortly up to 28% (~7.8 %RH) at system shut down.

The high absolute error at system startup and shut down are again attributed to the omitted inertia of the sorption wheel and mainly results from the error in predicted temperature. This becomes obvious if the relative error of the return air humidity after sorption wheel is regarded, which is only 10% (~1.2 g kg^{-1}) in maximum at system startup and -10% (~1.4 g kg^{-1}) in maximum at system shut down (Fig. 5-10). The average relative error over the whole period is 7 % (1.7%RH) for the relative and 3.5 % (0.5 g kg^{-1}) for the absolute humidity of the return air at sorption wheel outlet.

For supply air similar errors can be observed. Here for the relative humidity the relative errors observed are between -10 % (~2%RH) and +10%(~2%RH) with strong fluctuations in between. This of course results in large fluctuations of the absolute humidity with relative errors between –3 % (~0.24 g kg^{-1}) and –12 % (~0.96 g kg^{-1}). The average relative errors are +1.9 % (0.3%RH) for relative humidity and -7.2 % (0.51 g kg^{-1}) for absolute humidity at sorption wheel outlet. As already discussed above, the main reason for the large deviations at system startup and shut down is the omitted inertia of the sorption wheel. Since this error occurs only for very short time periods, the influence on the overall system performance is negligible low. The large fluctuations of relative and absolute humidity result from the fluctuations of the measured ambient air temperature and ambient air relative humidity. In the real sorption wheel these fluctuations are buffered by the thermal capacity of the sorption wheel. In the simulation a static model is used. Therefore, no storage effects are considered and the outlet conditions vary with the inlet conditions. However, if the measurement inaccuracies of humidity sensors at low relative humidity are considered, which can easily reach 20 % and more, the relative errors found are acceptable. Therefore, all together the model can be regarded as sufficiently accurate.

5.4.2 HEAT EXCHANGER

As described in section 2.3.2 a simple efficiency model is used for the rotation heat exchanger. The heat exchanger is operated at 1500 m^3h^{-1} most of the time with 10 rotations per minute. At an air volume flow rate of 1500 m^3h^{-1} on both sides the heat exchanger reaches a heat recovery efficiency of 84 % which is

considered in the model. For higher air volume flow rates the efficiency decreases slightly to 80 % at 3000 m³/h. This nearly linear decrease in efficiency is considered in the model by a correction factor. For validation of the model measured performance data of the installed system was used. Fig. 5-11 shows as an example the measured and predicted performance of the heat exchanger at variable air temperatures. A comparison of the heat exchanger outlet temperatures show a very good correlation between measured and predicted temperatures. At startup of the heat exchanger the relative error increases shortly to 10% (3 K) on the supply air side and to slightly below -10% (3 K) on the return air side. During operation the absolute error varies around 3% (~1.1 K) on the supply air side and around 1.5 % (0.4 K) on the return air side. The average absolute error is 1.1% (0.3 K) on the return air side and 2.6% (0.8 K) on the supply air side. The larger errors at system startup can be attributed to the omitted inertia of the heat exchanger wheel. All together a high accuracy is reached with the quite simple model which is sufficient for the analyses performed within this work.

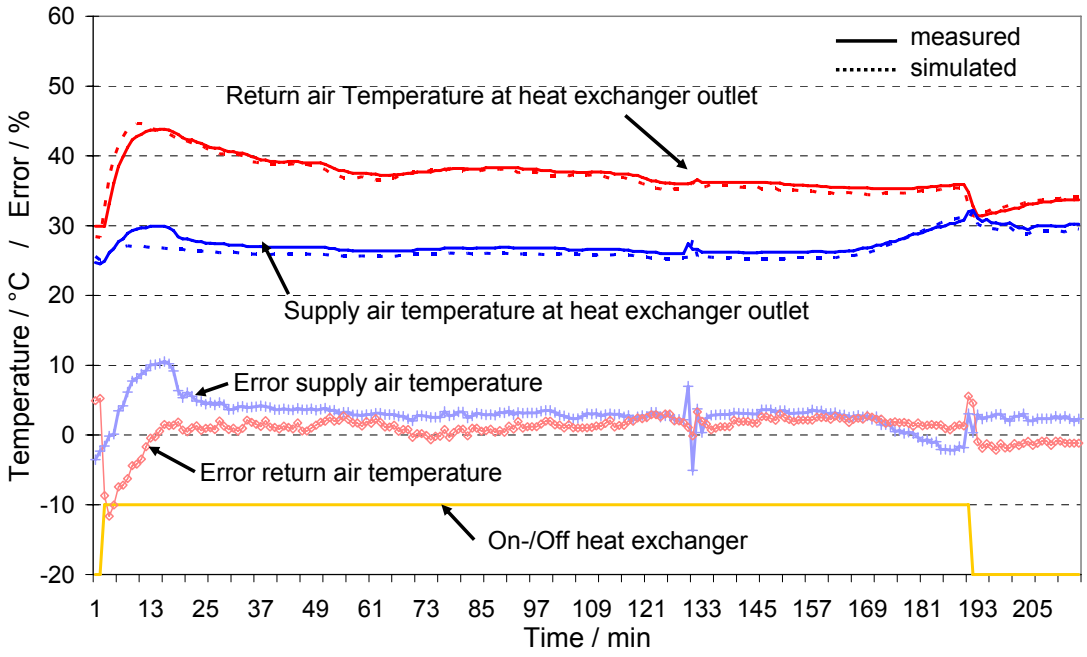

Fig. 5-11: Comparison of measured and simulated performance of the heat exchanger with 1.500 m^3h^{-1} air volume flow rate on the return and supply air side

5.4.3 RETURN AIR HUMIDIFIER

As described in section 2.3.3 a dynamic simulation model has been developed for the return air humidifier which considers the water storage capacity of the matrix used. For model validation and parameter fit, measured performance data of the installed DEC system were used. The parameters of the model found for the installed humidifier are shown in Fig. 5-12.

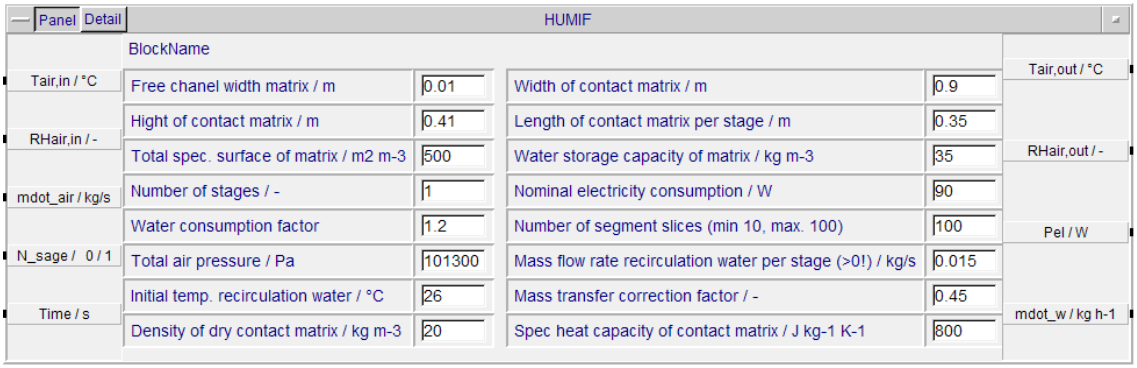

Fig. 5-12: Parameters of the return air humidifier model

A comparison of measured and simulated performance of the humidifier is shown in Fig. 5-13 for 3000 $m^3\ h^{-1}$ air volume flow rate and in Fig. 5-14 for 1500 $m^3\ h^{-1}$ air volume flow rate. As visible from these two figures a very good correlation between model and real humidifier performance is reached for different air volume flow rates. Larger errors only occur shortly at startup and after shut down at the very end of the humidifier drying process. Here the relative errors can increase up to 20% (12%RH / 6.4 K) but only for a quite short time period. The reasons for the large errors at the very end of the matrix drying process are diffusion resistances of the matrix structure at low water content, which are not considered in the model. However, the average relative errors over the whole period are below 1 % (0.9%RH / 0.2 K) for both analysed air flow rates. Therefore, a very precise model has been developed which predicts the humidification performance of the return air humidifier not only during operation but also at system startup and after cut off of the water supply during the drying phase of the matrix with sufficient accuracy, even at different air volume flow rates.

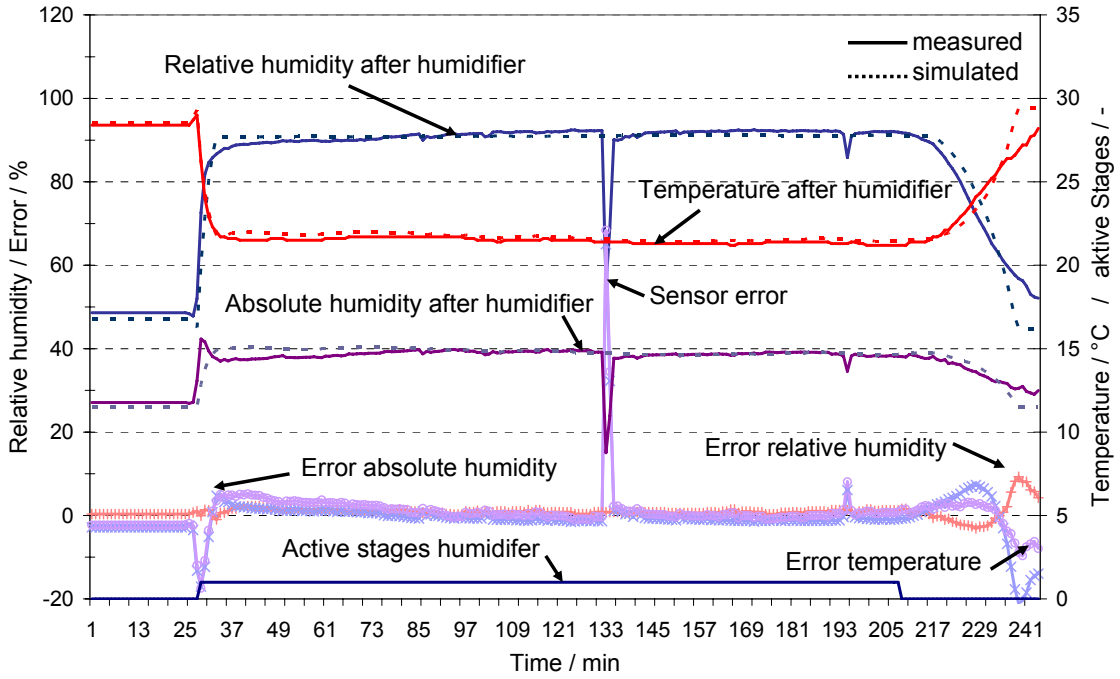

Fig. 5-13: Comparison of measured and simulated performance of the return air humidifier at 3000 m^3h^{-1} air volume flow rate

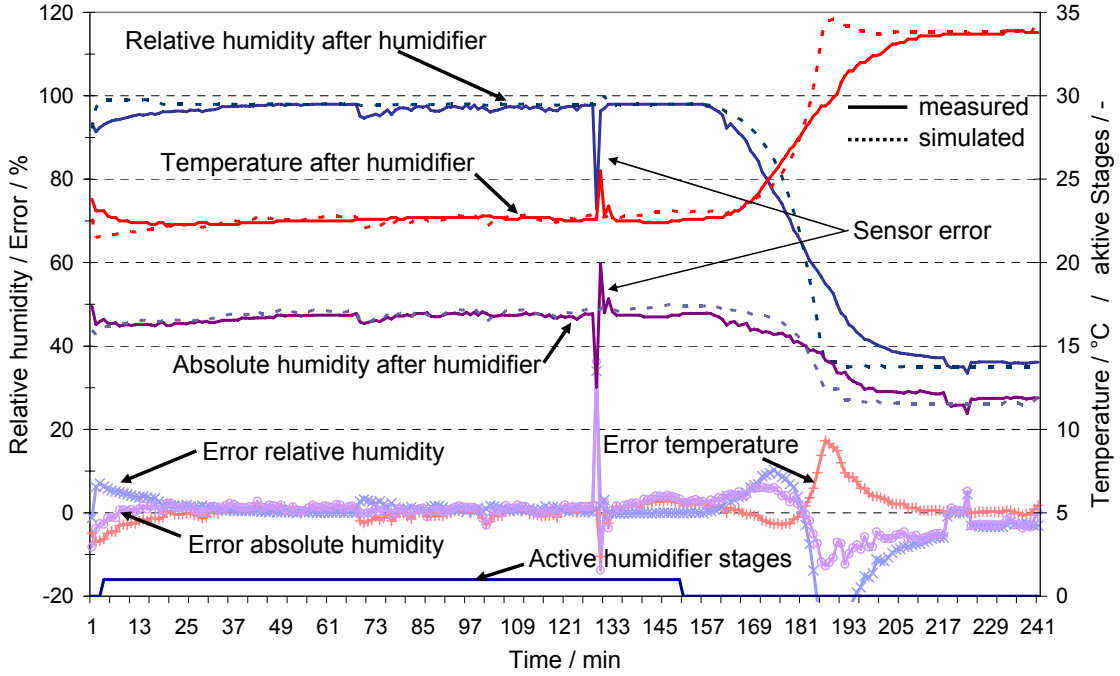

Fig. 5-14: Comparison of measured and simulated performance of the return air humidifier at 1500 m^3h^{-1} air volume flow rate

5.4.4 SUPPLY AIR HUMIDIFIER

As described in section 5.3.1 a hybrid humidifier has been integrated in the system for supply air humidification. This humidifier consists of a spray humidification part with adjacent ceramic matrix for additional humidification. This humidifier shows nearly the same behaviour as a pure contact matrix humidifier but is much more controllable. However, the development of a fully dynamic model for this type humidifier is very complex and difficult to solve. Therefore, in principle the same model is used as described for the return air humidifier in section 2.3.3. In order to be able to describe properly the seven control stages seven humidifiers are connected in series. Since the ceramic contact matrix is getting more and more saturated with increase in water supply the water storage capacity of the seven stages decreases with each additional stage. Fig. 5-15 represents the analogous model build up of seven contact matrix humidifier stages. For model validation and parameter fit measured performance data of the installed DEC system were used. Most of the parameters are the same for each of the humidifier stages as shown in Fig. 5-16 and Table 5-7.

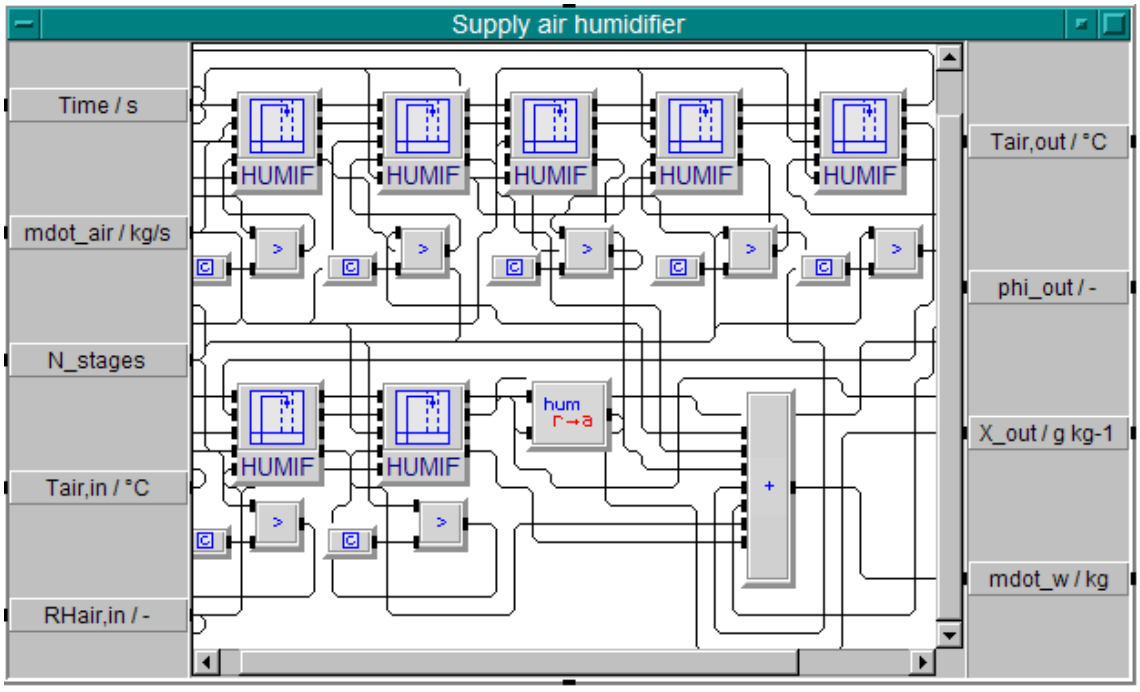

Fig. 5-15: Analogous model of the hybrid supply air humidifier build of contact matrix humidifier stages

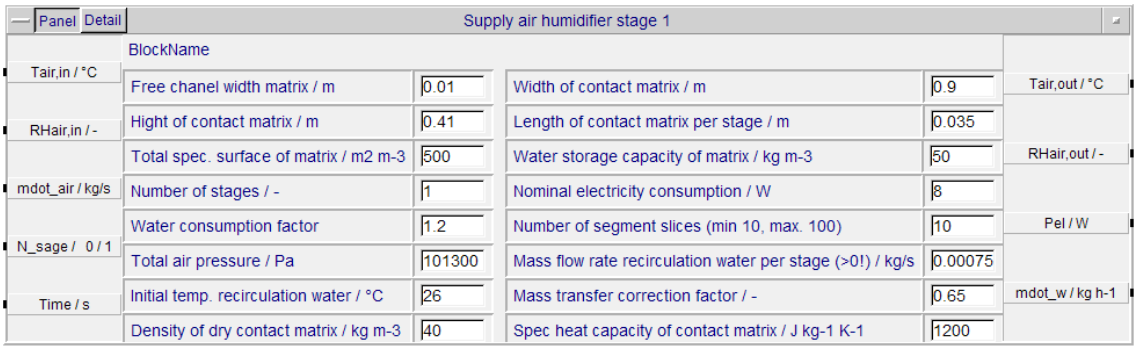

Fig. 5-16: Block template of the dynamic humidifier model with the parameters of the 7 humidifier stages as example for stage 1

The water storage capacity of the contact matrix used in the simulations is shown in Table 5-7 for each of the humidifier stages.

Table 5-7: Water storage capacity used for the humidifier stages

Humidifier stage	1	2	3	4	5	6	7
Water storage capacity of the matrix [kg m^{-3}]	50	40	35	25	15	8	2

A comparison of measured and simulated performance of the humidifier is shown in Fig. 5-17 for 1500 m^3 h^{-1} air volume flow rate and varied humidifier stages and in Fig. 5-18 for 3000 m^3 h^{-1} and constant air volume flow rate. As visible from these two figures a very good correlation between model and real humidifier performance is reached for different air volume flow rates. Fig. 5-17 furthermore demonstrates, that the simplified model also describes the performance of the supply air humidifier with different humidifier stages activated very precisely. Larger relative errors in predicted relative humidity only occur for a short time period at startup with errors up to 10% (6%RH) and after shut down at the very end of the humidifier drying process with errors up to and slightly above 20% (11%RH). The reasons for the large errors at the very end of the matrix drying process are diffusion resistances of the matrix structure at low water content, which are not considered in the model.

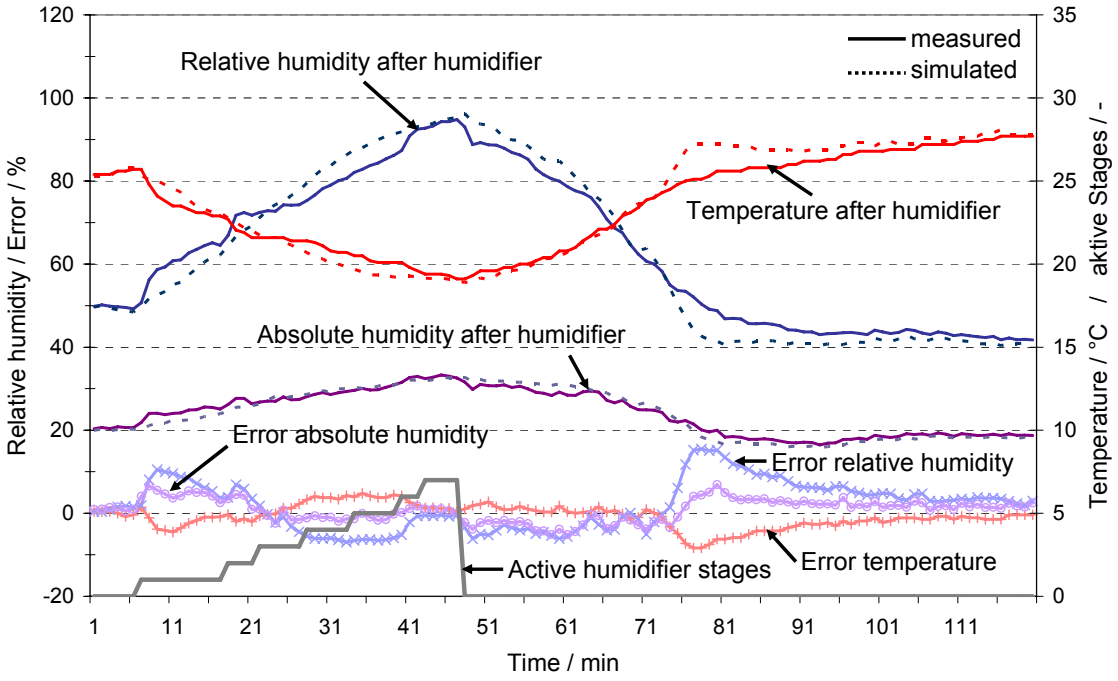

Fig. 5-17: Comparison of measured and simulated performance of the supply air humidifier at 1500 m^3h^{-1} air volume flow rate

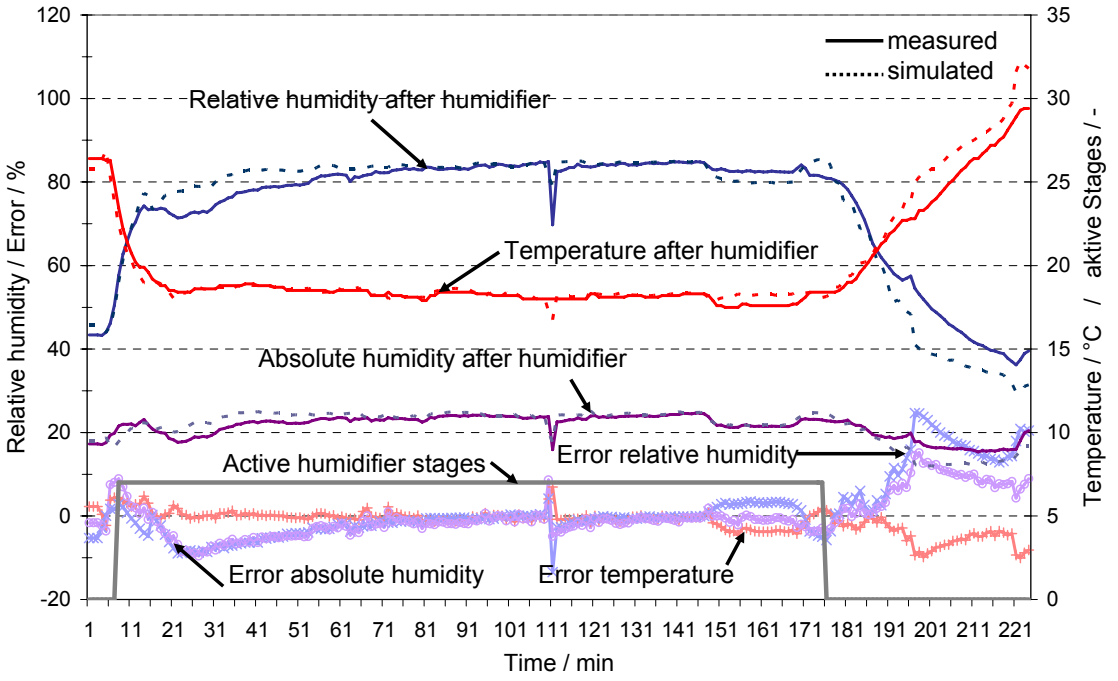

Fig. 5-18: Comparison of measured and simulated performance of the supply air humidifier at 1500 m^3h^{-1} air volume flow rate

For the predicted temperature and absolute humidity the relative error does not increase above 10 % (2.5 K / 1.4 g kg^{-1}) during the analysed periods. The average relative errors over the whole analysed periods are below 2 % (0.5 K / 1.2%RH / 0.2 g kg^{-1})for both analysed air flow rates. This clearly demonstrates that a quite precise model has been developed which predicts the humidification performance of the supply air humidifier not only during operation but also at system startup, for different humidifier stages and after cut off of the water supply during the drying phase of the matrix with sufficient accuracy.

5.4.5 SOLAR AIR COLLECTOR FIELD

As described in section 2.3.4 a dynamic model for solar air collectors has been developed in INSEL which is used for the simulation of the solar air collector field of the analysed DEC system of the University of Applied Sciences in Stuttgart. Fig. 5-19 offers a detailed view into the system model of the 20 m² solar air collector field including the tubing with a 5 m long tube on the supply side and a 8 m long tube on the return side, both with a diameter of 25 cm.

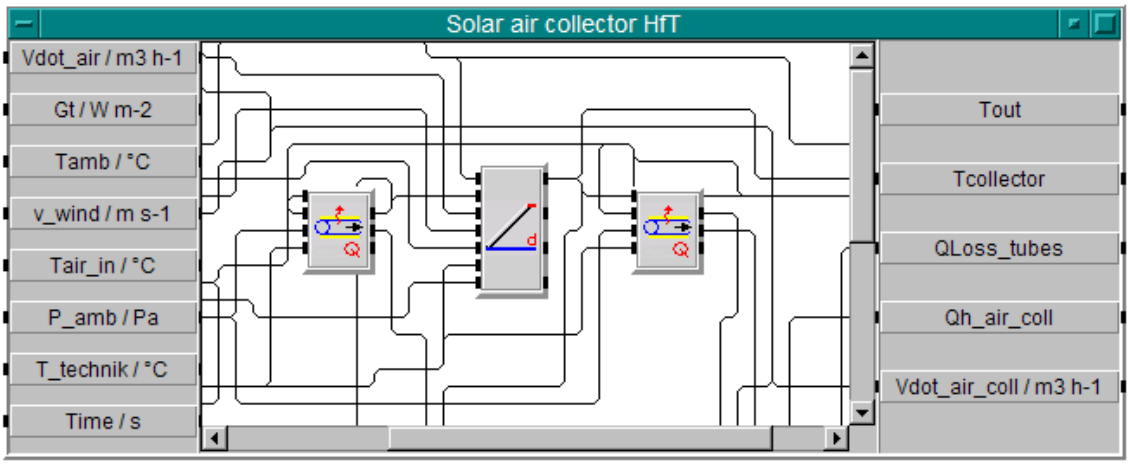

Fig. 5-19: Detailed view into the air collector system model with the dynamic collector and tubing model

The parameters used for the collector model can be found on the block template shown in Fig. 5-20.

Solar air collector field

Solar air collector (dynamic)

Vdot	Number of collectors in series	2	Optical efficiency	0.812	To
	Number of collectors in parallel	1	Insulation thickness	0.06	
Ti	Collector tilt angle	30	Insulation heat conductivity	0.04	
Gt	Collector length	10.40	Absorber heat conductivity	238	Tp
	Collector width	0.96	Emissivity glas cover	0.88	
Ta	Channel height	0.095	Emissivity absorber front	0.16	
	Channel width	0.060	Emissivity absorber back	0.085	Tb
vw	Number of channels	16	Emissivity channels	0.085	
	Plate thickness	0.0014	Distance absorber / front cover	0.020	
t	Thickness back cover material	0.002	Specific heat back cover material	500	
	Density back cover material	7800	Specific heat absorber material	500	Tc
pi	Density absorber material	2702			

Fig. 5-20: Block template of the dynamic air collector model with the parameters used for the collector field of the University of Applied Sciences in Stuttgart

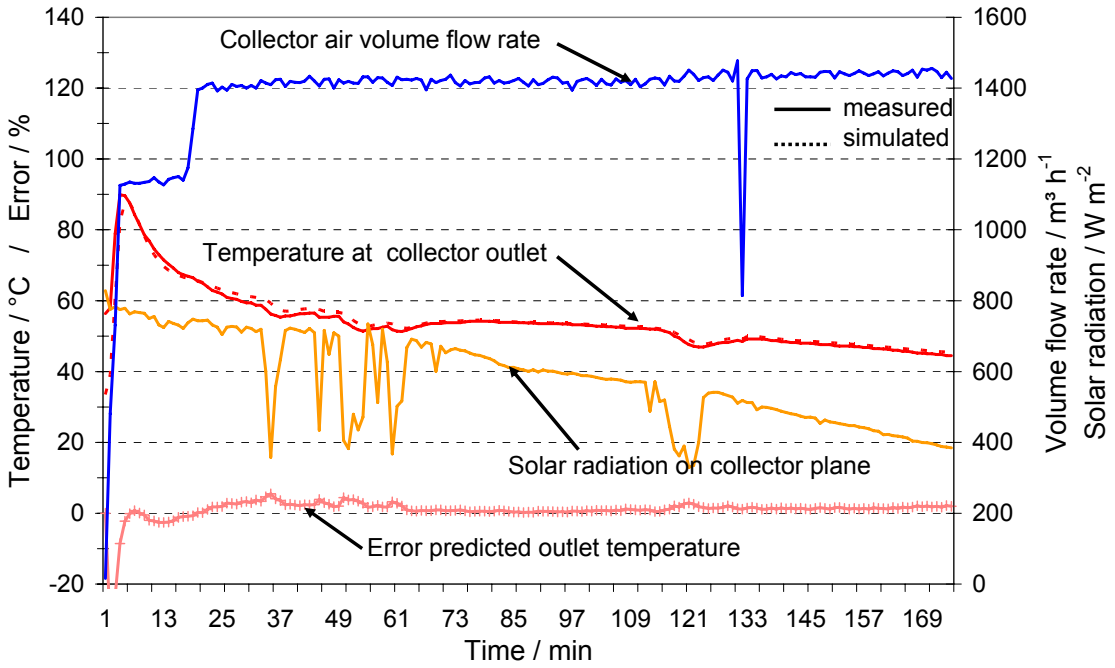

Fig. 5-21: Comparison of measured and simulated performance of the solar air collector field at 1500 m^3h^{-1} air volume flow rate

For model validation measured performance data of the installed DEC system are used. Fig. 5-21 shows the results for an afternoon of a day in July with single clouds with system startup after a period of no air flow rate in the

collector field. The results clearly demonstrate that the measured outlet temperature of the collector field is very well described by the simulated temperature, even at system startup and for larger fluctuations in solar irradiation. The average relative error is only 1.6 % (0.8 K) over the whole period shown in Fig. 5-21.

5.4.6 ROOM MODEL

-Thermal model

For the two seminar rooms connected to the DEC system a dynamic thermal building model based on existing blocks has been developed in INSEL for each room. This model consists of three internal walls, one internal floor, one internal ceiling, one external wall, a room block and a long-wave irradiation exchange block. The internal and external elements are modelled by the INSEL 'WALL' and 'WALLX' block. The WALL block solves the one-dimensional heat transfer equation for a interior wall / floor consisting of several layers with varying thickness and heat conductivity. Shortwave irradiance, convective heat flux from the room air and long-wave radiation flux from the other surfaces are given as boundary conditions. The WALLX block solves the one-dimensional heat transfer equation for an external wall consisting of several layers with varying thickness and heat conductivity. As boundary conditions, the exterior temperature and solar irradiance is given for the outside wall surface, on the inside shortwave irradiance, convective heat flux from the room air and long-wave radiation flux from the other surfaces are given as boundary conditions. The ROOM block calculates the room air temperature from the convective heat fluxes from all walls plus the convective heat input (heating or cooling system) onto the air node and the convective part of the internal heat gains. The output of the room block is the room air temperature at the end of the time step and the convective heat flux to each surface temperature node.

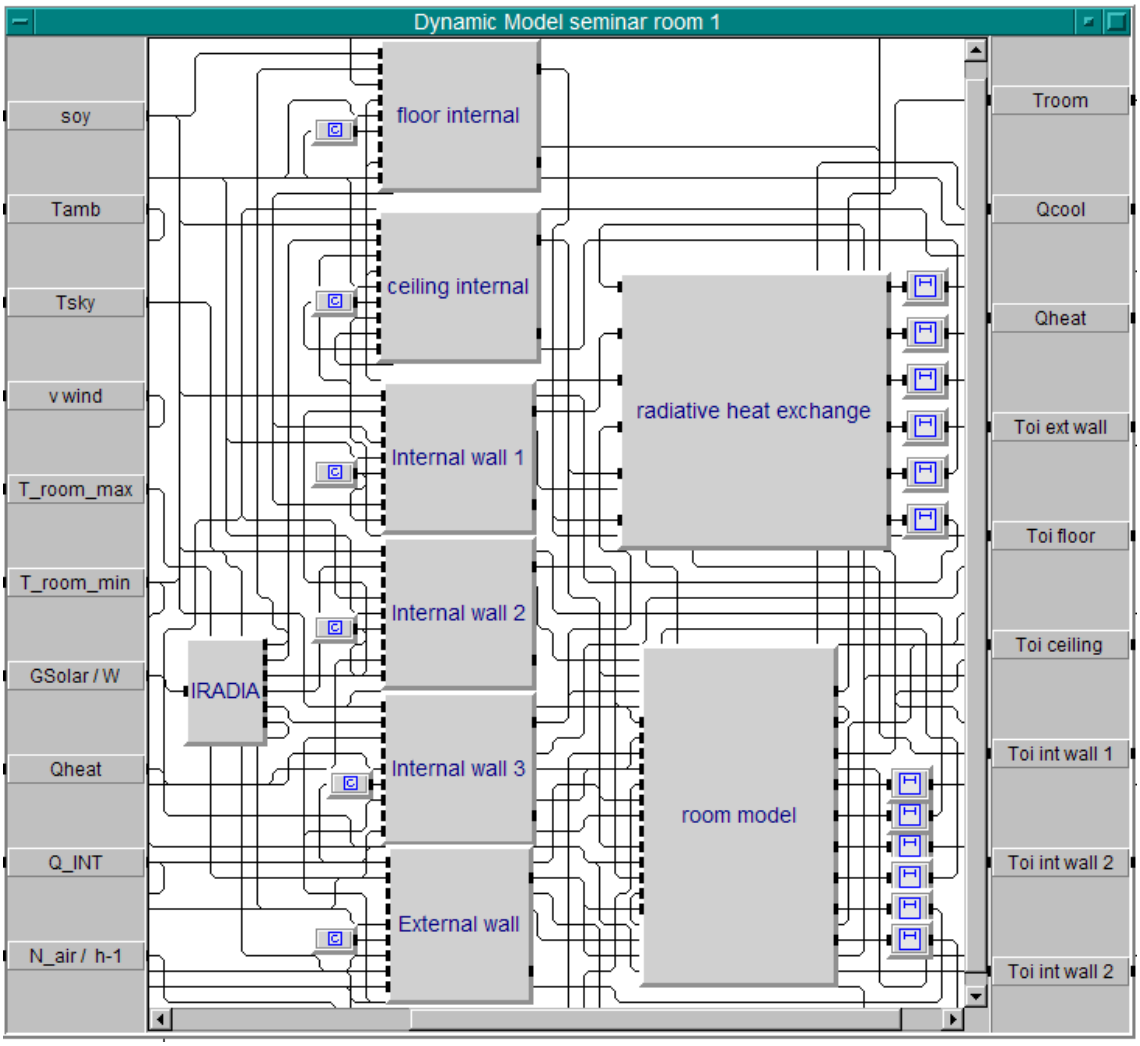

Fig. 5-22: Detailed view into the room model of one zone

The RADI block calculates the long-wave heat exchange between surface areas of different temperatures. In general, the radiative heat exchange has to be calculated considering the emission of each surface in direction of another surface, the reflection of that surface back to the original and finally the re-reflexion of the original surface. To simplify the calculations, the net long-wave emission of each surface is calculated from the own emission of the surface reduced by the absorbed irradiance at the surface, which comes from all the surrounding surfaces. For the surrounding surface intensities, their own emission is calculated and the reflection of the mean room radiation intensity is added. Actually there is no block available in INSEL for windows. To consider window areas, the heat losses through the windows are considered by an average U-value of the opaque part of the exterior wall. This average U-value is

considered through a reduced thermal resistance of the opaque part of the wall area. To consider the lower thermal capacity of the window area, the thermal capacity of the opaque wall is reduced to the average value of the opaque and glazed area of the wall. For window areas of the external wall below 50% a sufficient accuracy is reached with this simplified method. The solar gains of the windows are considered by the solar radiation on the window area multiplied by the transmission factors of the glazing and of external shading systems. The IRADIA block calculates the distribution of the transmitted shortwave solar radiation from the windows on the surface of internal walls. Since no geometrical model is implemented, the distribution of the solar radiation is only controlled by absorption coefficients which can be defined for each of the surfaces. The distribution is calculated for each surface by multiplying the solar radiation with the surface area and the absorption coefficient of the wall divided by the sum of all surface areas multiplied with their absorption coefficient. Reflections of the internal surfaces are not considered in this model.

For model validation the evaluation method for dynamic simulation models defined in the German standard VDI 6020 'Requirements on Methods of Calculation to Thermal and Energy Simulation of Buildings' is used. Here different examples are defined, which can be calculated and compared to validated results to ensure an accurate performance of newly developed simulation tools. Example number one with heavy room was chosen to demonstrate the validation of the dynamic building simulation model in INSEL. TRNSYS is used as reference simulation tool for result comparison. Example number 1 considers a room with 5 m depth, 3.5 m width and 3 m height with a volume of 52.5 m³ and floor area of 17.5 m². For room type S a room with heavy surrounding construction of the walls, floor and ceiling is considered. The details of constructions are shown in Table 5-8. A constant ambient air temperature of 22°C and a starting temperature of the room air and surrounding structure of 22°C is used in this example. The external wall has a window with an area of 7 m². The remaining opaque part of the wall is 3.5 m². The U-value of the window is 2.1 $Wm^{-2}K^{-1}$. Since no real window model is available in INSEL for

simplification the insulation thickness and heat capacity of the external wall are reduced in order to reach an average U-value of the external wall of 1.6 $Wm^{-2}K^{-1}$ and a reduced heat capacity which considers the light weight window. Short-wave solar radiation and long-wave ambient radiation are not considered in the example. During the simulations a constant convective heating load of 1000 W is applied to the room during 12 hours per day in the time from 6 am to 6 pm. A time period of 60 days is calculated and analysed.

Table 5-8: Construction details of the analysed example room

Type of element	Construction	d [m]	λ [$Wm^{-1}K^{-1}$]	ρ [$kg\ m^{-3}$]	c [$J\ kg^{-1}K^{-1}$]
Ceiling and floor	PVC covering	0.002	0.21	1300	1470
	Screed	0.045	1.40	2200	1050
	Rock wool	0.012	0.06	50	840
	concrete	0.15	2.035	2400	1050
Internal walls	Cavity blocks	0.24	0.56	1300	1050
Internal door	Beech, solid	0.040	0.21	700	2520
External wall	Concrete	0.24	2.035	2100	920
	Insulation	0.062	0.047	75	840
	Façade slab	0.025	0.45	1300	1050

The simulation results are shown in Fig. 5-23 together with the results from TRNSYS simulations using Type 56. A comparison between the resulting room air temperatures of the two simulation tools clearly demonstrates that the INSEL model nearly exactly delivers the same results as the TRNSYS simulations. The average relative error between the results of both simulation tools is only 0.85% (0.5 K).

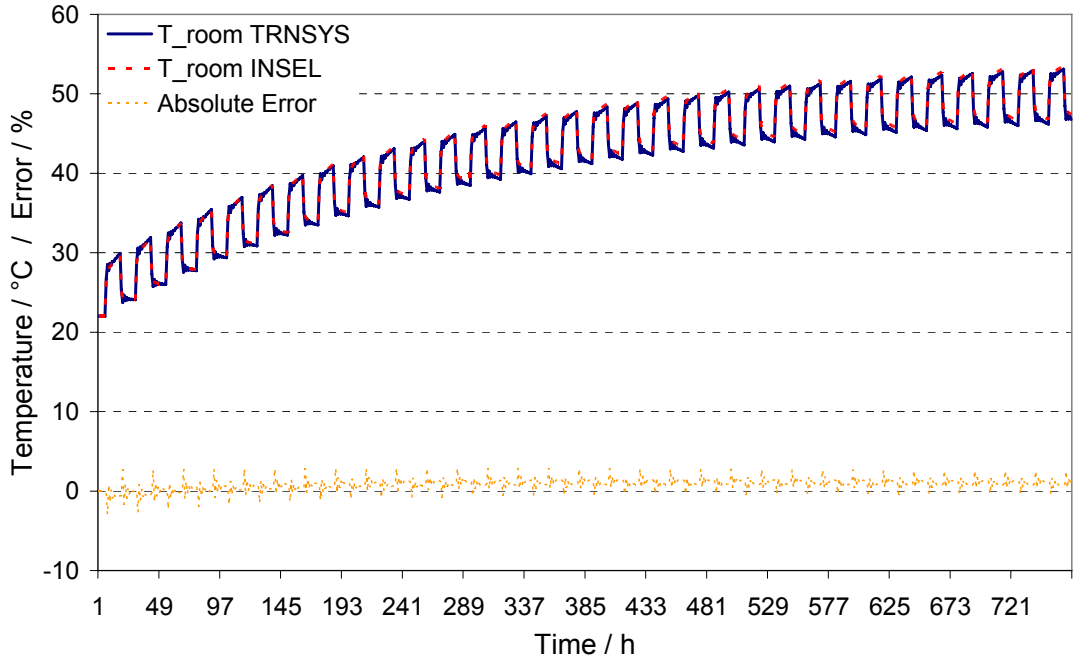

Fig. 5-23: Comparison between TRNSY and INSEL for the VDI 6020 example 1

-Humidity model

A simple static humidity balance model is used for the calculation of the absolute room air humidity content and resulting relative humidity. For simplification the storage of humidity in the surrounding structure and furniture etc. is not considered. As already mentioned in section 5.3.3 a humidity exposure of 50 g per hour is considered for each person at low degree of activity. To keep the humidity ratio and the CO_2-concentration of the room air within the comfort limit a minimum fresh air flow rate of 30 m³ per person and hour is considered in the simulations. The resulting average absolute humidity of the room / return air is calculated from equations 5-3:

$$x_{room,air} = x_{return,air} = \frac{x_{sup,air} \cdot \dot{V}_{sup,air} \cdot \rho_{air} + \dot{m}_{H_2O} \cdot N_{Pers}}{\dot{V}_{sup,air} \cdot \rho_{air}} \qquad (5\text{-}3)$$

The relative humidity of the room / return air is then calculated from empirical Equations 5-4 and 5-5 (Glück, 1991):

$$\varphi_{room,air} = \varphi_{return,air} = \frac{x_{room,air}}{x_{room,air} + 0.622} \cdot \frac{P}{p_s(T_{room})} \quad (5\text{-}4)$$

$$p_s(T) = 611 \exp\begin{pmatrix} -1.91275 \cdot 10^{-4} + 7.258 \cdot 10^{-2} T \\ -2.939 \cdot 10^{-4} T^2 + 9.841 \cdot 10^{-7} T^3 \\ -1.92 \cdot 10^{-9} T^4 \end{pmatrix} \quad (5\text{-}5)$$

With T: Room temperature in °C

5.4.7 CONVENTIONAL VENTILATION SYSTEM WITH COMPRESSION CHILLER AS REFERENCE SYSTEM

For comparison of the results of the analysed DEC system an energy efficient reference system has been defined (Fig. 5-24). This system consists of an efficient ventilation system with a heat exchanger, a cooling coil and a heating coil. For the analysed summer operation it is assumed, that the heat exchanger is only in operation if the outside temperature drops below 16°C to preheat the supply air. An electrical driven compression chiller supplies cooling energy to the cooling coil and a dry heat rejection system is used to reject the condensation enthalpy to the ambient. In case of dehumidification the supply air is cooled down to 14°C and needs to be heated up afterwards to avoid supply air temperatures below 16°C. To avoid additional heating energy from e.g. a gas boiler, in case of dehumidification the condensation energy of the chiller is used to heat the supply air to the lower supply air temperature limit, before the remaining heating energy is released to the ambient by the dry heat rejection system.

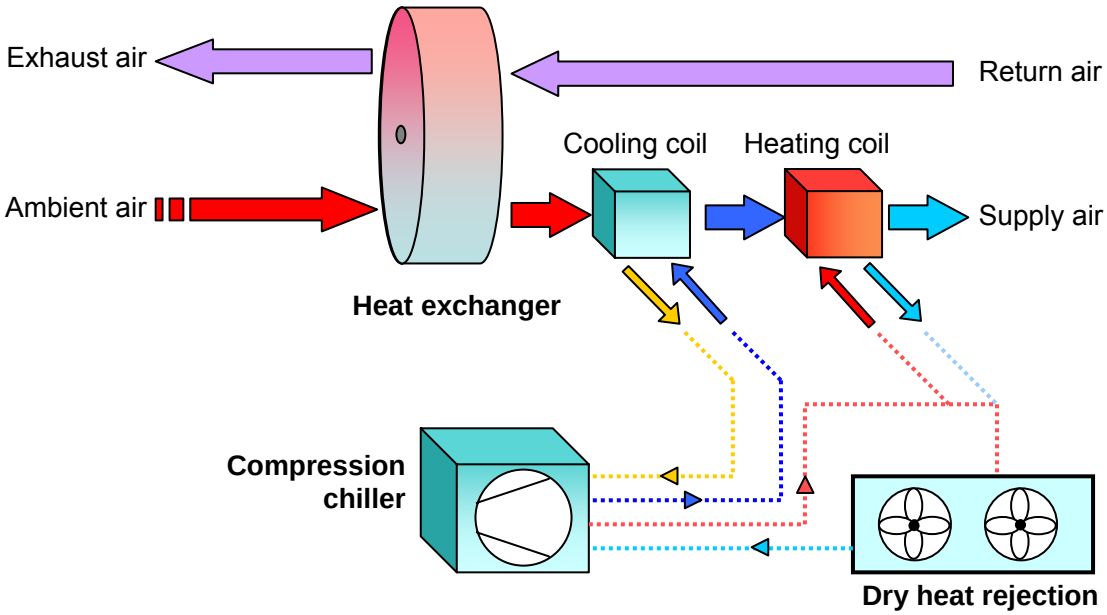

Fig. 5-24: Schematic diagram of the analysed reference air conditioning system

For the compression chiller an average COP of 2.8 is considered in the calculations. This value includes the electricity consumption of the chiller, of the dry heat rejection system and of all pumps. For the small power range and low cold water temperature of 6°C supply and 12°C return, the selected average COP describes already a quite highly efficient system (Yu et al., 2004). The electricity consumption of the ventilator is calculated from the pressure drop of the system at maximum air volume flow rate according to equation 5-6. Highly efficient ventilators with an efficiency of 70% are considered. The resulting pressure drops and electrical power demand at maximum air flow rate of 3000 $m^3\ h^{-1}$ are shown in Table 5-9 for the supply and return air side. The electricity consumption at lower air volume flow rate is calculated according to the proportional law from equation 5-1 (see section 5.4).

$$P_{el,\max} = \dot{V}_{\max} \cdot \Delta P_{total,\max} \cdot \frac{1}{\eta_{fan}} \qquad (5\text{-}6)$$

Table 5-9: Pressure rise, efficiency and nominal electrical power demand of the supply air and return air ventilator

	Supply air ventilator	Return air ventilator
Pressure drop of the system / Pa		
- Heat exchanger	100 Pa	100 Pa
- Cooling coil	150 Pa	--
- Heating coil	150 Pa	--
- Tubing and filters etc.	800 Pa	800 Pa
Total pressure drop	1200 Pa	900 Pa
Fan efficiency	70%	70%
Electrical power demand	1.4 kW	1.1 kW

The reference system is controlled to meet exactly the same room comfort conditions at exactly the same air volume flow rates as the best analysed desiccant system does. The cooling power provided to the seminar rooms by the reference system is therefore equal to the cooling power provided by the desiccant system. The cooling power provided by the chiller is set equal to the sum of sensible and latent cooling power, both calculated from the difference between ambient and supply air conditions for each time step.

5.5 SENSITIVITY ANALYSIS OF CONTROL PARAMETERS

The developed dynamic simulation model of the installed DEC system and the connected rooms described above was used to evaluate the influence of different control parameters on the overall primary energy efficiency of the installed DEC system. The primary energy ratio, which is defined as the cooling energy supplied to the room divided by the primary energy input caused by electricity consumption of the components (fans, pumps, etc.) and the additional heating energy demand, which is assumed to be provided by a gas boiler (equations (5-7) and (5-8)). The primary energy factors (PEF) used are 2.7 for electricity in Germany (GEMIS) and 1.1 for the gas boiler:

$$PER = \frac{\dot{Q}_{cool}}{\dot{Q}_{el} \cdot PEF_{el} + \dot{Q}_{h,add} \cdot PEF_{gas}} \tag{5-7}$$

$$\dot{Q}_{cool} = \dot{V} \cdot \rho_{air} \cdot (h_{\sup,air} - h_{ret,air}) \tag{5-8}$$

To visualise how the air volume flow rate influences the cooling power and the resulting primary energy ratio simulations were performed with different air volume flow rates at different supply air temperatures. For this analysis a fixed room temperature of 26°C and 55%RH and ambient air with 32°C and 40%RH were assumed. The resulting cooling power and primary energy ratios are shown in Fig. 5-25. The results clearly visualise that at constant supply air temperature an increase in air volume flow rate on the one hand significantly increases the cooling power but on the other hand significantly increases the electricity consumption. Therefore, the primary energy ratio decreases significantly with increasing air volume flow rate.

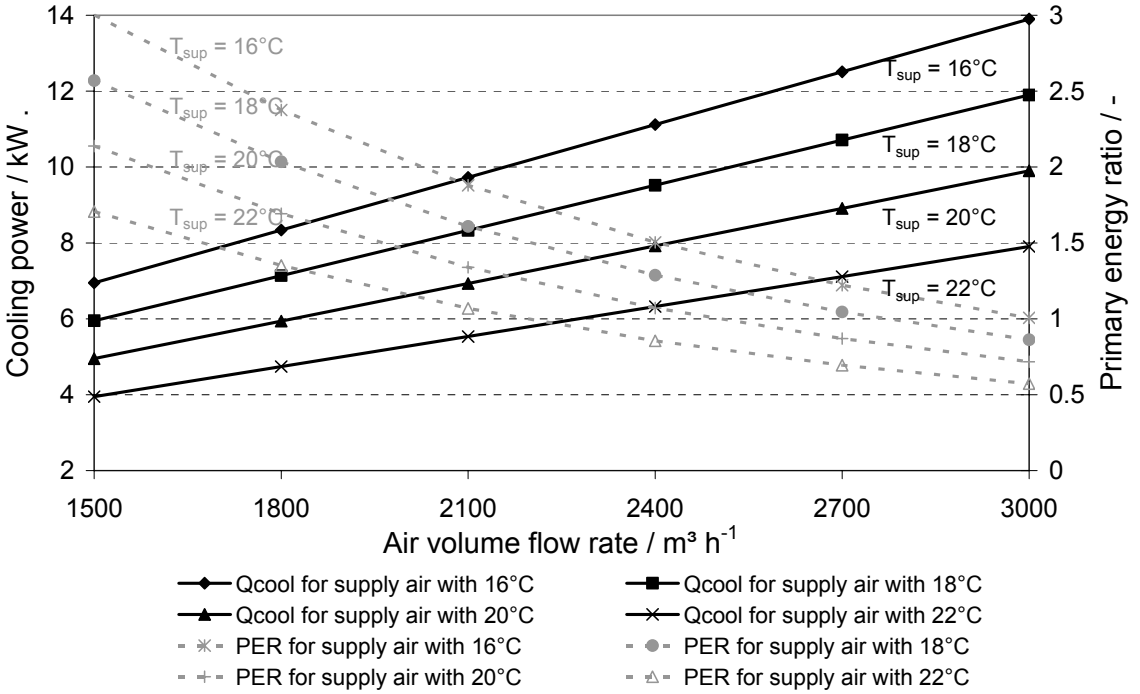

Fig. 5-25: Primary energy ratio of the DEC system in dependence of supply air temperature and air volume flow rate. Calculated for ambient air conditions of 32°C and 40%RH and for return air with 26°C and 55%RH and 100% solar fraction

If for example a cooling power of 7 kW shall be reached at 16°C supply air temperature an air volume flow rate of 1500 m³ h^{-1} would be sufficient. In this case the primary energy ratio reaches a value of 3.0. If the same cooling power shall be reached at 22°C supply air temperature, the air volume flow rate needs to be increased to 2700 m³ h^{-1}. The resulting primary energy ratio reaches only 0.7 which is less than one fourth of the value reached for 16°C supply air temperature and 1500 m³ h^{-1} air volume flow rate. This clearly demonstrate that from the primary energy point of view, for the analysed system the best strategy to cover the required cooling demand is to decrease the supply air temperature as far as possible and to use the increase of the air volume flow rate as the last possible option. Only for systems with very low pressure drops due to integrated bypasses and efficient system design (tubing and components with large cross sections) and highly efficient fans an increase of the air flow should be chosen as first choice.

Another fundamental question concerning the energy efficiency of DEC systems is, whether additional heating or additional cooling should be used in case of insufficient solar heat supply. To visualise the effect of the different options a simulation based analysis has been performed with the same ambient and room air conditions as described above but with a constant heat supply from the solar system of 8 kW which reaches around 50°C regeneration temperature. Then the additional heating input has been increased in steps of 1 kW.

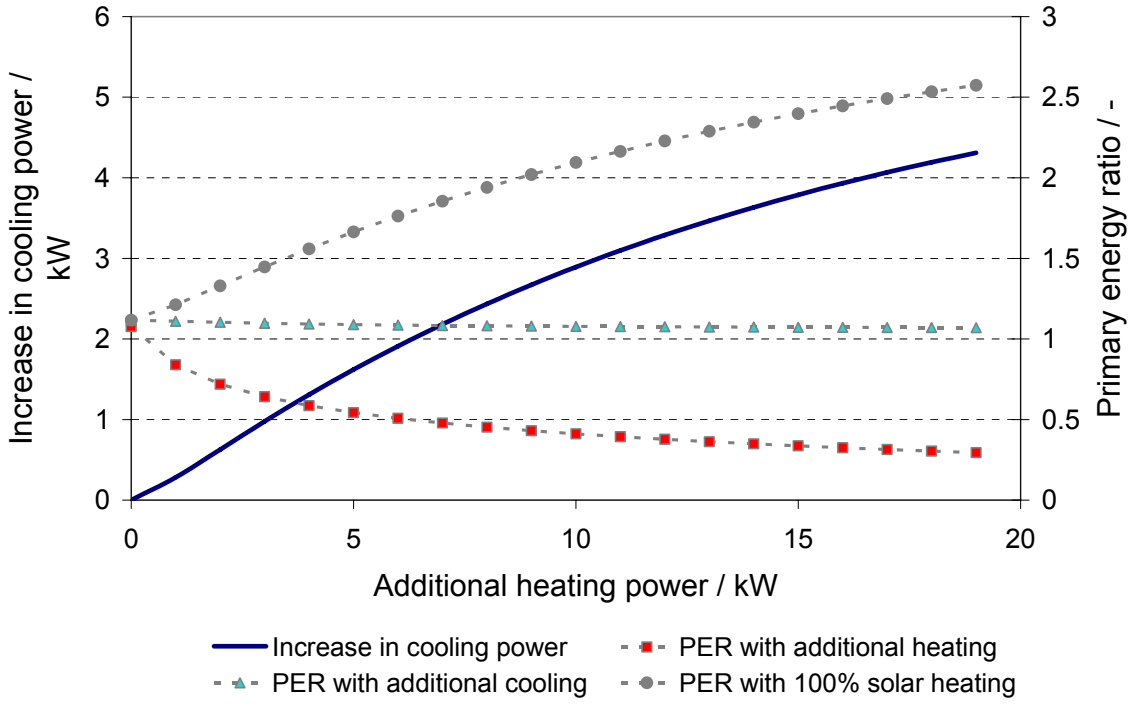

Fig. 5-26: Primary energy ratio of the DEC system in dependence of additional heating / cooling power. Calculated for 1500 $m^3\ h^{-1}$ air flow rate, ambient air with 36°C and 40%RH and return air with 26°C and 55%RH with the assumption that the solar system provides always 8 kW heating power .

The resulting increase in cooling power is shown in Fig. 5-26 as solid line. This line clearly shows that much more heating energy is required than increase in cooling power is reached. For an increase in cooling power of e.g. 3 kW the required additional heating power is 11 kW which is nearly a factor of four higher than the increase reached in cooling power. In consequence the primary energy ratio is drastically reduced from a value of 1.2 without additional heating to a value of 0.4. If additional cooling instead of additional heating is used to cover the 3 kW additional cooling power, the primary energy ratio decreases

only slightly to a value of 1.1. From the primary energy point of view it is therefore much more efficient (factor 3) to use additional cooling instead of additional heating. However, the overall best primary energy ratio of 2.2 would be reached if the solar system could cover the additional required heating demand or the heating demand would be supplied by another renewable energy source like renewable driven CHP systems.

5.6 PRIMARY ENERGY OPTIMISED CONTROL STRATEGY

Based on the results of the sensitivity analysis of the control parameters and the known problems of already existing control strategies a new primary energy optimised control strategy DEC systems has been developed. The exact functionality of this new control system is described and discussed in detail in the following three parts.

5.6.1 ARCHITECTURE AND FUNCTIONALITY OF THE DEVELOPED CONTROLLER

As visible from Fig. 5-27 the architecture of the developed controller is quite similar to standard control systems. It consists mainly of a sequence controller part which turns on or off the components of the DEC system in dependence of the room temperature and humidity. It starts with ventilation in free cooling mode at minimum air flow rate and switches to indirect humidification as soon as the room temperature increases above 23.5°C. If the room temperature further increases and reaches 24.5°C, the direct evaporative cooling mode is activated. The seven stages of the hybrid humidifier are controlled in order to reach 16°C supply air temperature. The supply air humidity is limited to 10 g/kg. If the room temperature reaches 25.5°C or the humidity of the ambient air increases above 10 g/kg the desiccant cooling mode is activated. In this case first the solar air collector is used before the solar heat exchanger is activated and heating energy from the vacuum tube collector is used to further heat up the supply air. A proportional controller is used to control the regeneration air temperature according to the measured room air temperature. As a last option the air volume flow control is activated if the room air temperature increases

above 26.5°C. A PID controller tries to control the air volume flow rate in order to keep the room temperature at 26°C.

Especially at lower ambient air temperatures such a simple control cascade can lead to conditions at which the indirect humidification mode is activated without providing real cooling power, or even heats up the ambient air. Additionally, in some cases the components are activated too fast after one another, even if dead times are implemented in the control. In consequence the DEC mode is activated although not required at the given load and ambient conditions. To overcome these problems a primary energy optimisation tool (PE-Optimiser) has been developed and implemented in the control system, which consist of an online tool based on simplified simulation models of all relevant components. The exact functionality of the PE-Optimiser is described separately in section 5.6.2.

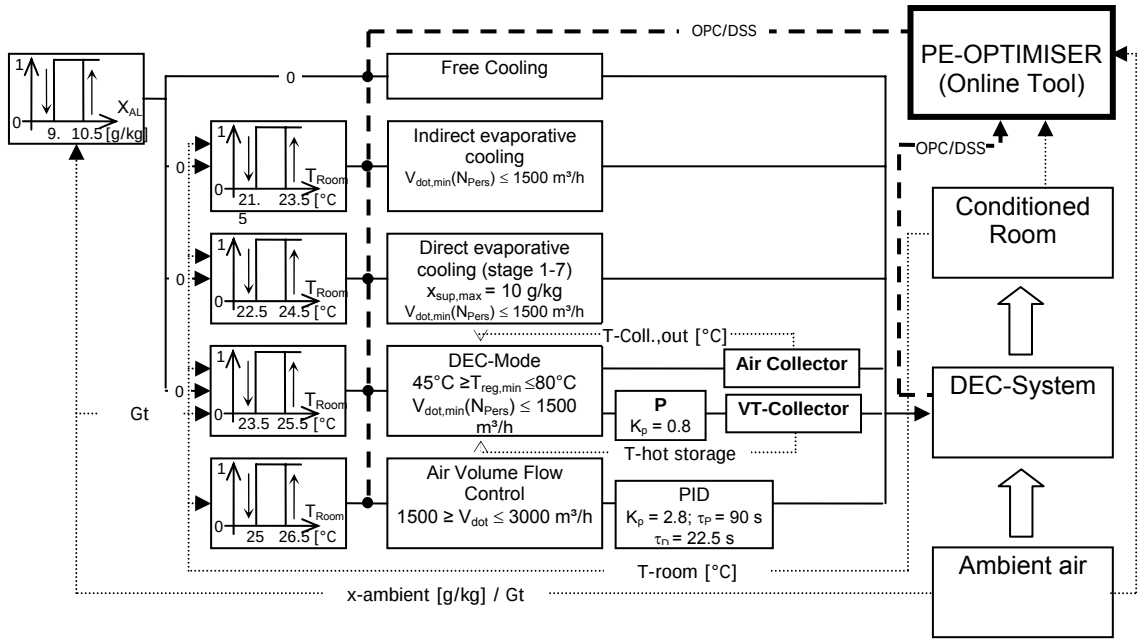

Fig. 5-27: Architecture of the developed new DEC controller

For the two seminar rooms two separate PID controllers are used to control the air volume flow rate of each room. The PID controller is defined in the general form as follows:

$$u(t) = K_p\left(e(t) + \frac{1}{\tau_i}\int_0^t e(t)dt + \tau_d \frac{de(t)}{dt} \right) \quad (5\text{-}9)$$

With K_p representing the proportional gain, τ_i the integral and τ_d the derivative time constant. The error function is given by e(t) which is the difference between the room temperature setpoint and the actual measured room temperature. Fig. 5-28 shows the functional principle of a PID controller. In the present case the lower limit of the PID controller is set to 0 which corresponds to the minimum air change rate of the connected seminar room of three air changes per hour (750 $m^3\ h^{-1}$). The upper limit of the PID controller is set to 1.0 which corresponds to the maximum air change rate per connected room of six air changes per hour (1500 $m^3\ h^{-1}$ for each of the two rooms). The two PID controllers are tuned in the simulation environment with the widely used Ziegler-Nichols' method (Ziegler and Nichols, 1942). With this method first only a proportional control is applied to the system and the proportional gain K_p is increased until the system starts to oscillate with constant amplitude and constant time period.

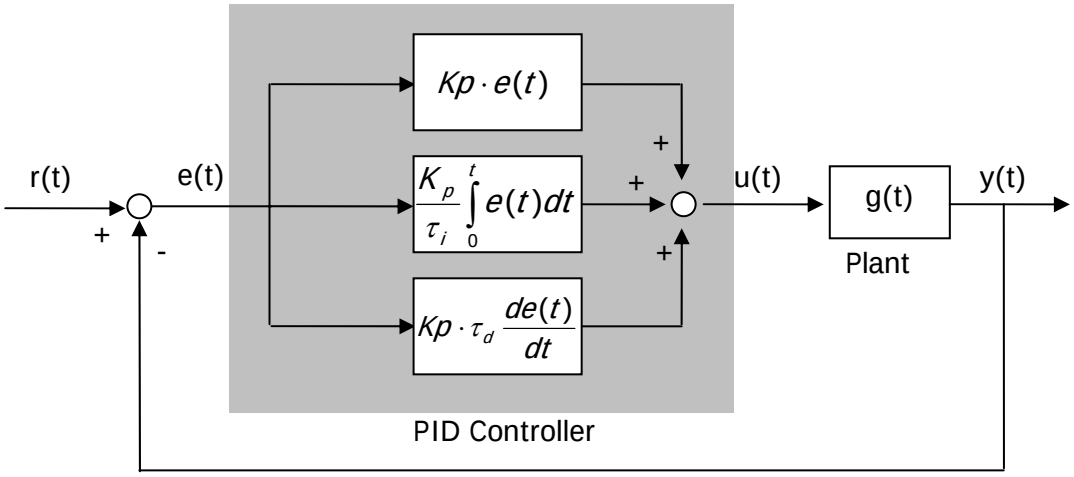

Fig. 5-28: PID controlled system

The resulting proportional gain is called the critical gain K_{pi} which in case of the volume flow rate control was equal to 4.7. With this proportional gain the room air temperature starts to oscillate with a period P_u of 180 s. With these two values the settings of the PID controller can be calculated according to the Ziegler-Nichols laws as follows:

$$K_p = 0.6 \cdot K_{pi} = 2.8; \qquad \tau_I = P_u \cdot 0.5 = 90s; \qquad \tau_D = \frac{P_u}{8} = 22.5s$$

Since the two seminar rooms are very similar, the same controller parameters can be used for both rooms.

A 'Conditional Integration' anti windup system is used, which sets the integrator to zero whenever a crisis exists. A crisis occurs when the error signal is large, the actuator is already saturated or the actuator is close to saturation and the present value of the control signal is driving it toward saturation (Paz, R. A., 2001). The following exponential error function has been used to avoid saturation of the integral term of the PID controller:

- Exponential error function:

$$\tilde{e}_i(t) = \frac{K_p}{\tau_i}\big(r(t) - y(t)\big) \cdot e^{-\left(100(u(t)-v(t))\right)^2} \tag{5-10}$$

Here u(t) is the resulting control signal and v(t) is the resulting control signal saturated to the possible maximum / minimum values of the control signal, e.g. $u(t)_{max}$ = +1 and $u(t)_{min}$ = -1. If the resulting control signal of the PID controller increases above or below these max / min values the saturated control signal v(t) is limited to +1 or -1.

- Resulting PID function:

$$u(t) = K_p \cdot e_p(t) + \int_0^t \tilde{e}_i(t)dt + K_p \cdot \tau_d \frac{de(t)}{dt} \tag{5-11}$$

The exponential error function is equal to $(K_p / \tau_i)\big(r(t) - y(t)\big)$ when u(t) = v(t) (no saturation). When u(t) ≠ v(t) (saturation), $\big(K_p / \tau_i\big)\big(r(t) - y(t)\big)$ is multiplied by a number that is closer to zero the further u(t) and v(t) are from each other. If u(t) is far enough from v(t), then $\tilde{e}_i(t)$ effectively becomes zero.

5.6.2 PE-OPTIMISER (ONLINE TOOL)

The PE-Optimiser permanently evaluates online the optimum system operation mode with the highest primary energy efficiency and transfers the recommended operation mode to the main system controller. Within this optimisation tool only the decision is taken, whether different operation modes are required or not to reach the maximum cooling capacity of the DEC system at highest possible primary energy efficiency. The activation command for the components comes from the sequence controller in dependence of the room air temperature and humidity. If the optimisation tool decides that some operation modes are not useful, the activation command of the cascade controller is ignored for these components. Additionally, the optimisation tool evaluates the optimum supply air humidifier stage in order to reach the lowest possible supply air temperature and to avoid supply air humidity values above 10 g/kg. The exact functionality of the optimisation tool is described in the following paragraphs.

Fig. 5-29 shows the typical operation ranges of the four possible operation modes which are calculated by the PE-Optimiser in dependence of the actual room air conditions. In the example shown here the operation ranges are calculated for a room air condition of 26°C and 50% relative humidity.

The decision whether the DEC system should be operated in free cooling/direct humidification mode (strategy I, Free cooling / direct humidification) depends on the temperature and humidity ratio of the ambient air. If the ambient air temperature is less than 2 K above the temperature of the return air after maximum humidification and the enthalpy of the ambient air is below 41 kJ kg^{-1}, no other operation mode than the free cooling or direct humidification mode is reasonable. In this case the lowest possible supply air temperature of 16°C can be reached without increasing the supply air humidity above the upper limit of 10 g/kg. For the detection whether the DEC system should be operated in this mode, first the enthalpy of the supply air is calculated according to equation (5-

12). The naming convention for the temperature and humidity variables is shown in Fig. 5-30.

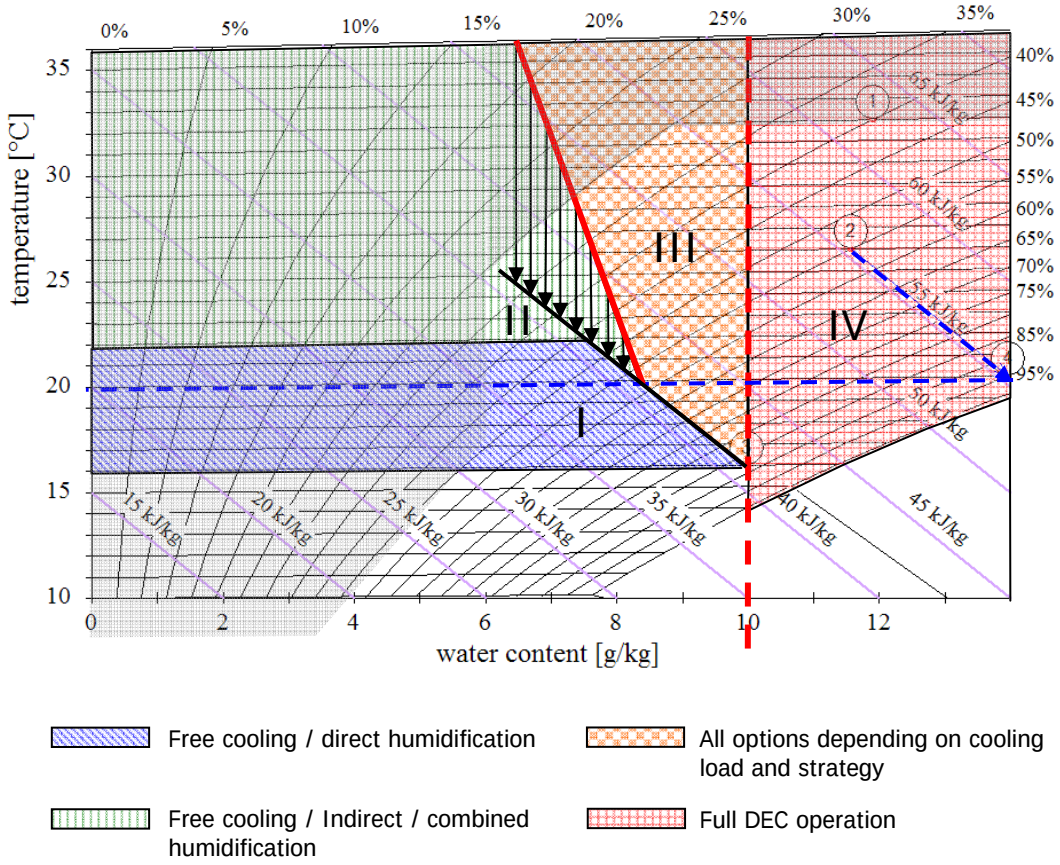

Fig. 5-29: Possible operation modes calculated by the PE-Optimiser for room air conditions of 26°C and 50% relative humidity

If the enthalpy of the ambient air is below 41 kJ kg^{-1} additionally the return air temperature after maximum humidification needs to be calculated from the measured return air conditions. The reachable relative return air humidity depends on the humidification efficiency of the return air humidifier which can be assumed to be constant at 95% independent of the actual air flow rate and return air humidity.

$$\begin{aligned} h_{humidair,S1} &= h_{air,S1} + x_{air} \cdot h_{D,S1} \\ &= \left(c_{air} + x_{ai,S1} \cdot c_D\right) \cdot T_{air,S1} + x_{air,S1} \cdot h_{ev}\left(T_{air,S1}\right) \end{aligned} \tag{5-12}$$

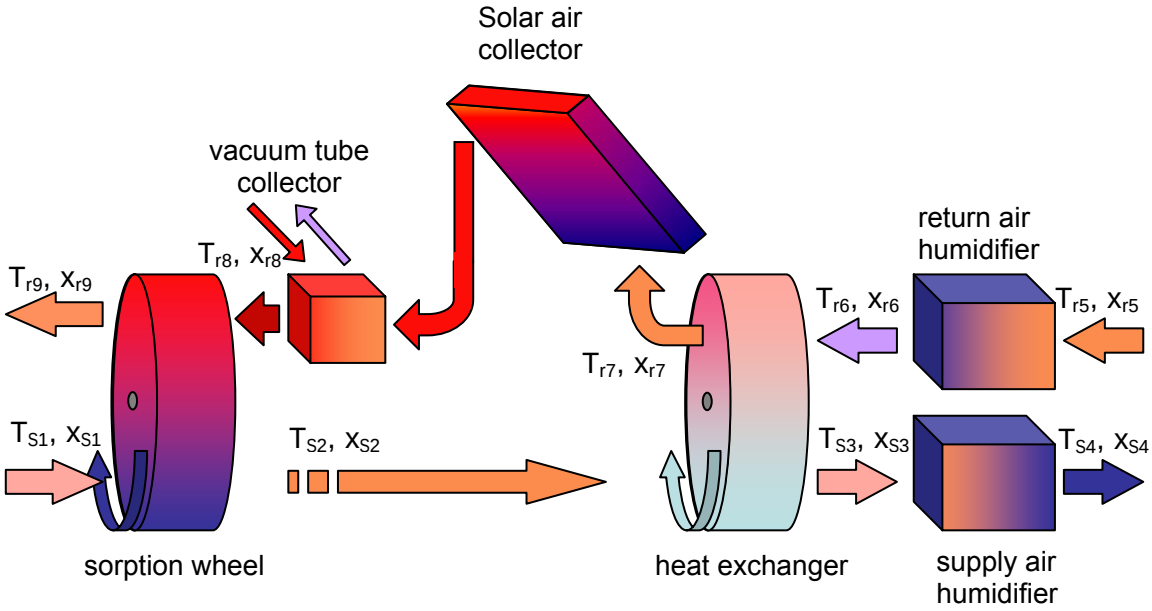

Fig. 5-30: System scheme with numbered temperature and humidity variables

The absolute return air humidity and temperature after the return air humidifier is calculated from equations (5.13) to (5.15). Considering an isenthalpic humidification process, the temperature of the return air is then given by the enthalpy equation resolved for the return air temperature. Since the evaporation enthalpy in equation (5.15) also depends on the return air temperature, the equation is still implicit. Due to the implicit character of the equation, the return air temperature needs to be solved iteratively.

$$p_{s,r6} = 611 \cdot \exp\left(\begin{matrix} -1.91275 \cdot 10^{-4} + t_{r6} \cdot 7.258 \cdot 10^{-2} - t_{r6}^{\,2} \cdot 2.939 \cdot 10^{-4} \\ + t_{r6}^{\,3} \cdot 9.841 \cdot 10^{-7} - t_{r6}^{\,4} \cdot 1.920 \cdot 10^{-9} \end{matrix}\right) \qquad (5\text{-}13)$$

$$x_{r6} = 0.622 \cdot \left(\frac{p_{s,r6} \cdot RH_{r6}}{p_{air} - p_{s,r6} \cdot RH_{r6}} \right) \qquad (5\text{-}14)$$

$$T_{r6} = \frac{h_{r6} - x_{air,r6} \cdot h_{ev}(T_{r6})}{c_{air} + x_{air,r6} \cdot c_D} \qquad (5\text{-}15)$$

If the ambient air temperature is more than 2 K above the return air temperature after maximum humidification and the enthalpy of the ambient air is below 41 kJ kg^{-1} operation strategy II is activated, which allows either free cooling, indirect humidification or combined humidification as operation modes of the DEC system. For ambient air conditions with a temperature above the return air temperature after maximum humidification with an air enthalpy greater than 41 kJ kg^{-1} the decision whether strategy II or III is activated strongly depends on the performance of the heat exchanger. The inclination of the border line between strategy II and strategy III increases with increasing heat exchanger efficiency. The maximum inclination of 90° would be reached for a theoretical heat exchanger efficiency of 100%. In the optimisation tool the position and inclination of the border line between strategy II and III is calculated dynamically for each operation condition of the DEC system using the measured return air and ambient air conditions. First the supply air temperature after the heat exchanger is calculated for the indirect humidification mode according to Equation (5-16) assuming a constant heat exchanger efficiency. If the lowest supply air temperature can be reached by direct humidification without increasing the supply air humidity above the upper limit of 10 g/kg the enthalpy of the supply air after the heat exchanger should not exceed a value of 41 kJ/kg. With this condition the upper limit of the absolute ambient air humidity can be calculated from Equation (5-17) and is used for the decision whether strategy II or III is valuable or not. For ambient air conditions below the calculated upper limit of the absolute ambient air humidity strategy II and for ambient air conditions with higher absolute humidity strategy III is activated.

$$\phi = \frac{T_{s2} - T_{s3}}{T_{s2} - T_{r6}} \qquad T_{s3} = T_{s2} - \phi \cdot \left(T_{s2} - T_{r6}\right) \tag{5. 16}$$

$$h_{s3,\max} = 41 kJ / kg$$

$$h_{s3,\max} = h_{L,s3} + x_{\max.s3} \cdot h_{D,s3} = \left(c_{L,s3} + x_{\max,s3} \cdot c_D\right) \cdot T_{s3} + x_{\max,s3} \cdot h_{ev}\left(T_{s3}\right) \quad (5.\ 17)$$

$$x_{\max,s3} = \frac{41 kJ / kg - T_{s3} \cdot c_{L,s3}}{T_{s3} \cdot c_D + h_{ev}\left(T_{s3}\right)}$$

If strategy III is activated all operation modes are possible. In this case the controller of the DEC system is allowed to select all possible operation modes according to the room air temperature in the connected rooms. If the absolute humidity of the ambient air increases above the upper limit of 10 g kg^{-1} the optimisation tool activates strategy IV which forces the controller to operate the DEC system in full desiccant operation mode.

As described above, the positions of the borders between the operation strategies of the decision scheme are calculated dynamically in the optimisation tool from the actual measured room air conditions. Irrespective of the room air conditions the position of the border between Strategy II and III depends on the quality of the heat exchanger. The border between Strategy III and IV depends on the maximum possible supply air humidity in order to keep the room air conditions within thermal comfort limits. The logic functionality of the PE-Optimiser is shown in Fig. 5-31.

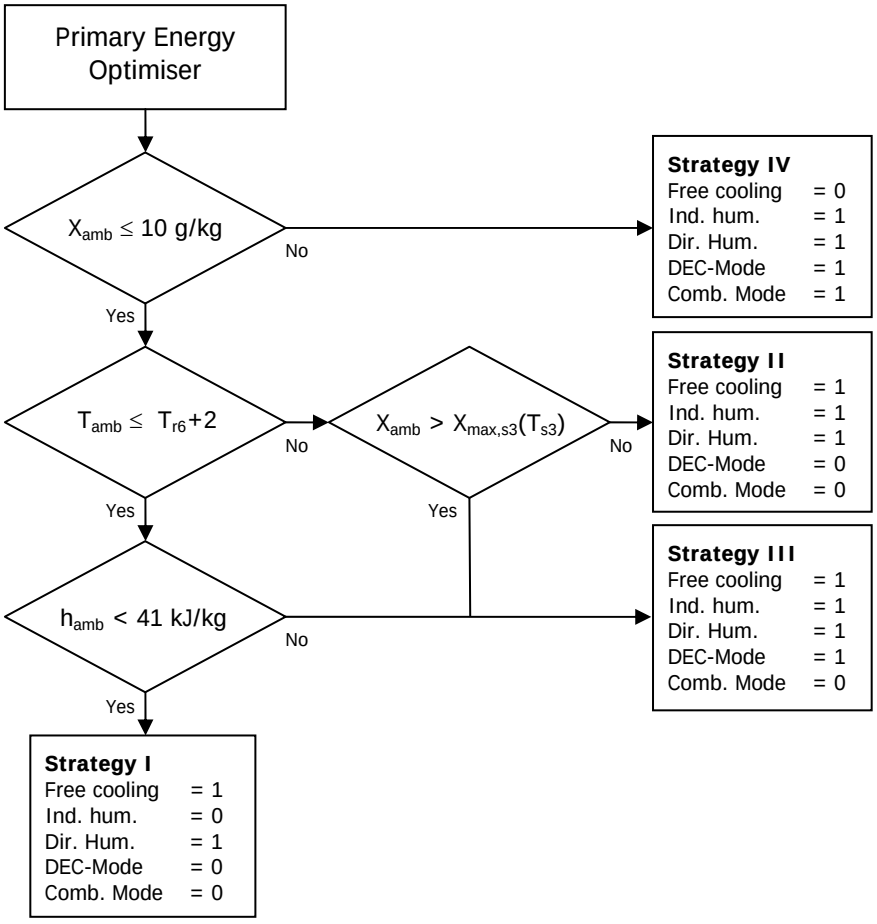

Fig. 5-31: Functionality of the Primary Energy Optimiser

5.6.3 OPTIMISED CONTROL OF THE SUPPLY AIR HUMIDIFIER

The main problem of the control of humidifiers results from their relatively high inertia. To overcome this problem longer dead times are commonly integrated in the system. This means that a waiting function is implemented in the control to avoid a too fast activation of the humidifier stages which would result in too high supply air humidity or to low supply air temperatures. On the other hand a long waiting time also hinders a fast adaption of the optimum supply air conditions which leads to longer periods of unsatisfactory supply air temperatures and may cause unnecessary further actions of the sequence controller. Therefore, for a fast and accurate control of the supply air humidifier a simple simulation based control tool has been implemented in the PE-Optimiser. This tool evaluates the supply air conditions after the heat exchanger and calculates the upper limit of

the supply air humidity, which is possible without decreasing the supply air temperatures below the lower temperature limit of 16°C at the given conditions. To do this the tool first calculates the supply air enthalpy after the heat exchanger from equation (5-18). Assuming an isenthalpic humidification process the supply air enthalpy doesn't change by humidification in the supply air humidifier. If the temperature after humidification is fixed to the minimum supply air temperature of 16°C the maximum absolute humidity of the supply air after humidification can be calculated by equation (5-19) and the maximum possible increase in supply air humidity is given by equation (5-20) :

$$h_{S3} = \left(c_{L,S3} + x_{S3} \cdot c_D\right) \cdot T_{S3} + x_{S3} \cdot h_{ev}\left(T_{S3}\right) \tag{5. 18}$$

$$h_{S3} = h_{S4} = \left(c_{L,S4} + x_{\max,S4} \cdot c_D\right) \cdot T_{S4,\min} + x_{\max,S4} \cdot h_{ev}\left(T_{S4,\min}\right)$$

$$x_{\max,S4} = \frac{h_{S3} - T_{\min,S4} \cdot c_{L,S4}}{T_{\min,S4} \cdot c_D + h_{ev}\left(T_{\min,S4}\right)} \tag{5. 19}$$

$$\Delta x_{\max} = x_{\max,S4} - x_{S3} \tag{5. 20}$$

To evaluate the optimum humidifier stage for the maximum possible increase in supply air humidity performance characteristics of the supply air humidifier have been calculated using the validated humidifier model described in section 2.3.3 and 5.4.4. These performance characteristics were calculated for the most common supply air temperature after the heat exchanger of 24°C. The relative humidity was varied between 30 and 90%. The resulting performance characteristics are shown in Fig. 5-32 for the seven stages of the humidifier. From this characteristics and the calculated maximum possible increase in supply air humidity the required humidifier stage is given. Values between the lines of the performance characteristic are linearly interpolated. The resulting humidifier stage is transferred as control suggestion to the sequence controller. For fine tuning the sequence controller is allowed to increase or decrease one humidifier stage only.

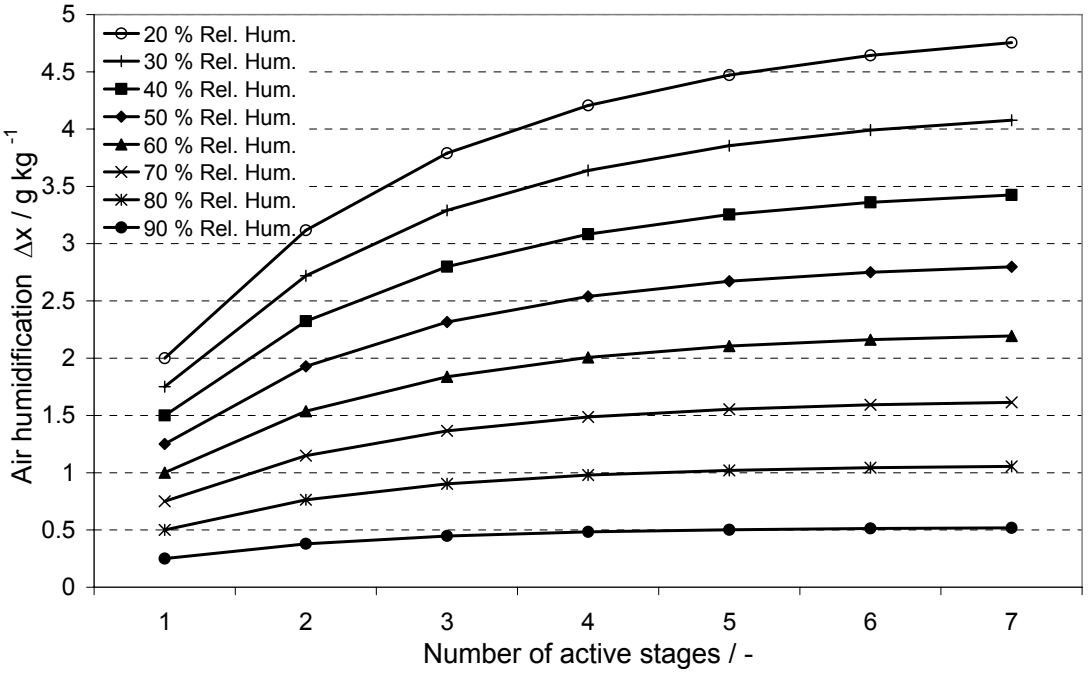

Fig. 5-32: Performance characteristics of the supply air humidifier in dependence of the supply air relative humidity at humidifier inlet and the number of active humidifier stages (calculated for 24 °C air inlet temperature)

The performance of the optimised humidifier control is shown in Fig. 5-33 for one typical day in July with low humidity of the ambient air. From this figure it becomes obvious that the optimised humidifier control operates very well even for large and sudden changes in supply air volume flow rate during the breaks between the lessons with only a few people left in the rooms. The supply air temperature and absolute humidity shows a quite smooth trend and only drops very shortly below the lower limit of 16°C at the beginning of the breaks between the lessons. In this case the supply air humidity very shortly increases significantly above 10 g/kg. However, since the air flow rate is low during these conditions, the influence on the room air temperature (nearly equal to the return air temperature) and room air humidity is low. It becomes also obvious, that the DEC system is operated in supply air humidification only although the room temperature increases nearly up to 26°C. This results from the fact that the lowest supply air temperature of 16°C can be reached by supply air

humidification without decreasing the absolute supply air humidity above 10 g kg^{-1}. Therefore, all other options are blocked by the PE-Optimiser

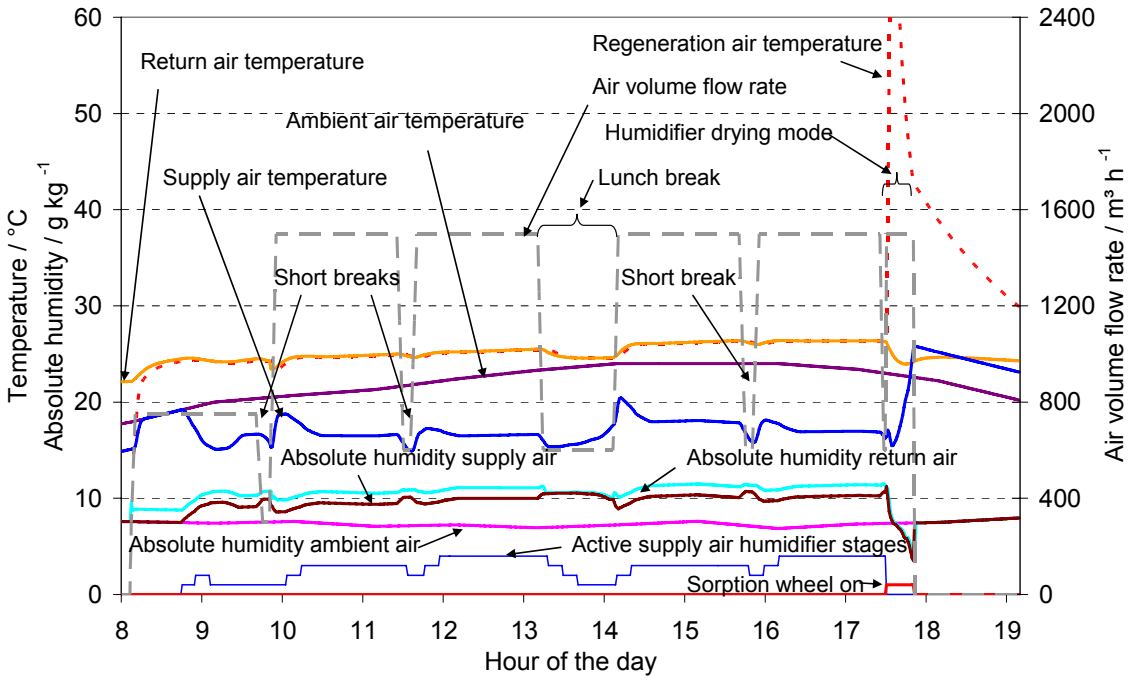

Fig. 5-33: Performance of the supply air humidifier control for one day in July with low humidity of the ambient air

5.6.4 POSSIBLE IMPLEMENTATION OF THE NEW CONTROLLER AND PE-OPTIMISER

The developed new sequence controller code can be directly implemented into the programming of the Siemens Visonic control unit, which is programmed in COLBAS. For the PE-Optimiser there are in principle two options. Option one would be to program the simple models of the PE-Optimiser directly as functions in the controller code. COLBAS allows the programming of loops, which are needed for the required iterative solution of some of the equations. The developed internal function is then called by the main control routine to get the control suggestions from the PE-Optimiser at each time step. The internal time step of the controller is 10 seconds.

The second option is to use the OPC interface provided by the Siemens Desigo control program and to directly use the developed PE-Optimiser in INSEL. In

this case an OPC client in INSEL reads the actual measured ambient air conditions from the OPC server, transfers them to the INSEL PE-Optimiser model which calculates the suggested operation mode of the DEC system and writes the result back to the OPC server for each time step. In addition to the operation mode of the DEC system also the suggested humidifier stage of the supply air humidifier is calculated from the measured supply air conditions after the heat exchanger wheel. The resulting humidifier stage is also written to the OPC server. For the suggested operation modes of the DEC system and the suggested humidifier stage virtual data points need to be defined in the control code which are then read form the OPC server and used in the control code. A time step of 1 minute would be sufficient in this case but could also be reduced down to 10 s. The possible external implementation of the optimisation tool via OPC is visualised in Fig. 5.4, which can be found in section 5.3.2., where the implementation was already discussed in principle.

5.7 SIMULATION BASED PERFORMANCE ANALYSIS

5.7.1 ANALYSED CONTROL OPTIONS

To demonstrate the efficiency of different standard control strategies compared to the developed new system controller with primary energy optimisation tool, simulations have been performed for a typical cooling period (May to September). The four different cases listed below together with the control sequences are analysed. In case 1 (as worst case) a standard control which starts with free cooling, followed by the increase of the air volume flow rate up to the maximum flow rate before the other options like indirect humidification, combined humidification and full desiccant mode are considered. In case 2 an electricity optimised control is used which tries to cover the cooling load at the lowest possible air flow rate using first all other options before the air volume flow control is used as last option. This control is similar to the control used for the sequence controller of the primary energy optimised control described in section 5.6 but without PE-Optimiser. Case 3 considers the primary energy optimised control including the PE-Optimiser as described in section 5.6. In

case 4 the reference ventilation system with compression chiller is analysed, which is described in section 5.4.7.

Case 1: Standard control cascade (1st free cooling / 2nd volume flow control / 3rd indirect humidification/4th combined humidification / 5th DEC mode)

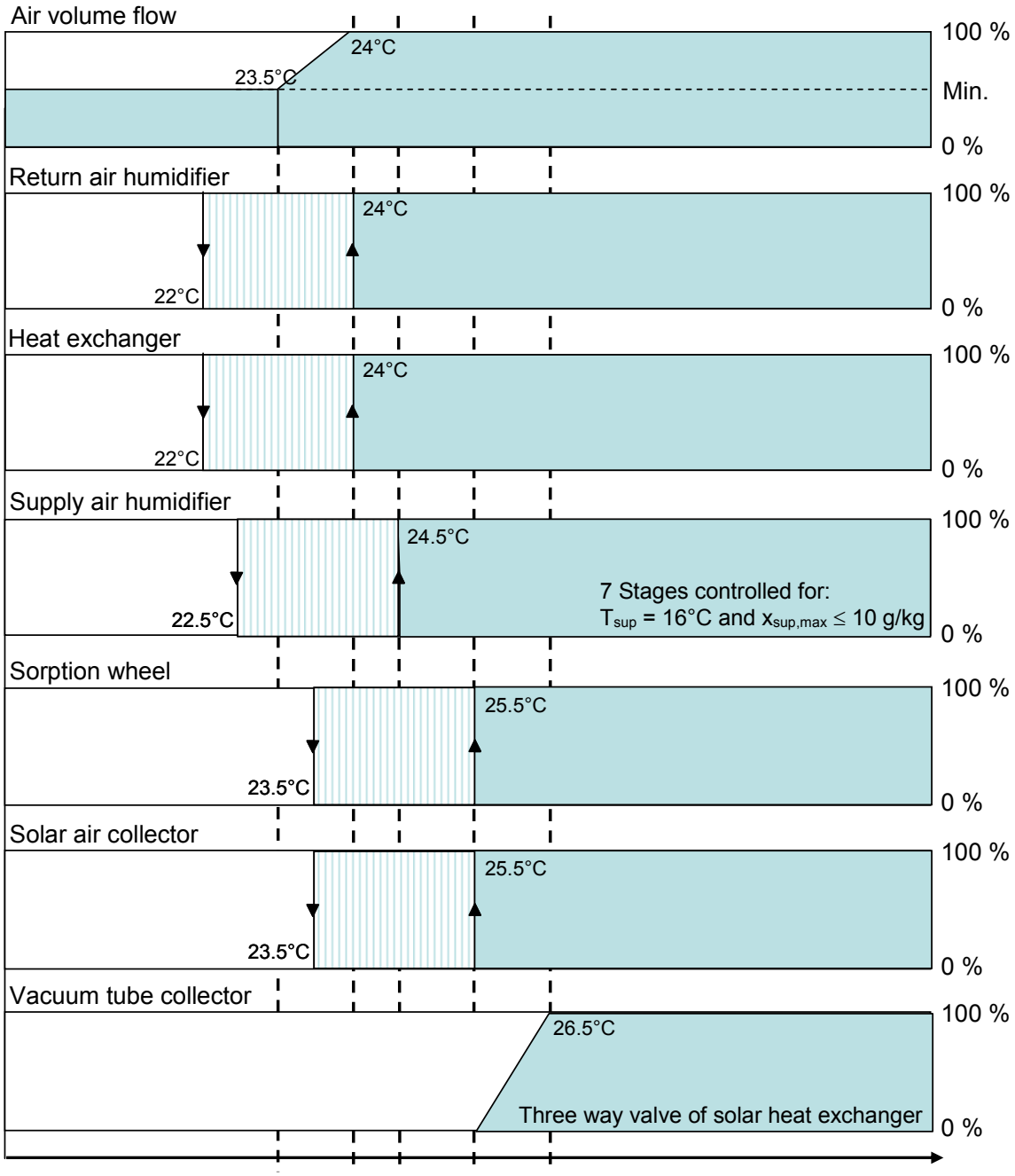

Fig. 5-34: Control cascade of the standard control

Case 2: Electricity optimised standard control cascade (1st free cooling / 2nd indirect humidification / 3rd combined humidification / 4th DEC mode / 5th volume flow control)

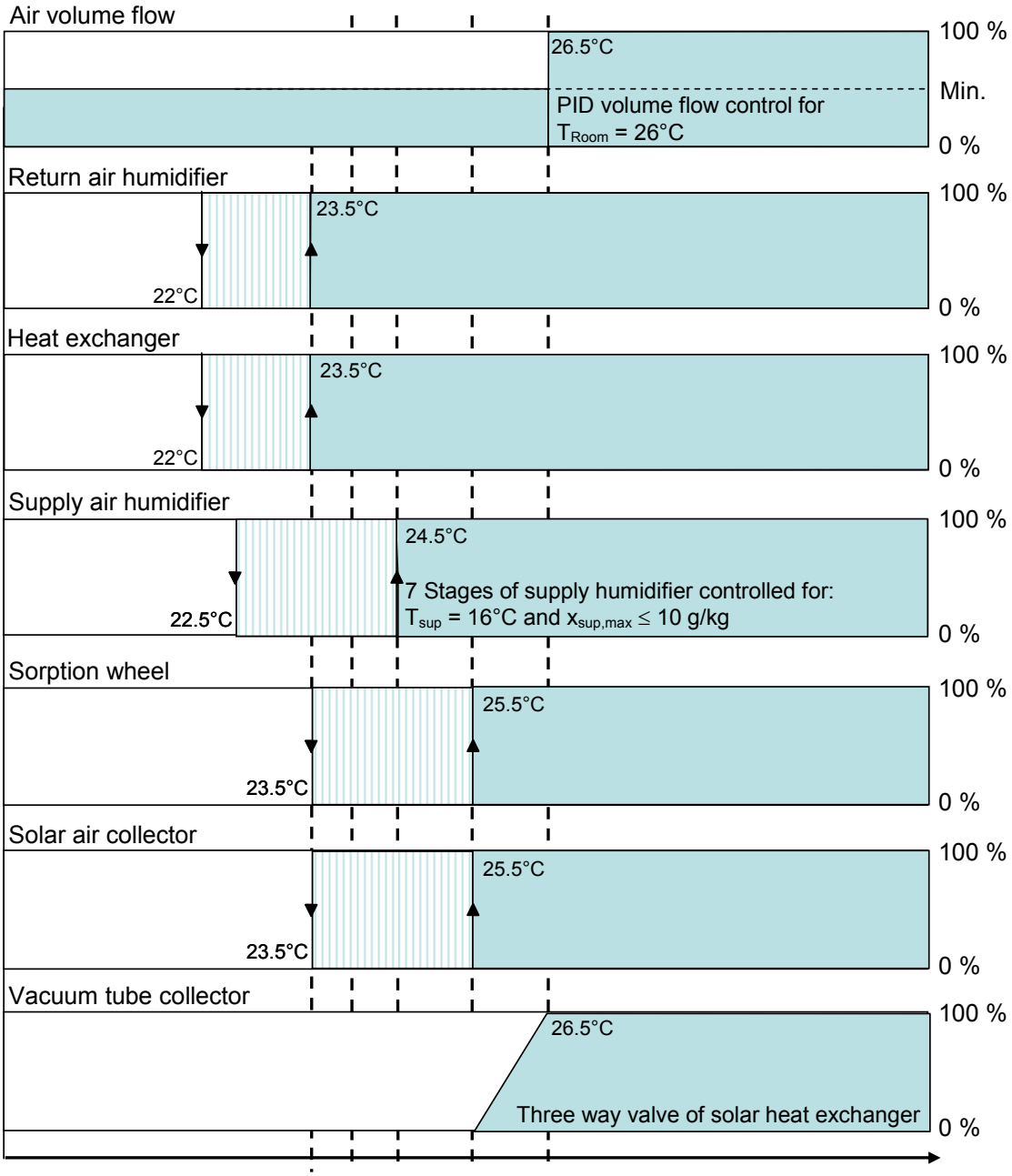

Fig. 5-35: Control cascade of the electricity optimised standard control

Case 3: Advanced model based control with PE-Optimiser

→ See section 5.6 for details

Case 4: Electricity optimised reference system (Ventilation system with air volume flow control / compression chiller with average COP of 2.8)

→ See section 5.4.7 for details

5.7.2 WEATHER DATA

A IWEC weather data set of Stuttgart (Energy Plus) with ambient temperature, relative humidity and solar radiation on the horizontal has been used for the simulations of the four different cases. The distribution of the ambient air temperature and relative humidity of the analysed period from May to September is shown in Fig. 5-36.

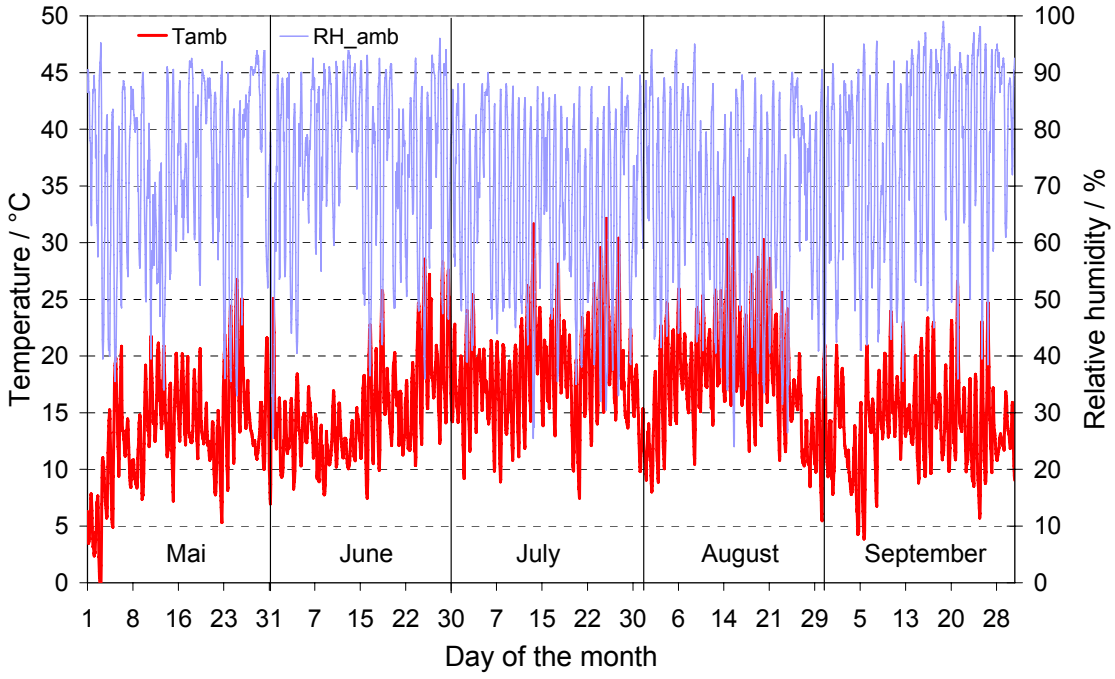

Fig. 5-36: IWEC weather data of Stuttgart (Source Energy Plus)

5.8 SIMULATION RESULTS AND DISCUSSION

5.8.1 OVERALL ENERGY EFFICIENCY

The main results are shown in Fig. 5-37 and Fig. 5-38, where the electrical COP and the primary energy ratio (PER) are compared for all analysed cases. For all analysed desiccant cases the required heating energy for regeneration of the sorption wheel is completely covered by the two solar systems described above. Therefore, the primary energy consumption of the analysed cases with DEC system only depends on the electricity consumption of the ventilators (main part) and the other components (pumps, wheels etc.).

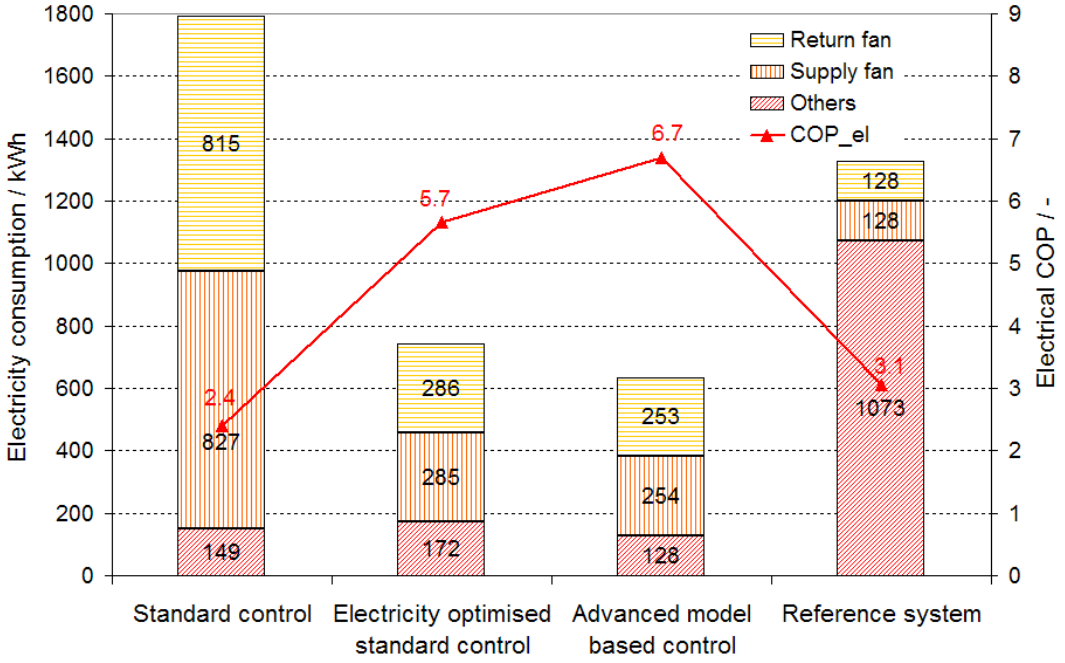

Fig. 5-37: Simulation results for the overall electricity consumption and the resulting electrical COP

As visible from Fig. 5-37, the highest electricity consumption of 1800 kWh and therefore the lowest electrical COP of 2.4 results for the DEC system with non optimised standard control (Case 1). If the standard control is replaced by the electricity optimised control (Case 2) the electricity consumption is reduced by 58% and an electrical COP of 5.7 is reached. The main difference between these two control strategies becomes obvious if Fig. 5-39 is regarded, which

shows a statistic of the frequency distribution of the air flow rates of all analysed cases. The DEC system with non optimised standard control in Case 1 uses the increase in air flow rate as first control option and is therefore much more often operated at higher air flow rates than the system with electricity optimised control, where the volume flow control is the last possible control option to keep the room air temperature within comfort limit. The much lower operational hours at high air flow rate reduce the electricity consumption of the supply and return air ventilator significantly.

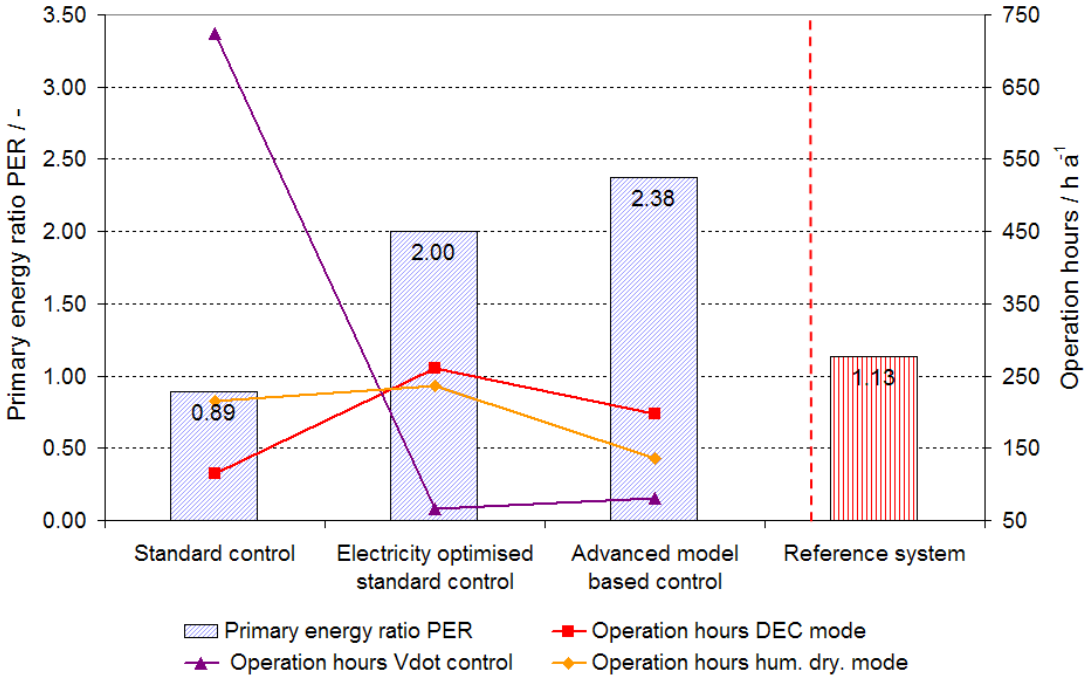

Fig. 5-38: Simulation results for the overall primary energy ratio of the analysed cooling period

If the primary energy ratio in Fig. 5-38 is regarded it becomes obvious, that the high electricity consumption of the non optimised standard control results in a low primary energy ratio of 0.89 which is 56 % lower than the primary energy ratio of the DEC system with electricity optimised control which reaches a quite high value of 2.0. In the same figure the operational hours in different operation modes are compared. This clearly shows that the standard control in Case 1 operates the system more the 720 hours in ventilation control mode whereas

the electricity optimised control uses this control option only during 65 hours for the whole analysed cooling period. Since the electricity optimised control option tries to operate the system at the lowest possible supply air temperature before the air volume flow is increased, the system operates much more frequently in full desiccant mode (260 h) than the standard control (115 h) does. Fig. 5-40 shows the fraction of the different operation modes of the analysed cases on the overall operational time of the analysed DEC system. Here it becomes obvious that the standard control operates the system only during 15 % of the total operation time in desiccant mode. For the electricity optimised control the operational hours in desiccant mode are nearly doubled and a fraction on total operation time of the DEC system of 29 % is reached. The standard control operates the system with 17 % of the total operational time much more often in indirect humidification mode as the electricity optimised control which uses this option only during 3 % of the total operational time. The reason for this is that at high air flow rates the cooling load can be very often covered with indirect humidification. All other control modes are used with nearly the same frequency.

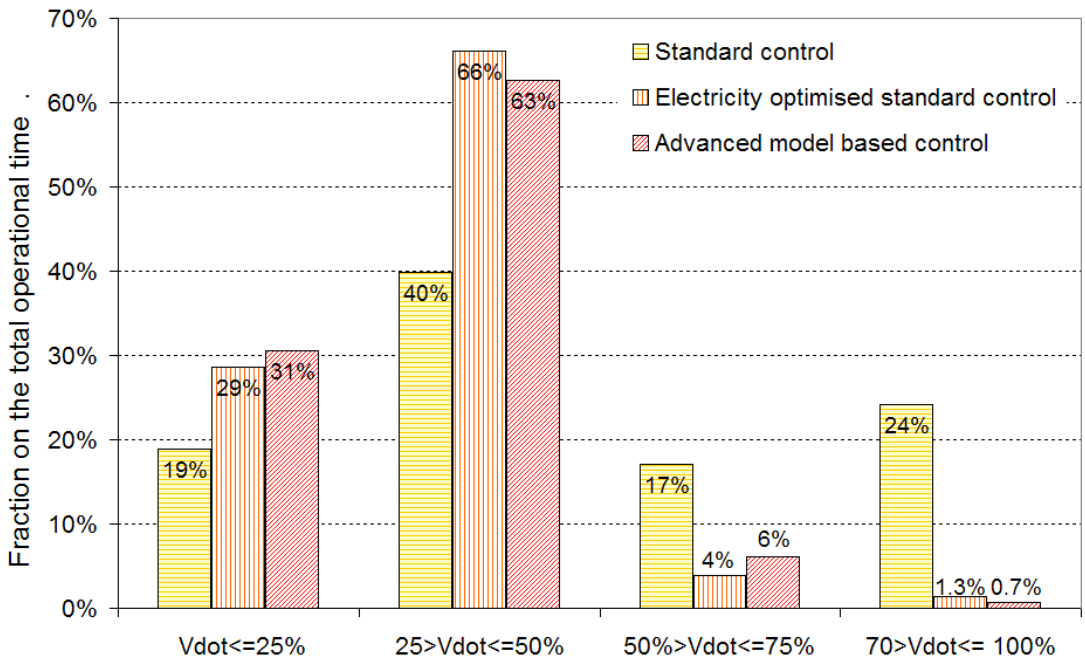

Fig. 5-39: Distribution of the air volume flow rate of the three analysed cases

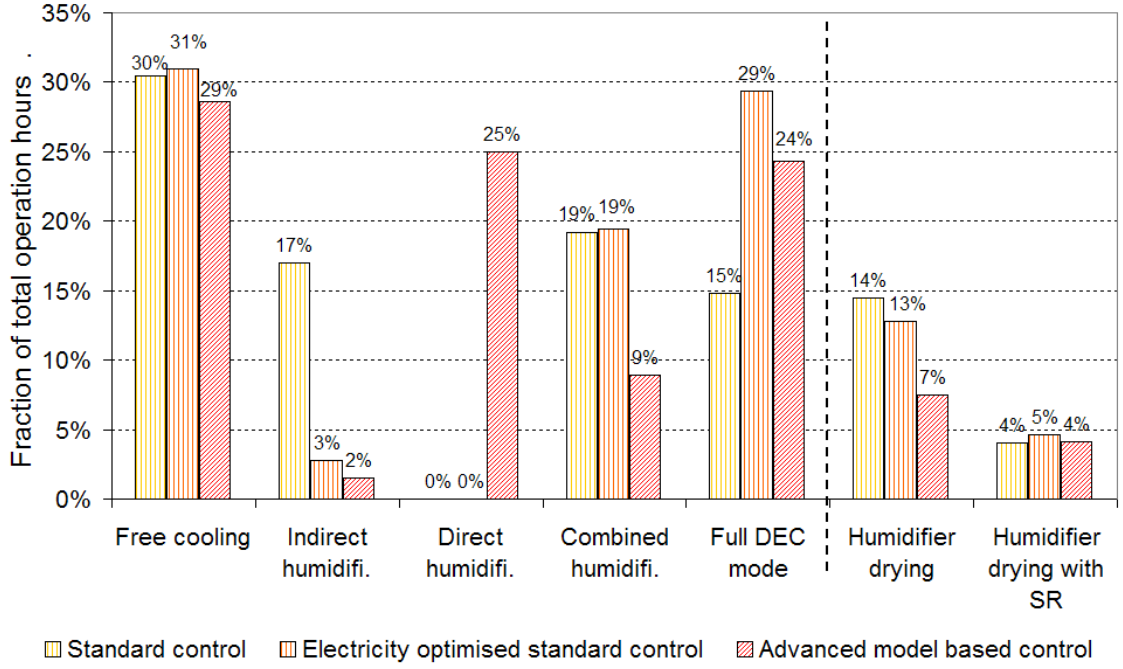

Fig. 5-40: Distribution of the DEC operation modes for the three analysed cases

If the developed advanced model based control is applied, the DEC system reaches a PER of 2.38, which is 19 % higher than for the electricity optimised standard control and more than a factor two better as the reference system. The better overall performance compared to the electricity optimised standard control results mainly from lower operation hours in humidifier drying mode and lower operation hours in full desiccant mode as visible from Fig. 5-40. This significantly reduces the electricity consumption by 15% compared to the electricity optimised control to a value of 635 kWh which results in an electrical COP of 6.7. For comparison, the analysed reference cooling system with compression chiller reaches a primary energy efficiency of 1.13. This is more than a factor of two lower than the value reached for the advanced model based control, but already 27% better than the value reached for the DEC system with standard control. This clearly demonstrates that an energy efficient control of the DEC system is very important in order to reach a higher efficiency than efficient standard systems with compression chiller.

The advanced model based control is based on the same sequence controller as used for the electricity optimised control but is supported by the primary energy optimiser. This model based tool is operated as online tool and evaluates permanently the operation mode with the highest primary energy efficiency at the actual weather conditions. All other control options are blocked in the sequence controller. The main difference between these two control options becomes visible from Fig. 5-40. Here it is clearly visible, that the advanced model based control operates the DEC system very often (25% of the total operational time) in direct humidification mode, whereas this option is not considered at all by the standard and the electricity optimised control. The indirect humidification mode is very seldom used by both, the electricity optimised standard and the advanced model based control. A significant difference is visible for the combined humidification which the advanced model based control uses less than half of the time as the other two options do. Since the supply air humidifier operates in direct humidification mode very often only with one or two stages, the required operation time of the ventilators for humidifier drying is much lower than in case of indirect humidification, where always the complete contact matrix is wetted. Therefore, the additional operation time in humidifier drying mode is much shorter for the advanced model based control. This significantly reduces the electricity consumption of the system. Additionally, at direct humidification mode, often lower supply air temperatures are supplied to the rooms than in indirect humidification mode, which reduces the peak cooling load in the early afternoon and therefore reduces the operation time in full desiccant mode. The operation in full desiccant mode is therefore with 24 % of the total operational time lower than in case of the electricity optimised control (29%) but is still significantly higher than in case of the standard control (15%).

The humidifier drying significantly reduces the efficiency of the DEC systems. A fast drying process is therefore important for a high overall efficiency. From Fig. 5-40 it becomes obvious, that for all control cases the humidifier drying is quite frequently supported by the sorption wheel and solar air collectors. This reduces

the operation time and electricity consumption of the fans and increases the energy yield of the solar air collectors.

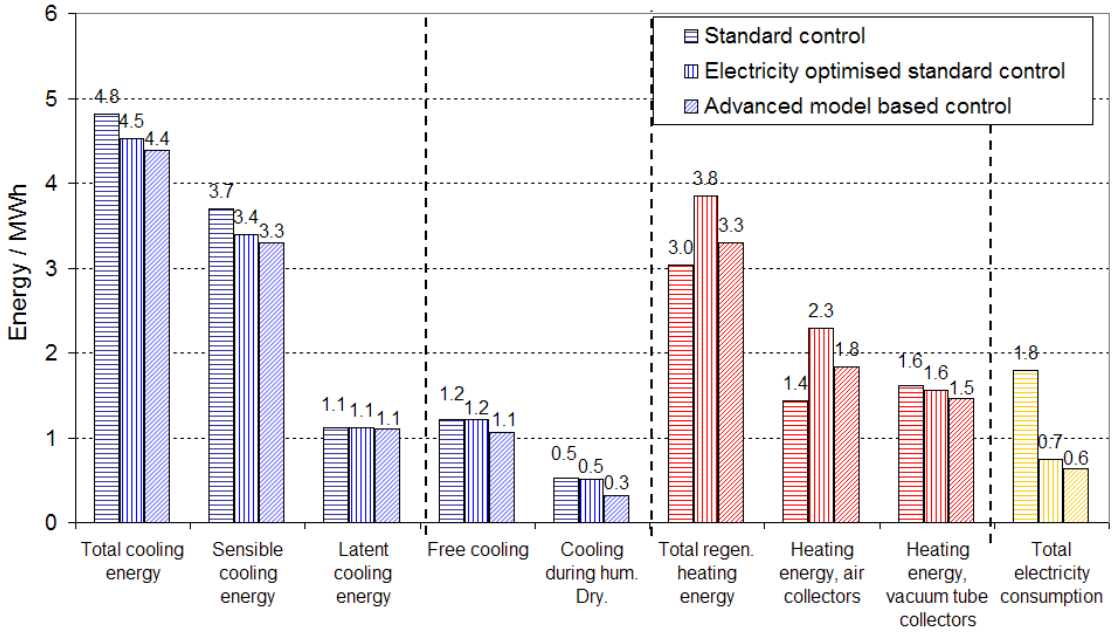

Fig. 5-41: Energy overview of the three analysed cases

The overall cooling energy supplied to the seminar rooms and the required heating energy are shown in Fig. 5-41 for all control options together with the resulting electricity consumption. Here it becomes obvious that the DEC system with standard control supplies the highest amount of cooling energy of 4.8 MWh but also has the highest electricity input of 1.8 MWh. On the other hand the lowest amount of heating energy is used from the solar system in this case, which can be attributed to the low operation hours in full desiccant mode as discussed before. The amount of cooling energy supplied to the seminar rooms is 4.5 MWh for the electricity optimised standard control and 4.4 MWh for the model based control. The main difference in cooling energy results from the sensible part whereas the latent cooling part is the same with 1.1 MWh for all control options. The additional cooling energy supplied to the rooms during the humidifier mode is 0.5 MWh in case of the standard and electricity optimised control and only 0.3 MWh in case of the advanced model based control. The reason for this has been discussed before and results from the lower operation

times in humidifier drying mode of the advanced model based control which often uses direct humidification.

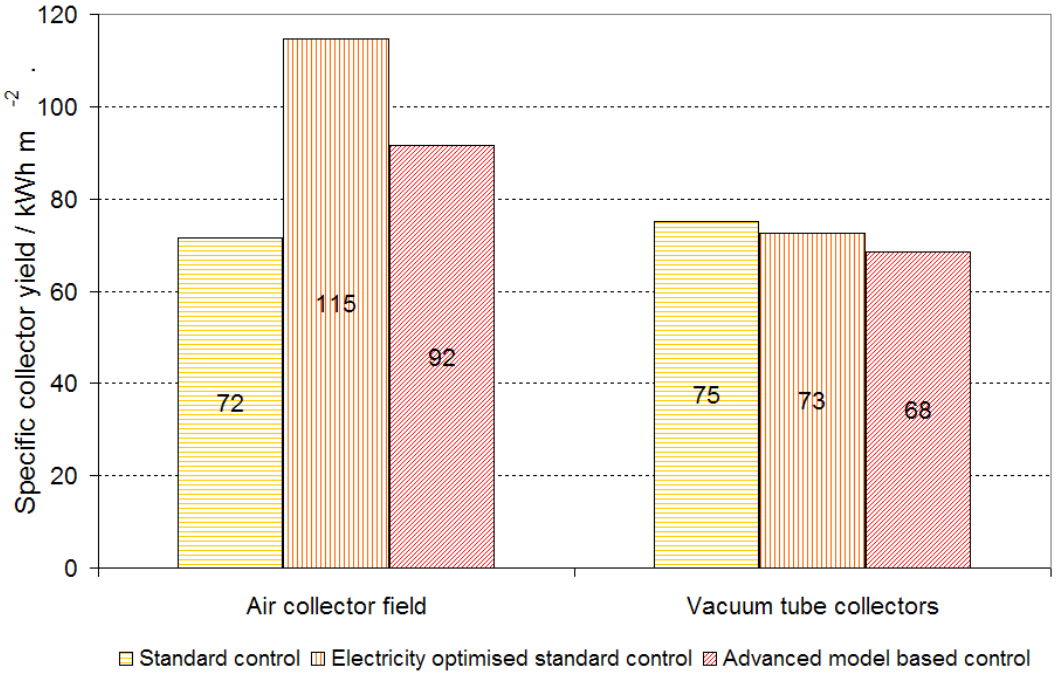

Fig. 5-42: Specific collector yield of the three analysed control options

As visible from Fig. 5-42 very low specific collector yields are reached during the analysed cooling period for both, the solar air collector with values between 72 kWh m^{-2} and 115 kWh m^{-2} and the vacuum tube collector field with values between 68 and 75 kWh m^{-2}. This is very typical for desiccant cooling systems in regions with moderate climate and 100 % solar fraction on the heating energy demand. Here the operational hours in desiccant mode are typically very low. For the solar air collector the highest values are reached for the electricity optimised control followed by the advanced model based control, which very frequently use the solar air collector at low air volume flow rates. Since the vacuum tube collector field is used as backup system it is more often used by the standard control which always uses high air flow rates in desiccant mode but operates only half of the time in desiccant mode than the optimised control does. The reason is, that at the high air flow rates the air collector does very often not reach the required regeneration temperature level and support is needed from the water based system.

5.8.2 DETAILED PERFORMANCE COMPARISON

To demonstrate the performance of the three different control strategies analysed for the DEC system, the detailed system performance of one Friday in July is shown in Fig. 5-43 to Fig. 5-45 for the different analysed cases. The system with standard control (Fig. 5-43) starts the operation in free cooling mode at ambient temperatures below 18°C. Between 8am and 9:30am only one of the two seminar rooms is occupied. Therefore, the minimum air flow rate is only 750 m³ per hour. Since the room air temperature increases from 22°C to 23.5°C after 10 minutes of operation the air volume flow control is activated and increases the air volume flow rate. After another 10 minutes of operation the room temperature increases above 24°C and the indirect humidification mode is activated (see also control sequence in Fig. 5-34). In consequence the supply air temperature decreases and the proportional controller reduces the air volume flow rate. Due to increasing external loads the air volume flow rate increases linear to 1300 m³ per hour until the first short break. During the break it is assumed that only a few students remain in the seminar room. Therefore, the air volume flow rate decreases to 600 m³ per hour during the break and increases quite fast to the maximum air flow rate of 3000 m³ per hour after the break, when both seminar rooms are fully occupied. Shortly after the maximum air flow rate is reached the room air temperature increases above 24.5°C and the supply air humidifier is activated. Since the room temperature remains below 25.5°C and above 22.5°C this operation mode is kept constant during the remaining occupation of the seminar room including one break with reduced air volume flow rate. After the last lesson the humidifier drying mode is activated to ensure dry humidifiers at system shut down. Since the air collector is able to deliver heating energy for the regeneration process, the air collector and the sorption wheel are activated to reduce the time required to dry the humidifiers. As described in section 5.3.1 for a higher overall efficiency at regeneration mode only half of the actual air flow rate is passed through the air collectors and mixed afterwards with the remaining air flow rate. The drying process of the humidifiers takes nearly one hour at half air flow rate. The drying process time

could be reduced if the maximum air flow rate would be used. However, since the electricity consumption of the fans increases with the third power of the air flow ratio (see Equation 5-1) this would significantly increase the electricity consumption of the system although the operation time is reduced by 40%.

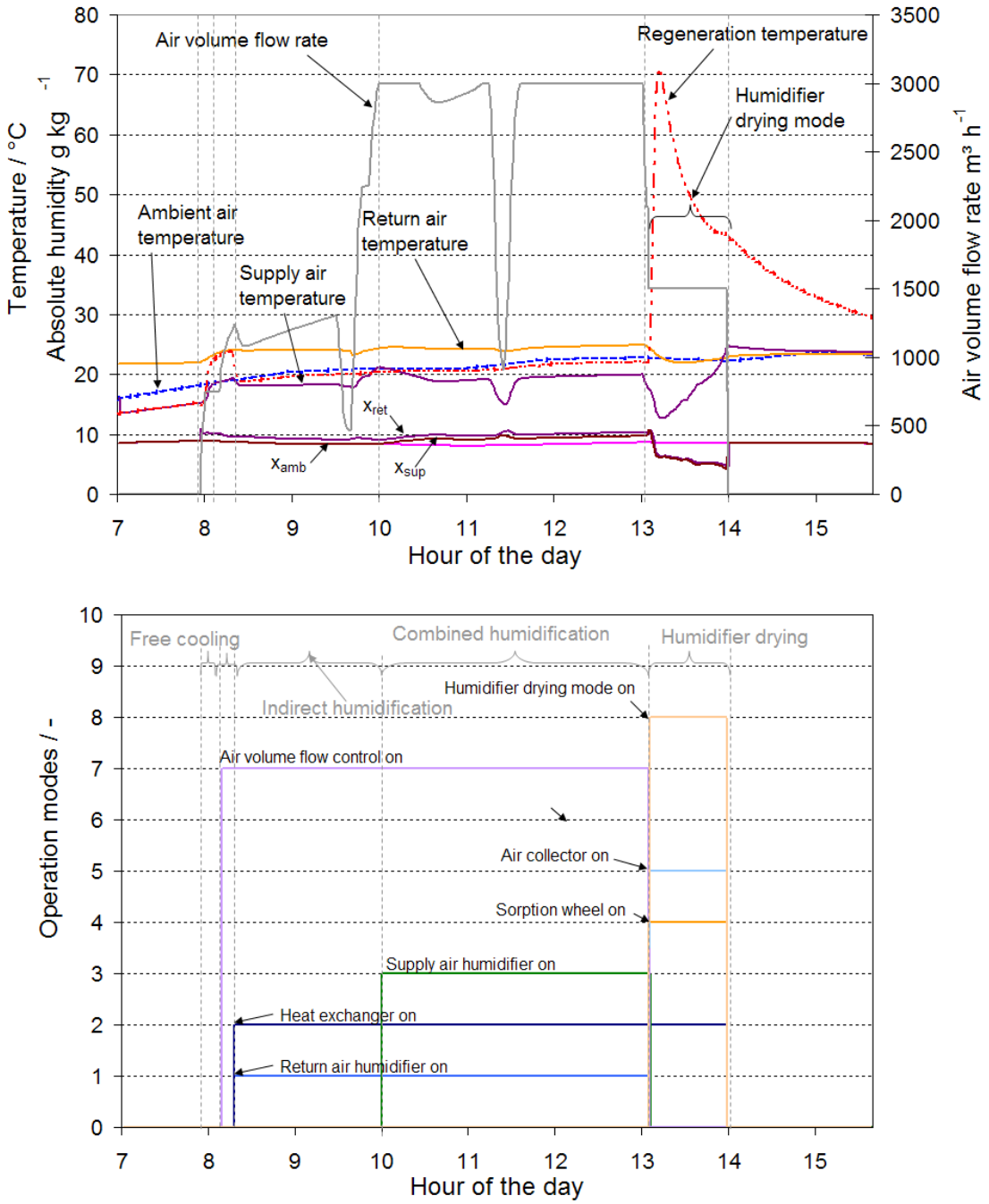

Fig. 5-43: DEC system with 'standard control' (Case 1); performance of a Friday in July

The performance of the system with electricity optimised control is shown in Fig. 5-44. The system starts also in free cooling mode at the lower limit of supply air flow rate of 750 m³ per hour. After 10 minutes of operation the room air temperature increases above 23.5°C and the indirect humidification mode is activated. However, at the given ambient and return air conditions this mode does not really provide cooling power. Therefore, the room temperature further increases to 24.5°C and the supply air humidifier is activated which increases the humidifier stages until the upper limit of the supply air humidity of 10 g kg^{-1} is reached. In consequence the supply air temperature is significantly decreased to 17°C and the room temperature is kept relatively constant below 25.5 °C.

After the second short break the room temperature increases above 25.5°C and at 11:45am the desiccant mode with sorption wheel and air collector is activated. The high regeneration temperature of 78°C at system startup significantly decreases the supply air temperature which shortly decreases slightly below 16°C. Since the regeneration temperature decreases and some stages of the supply humidifier are deactivated, the supply air temperature increases again above 25.5°C. Since the temperature of the air at air collector outlet is below 60°C, the solar heat exchanger fed by the hot water storages of the vacuum tube collector field is activated with proportional control of the regeneration air temperature. Since first cold water from the tubing is pumped into the solar heat exchanger the regeneration temperature is cooled and drops very fast below 30°C before it increases slightly above 50°C and is then decreased again by the proportional control to 42°C at the end of the last lesson.

After the last lesson the solar heat exchanger is switched off and the humidifier drying mode is activated. The solar air collector and the sorption wheel remain in operation for a faster drying process which again requires nearly one hour of operation at half air flow rate.

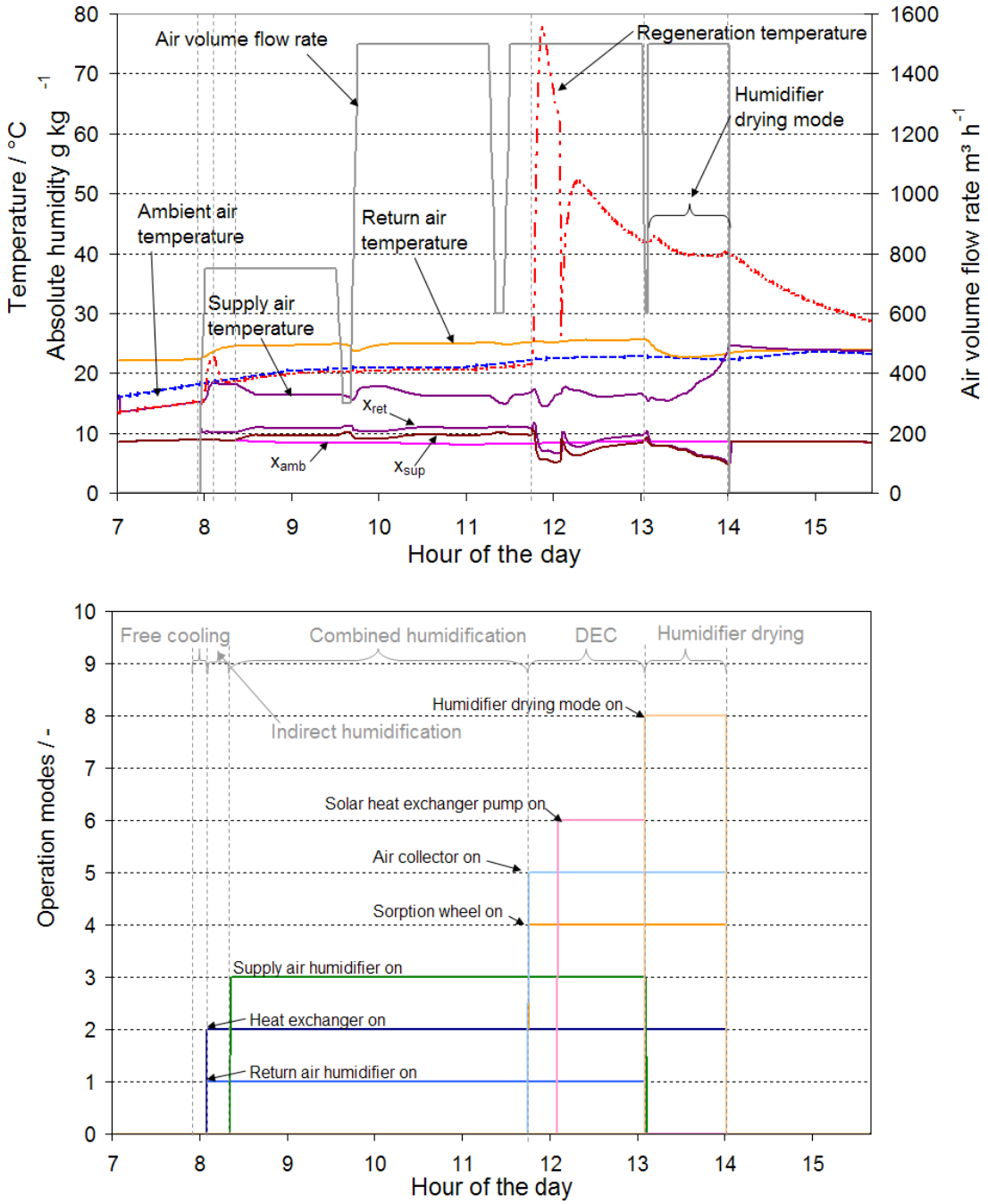

Fig. 5-44: DEC system with 'electricity optimised control' (Case 2); performance of a Friday in July

The advanced model based control shown in Fig. 5-45 starts also in free cooling mode but blocks the activation of the indirect humidification at low ambient air temperatures. Therefore, the indirect humidification mode is not activated although the room temperature increases above 23.5°C. As soon as the room temperature reaches 24.5°C the supply air humidifier is activated which increases the humidifier stages with optimised control until the upper limit of the supply air humidity is reached.

At 8:40am the ambient and return air conditions are in a region where the PE-Optimiser stops to block the indirect humidification. Since the room air temperature is still above 23.5°C the indirect humidification is activated. In consequence the supply air temperature drops slightly below 16°C and the number of active supply air humidifier stages is decreased. The system remains in combined humidification operation until 12:00am when the room temperature increases above 25.5°C and the sorption wheel and air collector are activated (15 minutes later than in Case 2). In consequence of the high regeneration temperature at system startup, the supply air temperature is significantly reduced and the room air temperature drops below 25.5°C.

The later startup of the sorption mode compared to the electricity optimised control can be attributed to the earlier activation of the direct humidification mode which provided more cooling energy to the seminar rooms during the early morning. After the last lesson the solar heat exchanger is switched off and the humidifier drying mode is activated with similar performance as already described for the electricity optimised control.

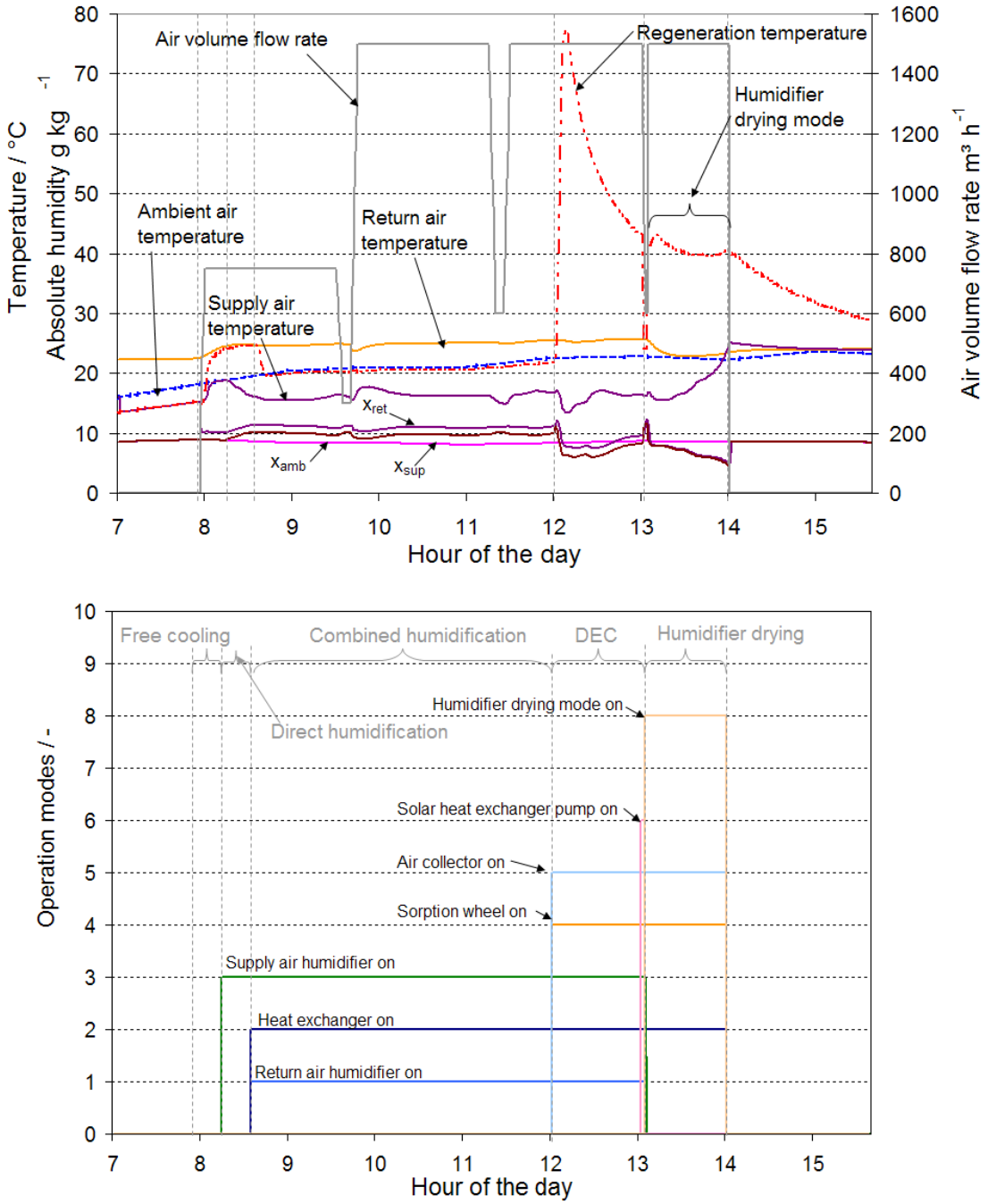

Fig. 5-45: DEC system with 'advanced model based control' (Case 3); performance of a Friday in July

The main difference between the electricity optimised and the advanced model based control becomes obvious if a day with relatively low ambient air temperature and humidity is regarded. Fig. 5-46 represents such a typical day in July and shows the performance of the electricity optimised control. The

regarded day is a Monday with a longer break of nearly 3 hours during the morning from 11:15am to 02:00pm. The system starts in free cooling mode until the room temperature increases above 23.5°C and the indirect humidification mode is activated. The indirect humidification mode does not really provide much additional cooling power, which is visible in the low difference between the ambient air temperature and the supply air temperature. In consequence the room temperature further increases up to 24.5°C and the supply air humidifier is set in operation. This significantly reduces the supply air temperature and the room air temperature of the two seminar rooms is kept below 25.5 °C during the remaining classes. At the beginning of the longer break the humidifier drying mode is activated together with the sorption wheel and the solar air collector for fast humidifier drying. During the afternoon lessons the performance of the DEC system is similar with the activation of the combined humidification followed by the direct humidification. At 16:15 the room air temperature increases above 25.5°C and the sorption wheel is set in operation together with the solar air collector. This significantly reduces the supply air temperature which leads to a drop in room air temperature. Due to low solar radiation the regeneration temperature after the solar air collector decreases very fast below the minimum operation temperature of 35°C and the air collector and sorption wheel are switched off. At the end of the last lesson the humidifier drying mode is activated, but only very shortly supported by the sorption wheel and solar air collector. If in comparison to this the performance of the advanced model based control in Fig. 5-47 is regarded, a completely different control is visible. The system starts also in free cooling mode but the indirect humidification mode is blocked by the controller, since at the given ambient and room air conditions no efficient cooling energy can be provided by this system. As soon as the room temperature increases above 24.5°C the direct humidification mode is activated and remains in operation for the rest of the morning lessons. The room temperature remains below 25.5°C and therefore no further mode is activated in the morning.

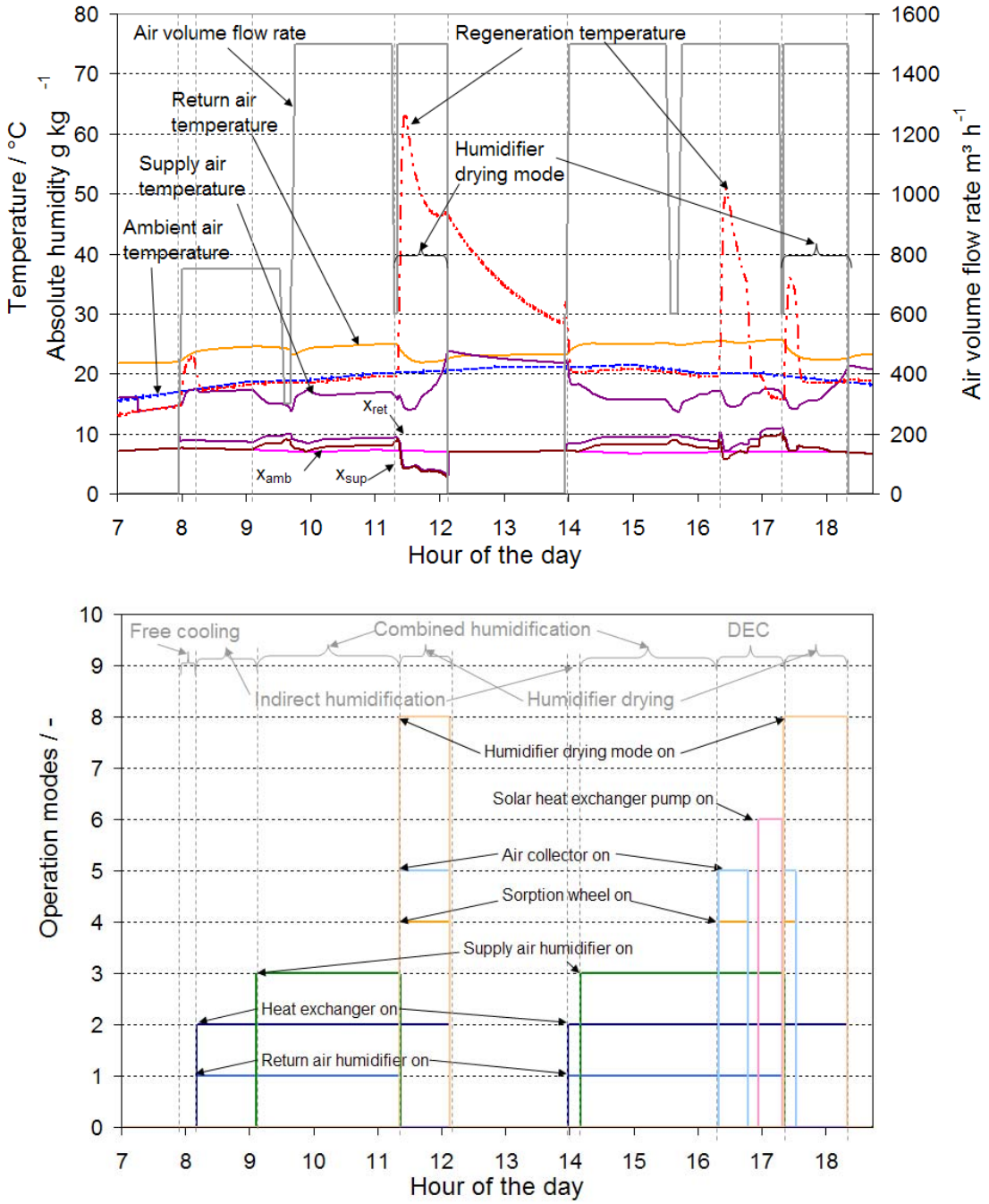

Fig. 5-46: DEC system with 'electricity optimised control' (Case 2); performance of a Monday in July with low ambient air temperature

The humidifier drying mode after the last morning lesson is supported by the solar air collector and desiccant wheel. Since only the supply air humidifier was in operation with a few stages, the drying process is much faster in this case.

After the break the system again starts in free cooling mode followed by direct humidification. The indirect humidification is still blocked by the controller.

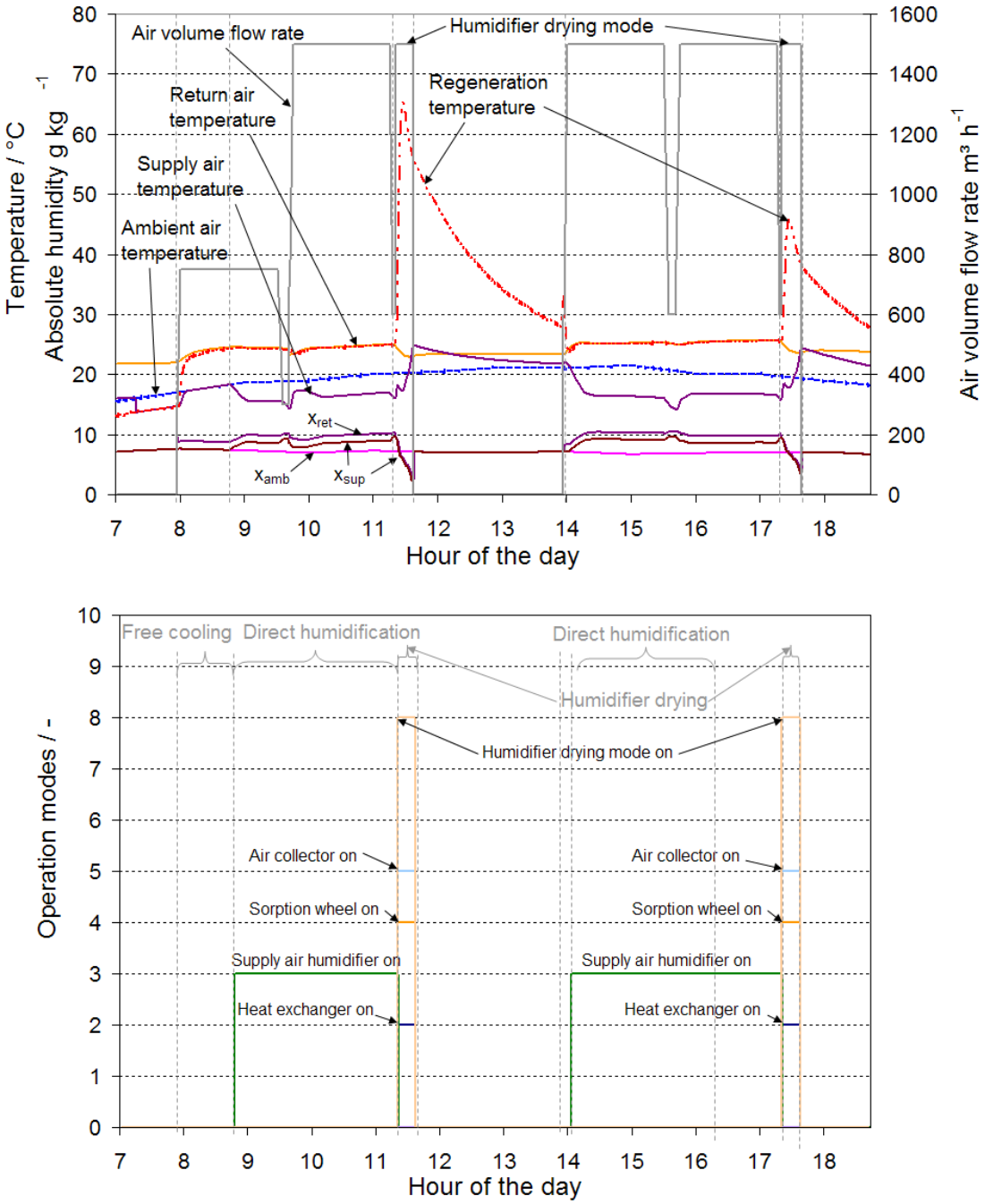

Fig. 5-47: DEC system with 'advanced model based control' (Case 3); performance of a Monday in July with low ambient temperature

Since the DEC system is able to provide the lowest possible supply air

temperature already in direct humidification mode the only remaining option to increase the cooling power is the increase in air flow rate. Therefore, the activation of the sorption mode is also blocked by the controller although the room temperature increases slightly above 25.5°C. Since the room temperature stays below 26.5°C the air volume flow control with PID control for 26°C room temperature becomes not active. The humidifier drying mode at the end of the day is again much shorter than for the electricity optimised control.

5.8.3 THERMAL COMFORT

Thermal comfort as defined in the standard ISO 7730 and the ASHRAE standard 55 uses the PMV index, which represents a supposed thermal comfort vote based on four physical measured parameters (air temperature, mean radiant temperature, air velocity and relative humidity) and two person based parameters (clothing insulation and activity level). From the predicted mean vote, the percentage of dissatisfied with general comfort (PPD) are calculated. Depending on the comfort category chosen, the PPD should be smaller than 6% (category A) up to 15% (category C). In the US, the ASHRAE Standard 55-2004 places an upper limit on the allowable operative temperature of 28°C, or 27°C when the moisture content increases to the limiting value of 12 g kg^{-1} of dry air (ASHRAE, 2004). In Germany, the allowed excess in room temperature level above 25 to 27°C (depending on the climatic zone) is 10% of all working hours (DIN 4108-2). For climatic zones as in Stuttgart where the average monthly temperatures during summer are above 18°C, it is acceptable within German regulations to exceed 27°C room temperature during 10% of all operational hours of the year.

To compare the obtained comfort level of the three analysed DEC control strategies the increase of room temperature above 26°C and 26.5°C is analysed and compared. The results shown in Fig. 5-48 clearly demonstrates that the room temperatures of seminar room 1 much more often increase above 26°C in case of the DEC system with electricity optimised control (Case 2) and

the DEC system with advanced model based control (Case 3) than in case of the standard control (Case 1). However, the hours above 26°C are still very low with only 12 hours for the standard control, 47 hours for the electricity optimised control and 54 hours for the advanced model based control. However, 26.5°C are only increased during 1 to 5 hours during the whole cooling period. For none of the analysed control cases 27°C is ever reached. The results for seminar room 2 are very similar and therefore not shown and discussed here separately.

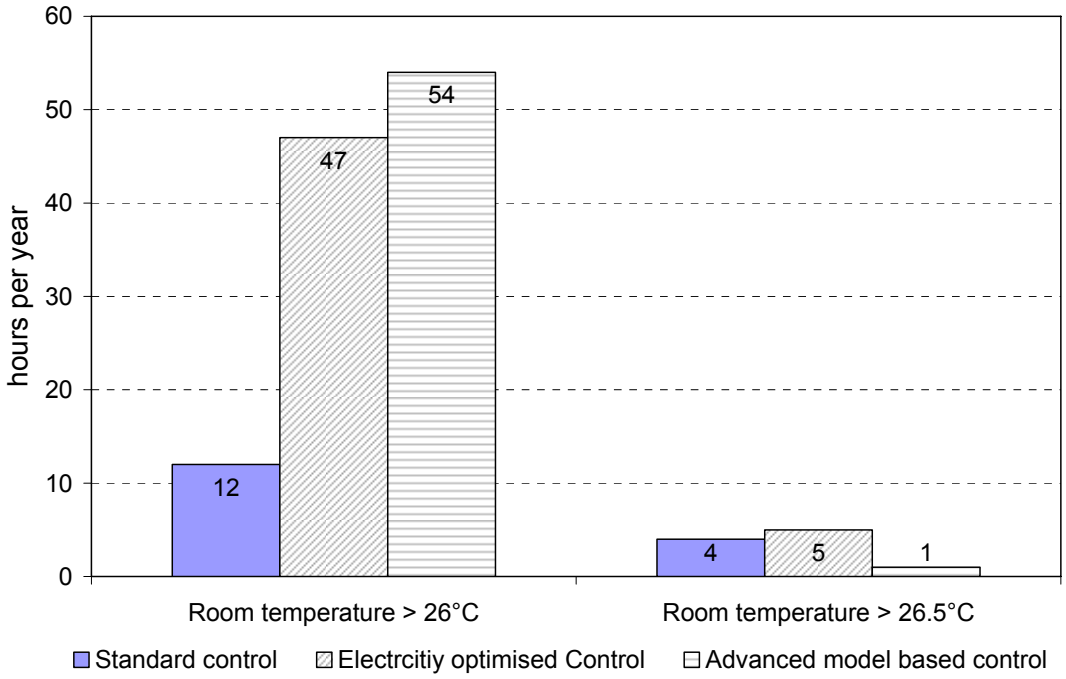

Fig. 5-48: Statistic of room temperatures obtained for the three analysed control options of the DEC system

Additionally, the hourly room air conditions during occupation over the whole analysed cooling period from May to October are compared to the acceptable ranges of operative temperature and humidity for people in typical summer and winter clothing during light, primarily sedentary activity (≤ 1.2 met) as defined in ASHRAE 55, Appendix A for 10 % dissatisfaction criterion. As visible from the results shown in Fig. 5-49 to Fig. 5-51 the room air conditions are almost always within the acceptable comfort ranges for all analysed DEC control cases. There

are only very few hours with room air conditions slightly outside the comfort ranges of ASHRAE 55. There is also nearly no difference between comfort conditions reached especially for the electricity optimised and the advanced model based control. The difference between the standard control and the two advanced control strategies is that the acceptable comfort range is used in the whole range in case of the advanced strategies whereas the stand control keeps the room air conditions more in the middle of the acceptable comfort range.

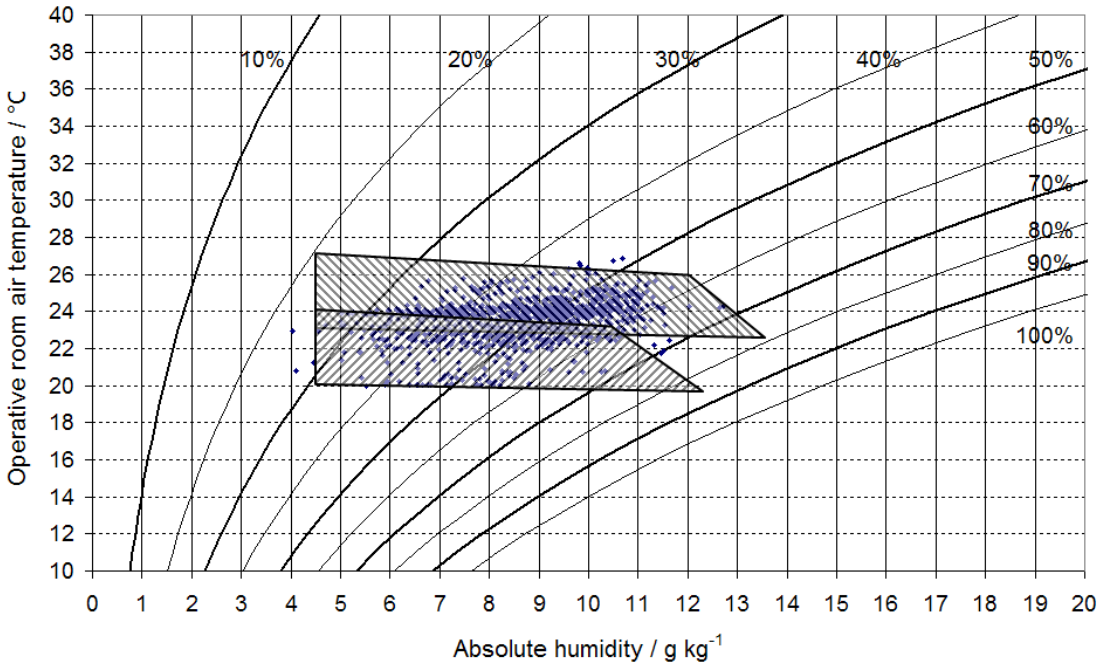

Fig. 5-49: Calculated operative temperatures and absolute humidity together with the ASHRAE 55 standard comfort limits for summer (upper area) and winter conditions (lower area) for the DEC system with standard control (Case 1)

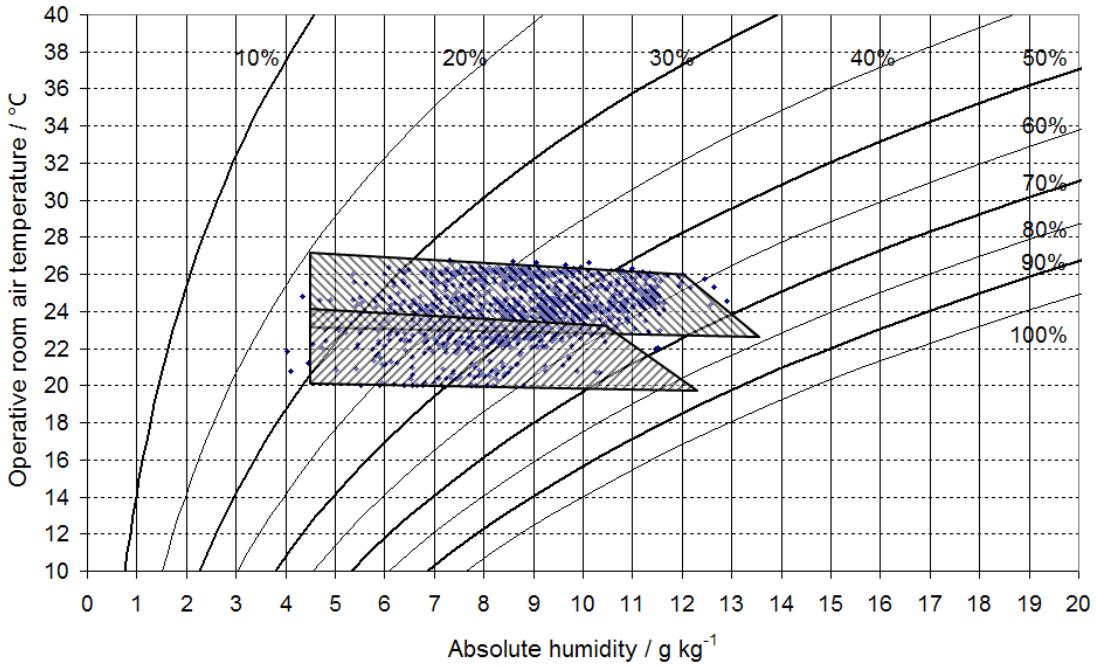

Fig. 5-50: Calculated operative temperatures and absolute humidity together with the ASHRAE 55 standard comfort limits for summer (upper area) and winter conditions (lower area) for the DEC system with electricity optimised control (Case 2)

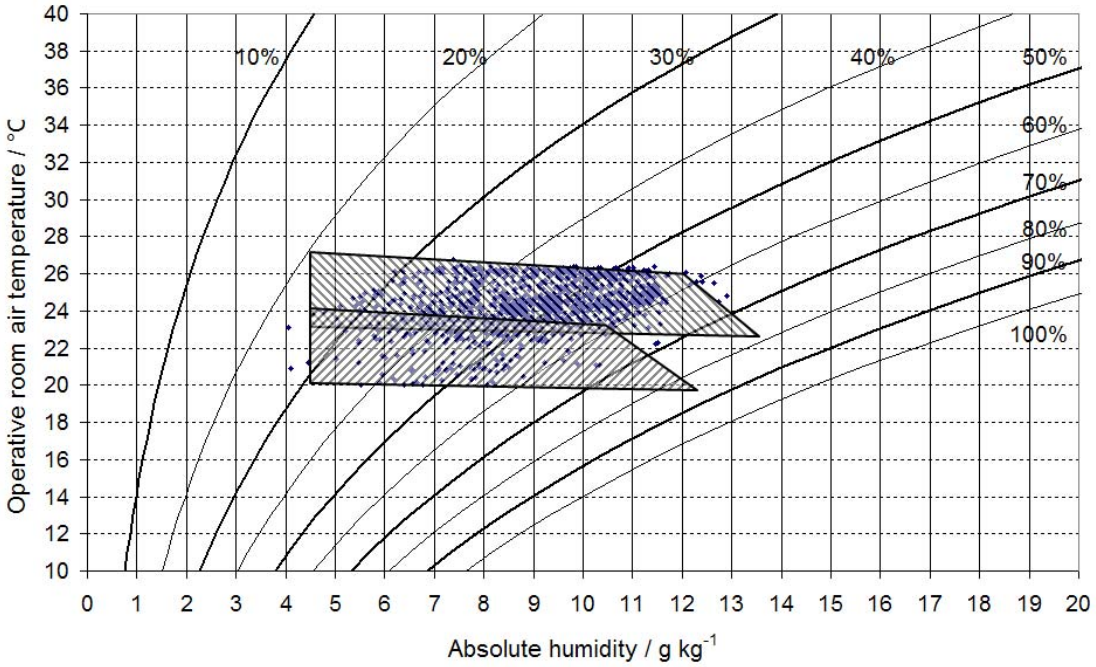

Fig. 5-51: Calculated operative temperatures and absolute humidity together with the ASHRAE 55 standard comfort limits for summer (upper area) and winter conditions (lower area) for the DEC system with advanced model based control (Case 3)

5.8.4 FURTHER OPTIMISATION POTENTIALS

As discussed in section 5.8.2 the analysed DEC system reaches a quite high primary energy ratio if the advanced model based control is used. Since the installed DEC system has so far no bypass possibilities for the sorption wheel, in all the simulations it was assumed that 100% of the return air is always passed through the sorption wheel. From detailed performance analyses it is known, that the performance of the desiccant wheel does not change remarkable if the regeneration air volume flow rate is reduced to 70% of the supply air volume flow rate (Schürger, 2007). This significantly reduces the required heating energy and the electricity consumption of the return air fan due to lower pressure drops in the sorption wheel and in the solar air collectors. A further improvement is reached if a bypass is used for the sorption wheel if this is not required. Under consideration of these two optimisation potentials a further simulation run with the advanced model based control was performed to evaluate the increase in overall system efficiency. These simulations of the improved system with advanced model based control revealed a significant reduction of the electricity consumption of 6% compared to the non optimised system. The resulting primary energy ratio is 2.55. This is 7% higher than for the non optimised system with the same control which reached a primary energy ratio of 2.38. These results clearly highlight the importance of an efficient system design with as low pressure losses as possible of all components including the tubing.

5.9 CONCLUSIONS

A new primary energy optimised system controller for DEC systems has been developed and tested in the simulation environment on a DEC demonstration plant of the University of Applied Sciences in Stuttgart which supplies two seminar rooms with fresh and cool air. The maximum air flow rate of the purely solar driven system is 3000 $m^3\ h^{-1}$. For heating energy supply the system is equipped with a 20 m^2 solar air collector field and a 21.6 m^2 vacuum tube collector field. The developed system controller consists of an electricity optimised sequence controller which switches on or off the different components of the DEC system in dependence of the room air temperature and ambient air conditions. This sequence controller is supported by a primary energy optimisation tool, which is operated as online simulation tool and evaluates for each time step the optimum operation condition with the lowest primary energy consumption of the DEC system. The results are transferred to the sequence controller, where the activation of the different operation modes are either blocked or accepted by the optimisation tool. This helps to avoid the activation of senseless or inefficient operation modes. The control of supply air humidifiers is always very difficult due to their high inertia especially when switched on or off. This can lead to largely fluctuating operation modes with an inefficient operation of the DEC system. To avoid such conditions and to improve the control the developed and validated dynamic humidifier model was used to calculate performance characteristics of the supply air humidifier. These performance characteristics are used in the optimisation tool to evaluate the optimum number of active stages of the seven possible stages of the supply air humidifier at the given inlet air conditions to avoid supply air temperatures below 16°C and absolute supply air humidity above 10 g kg^{-1}. The suggested humidifier stage is then transferred to the sequence controller who is allowed to increase or decrease the suggestion by one stage only for fine tuning. It could be demonstrated, that with this control the required supply air conditions are very fast reached at a stable operation of the DEC system.

The developed and validated dynamic simulation model of the whole DEC system was used for sensitivity analyses to evaluate the influence of air volume

flow control and additional heating or cooling on the overall system efficiency. The results clearly demonstrated that from the primary energy point of view, the increase of air volume flow should be used as last option if sufficient solar heating energy supply is available. Furthermore, it could be shown that additional cooling instead of additional heating leads to a much better primary energy efficiency of the system. In case of additional cooling the primary energy efficiency remains nearly constant at a value of around 1.2 whereas the primary energy efficiency in case of additional heating significantly decreases with increasing heating energy demand down to a value of 0.3. The highest primary energy efficiency is of course reached if the required heating energy can be completely covered by the solar system or other renewable sources. In this case primary energy ratios of up to 2.6 at full desiccant mode are possible.

To demonstrate the efficiency of the new model based controller simulations were performed for the demonstration plant with the validated dynamic simulation model for a typical cooling period from May to September. Three different cases with different controllers were considered, one with a standard control (Case 1) which uses the air volume flow control as first control option, one with an electricity optimised control (Case 2) which uses the air volume flow control as last possible option and an advanced model based control (Case 3) with the same sequence controller as for the electricity optimised control but with support from the primary energy optimiser which is used as an online tool. The results clearly demonstrated that the highest electricity consumption of 1800 kWh and therefore the lowest electrical COP of 2.4 results for the DEC system with non optimised standard control. If the standard control is replaced by the electricity optimised control the electricity consumption is reduced by 58% and an electrical COP of 5.7 is reached. The advanced model based control further reduces the electricity consumption by another 15 % and reaches a high electrical COP of 6.7. If the primary energy efficiency is regarded, the results show that a primary energy ratio of 2.38 can be reached in the best case for the advanced model based control. This is 19 % better compared to a system with electricity optimised standard control and by a factor two better than a good reference ventilation system with compression chiller. It is also shown, that an intelligent fan speed control is crucial for DEC systems in order

to compete with standard air conditioning systems. The analysed DEC system offers further optimisation potential through the implementation of a bypass of the sorption wheel and a reduction of regeneration air volume flow rate to 70% of the supply air volume flow rate. This optimised system setup has been analysed for the advanced model based control. The resulting overall primary energy efficiency was 2.55 which is 7 % higher than reached for the original system setup. This again highlights the importance of system constructions with low pressure losses of the components and the connected air channels.

The influence of the DEC system control on the reached thermal comfort conditions is also analysed. The results show that similar room air conditions are reached for the three analysed DEC control options. The room air conditions are almost always within the acceptable comfort ranges of ASHRAE 55. For all analysed control cases there are only very few hours with room air conditions slightly outside the comfort ranges. The room air temperatures are always below 27°C and only between 12 and 57 hours slightly above 26°C. Therefore, it can be concluded that for all cases room air conditions with good thermal comfort are reached.

6. SUMMARY

Solar cooling is a promising technology for CO_2 reduction in the fast growing air conditioning market for buildings. Therefore, the interest in this technology has significantly increased during the last 10 years and several demonstration plants have been installed in different European countries. These systems comprise solar driven closed absorption and adsorption cooling systems and open desiccant evaporative cooling systems (DEC). The first companies started to commercialise also small scale absorption cooling machines. However, due to lack of experience, not all of the installed systems operate energy efficiently and some are even worse than conventional systems with a compression chiller from the primary energy point of view. The main reasons for this are a suboptimal system control combined with a poor system design, which leads to low solar fractions and high electricity consumption of the pumps, fans and heat rejection systems. Often several separately controlled components were put together to form a 'cooling system'. Within IEA task 38 (International Energy Agency Solar Heating and Cooling Programme) several attempts are made to overcome these shortcomings. Optimised design guidelines supported by simple simulation based design tools are developed to improve the system design. Furthermore, guidelines for an optimised control of different systems derived from the experiences gained from installed systems are collected and published. In parallel standardised solar cooling kits with optimised components and optimised system controllers are developed by companies like SolarNext AG in Rimsting, Germany. The present work tries to support this process and presents guidelines for the optimised system design and control of solar driven closed absorption cooling systems. For DEC systems an innovative electricity optimised sequence controller has been developed which is support by model based primary energy optimisation tool (online tool) for control optimisation.

Simulation based analyses of design issues and control strategies are the main focus of this work. The simulation environment used and the models developed are introduced and described in detail in chapter 2. All models are validated against measured performance data of installed systems to ensure correct and high quality results.

6.1 SOLAR DRIVEN CLOSED ABSORPTION COOLING SYSTEMS

6.1.1 DIMENSIONING STRATEGIES FOR SOLAR DRIVEN ABSORPTION COOLING APPLICATIONS IN OFFICE BUILDINGS

The design, performance and economics of solar thermal driven absorption chiller systems for office building applications are addressed in chapter 3. The influence of different building load profiles caused by high external or internal loads, different building orientations and locations on the required solar system design for 80% solar fraction are analysed for a common maximum required cooling power. Additionally, the influence of different system technologies and control strategies on the required system design are regarded. Here systems with either constant (90°C) or flexible (70°C-95°C) generator inlet temperatures, wet or dry heat rejection systems and different temperature levels of the cold distribution system (6°C/12°C and 15°C/21°C) are analysed. These investigations showed that to achieve a given solar fraction of 80% of the total heat demand of the ACM largely different collector surfaces and storage volumes are required, depending on the characteristics of the building load file, the chosen system technology and control strategy. The required collector areas for 80% solar fraction vary in maximum by a factor of two between 1.8 and 3.6 m² per kW of maximum cooling power. The best system performance with the lowest required collector area is reached if the absorption cooling system is operated at flexible generator temperatures with preferably high cold water distribution temperatures. In this case a specific collector area of below 1.8 m^2 kW^{-1} is sufficient for a building with low internal loads which is more than 40% less than for the same system operated at constant generator temperature. In case of the constant generator inlet temperature also the selected collector mass flow rate clearly influences the required collector area. If the solar system is designed for a typical low flow arrangement with 15 kg m^{-2} h^{-1} the required collector area for the same system and load file is 30% higher

than with the collector field operated at the double mass flow rate of 35 kg m^{-2} h^{-1} (optimum). For flexible generator temperatures the influence of the specific collector mass flow rate is much lower but still shows a slight optimum at 35 kg m^{-2} h^{-1}. Higher mass flow rates in both cases decrease the performance of the solar system since the temperature lift in the collector field is often too low.

Apart from the collector mass flow rate, also the building load characteristic influences the required collector area, which varies by 15% for different orientations and by a factor of 2 if buildings with either high external or high internal loads are considered. For the location Madrid, 80% solar fraction are possible for surface areas between 2 and 4 m^2 per kW of cooling power, the higher values occurring for larger full load hours. For each MWh of cooling energy demand, between 1.6 and 3.6 m^2 collector surface are required for the Spanish site and between 4.6 and 6.2 m^2 for a German installation. The total system costs for commercially available solar cooling systems are between 180 and 270 € MWh^{-1} cold, again depending on the cooling load file and the chosen control strategy. The total costs are dominated by the costs for the solar thermal system and the chiller itself. For a more moderate climate with low cooling energy demand, the costs can rise as high as 680 € per MWh cold. The work shows that dynamic system simulations are necessary to determine the correct solar thermal system size and to reach a given solar fraction of the total heating energy requirement. In general it can be concluded that the best energetic and economic performance of the solar cooling system is reached for applications with long full load hours and if the absorption chiller is operated at flexible generator inlet temperatures (70°C to 90°C). All together the results of chapter 3 indicate that a design of solar cooling systems based on the maximum cooling load of a building is not recommendable. A much better energetic and economic performance is reached if the solar cooling system is designed to cover only a part (40% to 60%) of the maximum cooling load. This leads to high full load hours of the system and a good average thermal COP.

6.1.2 MODEL BASED CONTROL STRATEGY OPTIMISATION OF SOLAR DRIVEN ABSORPTION COOLING SYSTEMS

To analyse the effect of different control strategies on the system performance and primary energy efficiency in Chapter 4 more detailed analyses are performed. Dynamic simulation models are developed and used for these analyses which consider also the electricity consumption of the ACM, all connected pumps and of the fan of the heat rejection system apart from the thermal performance. The results obtained clearly demonstrate that a good system design with high solar fractions and low electricity consumptions combined with an intelligent system control is required for solar cooling systems in order to compete with standard compression chillers. Considering all results it can be concluded that a proper fan speed control of the cooling tower / dry heat rejection ventilator, as well as a ΔT mass flow control of the cold water distribution pump, are essential to obtain a high electrical COP of 8.0 and above. The highest total primary energy ratio of 2.2 and therefore the best overall efficiency is obtained if additionally the generator temperature is allowed to vary between 70°C and 90(95)°C and if the lowest possible set point for the absorber/condenser inlet temperature is used. For further improvement of the primary energy efficiency, the electricity consumption of the remaining main electricity consumers (absorber and condenser pump 37%, the collector pumps 28%, and the absorption machine itself 23%) needs to be reduced. Apart from the utilisation of highly energy efficient pumps with mass flow control the pressure drops in the system need to be reduced by constructive changes in the heat exchangers and the spray nozzles. For the absorber and condenser cooling water pump a reduction potential of 30% can be expected. If the solar system is operated as a pure water system with special frost protection control the heat exchanger between solar circuit and hot water storage can be omitted and the electricity consumption of the solar circuit is reduced by up to 50%. For the new generation of EAW chillers only one internal pump will be required. A reduction of electricity consumption by at least 30% is expected. Considering all reduction potentials the electrical COP could be improved by nearly 40% to a

value of 13 and above. This would increase the primary energy ratio by 18% to a value of 2.6 in the best case (case 3.2). If the additional heating is replaced by additional cooling the overall improvement in primary energy ratio (including the reduced electricity consumption of the components) is 50%. In this case primary energy ratios between 2.8 and 3.2 are reachable. This clearly demonstrates, that from the primary energy point of few additional cooling should be used instead of additional heating.

Purely solar driven absorption chillers often suffer from a quite late system startup, since first the collector field and connected hot water storage need to be heated up to the required startup temperature of 80°C and above. Therefore, such systems do not start to produce cold water before 11am or later. To reduce this startup process optimised control strategies for storage charge and discharge of solar driven absorption cooling systems are developed and analysed in chapter 4.2. The analyses are performed in the simulation environment INSEL where a detailed dynamic simulation model of the 15 kW chillii® solar cooling system of the SolarNext AG in Rimsting Germany has been developed and validated against measured performance data. Four different control strategies were developed and analysed: A standard control as reference system which always uses the full hot water storage volume and improved control strategies with storage bypass, with partitioned upper part of the storage tank and a control which combines the partitioned storage with a bypass. The developed control algorithms have been tested and improved in the dynamic simulation environment for different weather conditions. The validated control codes were then used to analyse the overall performance of the solar cooling system for three different typical hot summer days. It could be shown, that through the implementation of a storage bypass the start up time can be significantly reduced by 1h 40 min in the worst and nearly 2 h in the best case. For the partitioned storage case, the start-up time is between 12 and 20 minutes later. The overall best performance with the most stable system operation is reached for the combined bypass and partitioned storage control. This control produces, compared to the standard control (full storage), 19% more cooling energy production on a cloudless or slightly clouded day and 33%

more cooling energy production on a day with some clouds in the early morning and heavy rain in the early afternoon. Considering all results obtained, clear recommendations for an optimised system design with high primary energy efficiency have been developed which are shown in chapter 4.6.

6.2 MODEL BASED DEVELOPMENT OF PRIMARY ENERGY OPTIMISED CONTROL STRATEGIES FOR OPEN DESICCANT EVAPORATIVE COOLING SYSTEMS

For desiccant evaporative cooling systems (DEC) typically sequence controllers are used to adjust the cooling power of the DEC system to the cooling load of the connected rooms or building. These controllers switch on or off single components of the DEC system in dependence of the deviation between the setpoint and the actual measured room temperature. At cool and dry ambient air conditions in some controls first the air volume flow is increased, afterwards the return air humidifier and the heat exchanger between supply and return air are activated before the supply air humidifier is switched on for combined humidification. The sorption mode with startup of the sorption wheel and return air heater is very often considered as the last control option in the control sequence if the maximum room air humidity is exceeded or if the supply air humidifier operates at full load and still more cooling energy is required to keep the room air below the upper threshold. Therefore, common problems of installed DEC systems are very low solar system efficiencies of the installed collector fields and moderate primary energy efficiencies with values between 1.2 and 1.7. To improve the primary energy efficiency of DEC systems new control strategies try to operate the DEC as long as possible at the minimum air flow rate and first try to reach the lowest possible supply air temperature before the air volume flow rate is increased. Additionally, improved systems are operated at variable regeneration temperatures, which are adapted according to the load and the available solar energy. This significantly increases the solar fraction and thereby the solar system efficiency. However, since the sequence controllers switch on or off the components mainly according to the room air

conditions, often the indirect humidification mode is activated without providing a remarkable cooling power and in some cases even is heating up the supply air. Further control problems occur due to the quite long dead times especially of the humidifiers, which take typically up to 10 minutes until they reach their full cooling power and more than 20 minutes after switch off until their humidification efficiency starts to decrease slowly. Therefore, dead times are implemented in the control to avoid fluctuating control conditions. However, too long dead times also can lead to uncomfortable room air conditions and in consequence to an activation of the full desiccant mode is also not really required. To overcome these shortcuts a new primary energy optimised system controller for DEC systems has been developed and tested in the simulation environment on a DEC demonstration plant of the University of Applied Sciences in Stuttgart. The developed system controller consists of an electricity-optimised standard sequence controller which is supported by a primary energy optimisation tool. The so called PE-optimiser is operated as online simulation tool and evaluates for each time step the optimum operation condition with the lowest primary energy consumption of the DEC system. The results are transferred to the sequence controller, where the activation of the different operation modes are either blocked or accepted by the optimisation tool. To improve the control of the supply air humidifier stages, special performance characteristics of the humidifier derived from dynamic simulations are used in the optimisation tool to avoid supply air temperatures below 16°C and absolute supply air humidity above 10 g kg^{-1}. With these characteristics the optimum number of active stages of the seven possible stages of the supply air humidifier are determined for the given inlet air conditions. The suggested humidifier stage is then transferred to the sequence controller who is allowed to increase or decrease the suggestion by one stage only for fine tuning. It could be demonstrated, that with this control the required supply air conditions are reached very fast at a stable operation of the DEC system.

To analyse the impact of the new model based controller on the overall system efficiency simulations were performed for the demonstration plant for a typical cooling period from May to September. Here the following three cases are

considered and compared:

- Case 1: Standard control with air volume flow control as first option
- Case 2: Electricity optimised control with the air volume flow control as last possible option
- Case 3: Advanced model based control with the same sequence controller as for case 3 but with support from the primary energy optimiser (online tool)

The highest electricity consumption of 1800 kWh and therefore the lowest electrical COP of 2.4 were obtained for case 1 with the DEC system with non optimised standard control. If the standard control is replaced by the electricity optimised control (case 2) the electricity consumption is reduced by 58% and an electrical COP of 5.7 is reached. The advanced model based control in case 3 further reduces the electricity consumption by another 15 % and reaches a high electrical COP of 6.7. If the primary energy efficiency is regarded, the results show that a primary energy ratio of 2.38 can be reached in the best case for the advanced model based control. This is 19 % better compared to a system with electricity optimised standard control and by a factor two better than a good reference ventilation system with a compression chiller.

Altogether it can be concluded, that an intelligent fan speed control is crucial for DEC systems in order to compete with standard air conditioning systems. The implementation of a bypass of the sorption wheel and the reduction of the regeneration air volume flow rate to 70% instead of 100% could further improve the analysed DEC system. For the advance model based control (case 3) this improvements could increase the primary energy efficiency to a value of 2.55 which is 7 % higher than reached for the original system setup. This highlights the importance of system constructions with low pressure losses of the components and the connected air channels.

7. CONCLUSIONS AND OUTLOOK

7.1 SOLAR DRIVEN CLOSED ABSORPTION COOLING SYSTEMS

Within the present work detailed simulation based analyses on the design of solar driven absorption cooling systems have been carried out in chapter 03 for office buildings located in Madrid and Stuttgart. It could be shown that apart from the climatic conditions the system configuration and especially the required size of the solar collector field to cover 80% of the absorption chillers heating energy demand strongly depends on the operation conditions of the chiller and on the cooling load characteristics of the building. The collector areas vary between 1.6 and 3.5 m² per MWh cooling energy demand for office buildings in Madrid with the same maximum cooling power but different load profiles. The same analyses for office buildings in Germany gave required collector areas between 4.6 and 6.2 m² per MWh cooling energy demand. The resulting cooling costs are between 180 and 270 € per MWh of cooling energy produced in Spain with the lower value for an office building with high internal loads and long operation times of the chiller. These values can easily rise up to 680 € per MWh of cooling energy produced for an office building with the same maximum cooling load but located in Germany. All together, the outcomes and conclusions of the study in chapter 3 can be summarised as follows:

- Both the buildings location and its load characteristic strongly influence the required collector area for 80% solar fraction of the absorption chillers heating energy demand by a factor of 2 to 3
- Different system configuration and operation conditions of the absorption chiller additionally influence the required collector area for 80% solar fraction by a factor of up to 1.8
- Long operation times of the chiller increase the required collector area but significantly reduce the solar cooling cost. Therefore, hot climates with long lasting cooling periods are advantageous for solar cooling applications
- A system design only according to the maximum cooling load of the building is not recommendable

For a reliable system design, up to now, only detailed dynamic system simulations deliver reliable results, which consider the operation conditions and system configuration of the chiller and the cooling load characteristics of the building. However, for a broad application of solar cooling systems simpler design tools are required. Therefore, in a future work a study should be carried out which systematically compares simplified design methods, based on required cooling power and cooling energy, with dynamic system simulations for different climatic conditions, building types and operation regimes of the solar cooling system. This will help to clearly understand the weak points of the simplified methods and could result in strategies for the improvement of these methods.

Apart from the design methods the system control has a decisive influence on the overall energy efficiency of solar driven absorption cooling systems. The different influencing factors have been analysed systematically in chapter 4 to highlight the most important control issues in order to reach high primary energy efficiencies. These analyses are based on a dynamic system simulation model developed for an existing solar cooling system, which has been validated against measured performance data. It could be shown, that badly controlled solar driven absorption cooling systems are even worse than comparable standard systems with efficient compression chillers. Efficient conventional systems reach primary energy ratios of slightly above one. Well controlled and designed solar cooling systems can easily reach primary energy ratios of 1.8 to 2.3. From all analyses performed in chapter 4.4 it can be concluded that the most important control issues for an efficient system operation of solar driven absorption chillers are:

- The implementation of a fan speed control of the cooling tower
- The use of a ΔT mass flow control of the cold distribution pump
- The use of variable generator inlet temperatures either controlled according to the cooling load or allowed to vary according to the temperature in the hot water storage tank

Apart from these control issues also optimisation potentials concerning the hardware installation are regarded, which could help to further improve the efficiency of future systems. Optimisation measures discussed mainly focus on the reduction of electricity consumption of the system.

Possible further optimisation measures found in chapter 4.4 are:

- Improvement of the system hydraulics to reduce pressure drops in the system
- Installation of highly efficient pumps with mass flow control
- Improvements of the solar system through the implementation of pure water systems (no heat exchanger, no secondary solar pump)
- Improvements of future absorption chillers with less power demand for the solution pump and control panel

All measures together gave a reduction potential of 40 % for the electricity consumption compared to the existing analysed system which increases the electrical COP form original around 10 to values of 13 and above. In this case the primary energy ratio would increase by 18% to values of 2.2 to 2.6.

Furthermore, it was analysed what happens if the additional heating would be replaced by additional cooling. Together with the reduction of electricity consumption mentioned above, with this measure primary energy ratios of 2.8 to 3.2 would be possible. From this it can be concluded that the use of additional cooling instead of additional heating further improves the primary energy efficiency by another 18%.

For a high solar contribution on the cooling energy demand of buildings an early system startup of the solar cooling system is required. However, typical standard solar driven absorption cooling systems do not start operation before 11am since the water in the hot water storage tank first needs to be heated up to the required startup temperature which is in the region of 80°C. To reduce the startup time, a segmentation or bypass of the hot water storage tank is required. In order to guarantee a stable system operation also on partly clouded days,

improved control strategies for storage charge and discharge and for the absorption chiller startup are required. This issue was addressed in chapter 4.5 where control strategies have been developed and tested in the simulation environment for system configurations with bypass of the hot water storage, for a segmented storage tank with a small upper volume and for a combination of both. It could be shown that the implementation of a hot water storage bypass combined with a good storage charge and discharge control strategy reduces startup time of the absorption chiller by 1 hour and 40 minutes and increases the solar coverage of the cooling energy demand of a typical office building from 72% without bypass up to 90%. The main outcomes can be summarised as follows:

- For purely solar driven absorption cooling systems a bypass and/or a segmentation of the hot water storage tank is very important for an early system startup and a high solar coverage of the cooling energy demand
- Improved storage charge and discharge control strategies are required and are shown in chapter 4.5 for systems with bypass, storage segmentation and a combination of both.

From all the results obtained in chapter 4 clear recommendations for the design and control of solar cooling systems have been developed. These recommendations are summarised in chapter 4.6. In a next step, all these recommendations should be considered and implemented for a number of newly installed systems, which should be equipped with a detailed performance monitoring. This could help to demonstrate highly efficient solar driven absorption cooling systems. Apart from cost reductions, this is one of the most important issues in order to reach a significant market penetration of this new and innovative technology.

7.2 PRIMARY ENERGY OPTIMISED CONTROL STRATEGY FOR OPEN DESICCANT EVAPORATIVE COOLING SYSTEMS

A new innovative model based control strategy has been developed in chapter 5 for desiccant evaporative cooling systems applicable for moderate climatic conditions. The system controller consists of a quite standard sequence controller but with electricity optimised control strategy (increase of air volume flow as last control option). This sequence controller switches on or off the different components of the desiccant cooling system according to the room temperature to cover the cooling load of the connected room. A primary energy optimisation tool (online tool) supports the sequence controller and evaluates permanently the best operation mode of the desiccant cooling system under consideration of the actual room and ambient air conditions. The optimum operation mode is then transferred to the sequence controller where except of the suggested mode all other operation modes of the desiccant system are blocked. The efficiency of the new controller has been tested in the simulation environment on a dynamic simulation model of the analysed DEC system. To ensure accurate results the developed simulation model has first been validated against measured performance data of the system. It could be shown, that an open desiccant cooling system with the new system controller can reach a primary energy ratio (PER) of 2.38. This is nearly a factor of three higher compared to a badly controlled standard DEC system (PER = 0.89). A DEC system with electricity optimised standard control reaches a primary energy ratio of 2.0. For comparison, an energy efficient standard ventilation system with compression chiller and air volume flow control reaches a primary energy ratio of 1.1 or slightly above.

The main conclusions found in chapter 5 are:

- DEC systems with solar heat supply are not necessarily better than efficient standard air handling units with cold supply from compression chillers
- A good system design with low pressure drops of the components and the tubing and an energy efficient control are essential for a high primary energy efficiency of DEC systems

- DEC systems with electricity optimised sequence controller use the increase in air flow rate as last control option and reach a primary energy efficiency which is nearly a factor of two better compared to efficient conventional systems
- A simulation based primary energy optimisation tool has been developed which supports an electricity optimised sequence controller and blocks meaningless and inefficient operation modes and improves the supply humidifier control
- With the primary energy optimisation tool the primary energy efficiency of the system is significantly improved by 19 %

In future work the developed control strategy with support form the primary energy optimiser will be implemented in the controller of the DEC system at the University of Applied Sciences in Stuttgart and tested under real operation conditions. Here, the primary energy optimiser will either be operated as external optimisation tool which communicates via OPC with the control unit or it will be directly programmed in the control unit as internal function which is frequently called by the system controller in order to get suggestions for the optimum operation mode. For a broad application of the new controller analyses of necessary adaptations for its utilisation in different climatic regions of Europe are required.

7.3 CLOSED ABSORPTION COOLING SYSTEMS VERSUS OPEN DESICCANT EVAPORATIVE COOLING SYSTEMS

Within this study solar driven closed absorption cooling systems and open desiccant cooling systems with heat supply from solar collectors have been analysed in detail in chapter 4 and 5 for moderate German weather conditions. The results found clearly demonstrate that, if efficiently controlled, both systems are able to cover the cooling load of the building at much higher primary energy efficiency than standard systems with compression chillers. The primary energy ratios reached are in both cases in region of 2.0 and above. Both systems can

therefore be regarded as equally efficient. DEC-systems offer the possibility to use cheap solar air collectors. On the other hand the supply and return air humidifiers can lead to hygienic problems with risk of legionella bacteria infections if the system is not properly maintained. Therefore, some people avoid this efficient technology.

The main difference between the two systems is that the cooling power provided to the room is directly coupled with the fresh air supply of the rooms in case of the DEC system whereas the closed absorption chiller allows water based cold distribution. Highly energy efficient DEC systems are equipped with an air volume flow control which increases or decreases the air volume flow according to the cooling load in the connected rooms. The lower limit of the air volume flow rate is typically the required minimum fresh air supply. For thermal and acoustic comfort reasons the air change rate is typically limited to 6 air changes per hour. This limits the maximum cooling power of air handling units at 18°C supply and 26°C return temperature to 38 W per square meter conditioned space (at room height of 2.8 m). Chilled ceilings reach a cooling power of 50 W/m² to 80 W/m². These systems are supplied with cold water which can be provided by a solar driven absorption chiller. In modern office buildings maximum cooling loads of more than 50 W per square meter conditioned space can occur especially in rooms with high computer density and highly glazed façades.

DEC systems or other air handling units are normally not able to cover such high cooling loads if thermal and acoustic comfort issues need to be considered. In this case additional cooling devices like e.g. chilled suspended ceilings or thermally activated concrete ceilings are required. In innovative modern office buildings therefore the air handling units are typically designed to cover only the fresh air supply and to remove air pollutants emitted by e.g. furniture and carpets. Therefore, they are normally not designed for more than 2.5 air changes per hour. This limits the cooling power of the air handling unit to max. 15 W per square meter conditioned space. The remaining main part of the cooling load is then typically removed by either suspended chilled ceilings or thermally activated concrete ceilings (max. 30 to 40 W/m²).

If such a building shall be equipped with a solar cooling system, the decision is often for water based closed absorption or adsorption cooling systems. These systems are able to supply cooling energy at the same time to the chilled ceilings and to the air handling units. Since the solar cooling technology is still costly and the available roof area for collectors is often limited, the application of both solar cooling technologies is normally not considered. On the other hand, rooms with a high person density like seminar rooms, meeting rooms or canteens require high fresh air flow rates to ensure a good air quality. If the external loads are not too high the cooling loads are often below 38 W/m². Therefore, such rooms offer good conditions for the application of DEC systems. Furthermore, production halls of manufacturing companies with a high fresh air demand caused by pollutants offer good application potentials for open desiccant evaporative cooling systems especially if the room temperatures need to be limited to keep the products within the required accuracy tolerances. In these cases often also waste heat from the production process can be used to heat or preheat the regeneration air of the DEC system.

To summarise the discussion it can be concluded, that the two solar cooling technologies are equally efficient from the primary energy efficiency point of view. The decision which technology is applied strongly depends on the application and the preferences of the investor. Especially rooms with high fresh air needs offer good potentials for the application of open desiccant cooling systems. Office buildings with high internal and high external loads often require additional cooling devices apart from the air handling unit. These are typical applications for solar driven closed absorption or adsorption cooling systems.

For hot and humid climates the situation is different, since the supply air needs to be dehumidified for a long time period of the year. Here the application of both technologies to the same building could be interesting, if the DEC system removes mainly the latent load and the absorption chiller the sensible load of the building. However, so far there are no detailed analyses available which highlight such a combined application. Therefore, in a future work the question should be addressed how both systems can be applied and combined to reach the highest possible overall system energy efficiency.

REFERENCES

Albers, J., Kemmer, H., Ziegler, F., Solar driven absorption chiller controlled by hot and cooling water temperature,3rd International Conference Solar Air-Conditioning, 30th September – 2nd October, Palermo, Sicily, Italy, proceedings pp 338-343, 2009

Albers, J., Ziegler, F., Analysis of the part load behavior of sorption chillers with thermally driven solution pumps, ISBN: 2-913149-32-4, in: Proceedings of the 21st IIR International Congress of Refrigeration, International Institute of Refrigeration (IIR), Washington D.C., USA, August 17–22, 2003.

Albers, J.: TRNSYS Type107 Part load simulation of single staged absorption chillers in quasi steady states - Contribution to a design tool for solar assisted air conditioning systems developed in IEA TASK25 Subtask B, IEMB-Report 2-67/2002.

Altfeld, K., Exergetische Optimierung flacher solarer Lufterhitzer, VDI Forschungsberichte Reihe 6, Nr. 175, VDI Verlag, 1985

ASHRAE, ASHRAE Handbooks - Fundamentals, 1989

ASHRAE, ANSI/ASHRAE Standard 55-1992, Thermal environmental conditions for human occupancy, 1992.

ASHRAE (2004) Thermal Conditions for Human Occupancy American National Standards Institute (ANSI) and ASHRAE , Atlanta, GA . Standard, No. 55-2004

Atmaca, I., Yigit, A., Simulation of solar-powered absorption cooling system, Renewable Energy 28 (2003).

Berliner, P., Kühltürme. Berlin, Springerverlag 5. Auflage, 1972

Bosnjakovic, V., Vilicic, M., Slipcevic, B., Einheitliche Berechnung von Rekuperatoren. VDI-Forschungsheft 432, Band 17, 1951

Devres, Y. O., Psychrometric properties of humid air: Calculation procedures in: Applied Energy 48 1994

DesignBuilder, http://www.designbuilder.co.uk

EAW, Absorption chiller Wegracal SE 15 - technical. Company product information, EAW Energieanlagenbau GmbH, Germany, 2003.

Eicker, U. . Solare Technologien für Gebäude (Solar technologies for buildings) (1st edit.) Stuttgart, Germany: Verlag B. G. Teubner, 2001

Eicker, U., Schürger, U., Schumacher, J. ,Betriebserfahrungen und Potentiale sorptionsgestützter Klimaanlagen mit Solarluftkollektoren: Optimierung des solaren Ertrags durch Simulation unterschiedlicher Regelungsstrategien' 16. Symposium Thermische Solarenergie. Staffelstein. Seite 404-409, 17.-19. Mai 2006.

EnergyPlus v5.0; http://www.energyplus.gov

Engler, M., Grossmann, G., Hellmann, H.-M., Comparative simulation and investigation of ammonia–water: absorption cycles for heat pump applications, International Journal of Refrigeration 20 (7) (1997) 504–516.

Florides, G. A., Kalogirou, S. A., Tassou, S. A., Wrobel, L. C., Modelling, simulation and warming impact assessment of a domestic-size absorption solar cooling system, Applied Thermal Engineering 22 (12), 2002.

Gassel, A., Kraft-Wärme-Kälte-Kopplung und solare Klimatisierung, Habilitationsschrift TU Dresden, 2004.

Ginestet, S., Stabat, P., Marchio, D. , Control strategies of open-cycle desiccant cooling systems minimising energy consumption, eSim 2002, The Canadian conference on building energy simulation, September 11th-13th, Montréal 2002

Ginestet, S. Stabat, P., Marchio, D., Control design of open-cycle desiccant cooling systems using a graphical environment tool, Building Service Engineering Research and Technology, Vol. 24, No. 4, 257-269, 2002

Glück, B., Zustands- und Stoffwerte (Wasser, Dampf, Luft), Verbrennungsrechnung. Verlag für Bauwesen Berlin 1991

Grossmann, G., Solar powered systems for cooling, dehumidification and air conditioning, Solar Energy 72 (2002) 53–62

Henning, H.-M., Solar-assisted Air-conditioning in Buildings—A Handbook for Planners, Springer-Verlag, 2004 ISBN: 3-211-00647-8.

Henning, H.-M., Solare Klimatisierung—Stand der Entwicklung Fraunhofer-Institut für Solare Energiesysteme ISE Tagung Solares Kühlen, Wirtschaftskammer Österreich, Wien, May 7, 2004.

Henning, H.M., Hindenburg, C., Erpenbeck, T., Santamaria, I. S. The potential of solar energy use in desiccant cooling cycles, International Journal of Refigeration, Volume 24, Issue 3, May 2001, 220 – 229

INSEL 7.0 Block Reference Manual, www.insel.eu

Jakob, U., Eicker, U., Taki, A. H., Cook, M. J., Development of an optimised solar driven Diffusion-Absorption Cooling Machine, ISBN: 91-631-4740-8, in: Proceedings of the ISES Solar World Congress 2003, International Solar Energy Society (ISES), Göteborg, Sweden, June 16–19, 2003.

Jakob, U., Investigations on solar powered diffusion–absorption cooling machines, PhD Thesis, De Montfort University Leicester, 2005.

Kast, W., Adsorption aus der Gasphase (Adsorption from gas phase). Weinheim, Germany: VCH Verlagsgesellschaft mbH, 1988

Kim, D.S., Machielsen, C. H. M., Evaluation of air-cooled solar absorption cooling systems, in: ISHPC ’02, Proceedings of the International Sorption Heat Pump Conference, Shanghai, China, September 24–27, 2002

Kim, D.S., Wang, L., Machielsen, C.H.M., Dynamic modelling of a small-scale NH3/H2O absorption chiller, ISBN: 2-913149-32-4, in: Proceedings of the 21st IIR International Congress of Refrigeration, International Institute of Refrigeration (IIR), Washington, D.C., USA, August 17–22, 2003

Knapp, K., Solare Kühlung im Museum Ritter Waldenbuch, Proceedings Fünftes Symposium Solares Kühlen in der Praxis, Band 89, pp 69-80, Stuttgart 2008

Kohlenbach, P., Solar cooling with absorption chillers: Control strategies and transient chiller performance, Dissertation Technische Universität Berlin, 2006

Kühn, A., Ciganda, J.L.C., Ziegler, F., Comparison of control strategies of solar absorption chillers, Eurosun 2008, 1st International Congress on Heating, Cooling and Buildings, 7th to 10th October, Lisbon, Portugal, 2008

Mendes, L. F., Collares-Pereira, M., Ziegler, F., Supply of cooling and heating with solar assisted heat pumps: an energetic approach, International Journal of Refrigeration 21 (2) (1998) 116–125.

Merkel, F., Verdunstungskühlung, Zeitschrift des Vereins Deutscher Ingenieure (VDI) 70, pp. 123-128, 1925

Mc Neely, LA., Thermodynamic properties of aqueous solutions of lithium bromide. ASHRAE Transactions 1979; 85(Part 1), pp. 413 – 434, 1979

Núnez, T., Mehling, F., Heating and cooling with a small scale solar driven adsorption chiller combined with a borehole system – recent Results -, 3rd International Conference Solar Air-Conditioning, 30th September – 2nd October, Palermo, Sicily, Italy, proceedings pp 354-360, 2009

Park, C., D.R. Clark, and G.E. Kelly, An Overview of HVACSIM+, A Dynamic Building/HVAC/Control Systems Simulation Program , Proceedings of the 1st Annual Building Energy Simulation Conf., Seattle, WA, August 21-22, 1985.

Pietruschka, D., Dalibard, A., Eicker, U., Large capacity solar adsorption cooling at the Festo company", Oral presentation at the Solar Cooling Conference in the frame of Clean Energy Power CEP, Stuttgart 2009

Qureshi, B.A., Zubair, S.M., A complete model of wet cooling towers with fouling in fills, Applied Thermal Engeniering 26, pp. 1982-1989, 2006

Recknagel and Sprenger and Schramek, Taschenbuch für Heizung und Klimatechnik (for Heating and Air) (68th edit.), München Germany: Oldenbourg Verlag.

Safarik, M., "Solare Kuehlprojekte mit Wasser-LiBr Absorptionskältetechnik", Proceedings Fünftes Symposium Solares Kühlen in der Praxis, Band 89, pp 81-89, Stuttgart 2008

Schoelkopf, W., Kuckelkorn, J., Verwaltungs- und Bürogebäude—Nutzerverhalten und interne Wärmequellen, OTTI Kolleg Klimatisierung von Büro- und Verwaltungsgebäuden, Regensburg 9/2004.

Schumacher, J., Digitale Simulation regenerativer elektrischer Energieversorgungssysteme, Dissertation Universität Oldenburg, 1991

Schürger, U., Eicker, U., Schumacher, J. ,Betriebserfahrungen und Untersuchungen von DEC-Anlagen: Regelungsoptimierung und Energieanalysen` Tagungsband 4. Symposium Solares Kühlen in der Praxis, Band 74, Seite 59-72, 3.-4. April 2006.

Schürger, U., Investigation into solar powered adsorption cooling systems, PhD Thesis, Institute of Energy and Sustainable Development, De Montfort University Leicester, March 2007

Schweigler, C., Storkenmaier, F., Ziegler, F., Die charakteristische Gleichung von Sorptionskälteanlagen, in: Proceedings of the 26th Deutsche Klima-Kälte- Tagung, Berlin, Germany, 1999.

SIMBAD, Simulation toolbox for Matlab-Simulink
http://kheops.champs.cstb.fr/Simbadhvac/

Sparber, W., Napolitano, A., Besana, F., Thür, A., Nocke, B., Finocchiaro, P., Nujedo Nieto, L. A., Rodriguez, J., Núnez, T., Comparative results of monitored solar assisted heating and cooling installations, 3rd International Conference Solar Air-Conditioning, 30th September – 2nd October, Palermo, Sicily, Italy, proceedings pp 344-353, 2009

Takagi, Y., Nakamaru, T., Nishitani, Y., An absorption chiller model for HVACSIM+, in: Proceedings of the International Building Performance Simulation Association, Toshiba Corporation, 1999.

Tommy, H. J. M., Simulation of a PV-Diesel Generator Hybrid System and Investment Analysis: Case Study of a Mountain Hostel, Master Thesis, Renewable Energy Group, Department of Physics, Carl von Ossietzky University Oldenburg, Germany, 1994.

TRNSYS 16: A TRaNsient SYstem Simulation program – Volume 5 Mathematical reference; Type 107: Single Effect Hot Water Fired Absorption Chiller; Page 155-158. Solar Energy Laboratory, University of Wisconsin-Madison. 2004.

Vitte, T., Brau, J., Chatagnon, N., Woloszyn, M., Proposal for a new hybrid control strategy for a solar desiccant evaporative cooling air handling unit, Energy and Buildings, Volume 40, 896-905, 2008

Walker, W.H., Lewis, W.K., McAdams, W.H., Gilliland, E.R., Principles of Chemical Engineering, third ed., McGraw-Hill Inc., New York, 1923

Wardono, B., Nelson, R.M., Simulation of a double effect LiBr/H2O absorption cooling system, ASHRAE Journal (October 1996) 32–38.

Webb, A., Unified theoretical treatment for thermal analysis of cooling towers, evaporative condensers and fluid coolers, ASHRAE Trans. 90 (2) pp. 398-415, 1984

Weidner, G., Low capacity absorption chillers for solar cooling applications, 3rd International Conference Solar Air-Conditioning, 30th September – 2nd October, Palermo, Sicily, Italy, proceedings pp 256-261, 2009

Willers, E., Neveu, P., Groll, M., Kulick, C., Meunier, F., Mostofizadeh, C., Wierse, M., Dynamic modelling of a liquid absorption system, in: ISHPC '99, Proceedings of the International Sorption Heat Pump Conference, Munich, Germany, March 24–26, 1999

Yu, F. W., Chan, K. T., Improved energy efficiency standards for vapour compression chillers serving buildings, Department of Building Services Engineering, The Hong Kong Polytechnic University, 2004

Ziegler, F., Sorptionswärmepumpen, Forschungsberichte des Deutschen Kälte und Klimatechnischen Vereins Nr. 57, Stuttgart, ISBN 3-932715-60-8, 1998.

Ziegler, J., Nichols, N., Optimum settings for automatic controllers, Transactions of ASME 64, 759-768, 1942

OWN PUBLICATIONS

[1] Eicker, U. and Pietruschka, D. 'Optimization and Economics of Solar Cooling Systems' Advances in building energy research (2009), Volume 3, pp 45–82 ISSN 1751-2549, 2009
[2] Eicker, U. and Pietruschka, D. 'Design and performance of solar powered absorption cooling systems in office buildings' Energy and Buildings (2009), Volume 41, Issue 1, January 2009, Pages 81-91
[3] Pietruschka, D. 'Solare Kühlung mit sorptionsgestützten Klimaanlagen – Primärenergetisch optimierter Betrieb durch innovative simulationsbasierte Regelstrategien-' Textbeitrag zum Energy 2.0-Kompndium 2010
[4] Pietruschka, D., Eicker, U., Hanby, V.'Primary energy optimised operation of solar driven desiccant evaporative cooling systems through innovative control strategies' proceedings 3rd International Conference Solar Air-Conditioning, Palermo, Italy, 30.09.2009 – 02.10.2009
[5] Dalibard, A., Biesinger, A., Pietruschka, D., Eicker, U. 'Optimisation potential of a large solar adsorption cooling plant' proceedings 3rd International Conference Solar Air-Conditioning, Palermo, Italy, 30.09.2009 – 02.10.2009
[6] Pietruschka, D., Eicker, U., Hanby, V. 'Primärenergetisch optimierter Betrieb von solaren sorptionsgestützten Klimaanlagen (DEC) durch innovative Regelstrategien' Tagungsband zum 19. Symposium Thermische Solarenergie. Ostbayerisches Technologie-Transfer-Institut e.V. (OTTI), Bad-Staffelstein (Mai 2009)
[7] Pietruschka, D., Dalibard, A., Eicker, U. 'Large capacity solar adsorption cooling at the FESTO company', Proceedings Conference Clean Energy Power CEP 2009, Stuttgart Messe, Germany, January 2009
[8] Dalibard, A., Pietruschka, D., Eicker, U. 'Dynamic simulation of large monitored solar adsorption cooling plant' Proceedings Eurosun 2008, Lisboa, 7-10th October, 2008
[9] Pietruschka, D., Jakob, U., Hanby, V., Eicker, U. 'Simulation based optimisation of a newly developed system controller for solar cooling and heating systems' Proceedings Eurosun 2008, Lisboa, 7-10th October, 2008
[10] Eicker, U., Dalibard, A., Pietruschka, D. ,Simulationsbasierte Überwachung und Optimierung einer großen Solaranlage zur solaren Kühlung und Heizungsunterstützung' Tagungsband zum 18. Symposium Thermische Staffelstein (2008)
[11] Pietruschka, D., Jakob, U., Eicker, U., Hanby, V. ,Optimierung und online Überwachung eines neuen Systemreglerkonzepts für kombinierte Anlagen zur solaren Kälteerzeugung und Heizungsunterstützung durch betriebsbegleitende Simulationen' Vortrag auf dem 18. Symposium Thermische Solarenergie. Ostbayerisches Technologie-Transfer-Institut e.V. (OTTI), Staffelstein (2008)

[12] Pietruschka, D., Dalibard, A. Eicker, U. ‚Planung, Inbetriebnahme und Messungen an einer solaren Adorptionskälteanlage der FESTO AG & CO. KG & Co. KG mit 1218 m² Kollektorfläche' Tagungsband 5. Symposium solares Kühlen in der Praxis, Stuttgart, 04/2008
[13] Dalibard, A., Pietruschka, D., Eicker, U., Schumacher, J. 'Performance analysis and optimisation through system simulations of renewable driven adsorption chillers' Proceedings of the 2nd International Conference Solar Air Conditioning, Tarragona, 10/2007
[14] Pietruschka, D., Jakob, U., Eicker, U., Hanby, V. 'Simulation based optimisation and experimental investigation of a solar cooling and heating system' Proceedings of the 2nd International Conference Solar Air Conditioning, Tarragona, 10/2007
[15] Pietruschka, D. , Dalibard, A., Eicker, U., Hanby, V. ‚Simulationsbasierte Planung solar betriebener Kälteanlagen an zwei Beispielen aus der Praxis' Tagungsband zum 17. Symposium Thermische Solarenergie. Ostbayerisches Technologie-Transfer-Institut e.V. (OTTI), Staffelstein (2007)
[16] Pietruschka, D., Eicker, U., Huber, M., Schumacher, J. 'Experimental Performance Analysis and Modelling of Liquid Desiccant Cooling Systems for Air Conditioning in Residential Buildings' International Journal of Refrigeration (2006), Vol 29/1, pp 110-124
[17] Pietruschka, D., Eicker, U., Schumacher, J. 'Simulation based design methods and economical analysis for solar driven absorption cooling systems' Proceedings of the International Conference EuroSun, Glasgow (2006)
[18] Eicker, U., Pietruschka, D., Schumacher, J. 'Energetic and economical performance of solar powered absorption cooling systems' Proceedings of the International Conference Solar Air Conditioning, Bad Staffelstein, 10/2005
[19] Pietruschka, D., Eicker, U., Huber, M., Schumacher, J. ‚Small Power Liquid Sorption Cooling for Building Ventilation Systems' Proceedings of the International Conference Solar Air Conditioning, Bad Staffelstein, 10/2005
[20] Eicker, U., Schumacher, J., Jakob, U., Pietruschka, D. ‚Energieeffizienz und Wirtschaftlichkeit solar betriebener Absorptionskältetechnik' Tagungsband zum 15. Symposium Thermische Solarenergie, Ostbayerisches Technologie-Transfer-Institut e.V. (OTTI), Staffelstein. 4/2005.

MODEL DEVELOPMENT

1. ABSORPTION CHILLER MODEL

1.1 STATIC ACM MODEL

In this chapter the solution of ACM equation system is shown for the external mean temperatures of the evaporator, absorber, generator and condenser. The ACM model is based on the characteristic equation as described in chapter 2.2.2.1.

With the simplified assumption of a linear heat exchange the external mean temperatures can be written in dependence of the inlet and outlet temperature:

$$t_i = \frac{\left(t_{i,in} + t_{i,out}\right)}{2};\ t_{out,i} = 2t_i - t_{in}$$

With this simplified correlation the equation system for the external and internal energy balances can be resolved for the unknown external mean temperatures as follows:

$$\dot{Q}_E = s_E \cdot \left(\Delta\Delta t - \Delta\Delta t_{\min,E}\right)$$

$$\dot{Q}_C = C_E \cdot s_E \cdot \left(\Delta\Delta t - \Delta\Delta t_{\min,E}\right)$$

$$\dot{Q}_A = A_E \cdot s_E \cdot \left(\Delta\Delta t - \Delta\Delta t_{\min,E}\right) + \dot{Q}_x$$

$$\dot{Q}_G = G_E \cdot s_E \cdot \left(\Delta\Delta t - \Delta\Delta t_{\min,E}\right) + \dot{Q}'_x$$

With

$$t_{x,out} = 2 \cdot t_x - t_{x,in}$$

The external energy flows can be written as:

$$s_E \cdot \left(\Delta\Delta t - \Delta\Delta t_{\min,E}\right) = 2 \cdot \dot{m}_E \cdot c_{H_2O} \cdot (-t_E + t_{E,in})$$

$$C_E \cdot s_E \cdot \left(\Delta\Delta t - \Delta\Delta t_{\min,E}\right) = 2 \cdot \dot{m}_C \cdot c_{H_2O} \cdot (t_C - t_{A,out})$$
$$= 2 \cdot \dot{m}_C \cdot c_{H_2O} \cdot (t_C - 2 \cdot t_A + t_{A,in})$$

$$A_E \cdot s_E \cdot \left(\Delta\Delta t - \Delta\Delta t_{\min,E}\right) + \dot{Q}_x = 2 \cdot \dot{m}_A \cdot c_{H_2O} \cdot (t_A - t_{A,in})$$

$$G_E \cdot s_E \cdot \left(\Delta\Delta t - \Delta\Delta t_{\min,E}\right) + \dot{Q}'_x = 2 \cdot \dot{m}_G \cdot c_{H_2O} \cdot (-t_G + t_{G,in})$$

If $\Delta\Delta t$ is replaced in the equations we get:

$$s_E \cdot \left(t_G - t_A - B \cdot t_C + B \cdot t_E - \Delta\Delta t_{\min,E}\right) = 2 \cdot \dot{m}_E \cdot c_{H_2O} \cdot (-t_E + t_{E,in})$$

$$C_E \cdot s_E \cdot \left(t_G - t_A - B \cdot t_C + B \cdot t_E - \Delta\Delta t_{\min,E}\right) = 2 \cdot \dot{m}_C \cdot c_{H_2O} \cdot (t_C - 2 \cdot t_A + t_{A,in})$$

$$A_E \cdot s_E \cdot \left(t_G - t_A - B \cdot t_C + B \cdot t_E - \Delta\Delta t_{\min,E}\right) + \dot{Q}_x = 2 \cdot \dot{m}_A \cdot c_{H_2O} \cdot (t_A - t_{A,in})$$

$$G_E \cdot s_E \cdot \left(t_G - t_A - B \cdot t_C + B \cdot t_E - \Delta\Delta t_{\min}\right) + \dot{Q}'_x = 2 \cdot \dot{m}_G \cdot c_{H_2O} \cdot (-t_G + t_{G,in})$$

This equation system can be solved for the unknown external inlet temperatures. Z1 to Z9 are used for simplification of the equation.

$$t_G - t_A - B \cdot t_C + t_E \overbrace{\left(B + \frac{2 \cdot \dot{m}_E \cdot c_{H_2O}}{s_E}\right)}^{=Z1} = \overbrace{\Delta\Delta t_{\min,E} + \frac{2 \cdot \dot{m}_E \cdot c_{H_2O}}{s_E}}^{=Z2} \cdot t_{E,in}$$

$$t_G - t_A \overbrace{\left(1 - \frac{4 \cdot \dot{m}_C \cdot c_{H_2O}}{C_E \cdot s_E}\right)}^{=Z3} - t_C \overbrace{\left(B + \frac{2 \cdot \dot{m}_C \cdot c_{H_2O}}{C_E \cdot s_E}\right)}^{=Z4} + B \cdot t_E$$
$$= \overbrace{\Delta\Delta t_{\min,E} + \frac{2 \cdot \dot{m}_C \cdot c_{H_2O}}{C_E \cdot s_E}}^{=Z5} \cdot t_{A,in}$$

$$t_G - t_A \overbrace{\left(1 + \frac{2 \cdot \dot{m}_A \cdot c_{H_2O}}{A_E \cdot s_E}\right)}^{=Z6} - B \cdot t_C + B \cdot t_E = \overbrace{\Delta\Delta t_{\min,E} - \frac{2 \cdot \dot{m}_A \cdot c_{H_2O}}{A_E \cdot s_E} \cdot t_{A,in} - \frac{\dot{Q}_x}{A_E \cdot s_E}}^{=Z7}$$

$$t_G \overbrace{\left(1 + \frac{2 \cdot \dot{m}_G \cdot c_{H_2O}}{G_E \cdot s_E}\right)}^{=Z8} - t_A - B \cdot t_C + B \cdot t_E = \overbrace{\Delta\Delta t_{\min,E} + \frac{2 \cdot \dot{m}_G \cdot c_{H_2O}}{G_E \cdot s_E} \cdot t_{G,in} - \frac{\dot{Q}'_x}{G_E \cdot s_E}}^{=Z9}$$

With these simplifications we get:

(1) $t_G - t_A - B \cdot t_C + t_E Z_1 = Z_2$

(2) $t_G - t_A Z_3 - t_C Z_4 + B \cdot t_E = Z_5$

(3) $t_G - t_A Z_6 - B \cdot t_C + B \cdot t_E = Z_7$

(4) $t_G Z_8 - t_A - B \cdot t_C + B \cdot t_E = Z_9$

If equation (1) is solved for t_G we get:

(1.1) $t_G = Z_2 + t_A + B \cdot t_C - t_E Z_1$

If t_G in equation (2) is replaced by equation (1.1) we get for t_A:

$$Z_2 + t_A + B \cdot t_C - t_E Z_1 - t_A Z_3 - t_C Z_4 + B \cdot t_E = Z_5$$

$$t_A - t_A Z_3 = Z_5 - Z_2 - B \cdot t_C + t_E Z_1 + t_C Z_4 - B \cdot t_E$$

$$t_A = \frac{Z_5 - Z_2 - t_C (B - Z_4) + t_E (Z_1 - B)}{1 - Z_3}$$

(2.1) $$t_A = \overbrace{\frac{Z_5}{1-Z_3} - \frac{Z_2}{1-Z_3}}^{=U1} - t_C \overbrace{\frac{(B - Z_4)}{1-Z_3}}^{=U2} + t_E \overbrace{\frac{(Z_1 - B)}{1-Z_3}}^{=U3}$$

(2.1) $t_A = U_1 - t_C U_2 + t_E U_3$

Now t_G and t_A are replaced in equation (3) by equation (1.1) and (2.1) and equation 3 is solved for t_C as follows

$$Z_2 + \frac{Z_5}{1-Z_3} - \frac{Z_2}{1-Z_3} - t_C \frac{(B - Z_4)}{1-Z_3} + t_E \frac{(Z_1 - B)}{1-Z_3} + B \cdot t_C - t_E Z_1$$
$$- \left(\frac{Z_5}{1-Z_3} - \frac{Z_2}{1-Z_3} - t_C \frac{(B - Z_4)}{1-Z_3} + t_E \frac{(Z_1 - B)}{1-Z_3} \right) Z_6 - B \cdot t_C + B \cdot t_E = Z_7$$

$$-t_C\frac{(B-Z_4)}{1-Z_3}+t_E\frac{(Z_1-B)}{1-Z_3}+B\cdot t_C-t_EZ_1$$
$$-\frac{Z_5Z_6}{1-Z_3}+\frac{Z_2Z_6}{1-Z_3}+t_C\frac{(B-Z_4)Z_6}{1-Z_3}-t_E\frac{(Z_1-B)Z_6}{1-Z_3}-B\cdot t_C+B\cdot t_E=Z_7-Z_2-\frac{Z_5}{1-Z_3}+\frac{Z_2}{1-Z_3}$$

$$-t_C\frac{(B-Z_4)}{1-Z_3}+B\cdot t_C+t_C\frac{(B-Z_4)Z_6}{1-Z_3}-B\cdot t_C$$
$$=Z_7-Z_2-\frac{Z_5}{1-Z_3}+\frac{Z_2}{1-Z_3}-B\cdot t_E+t_E\frac{(Z_1-B)Z_6}{1-Z_3}+t_EZ_1+\frac{Z_5Z_6}{1-Z_3}-\frac{Z_2Z_6}{1-Z_3}-t_E\frac{(Z_1-B)}{1-Z_3}$$

$$t_C\left(\frac{(B-Z_4)}{1-Z_3}\cdot(Z_6-1)\right)$$
$$=Z_7-Z_2-\frac{Z_5}{1-Z_3}+\frac{Z_2}{1-Z_3}+\frac{Z_5Z_6}{1-Z_3}-\frac{Z_2Z_6}{1-Z_3}+t_E\cdot\left(-B+\frac{(Z_1-B)Z_6}{1-Z_3}+Z_1-\frac{(Z_1-B)}{1-Z_3}\right)$$

$$t_C=\frac{\overbrace{Z_7-Z_2-\frac{Z_5}{1-Z_3}+\frac{Z_2}{1-Z_3}+\frac{Z_5Z_6}{1-Z_3}-\frac{Z_2Z_6}{1-Z_3}}^{=K_1}}{\left(\frac{(B-Z_4)}{1-Z_3}\cdot(Z_6-1)\right)}+t_E\cdot\frac{\overbrace{\left(-B+\frac{(Z_1-B)Z_6}{1-Z_3}+Z_1-\frac{(Z_1-B)}{1-Z_3}\right)}^{=K_2}}{\left(\frac{(B-Z_4)}{1-Z_3}\cdot(Z_6-1)\right)}$$

(3.1) $t_C=K_1+t_E\cdot K_2$

Finally t_G, t_A and t_C are replaced in equation (4) and equation is solved for t_E

$$(Z_2+U_1-(K_1+t_E\cdot K_2)U_2+t_EU_3+B\cdot(K_1+t_E\cdot K_2)-t_EZ_1)\cdot Z_8$$
$$-(U_1-(K_1+t_E\cdot K_2)U_2+t_EU_3)-B\cdot(K_1+t_E\cdot K_2)+B\cdot t_E=Z_9$$

$$Z_2Z_8+U_1Z_8-(K_1+t_E\cdot K_2)U_2Z_8+t_EU_3Z_8+B\cdot Z_8\cdot(K_1+t_E\cdot K_2)-t_EZ_1Z_8$$
$$-U_1+(K_1+t_E\cdot K_2)U_2-t_EU_3-B\cdot K_1-t_E\cdot B\cdot K_2+B\cdot t_E=Z_9$$

$$-K_1U_2Z_8-t_E\cdot K_2U_2Z_8+t_EU_3Z_8+B\cdot Z_8K_1+B\cdot Z_8t_E\cdot K_2-t_EZ_1Z_8$$
$$-U_1+K_1U_2+t_E\cdot K_2U_2-t_EU_3-B\cdot K_1-t_E\cdot B\cdot K_2+B\cdot t_E=Z_9-Z_2Z_8-U_1Z_8$$

$$
\begin{aligned}
&- t_E \cdot K_2 U_2 Z_8 + t_E U_3 Z_8 + t_E \cdot B \cdot Z_8 K_2 - t_E Z_1 Z_8 \\
&+ t_E \cdot K_2 U_2 - t_E U_3 - t_E \cdot B \cdot K_2 + B \cdot t_E \\
&= Z_9 - Z_2 Z_8 - U_1 Z_8 + K_1 U_2 Z_8 - B \cdot Z_8 K_1 + U_1 - K_1 U_2 + B \cdot K_1
\end{aligned}
$$

$$
\begin{aligned}
&t_E \cdot \left(- K_2 U_2 Z_8 + U_3 Z_8 + B \cdot Z_8 K_2 - Z_1 Z_8 + K_2 U_2 - U_3 - B \cdot K_2 + B\right) \\
&= Z_9 - Z_2 Z_8 - U_1 Z_8 + K_1 U_2 Z_8 - B \cdot Z_8 K_1 + U_1 - K_1 U_2 + B \cdot K_1
\end{aligned}
$$

$$
(4.1) \quad t_E = \frac{Z_9 - Z_2 Z_8 - U_1 Z_8 + K_1 U_2 Z_8 - B \cdot Z_8 K_1 + U_1 - K_1 U_2 + B \cdot K_1}{- K_2 U_2 Z_8 + U_3 Z_8 + B \cdot Z_8 K_2 - Z_1 Z_8 + K_2 U_2 - U_3 - B \cdot K_2 + B}
$$

1.2 CORRELATIONS USED IN THE ACM MODEL

1.2.1 LIQUID WATER AND WATER VAPOUR

-Enthalpy of water and water vapour

For the calculation of the liquid and vapour enthalpy of water the following empirical temperature dependent correlations provided by (Glück, B. 1991) are used in the ACM model. In the equations the temperature t is in °C.

$$h_{Water\ vapour} = 2501.482 + 1.789736 \cdot t + 8.957546 \cdot 10^{-4} \cdot t^2 - 1.3005254 \cdot 10^{-5} \cdot t^3$$

$$h_{H_2O} = -2.25 \cdot 10^{-2} + 4.2063437 \cdot t - 6.014696 \cdot 10^{-4} \cdot t^2 + 4.381537 \cdot 10^{-6} \cdot t^3$$

The error of the correlation is in the range from 10°C to 200°C smaller than 0.04%.

-Saturation pressure of water vapour

For the saturation pressure of water vapour the following empirical temperature dependent correlations also provided by (Glück, B. 1991) is used in the ACM model. In the equations the temperature t is in °C.

$$p_{S,r6} = 611 \cdot \exp\left(\begin{aligned}&-1.91275 \cdot 10^{-4} + t \cdot 7.258 \cdot 10^{-2} - t^2 \cdot 2.939 \cdot 10^{-4} \\ &+ t^3 \cdot 9.841 \cdot 10^{-7} - t^4 \cdot 1.920 \cdot 10^{-9}\end{aligned}\right)$$

1.2.2 PROPERTIES OF AQUEOUS LIBR SOLUTION

- Enthalpy of the aqueous LiBr solution

The enthalpy of the LiBr solution is calculated in dependence of the temperature and concentration from the correlations provides by (Mc Neely 1979) from the following equations.

$$h_{LiBr+H_2O}(t, X) = X \cdot h_{LiBr}(t) + (1 - X) \cdot h_{H_2O}(t) + \Delta h(t, X)$$

$$h_{LiBr}(t) = \sum_{i=0}^{4} a_i \cdot t_i$$

$$\Delta h = X \cdot (1 - X) \sum_{i=0}^{4} \sum_{j=0}^{3} b_{ij} \cdot (2X - 1)^i \cdot t^i$$

Table 1: Parameters of the enthalpy correlations for LiBr solution of Mc Neely

i	a_i	b_{i0}	b_{i1}	b_{i2}	b_{i3}
0	508.668	-1021.61	+36.8773	-0.186051	$-7.51277\ 10^{-6}$
1	-18.6241	- 533.308	+40.2847	-0.191198	0.0
2	$+9.85946\ 10^{-2}$	+483.62	+39.9142	-0.199213	0.0
3	$-2.50979\ 10^{-5}$	+1155.13	+33.3572	-0.178258	0.0
4	$+4.15801\ 10^{-8}$	+640.622	+13.1032	-0.077510	0.0

The enthalpy of liquid water is calculated according to the correlation of (Glück, B. 1991) shown in chapter 1.2.1.

- Concentration of the aqueous LiBr solution

For the calculation of the concentration of the LiBr solution in dependence of the temperature and surrounding vapour pressure a correlation provided by (Mc Neely 1979) is used which describes the solution temperature in dependence of the concentration and surrounding water vapour pressure. Since this equation can't be easily solved the concentration is calculated in an iteration process (Regula Falsi) where the concentration is varied until the temperature of the solution is equal to the know temperature value. The equation used is:

$$t_{LiBr}(X, p_s) = \sum_{i=0}^{4} a_i \cdot X_i^{\ i} + \left(\sum_{i=0}^{4} b_i \cdot X_i^{\ i} \right) \cdot t(p_s)$$

Table 2: Parameters of the temperature correlations for LiBr solution of Mc Neely

i	a_i	b_i
1	$1.6634856\ 10^{1}$	$-6.8242821\ 10^{-2}$
2	$-5.5338169\ 10^{2}$	$5.8736190\ 10^{0}$
3	$1.1228336\ 10^{4}$	$-1.0278186\ 10^{2}$
4	$-1.1028390\ 10^{5}$	$9.3032374\ 10^{2}$
5	$6.2109464\ 10^{5}$	$-4.8223940\ 10^{3}$
6	$-2.1112567\ 10^{6}$	$1.5189038\ 10^{4}$
7	$4.3851901\ 10^{6}$	$-2.9412863\ 10^{4}$
8	$-5.4098115\ 10^{6}$	$3.4100528\ 10^{4}$
9	$3.6266742\ 10^{6}$	$-2.1671480\ 10^{4}$
10	$-1.0153059\ 10^{6}$	$5.7995604\ 10^{4}$

The vapour temperature in dependence of the saturation pressure t(ps) is calculated from correlations provided by (Devres, Y. O. 1994).

1.3 DYNAMIC PART OF THE ACM MODEL

In this chapter the solution of the equation system of the dynamic part of the 15 kW EAW absorption chiller is shown. The idea and principle of the model is described in chapter 2.2.2.3. Despite of the heat storage in the single components the model also considers the heat losses to the environment and internal heat transfer. For the calculation of the internal heat transfer the temperature of the adjacent parts of the chiller is considered to be the one from the time step before. This simplifies the model and since very small time steps of 10s are used in the simulations the error made by this simplification is low.

A) Generator

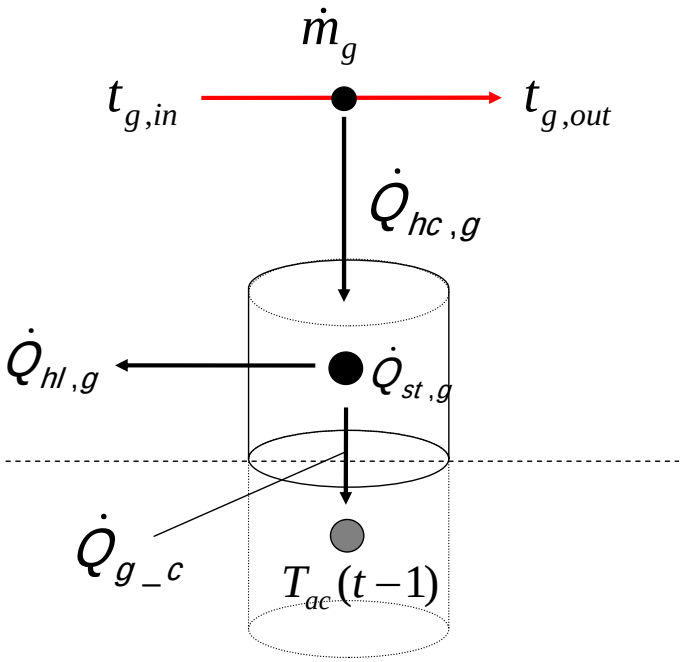

Fig. 1: Heat transfer and heat storage of the generator

- Heat balance of the external circuit

$$\dot{Q}_g = \dot{Q}_{hc,g}$$

$$\dot{m}_g \cdot c_{p,g} \cdot \Delta t \cdot \left(t_{g,in} - t_{g,out}\right) = UA_g \cdot \Delta t \cdot \left(\frac{t_{g,in} + t_{g,out}}{2} - \frac{T_g(t-1) + T_g(t)}{2} \right)$$

$$t_{g,out} \overbrace{\left(\dot{m}_g \cdot c_{p,g} + \frac{UA_g}{2} \right)}^{= C1} = t_{g,in} \overbrace{\left(\dot{m}_g \cdot c_{p,g} - \frac{UA_g}{2} \right)}^{= C2} + \overbrace{\frac{UA_g}{2}}^{= C3} \cdot T_g(t-1) + \overbrace{\frac{UA_g}{2}}^{= C3} \cdot T_g(t)$$

$$t_{g,out} = t_{g,in} \frac{C2}{C1} + T_g(t-1) \frac{C3}{C1} + T_g(t) \frac{C3}{C1}$$

- Internal heat balance

$$\dot{Q}_{st,g} = \dot{Q}_{hc,g} - \dot{Q}_{hl,g} - \dot{Q}_{g\_c}$$

$$C_g \cdot \left(T_g(t) - T_g(t-1)\right) = UA_g \cdot \Delta t \cdot \left(\frac{t_{g,in} + t_{g,out}}{2} - \frac{T_g(t-1) + T_g(t)}{2} \right)$$
$$- U_{tot,g} \cdot \Delta t \cdot \left(\frac{T_g(t-1) + T_g(t)}{2} - t_{amb} \right)$$
$$- U_{g\_c} \cdot \Delta t \cdot \left(T_g(t-1) - T_{ac}(t-1)\right)$$

- Solving the equation system for $T_g(t)$

Step 1

$$\frac{C_g}{\Delta t} \cdot T_g(t) - \frac{C_g}{\Delta t} \cdot T_g(t-1)$$
$$= \frac{UA_g}{2} \left(t_{g,in} + t_{g,in} \frac{C2}{C1} + T_g(t-1) \frac{C3}{C1} + T_g(t) \frac{C3}{C1} - T_g(t-1) - T_g(t) \right)$$
$$- \frac{U_{tot,g}}{2} \cdot \left(T_g(t-1) + T_g(t) - 2t_{amb}\right) - U_{g\_c} \cdot \left(T_g(t-1) - T_{ac}(t-1)\right)$$

Step 2

$$\frac{C_g}{\Delta t}\cdot T_g(t) - T_g(t)\cdot\frac{UA_g}{2}\left(\frac{C3}{C1}-1\right)+\frac{U_{tot,g}}{2}T_g(t)$$
$$=\frac{C_g}{\Delta t}\cdot T_g(t-1)+\frac{UA_g}{2}\left(t_{g,in}+t_{g,in}\frac{C2}{C1}+T_g(t-1)\frac{C3}{C1}-T_g(t-1)\right)$$
$$-\frac{U_{tot,g}}{2}\cdot\left(T_g(t-1)-2t_{amb}\right)$$
$$-U_{a\_g}\cdot\left(T_g(t-1)-T_a(t-1)\right)$$

$$T_g(t)\overbrace{\left(\frac{C_g}{\Delta t}-\frac{UA_g}{2}\left(\frac{C3}{C1}-1\right)+\frac{U_{tot,g}}{2}\right)}^{=Z1}$$

$$=T_g(t-1)\overbrace{\left(\frac{C_g}{\Delta t}+\frac{UA_g}{2}\left(\frac{C3}{C1}-1\right)-\frac{U_{tot,g}}{2}-U_{g\_c}\right)}^{=Z2}+t_{g,in}\overbrace{\frac{UA_g}{2}\left(1+\frac{C2}{C1}\right)}^{=Z3}$$
$$+t_{amb}\cdot U_{tot,g}+T_{ac}(t-1)\cdot U_{g\_c}$$

$$T_g(t)=T_g(t-1)\frac{Z2}{Z1}+t_{g,in}\frac{Z3}{Z1}+t_{amb}\cdot\frac{U_{tot,g}}{Z1}+T_{ac}(t-1)\cdot\frac{U_{g\_c}}{Z1}$$

- Without generator mass flow

$$\dot{Q}_{st,g} = \dot{Q}_{hl,g} + \dot{Q}_{g\_c}$$

$$C_g \cdot \left(T_g(t-1) - T_g(t)\right) = U_{tot,g} \cdot \Delta t \cdot \left(\frac{T_g(t-1) + T_g(t)}{2} - t_{amb}\right) + U_{g\_c} \cdot \Delta t \cdot \left(T_g(t-1) - T_{ac}(t-1)\right)$$

$$\frac{C_g}{\Delta t} \cdot T_g(t-1) - \frac{C_g}{\Delta t} \cdot T_g(t) = \frac{U_{tot,g}}{2} T_g(t-1) + \frac{U_{tot,g}}{2} T_g(t) - U_{tot,g} \cdot t_{amb} + U_{g\_c} \cdot T_g(t-1) - U_{g\_c} \cdot T_{ac}(t-1)$$

$$T_g(t)\underbrace{\left(\frac{C_g}{\Delta t} + \frac{U_{tot,g}}{2}\right)}_{=C1} = T_g(t-1)\underbrace{\left(\frac{C_g}{\Delta t} - \frac{U_{tot,g}}{2} - U_{g\_c}\right)}_{=C2} + U_{tot,g} \cdot t_{amb} + U_{g\_a} \cdot T_{ac}(t-1)$$

$$T_g(t) = T_g(t-1)\frac{C2}{C1} + t_{amb}\frac{U_{tot,g}}{C1} + T_{ac}(t-1)\frac{U_{g\_c}}{C1}$$

B) Evaporator

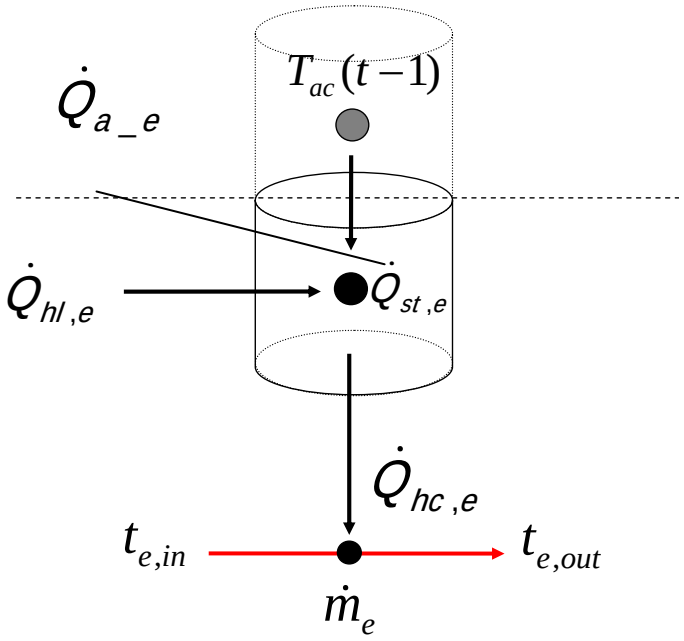

Fig. 2: Heat transfer and heat storage of the evaporator

- Heat balance of the external circuit

$$\dot{Q}_e = \dot{Q}_{hc,e}$$

$$\dot{m}_e \cdot c_{p,e} \cdot \Delta t \cdot \left(t_{e,out} - t_{e,in}\right) = UA_e \cdot \Delta t \cdot \left(\frac{T_e(t-1) + T_e(t)}{2} - \frac{t_{e,in} + t_{e,out}}{2}\right)$$

$$t_{e,out}\underbrace{\left(\dot{m}_e \cdot c_{p,e} + \frac{UA_e}{2}\right)}_{=C1} = t_{e,in}\underbrace{\left(\dot{m}_e \cdot c_{p,e} - \frac{UA_e}{2}\right)}_{=C2} + \underbrace{\frac{UA_e}{2}}_{=C3} \cdot T_e(t-1) + \underbrace{\frac{UA_e}{2}}_{=C3} \cdot T_e(t)$$

$$t_{e,out} = t_{e,in}\frac{C2}{C1} + T_e(t-1)\frac{C3}{C1} + T_e(t)\frac{C3}{C1}$$

- Internal heat balance

$$\dot{Q}_{st,e} = \dot{Q}_{hc,e} - \dot{Q}_{hl,e} - \dot{Q}_{a\_e}$$

$$C_e \cdot \left(T_e(t) - T_e(t-1)\right) = -UA_e \cdot \Delta t \cdot \left(\frac{T_e(t-1) + T_e(t)}{2} - \frac{t_{e,in} + t_{e,out}}{2}\right) + U_{tot,e} \cdot \Delta t \cdot \left(t_{amb} - \frac{T_e(t-1) + T_e(t)}{2}\right) + U_{a\_e} \cdot \Delta t \cdot \left(T_{ac}(t-1) - T_e(t-1)\right)$$

- Solving the equation system for $T_e(t)$

Step 1

$$\frac{C_e}{\Delta t} \cdot T_e(t) - \frac{C_e}{\Delta t} \cdot T_e(t-1) = \frac{UA_e}{2}\left(t_{e,in} + t_{e,in}\frac{C2}{C1} + T_e(t-1)\frac{C3}{C1} + T_e(t)\frac{C3}{C1} - T_e(t-1) - T_e(t)\right) + \frac{U_{tot,e}}{2} \cdot \left(2t_{amb} - T_e(t-1) - T_e(t)\right) + U_{a\_e} \cdot \left(T_{ac}(t-1) - T_e(t-1)\right)$$

Step 2

$$\frac{C_e}{\Delta t} \cdot T_e(t) - T_e(t)\frac{UA_e}{2}\left(\frac{C3}{C1} - 1\right) + T_e(t)\frac{U_{tot,e}}{2} = \frac{C_e}{\Delta t} \cdot T_e(t-1) + \frac{UA_e}{2}\left(t_{e,in} + t_{e,in}\frac{C2}{C1} + T_e(t-1)\frac{C3}{C1} - T_e(t-1)\right) + \frac{U_{tot,e}}{2} \cdot \left(2t_{amb} - T_e(t-1)\right) + U_{a\_e} \cdot \left(T_{ac}(t-1) - T_e(t-1)\right)$$

Step 2

$$T_e(t)\overbrace{\left[\frac{U_{tot,e}}{2}-\frac{C_e}{\Delta t}-\frac{UA_e}{2}\left(\frac{C3}{C1}-1\right)\right]}^{=Z1}$$

$$=T_e(t-1)\overbrace{\left[\frac{UA_e}{2}\left(\frac{C3}{C1}-1\right)-\frac{C_e}{\Delta t}-\frac{U_{tot,e}}{2}-U_{a\_e}\right]}^{=Z2}+t_{e,in}\overbrace{\frac{UA_e}{2}\left(1+\frac{C2}{C1}\right)}^{=Z3}$$

$$+U_{tot,e}t_{amb}+U_{c\_e}\cdot T_{ac}(t-1)$$

$$T_e(t)=T_e(t-1)\frac{Z2}{Z1}+t_{e,in}\frac{Z3}{Z1}+t_{amb}\frac{U_{tot,e}}{Z1}+T_{ac}(t-1)\frac{U_{a\_e}}{Z1}$$

Without evaporator mass flow

$$\dot{Q}_{st,e}=\dot{Q}_{hl,e}+\dot{Q}_{c\_e}$$

$$C_e\cdot\left(T_e(t)-T_e(t-1)\right)=U_{tot,e}\cdot\Delta t\cdot\left(t_{amb}-\frac{T_e(t-1)+T_e(t)}{2}\right)$$
$$+U_{a\_e}\cdot\Delta t\cdot\left(T_{ac}(t-1)-T_e(t-1)\right)$$

$$\frac{C_e}{\Delta t}\cdot T_e(t)-\frac{C_e}{\Delta t}\cdot T_e(t-1)=U_{tot,e}\cdot t_{amb}-\frac{U_{tot,e}}{2}\cdot T_e(t-1)-\frac{U_{tot,e}}{2}\cdot T_e(t)$$
$$+U_{a\_e}\cdot\left(T_{ac}(t-1)-T_e(t-1)\right)$$

$$T_e(t)\overbrace{\left(\frac{C_e}{\Delta t}+\frac{U_{tot,e}}{2}\right)}^{=C1}=T_e(t-1)\overbrace{\left(\frac{C_e}{\Delta t}\cdot-\frac{U_{tot,e}}{2}-U_{a\_e}\right)}^{=C2}+t_{amb}\cdot U_{tot,e}$$
$$+T_{ac}(t-1)\cdot U_{a\_e}\quad\cdot$$

$$T_e(t)=T_e(t-1)\frac{C2}{C1}+t_{amb}\frac{U_{tot,e}}{C1}+T_{ac}(t-1)\frac{U_{a\_e}}{C1}$$

C) Absorber/Condenser

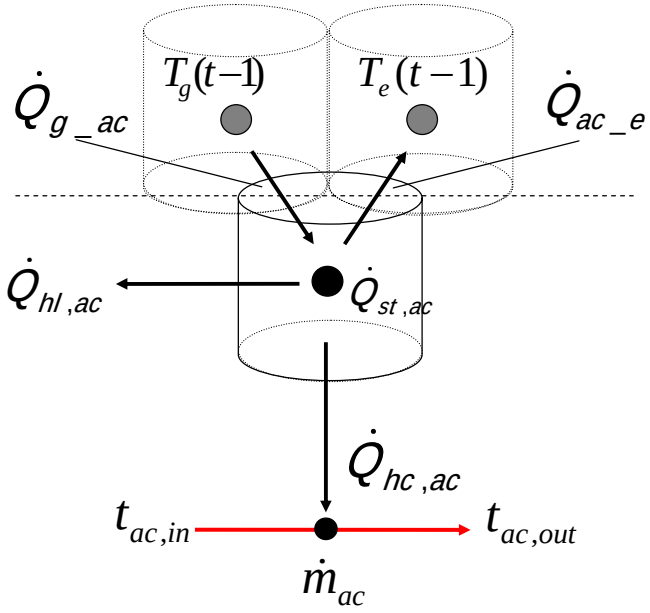

Fig. 3: Heat transfer and heat storage of the evaporator

- Heat balance of the external circuit

$$\dot{Q}_{ac} = \dot{Q}_{hc,ac}$$

$$\dot{m}_{ac} \cdot c_{p,ac} \cdot \Delta t \cdot \left(t_{ac,out} - t_{ac,in}\right) = UA_{ac} \cdot \Delta t \cdot \left(\frac{T_{ac}(t-1) + T_{ac}(t)}{2} - \frac{t_{ac,in} + t_{ac,out}}{2}\right)$$

$$t_{ac,out}\overbrace{\left(\dot{m}_{ac} \cdot c_{p,ac} + \frac{UA_{ac}}{2}\right)}^{=C1} = t_{ac,in}\overbrace{\left(\dot{m}_{ac} \cdot c_{p,ac} - \frac{UA_{ac}}{2}\right)}^{=C2} + \overbrace{\frac{UA_{ac}}{2}}^{=C3} T_{ac}(t-1) + \overbrace{\frac{UA_{ac}}{2}}^{=C3} T_{ac}(t)$$

$$t_{ac,out} = t_{ac,in}\frac{C2}{C1} + T_{ac}(t-1)\frac{C3}{C1} + T_{ac}(t)\frac{C3}{C1}$$

- Internal heat balance

$$\dot{Q}_{st,ac} = -\dot{Q}_{hc,ac} - \dot{Q}_{hl,ac} + \dot{Q}_{g\_ac} - \dot{Q}_{ac\_e}$$

$$C_{ac} \cdot \left(T_{ac}(t) - T_{ac}(t-1)\right) = -UA_{ac} \cdot \Delta t \cdot \left(\frac{T_{ac}(t-1) + T_{ac}(t)}{2} - \frac{t_{ac,in} + t_{ac,out}}{2}\right)$$
$$- U_{tot,ac} \cdot \Delta t \cdot \left(\frac{T_{ac}(t-1) + T_{ac}(t)}{2} - t_{amb}\right)$$
$$+ U_{g\_ac} \cdot \Delta t \cdot \left(T_g(t-1) - T_{ac}(t-1)\right)$$
$$- U_{ac\_e} \cdot \Delta t \cdot \left(T_{ac}(t-1) - T_e(t-1)\right)$$

- Solving the equation system for $T_{ac}(t)$

Step 1

$$\frac{C_{ac}}{\Delta t} \cdot T_{ac}(t) - \frac{C_{ac}}{\Delta t} \cdot T_{ac}(t-1)$$
$$= -\frac{UA_{ac}}{2}\left(-t_{ac,in} - t_{a,in}\frac{C2}{C1} - T_{ac}(t-1)\frac{C3}{C1} - T_{ac}(t)\frac{C3}{C1} + T_{ac}(t-1) + T_{ac}(t)\right)$$
$$- \frac{U_{tot,ac}}{2} \cdot \left(T_{ac}(t-1) + T_{ac}(t) - 2t_{amb}\right) + U_{g\_ac} \cdot \left(T_g(t-1) - T_{ac}(t-1)\right)$$
$$- U_{ac\_e} \cdot \left(T_{ac}(t-1) - T_e(t-1)\right)$$

Step 2

$$\frac{C_{ac}}{\Delta t} \cdot T_{ac}(t) - T_{ac}(t)\frac{UA_{ac}}{2}\left(\frac{C3}{C1} - 1\right) + T_{ac}(t)\frac{U_{tot,ac}}{2}$$
$$= \frac{C_{ac}}{\Delta t} \cdot T_{ac}(t-1) + \frac{UA_{ac}}{2}\left(t_{ac,in} + t_{ac,in}\frac{C2}{C1} + T_{ac}(t-1)\left(\frac{C3}{C1} - 1\right)\right)$$
$$- \frac{U_{tot,ac}}{2} \cdot \left(T_{ac}(t-1) - 2t_{amb}\right) + U_{g\_ac} \cdot \left(T_g(t-1) - T_{ac}(t-1)\right)$$
$$- U_{ac\_e} \cdot \left(T_{ac}(t-1) - T_e(t-1)\right)$$

Step 3

$$T_{ac}(t)\overbrace{\left[\frac{U_{tot,ac}}{2}+\frac{C_{ac}}{\Delta t}-\frac{UA_{ac}}{2}\left(\frac{C3}{C1}-1\right)\right]}^{=Z1}$$

$$=T_{ac}(t-1)\overbrace{\left[\frac{UA_{ac}}{2}\left(\frac{C3}{C1}-1\right)+\frac{C_{ac}}{\Delta t}-\frac{U_{tot,ac}}{2}-U_{ac\_e}-U_{g\_ac}\right]}^{=Z2}$$

$$+t_{ac,in}\overbrace{\frac{UA_{ac}}{2}\left(1+\frac{C2}{C1}\right)}^{=Z3}$$

$$+U_{tot,ac}t_{amb}+U_{ac\_e}\cdot T_e(t-1)+U_{g\_ac}\cdot T_g(t-1)$$

$$T_{ac}(t)=T_{ac}(t-1)\frac{Z2}{Z1}+t_{ac,in}\frac{Z3}{Z1}+t_{amb}\frac{U_{tot,ac}}{Z1}+T_e(t-1)\frac{U_{ac\_e}}{Z1}+T_g(t-1)\cdot\frac{U_{g\_ac}}{Z1}$$

Without evaporator mass flow

$$\dot{Q}_{st,ac}=\dot{Q}_{hl,ac}-\dot{Q}_{g\_ac}+\dot{Q}_{ac\_e}$$

$$\begin{aligned}C_{ac}\cdot\left(T_{ac}(t-1)-T_{ac}(t)\right)&=U_{tot,ac}\cdot\Delta t\cdot\left(\frac{T_{ac}(t-1)+T_{ac}(t)}{2}-t_{amb}\right)\\&-U_{g\_ac}\cdot\Delta t\cdot\left(T_g(t-1)-T_{ac}(t-1)\right)\\&+U_{ac\_e}\cdot\Delta t\cdot\left(T_{ac}(t-1)-T_e(t-1)\right)\end{aligned}$$

$$T_{ac}(t)\overbrace{\left(\frac{C_{ac}}{\Delta t}+\frac{U_{tot,ac}}{2}\right)}^{=C1}=T_{ac}(t-1)\overbrace{\left(\frac{C_{ac}}{\Delta t}\cdot-\frac{U_{tot,ac}}{2}-U_{g\_ac}-U_{ac\_e}\right)}^{=C2}+U_{tot,ac}t_{amb}$$

$$+U_{g\_ac}\cdot T_g(t-1)+U_{ac\_e}\cdot T_e(t-1)$$

$$T_{ac}(t)=T_{ac}(t-1)\frac{C2}{C1}+t_{amb}\frac{U_{tot,ac}}{C1}+T_g(t-1)\frac{U_{g\_ac}}{C1}+T_e(t-1)\frac{U_{ac\_e}}{C1}$$

D) Calculation of the heat transfer areas, the heat transfer coefficients and the thermal capacity:

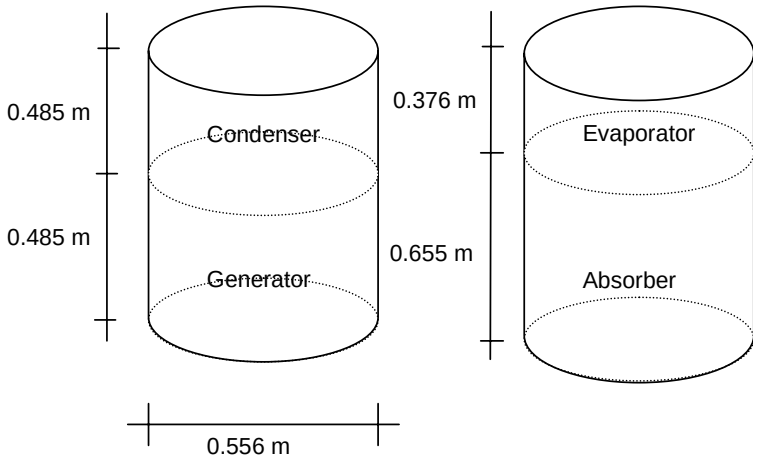

- System weight without liquid: 600 kg – 20% for structure = 460 kg
  Specific heat capacity of cupper: 380 J/kgK

- Separated weight and thermal capacity of components according to size

Generator/Condenser	= 115 kg;	$c_{G/C}$ = 43 700 J/K
Absorber	= 146 kg;	c_A = 55 480 J/K
Evaporator	= 84 kg	c_E = 31 920 J/K
Liquid weight:	= 100kg	
→ 25 kg liquid each		c_W = 104 500 J/K

- Heat transfer areas and coefficients:

1. Generator

-Area adjacent to ambient: $A = \left(\frac{0.556m}{2}\right)^2 \cdot \pi + 0.556m \cdot \pi \cdot 0.485m = 1.09m^2$

- Area adjacent to condenser: $A = \left(\frac{0.556m}{2}\right)^2 \cdot \pi = 0.24m^2$

- Heat transfer coefficient generator → condenser:

$$U_{g\_c} = h_{c,g} \cdot A_{g\_c} \cdot a_{TB} = 7.7 \frac{W}{m_2 K} \cdot 0.24m^2 \cdot 2 = 3.70 \frac{W}{K}$$

The factor for the larger thermal bridges a_{TB} is set to a value of 2.0

- Heat transfer coefficient generator → ambient:

$$U_{g\_amb} = \left(\frac{1}{\frac{1}{h_{c,g}} + \frac{1}{h_{c,amb}}} \right) \cdot A_{g\_amb} = \frac{1}{2 \cdot 0.13} \frac{W}{m_2 K} \cdot 1.09 m^2 = 4.19 \frac{W}{K}$$

2. Condenser

- Area adjacent to ambient: $A = \left(\frac{0.556m}{2} \right)^2 \cdot \pi + 0.556m \cdot \pi \cdot 0.485m = 1.09m^2$

- Area adjacent to generator: $A = \left(\frac{0.556m}{2} \right)^2 \cdot \pi = 0.24m^2$

- Heat transfer coefficient condenser→ generator:

$$U_{g\_c} = h_{c,g} \cdot A_{g\_c} \cdot a_{TB} = 7.7 \frac{W}{m_2 K} \cdot 0.24 m^2 \cdot 2 = 3.70 \frac{W}{K}$$

The factor for the larger thermal bridges a_{TB} is set to a value of 2.0

- Heat transfer coefficient condenser → ambient:

$$U_{c\_amb} = \left(\frac{1}{\frac{1}{h_{c,c}} + \frac{1}{h_{c,amb}}} \right) A_{g\_amb} = \frac{1}{2 \cdot 0.13} \frac{W}{m_2 K} \cdot 1.09 m^2 = 4.19 \frac{W}{K}$$

3. Absorber

- Area adjacent to ambient: $A = \left(\frac{0.556m}{2} \right)^2 \cdot \pi + 0.556m \cdot \pi \cdot 0.655m = 1.39m^2$

- Area adjacent to evaporator: $A = \left(\frac{0.556m}{2} \right)^2 \cdot \pi = 0.24m^2$

- Heat transfer coefficient Absorber→ Evaporator:

$$U_{a\_e} = h_{c,a} \cdot A_{a\_e} \cdot a_{TB} = 7.7 \frac{W}{m_2 K} \cdot 0.24 m^2 \cdot 2 = 3.70 \frac{W}{K}$$

The factor for the larger thermal bridges a_{TB} is set to a value of 2.0

- Heat transfer coefficient Absorber → Ambient:

$$U_{a\_amb} = \left(\frac{1}{\frac{1}{h_{c,a}} + \frac{1}{h_{c,amb}}} \right) A_{g\_amb} = \frac{1}{2 \cdot 0.13} \frac{W}{m_2 K} \cdot 1.39 m^2 = 5.35 \frac{W}{K}$$

4. Evaporator

- Area adjacent to ambient: $A = \left(\frac{0.556m}{2} \right)^2 \cdot \pi + 0.556m \cdot \pi \cdot 0.376m = 0.91m^2$
- Area adjacent to evaporator: $A = \left(\frac{0.556m}{2} \right)^2 \cdot \pi = 0.24m^2$
- Heat transfer coefficient Evaporator→ Absorber:

$$U_{a\_e} = h_{c,a} \cdot A_{a\_e} \cdot a_{TB} = 7.7 \frac{W}{m_2 K} \cdot 0.24 m^2 \cdot 2 = 3.70 \frac{W}{K}$$

The factor for the larger thermal bridges a_{TB} is set to a value of 2.0

- Heat transfer coefficient Evaporator → Ambient:

$$U_{e\_amb} = \left(\frac{1}{\frac{1}{h_{c,a}} + \frac{1}{h_{c,amb}}} \right) A_{g\_amb} = \frac{1}{2 \cdot 0.13} \frac{W}{m_2 K} \cdot 0.91 m^2 = 3.50 \frac{W}{K}$$

1.4 PERFORMANCE CHARACTERISTICS CALCULATED FOR THE AXIMA EWK 036 COOLING TOWER

For the AXIMA EWK 036 cooling tower several performance characteristics are calculated with the developed cooling tower model descried in chapter 2.2.3.1. The results are shown in the following graphs but not further discussed.

In a first step the cooling performance, water consumption and electricity demand of the Axima EWK has been calculated for fixed ambient conditions of 34°C, 45 % relative humidity and a water mass flow rate of 1.39 kg/s. The water inlet temperature and fan speed were varied between 30°C and 50 °C and 20 and 100%. The results are shown in Fig. 4 to Fig. 7.

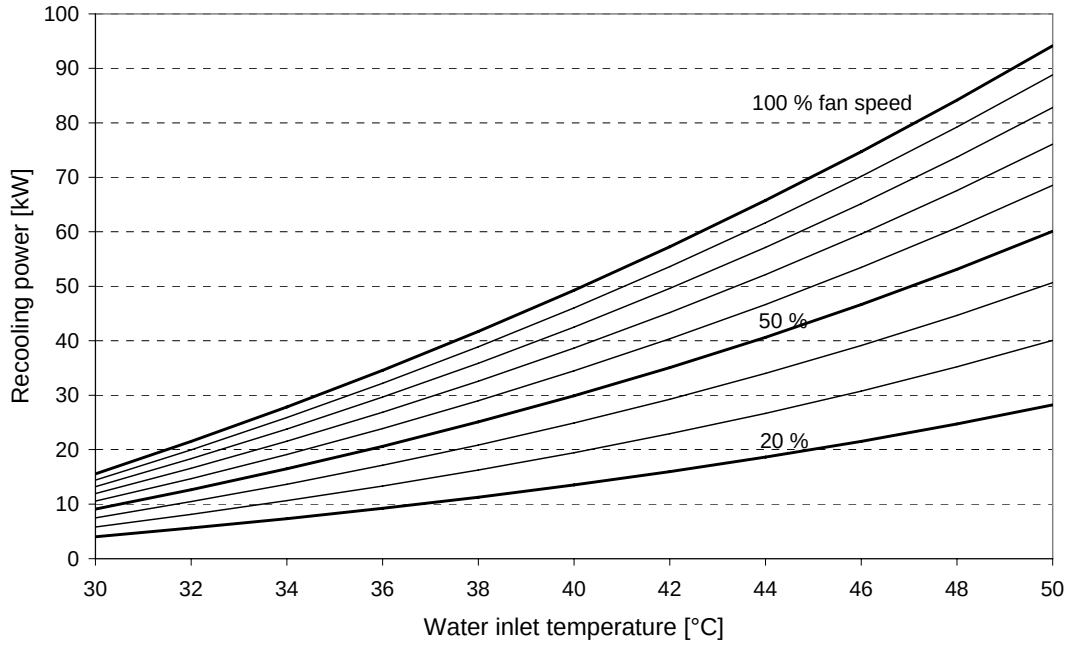

Fig. 4: Recooling power in dependence of the water inlet temperature and fan speed. Results are for 34°C ambient temperature and 45 % relative humidity and a water mass flow rate of 1.39 kg/s

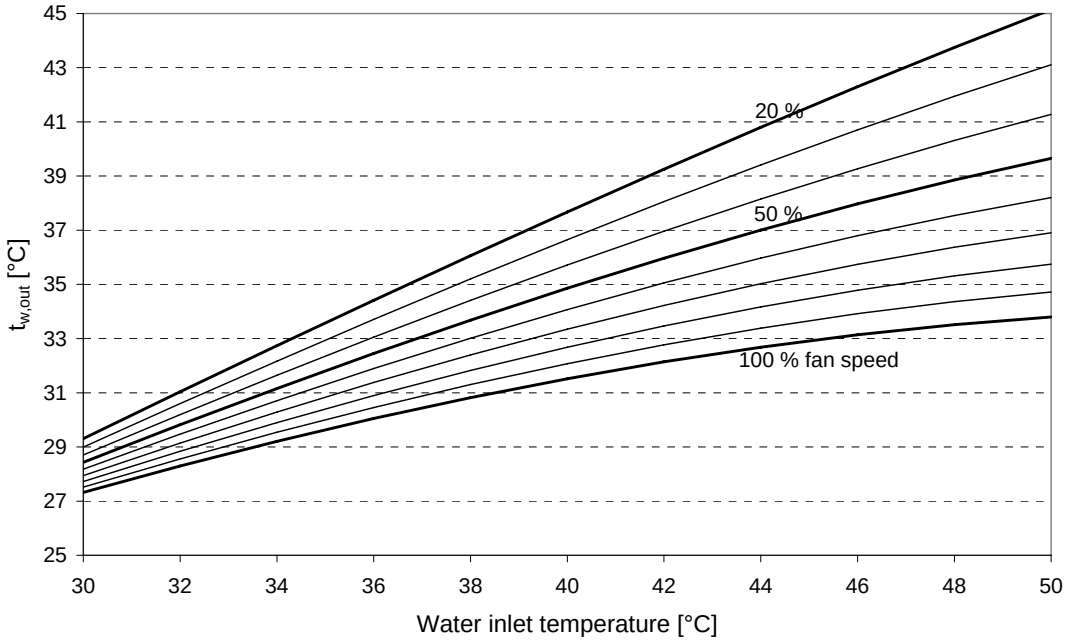

Fig. 5: Water outlet temperature in dependence of the water inlet temperature and fan speed. Results are for 34°C ambient temperature and 45 % relative humidity and a water mass flow rate of 1.39 kg/s

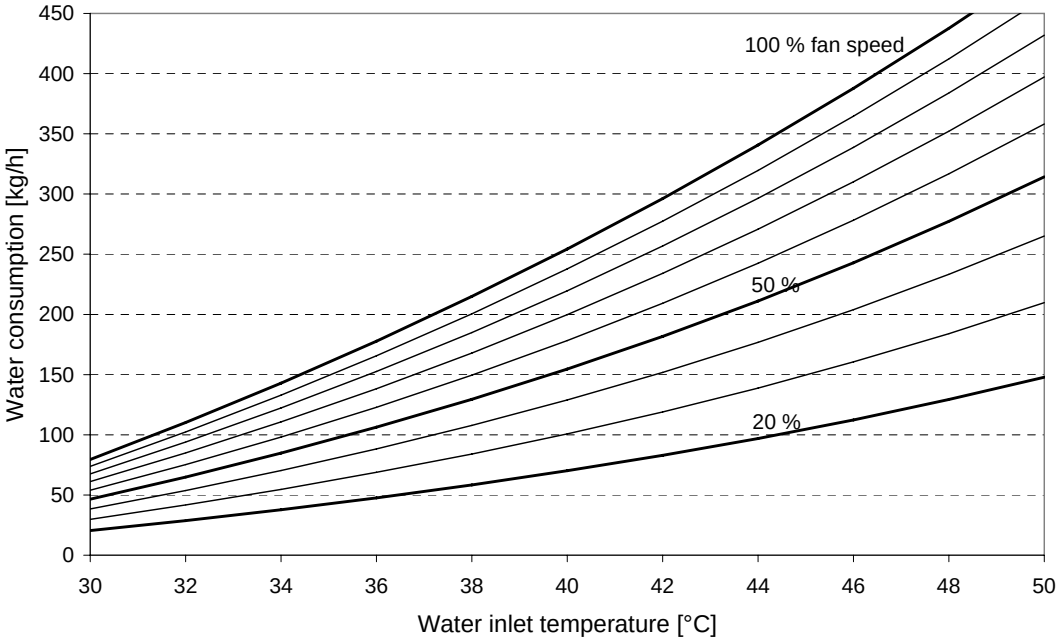

Fig. 6: Water outlet consumption in dependence of the water inlet temperature and fan speed. Results are for 34°C ambient temperature and 45 % relative humidity and a water mass flow rate of 1.39 kg/s

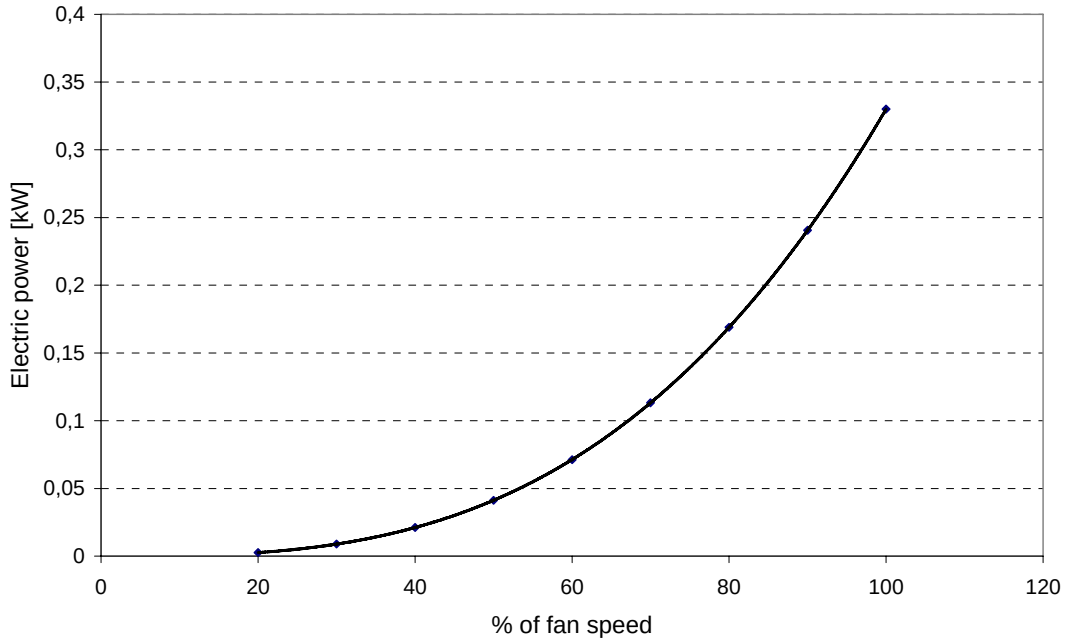

Fig. 7: Electricity consumption in dependence of the fan speed.

Additionally, the cooling performance and water consumption of the Axima EWK 036 wet cooling tower has been calculated for variable wet bulb temperatures of the ambient air and fixed water mass flow rate of 1.39 kg/s. The water inlet temperature was kept constant at 36°C and the van speed was varied between 20 and 100%. The results are shown in Fig. 8 to Fig. 10.

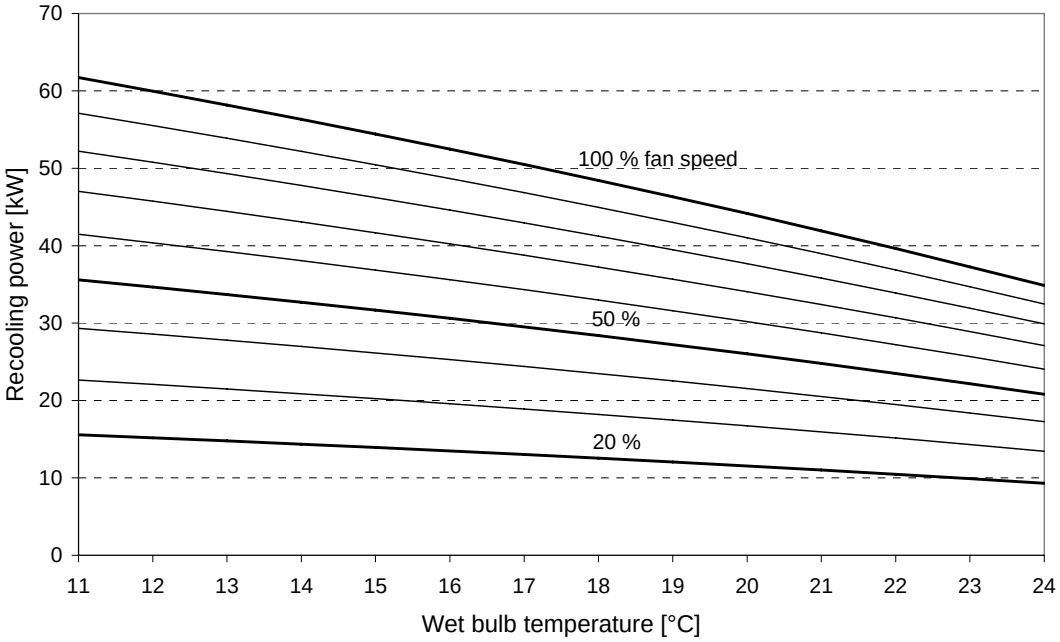

Fig. 8: Recooling power in dependence of the wet bulb temperature and fan speed. Results are for 36°C water inlet temperature and a water mass flow rate of 1.39 kg/s

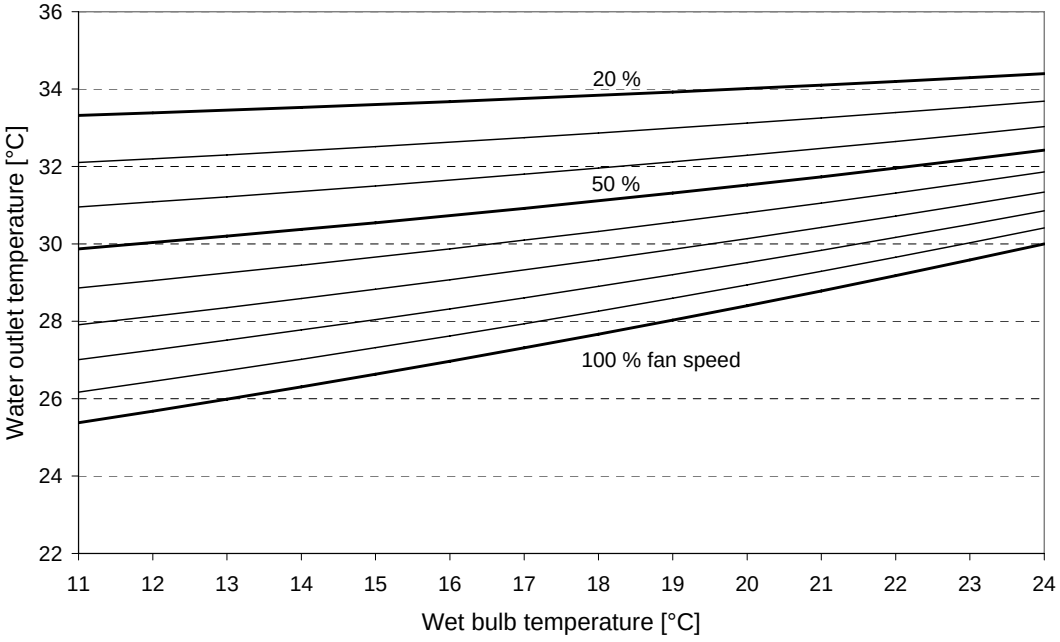

Fig. 9: Water outlet temperature in dependence of the wet bulb temperature and fan speed. Results are for 36°C water inlet temperature and a water mass flow rate of 1.39 kg/s

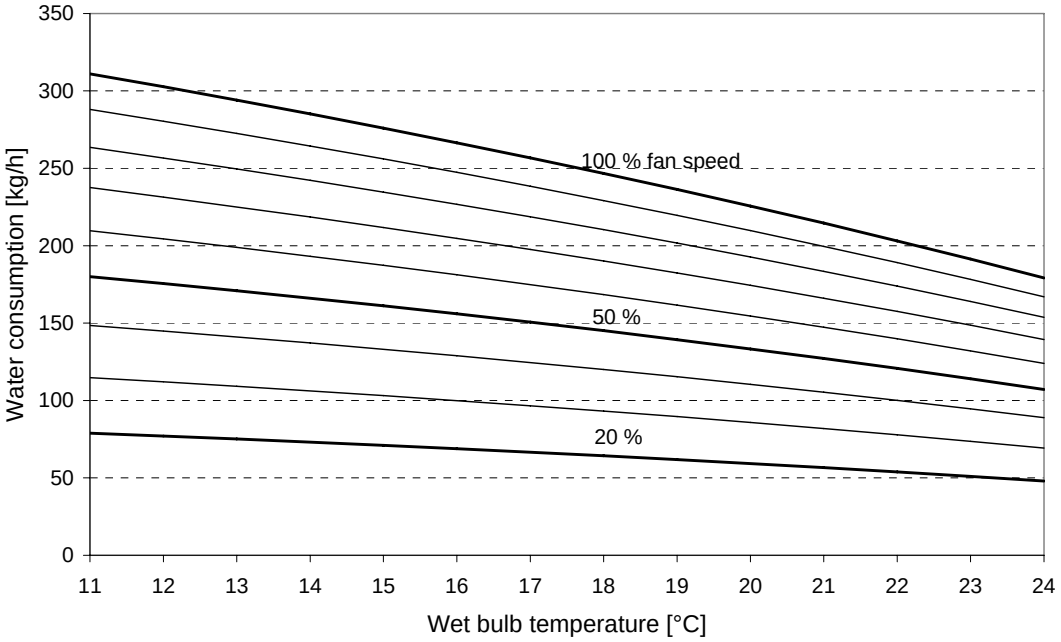

Fig. 10: Water outlet temperature in dependence of the wet bulb temperature and fan speed. Results are for 36°C water inlet temperature and a water mass flow rate of 1.39 kg/s

DESCRIPTION OF THE COMPONENTS OF THE SOLAR COOLING SYSTEM INSTALLED AT THE SOLARNEXT OFFICE BUILDING IN RIMSTING, GERMANY

1. ABSORPTION CHILLER CHILLII® ESC15

The installed LiBr absorption chiller chillii® ESC15 is equal to the EAW WGRACAL SE 15 chiller. The technical data of the chiller is shown in the table below:

Technical Data of the EAW WEGRACAL SE 15 Absorption Chiller

Cooling power	15 kW	Thermal COP	0.71
Cold water inlet	17 °C	Cold water outlet	11 °C
Cold water volume flow rate	1.9 $m^3 h^{-1}$	Nominal pressure loss	350 mbar
Nominal pressure	6 bar	Cold water connection	DN 25
Heating power	21 kW		
Hot water supply	90 °C	Hot water return	80.5 °C
Cold water volume flow rate	2.0 $m^3 h^{-1}$	Nominal pressure loss	250 mbar
Nominal pressure	6 bar	Cold water connection	DN 25
Recooling power	35 kW		
Cooling water supply	30 °C	Cooling water return	36 °C
Cold water volume flow rate	5.0 $m^3 h^{-1}$	Nominal pressure loss	900 mbar
Nominal pressure	6 bar	Cold water connection	DN 32
Voltage / Frequency	400 V / 230 V 50 Hz	Electrical power consumption	0,3 kW
Length	1.5 m	Width	0.75 m
Height	1.6 m	Weight	700 kg

2. COOLING TOWER AXIMA EWK 035

The open wet cooling tower installed in the solar cooling system is an Axima EWK cooling tower with a nominal cooling capacity of 35 kW at 30°C water supply and 36°C cooling water return temperature at ambient conditions with a wet bulb temperature of 24°C. The complete set of technical data is listed in the table below:

Technical Data of the Axima Wet Cooling Tower EWK 035

Cooling power	35 kW	Thermal COP	0.71
Cooling water inlet	36 °C	Cooling water outlet	30 °C
Ambient wet bulb temperature	24°C	Cooling water volume flow rate	5 $m^3 h^{-1}$
Nominal electrical power demand of cooling tower fan	330 W	Nominal rotation speed of fan	1420 m^{-1}
Total length	0.739 m	Total width	0.739 m
Total height	1.865 m	Height of contact matrix	0.610 m

3. COLD WATER STORAGE TANK

A 1000 l cold water storage tank (Citrinsolar PS1000/790) with 10 cm Armaflex isolation has been implemented in the system. Since the cold water distribution is operated at high temperature of 16°C supply and 18°C return temperature, the cold storage offers a storage capacity of 10 kWh if cooled down to the lower limit of 6°C.

4. HOT WATER STORAGE TANK

Two 1000 l Citrinsolar hot water storage tanks, Type PS1000/790 with 10 cm heat isolation have been implemented in the system. The two storage tanks are connected in parallel and therefore behave like one big storage tank, but with higher heat losses. The hot storage tank has several connections in different height for the collector supply which are controlled by magnetic valves. This offers the possibility to operate the storage tank with partitioned volume for faster temperature increase. A schematic diagram of the whole solar cooling installation visualises the hydraulic connections of the hot storage tank.

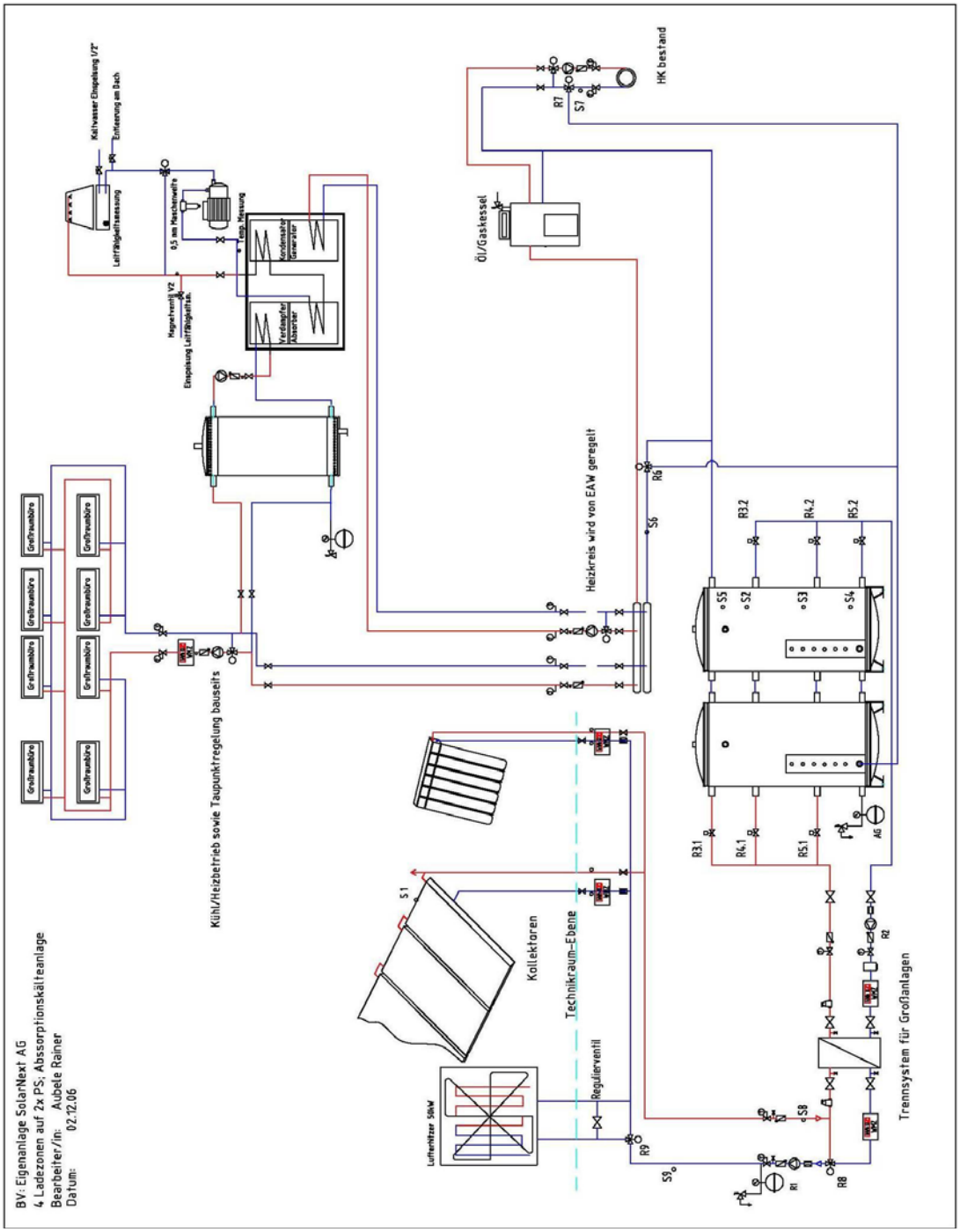

Schematic diagram of the installed chillii® solar cooling system

5. SOLAR COLLECTORS

Two collector fields, one with 37 m² Citrinsolar CS-100F flat plate collectors and one with 34 m² TH SLU1500/16 solar vacuum tube collectors all facing south with an inclination of 30° have been installed. The two collector fields are connected in parallel with the possibility to operate only the flat plate or the vacuum collectors or the whole collector field together (common operation mode). The technical data of the installed collectors are shown in the tables below:

Technical Data of the Citrinsolar CS-100F Flat Plate Collectors

Collector aperture area	1.903 m²	Collector absorber area	1.903 m²
Collector gross area	2.078 m²	Collector mass flow rate	162 l m^{-2} h^{-1}
Collector efficiency related to the collector aperture area			
maximum efficiency η_0	0.798	Linear heat loss coefficient a_1	3.34 W m^{-2} K^{-1}
Quadratic heat loss coefficient a_2	0.0075 W $m^{-2}K^{-2}$	Area related heat capacity	9.5 kJ m^{-2} K^{-1}

Technical Data of the SLU1500/16 SLU1500/16 Vacuum Tube Collectors

Collector aperture area	1.330 m²	Collector absorber area	0.880 m²
Collector gross area	1.620 m²	Collector mass flow rate	127 l m^{-2} h^{-1}
Collector efficiency related to the collector aperture area			
Maximum efficiency η_0	0.695	Linear heat loss coefficient a_1	1.36 W m^{-2} K^{-1}
Quadratic heat loss coefficient a_2	0.01 W m^{-2} K^{-2}	Area related heat capacity	44 kJ m^{-2} K^{-1}

6. SOLAR CIRCUIT EMERGENCY WATER TO AIR COOLER

To avoid stagnation in the collector circuit during periods of chiller shut down, a water to air cooler (KAMPMANN air heater TOP 474136) has been implemented in the system, which rejects the solar heat to the environment if the temperature in the collector return increases above 100 °C. After activation the solar circuit cooler remains in operation until the temperature in the collector return decreases below 90°C. The model of the dry heat rejection system described in Chapter 2.2.3.2 was used to simulate the performance of the system. The technical data described in the table below was used in the model:

Technical Data Dry Heat Rejection System, KAMPMANN Air Heater TOP 474136

Nominal cooling power	53.6 kW	Nominal hot fluid inlet temperature	90.0 °C
Nominal air temperature	35°C	Fan speed	450 min^{-1}
Air volume flow rate	3840 $m^3 h^{-1}$	Electrical power consumption ventilator	120 W
Hot fluid volume flow rate	2.47 $m^3 h^{-1}$	Density of hot fluid	1004 kg m^{-3}
Specific heat of hot fluid	3.9 kJ $kg^{-1} K^{-1}$	Nominal ambient air inlet temperature	20 °C
Total length of heat exchanger unit	0.8 m	Total width of heat exchanger unit	0.8 m

7. DETAILED LIST OF IMPLEMENTED SENSORS AND ACTUATORS

The following list gives an overview of the sensors and actuators implemented in the chillii® solar cooling system of the SolarNext AG in Rimsting. This list is very ambitious, which results from the fact, that the installed system was intended to be operated as test facility with the possibility to test different control strategies and control options. Therefore, not all of these sensors and actuators are really required for the control and observation of a standard solar cooling system.

Sensor and Actuator List:

Description	Unit	Variable
0. Weather Station		
- Temperature ambient air	°C	t_{amb}
- Relative humidity ambient air	%	Rh_{amb}
- global solar irradiation on the horizontal	W/m²	G_h
- global solar irradiation on the tiltet collector area	W/m²	G_t
- Wind speed	m²/h	v_W
- Wind direction	0 - 360° 0° = North 180° = South	
1. Solar System		
a) Collectors		
Description	Unit	Variiable
Temperature sensors		
- Collector temperature	°C	t_{col}
- Inlet (supply) temperatur of collector field	°C	$t_{C,h}$
- Outlet (return) temperature of collector field	°C	$t_{C,c}$
Volume flow sensors, electromagnetic flowmeters e.g. ABB		
- Volume flow collector circuit	m³/h	$\dot{V}_C$
Status collector pump	0/1 (on/off)	
Set points		
Collector outlet temperature (mass flow control)	°C	
Volume flow setpoint collector pump	% (0-100)	

b) Hot Water Storage Tank

Description	Unit	Variable
Temperature sensors heat storage tank supply circuit (only for external HE)		
- Supply temperatur HE collector	°C	$t_{He,o}$
- Return temperature HE collector	°C	$t_{He,i}$
Temperature sensors heat storage tank (sensors on the metall surface)		
- 5 Temperature sensors at different hight	°C	$t_{St,1} \dots t_{St,5}$
Temperature sensors load circuit		
- Outlet temperature from heat storage tank to load	°C	$t_{St,h}$
- Return temperature from load to heat storage tank	°C	$t_{St,c}$
Volume flow sensors, electromagnetic flowmeters e.g. ABB		
- Volume flow storage tank / HE collector	m³/h	$\dot{V}_{HE}$
- Volume flow storage tank to load	m³/h	$\dot{V}_{G,St}$

3. Absorption Cooling Machine External Sensors

Temperature sensors		
- Generator inlet temperature	°C	$t_{G,i}$
- Generator outlet temperature	°C	$t_{G,o}$
- Absorber/Condenser inlet temperature	°C	$t_{AC,i}$
- Absorber/Condenser outlet temperature	°C	$t_{AC,o}$
- Evaporator inlet temperature	°C	$t_{E,i}$
- Evaporator outlet temperature	°C	$t_{E,o}$
Volume flow sensors, electromagnetic flow meters e.g. ABB		
- Generator	m³/h	$\dot{V}_G$
- Absorber/Condenser --> Cooling Tower	m³/h	$\dot{V}_{AC}$
- Evaporator	m³/h	$\dot{V}_E$
Status		
- Generator pump	0/1 (on/off)	
- Absorber/Condenser pump --> Cooling Tower	0/1 (on/off)	
- Evaporator pump	0/1 (on/off)	
- Free Cooling mode	0/1 (open/shutt)	AH1 - AH3
Set points		
- Generator inlet temperature	°C	
- Absorber inlet temperature	°C	
- Evaporator inlet temperature	°C	
- 3-Way mixing valve generator circuit	% (0-100)	
- 3-Way mixing valve Absorber/Condenser to Cooling Tower circuit	% (0-100)	

3. Cold Storage Tank

Description	Unit	Variable
Temperature sensors cold storage tank (sensors on the metall surface)		
- 5 Temperature sensors at different hight	°C	$t_{CSt,1}$ … $t_{CSt,5}$

4. Cold Distribution

Temperature sensors		
- Supply water temperature cooling circuit	°C	$t_{CB,s}$
- Return water temperature cooling circuit	°C	$t_{CB,r}$
Volume flow sensors, electromagnetic flowmeters e.g. ABB		
- cooling circuit building	m³/h	$\dot{V}_{CB}$
Status pump		
- Status cold distribution pump	0/1 (on/off)	
Set points		
Cooling circuit supply temperature	°C	
Mass flow set point cold distribution pump	% (0-100)	

5. Cooling Tower

Temperature sensors		
- Water inlet temperature cooling tower	°C	$t_{CT,i}$
- Water outlet temperature cooling tower	°C	$t_{CT,o}$
Volume flow sensors, electromagnetic flowmeters e.g. ABB		
- cooling water	m³/h	$\dot{V}_{CT}$
		$\dot{V}_{Air}$
Status ventilator		
- Status ventilator	0/1 (on/off)	
Set points		
- Cooling circuit supply temperature	°C	
- Fan speed cooling tower (Ventilator motor control)	% (0-100)	

6. Electricity Consumption and Power Meters

a) Electrical power input		
- Pumps of the solar collectors	W	$P_{el,S}$
- ACM	W	$P_{el,ACM}$
- External pumps ACM	W	$P_{el,P}$
- Cold distribution of the building	W	$P_{el,dist}$
- Cooling tower	W	$P_{el,CT}$

OPTIMISED CONTROL SEQUENCES OF THE FOUR ANALYSED STORAGE CHARGE AND DISCHARGE CASES (SEE CHAPTER 4.5.3)

Case 1: Full storage volume always used

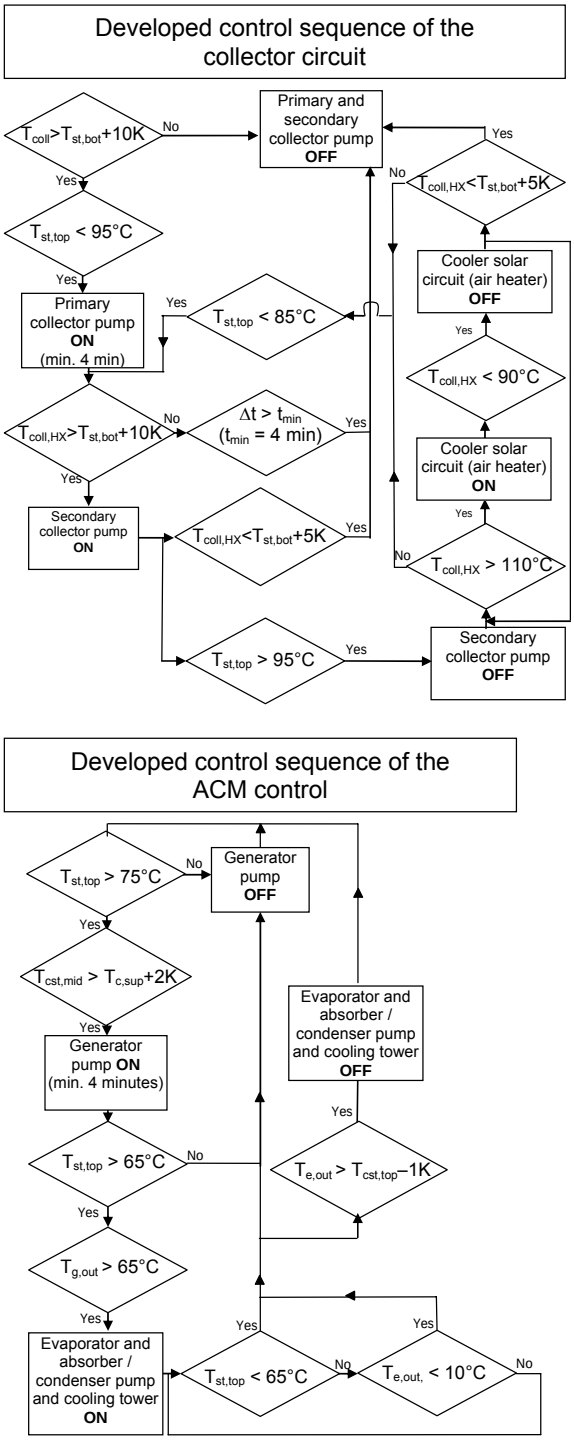

Case 2: Full storage with bypass

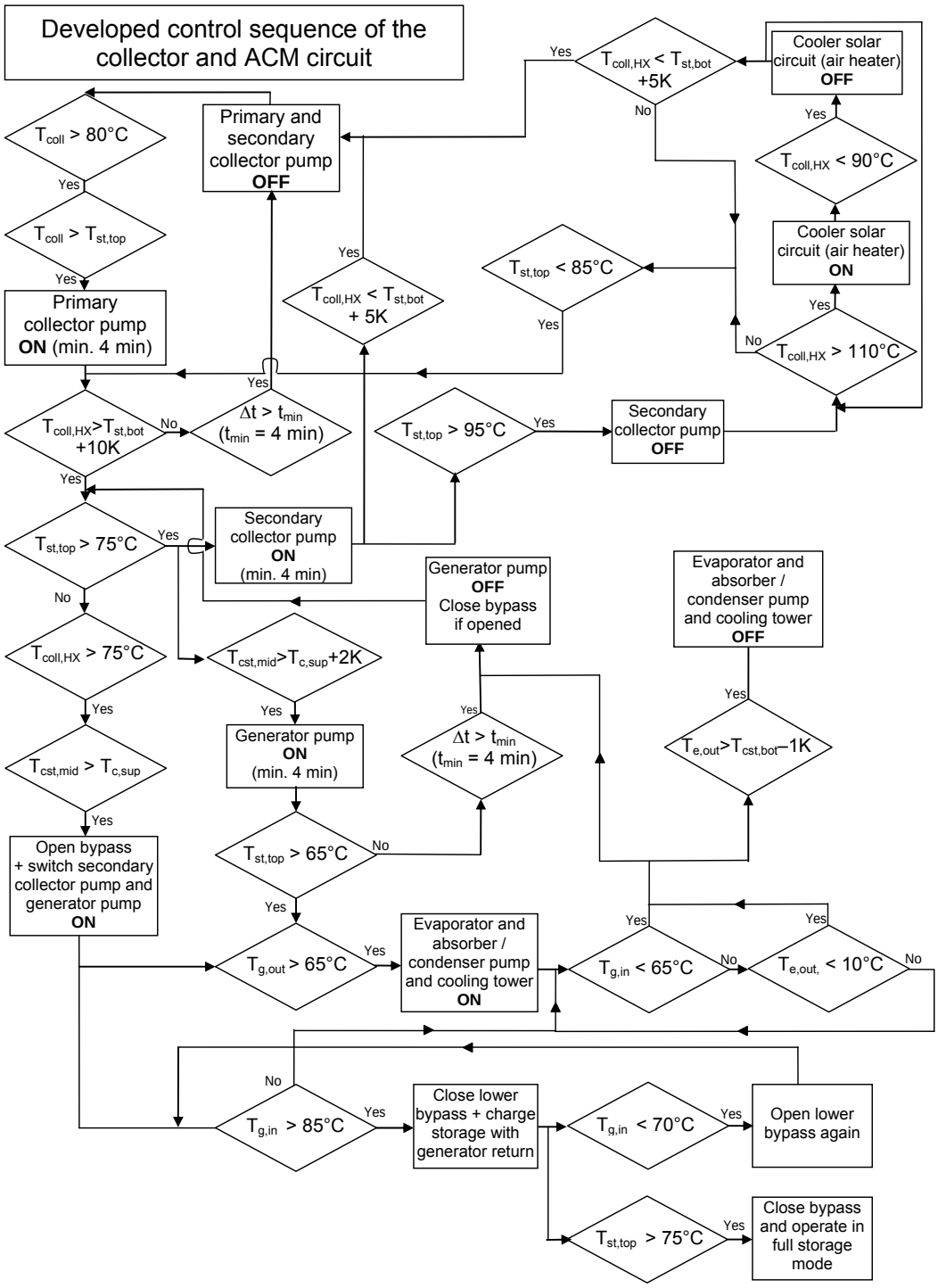

Case 3: Partitioned storage with 300 l top volume

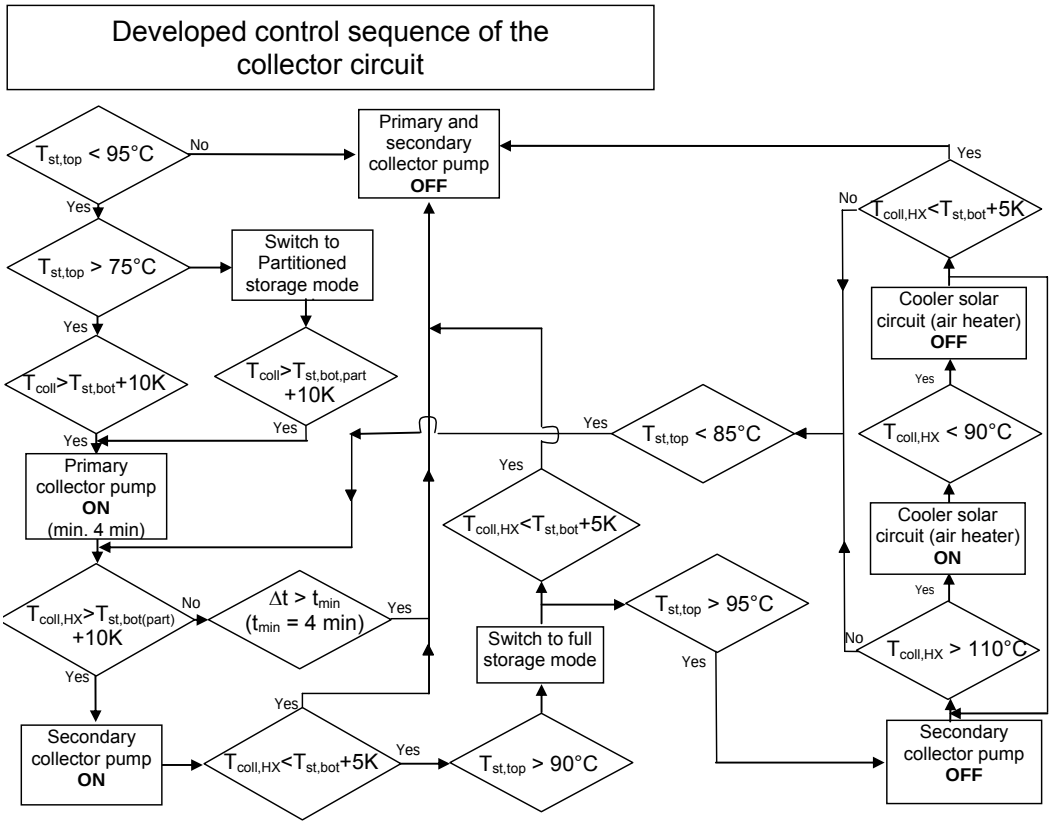

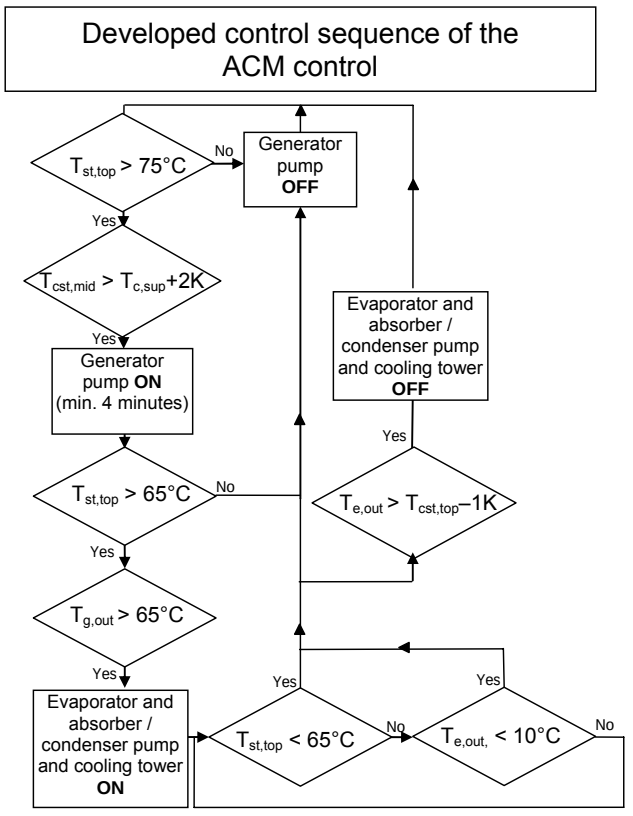

Case 4: Partitioned storage and bypass

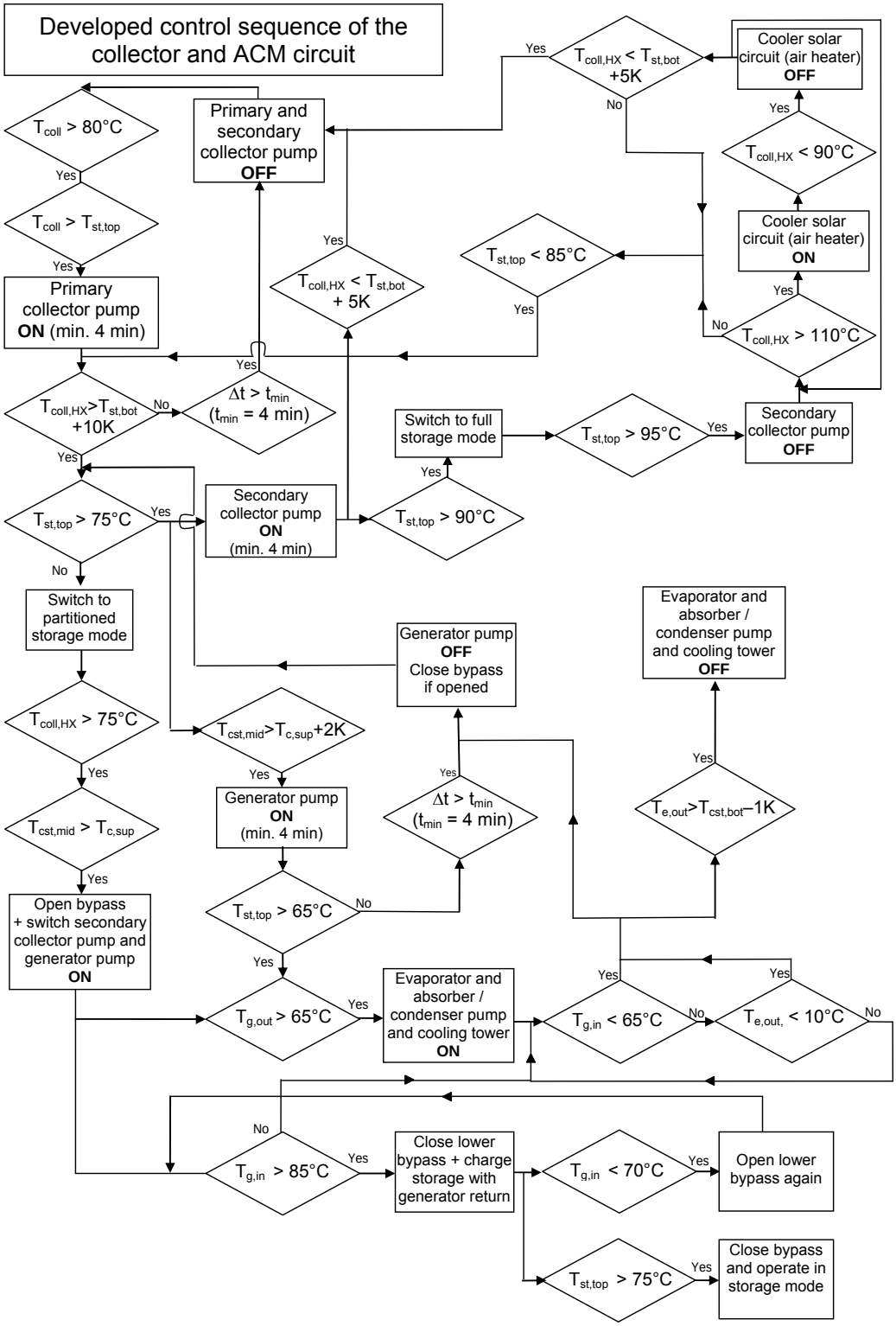

DETAILED SIMULATION RESULTS OF THE FOUR ANALYSED STORAGE CHARGE AND DISCHARGE CASES (SEE CHAPTER 4.5.5)

1. Simulation results for 21st June 2008

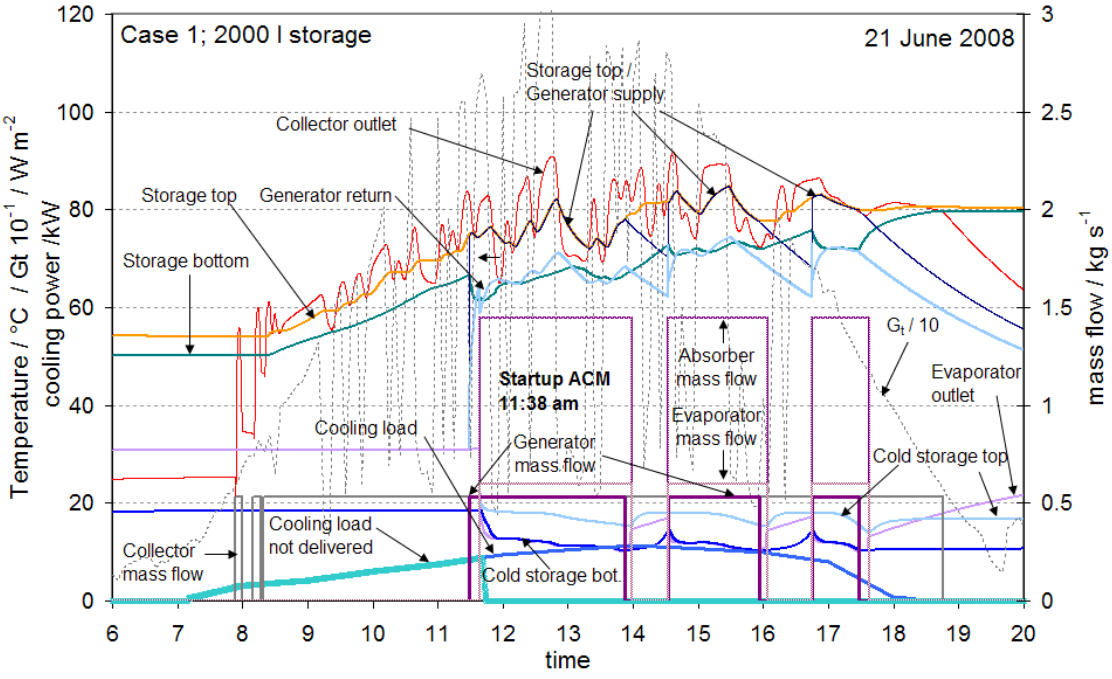

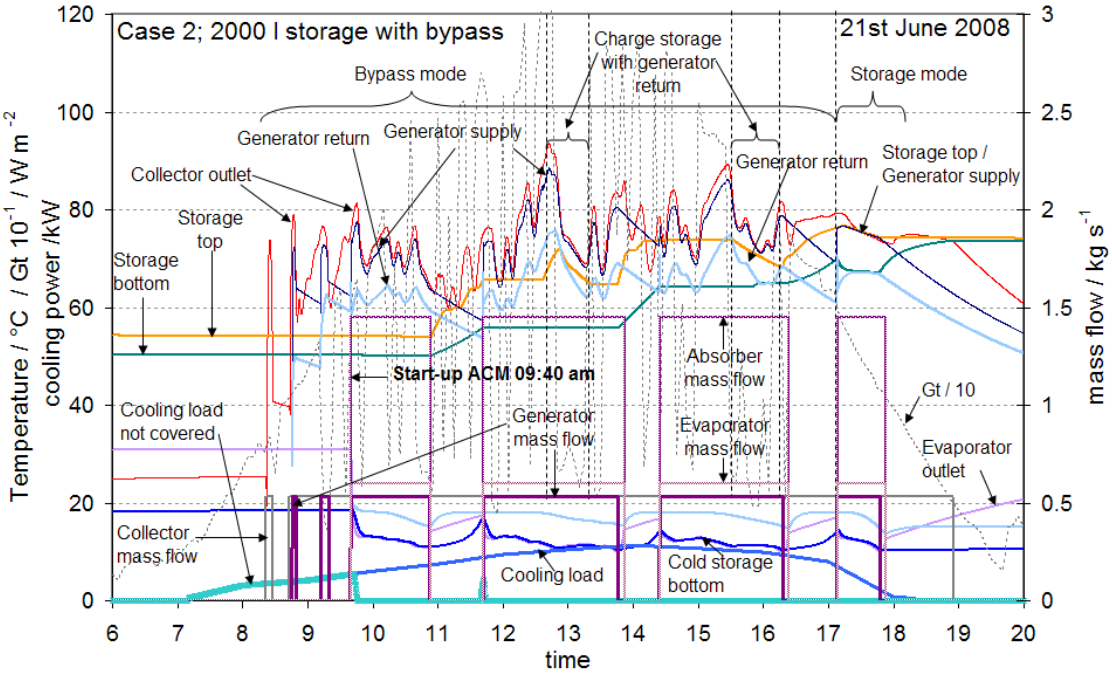

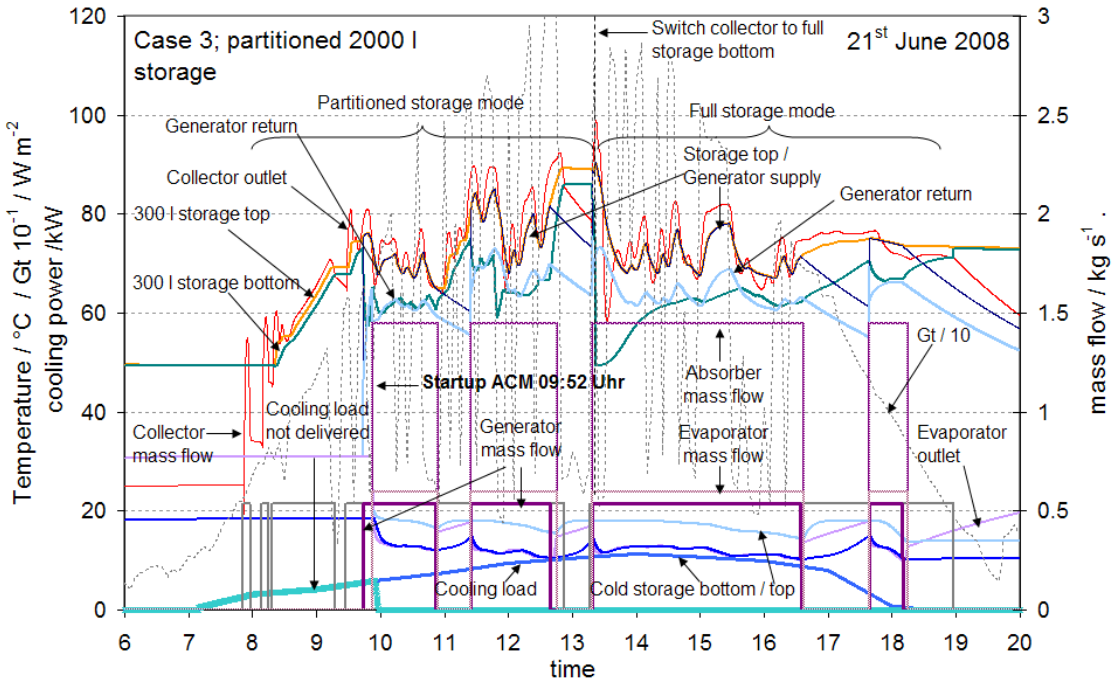
Case 3; partitioned 2000 l storage
21st June 2008
Switch collector to full storage bottom
Partitioned storage mode
Full storage mode
Generator return
Collector outlet
300 l storage top
300 l storage bottom
Storage top / Generator supply
Generator return
Startup ACM 09:52 Uhr
Absorber mass flow
Gt / 10
Cooling load not delivered
Collector mass flow
Generator mass flow
Evaporator mass flow
Evaporator outlet
Cooling load
Cold storage bottom / top
Temperature / °C / Gt 10-1 / W m-2
cooling power /kW
mass flow / kg s-1
time

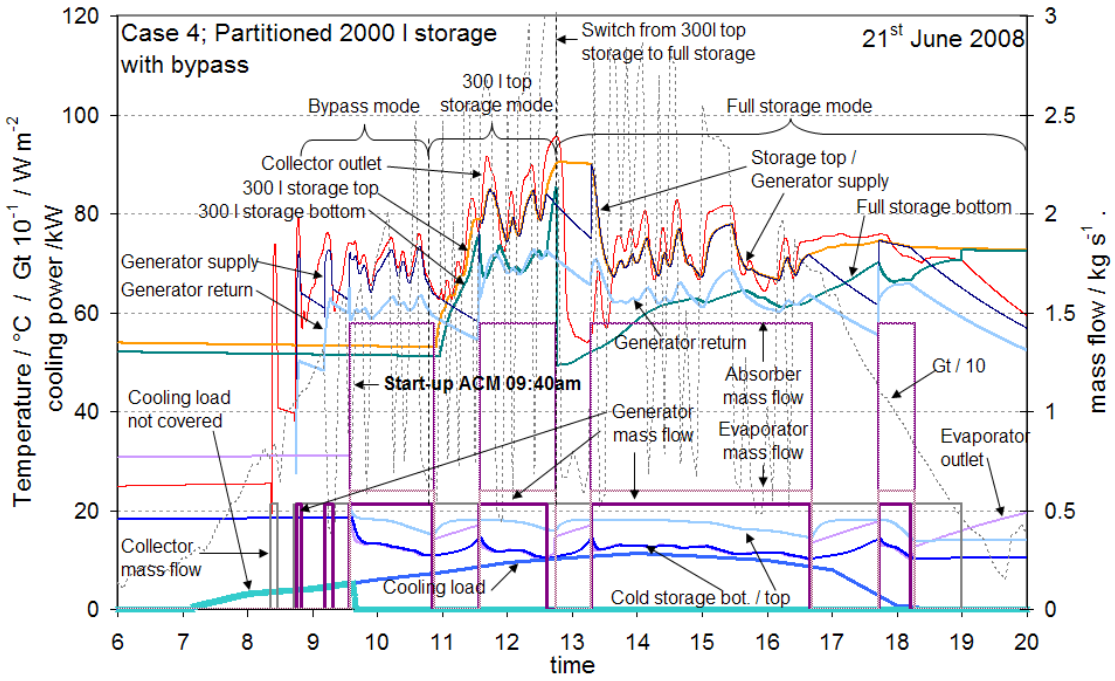
Case 4; Partitioned 2000 l storage with bypass
21st June 2008
Switch from 300l top storage to full storage
300 l top storage mode
Bypass mode
Full storage mode
Collector outlet
300 l storage top
300 l storage bottom
Storage top / Generator supply
Full storage bottom
Generator supply
Generator return
Generator return
Start-up ACM 09:40am
Absorber mass flow
Gt / 10
Cooling load not covered
Generator mass flow
Evaporator mass flow
Evaporator outlet
Collector mass flow
Cooling load
Cold storage bot. / top
Temperature / °C / Gt 10-1 / W m-2
cooling power /kW
mass flow / kg s-1
time

2. Simulation results for 10th July 2008

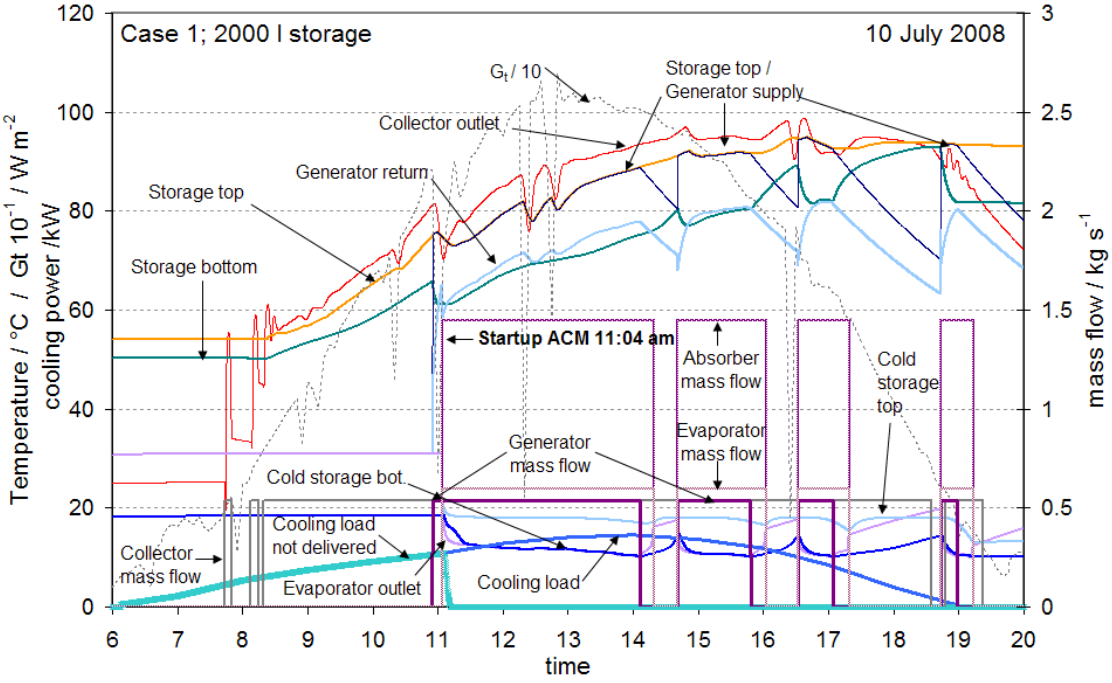

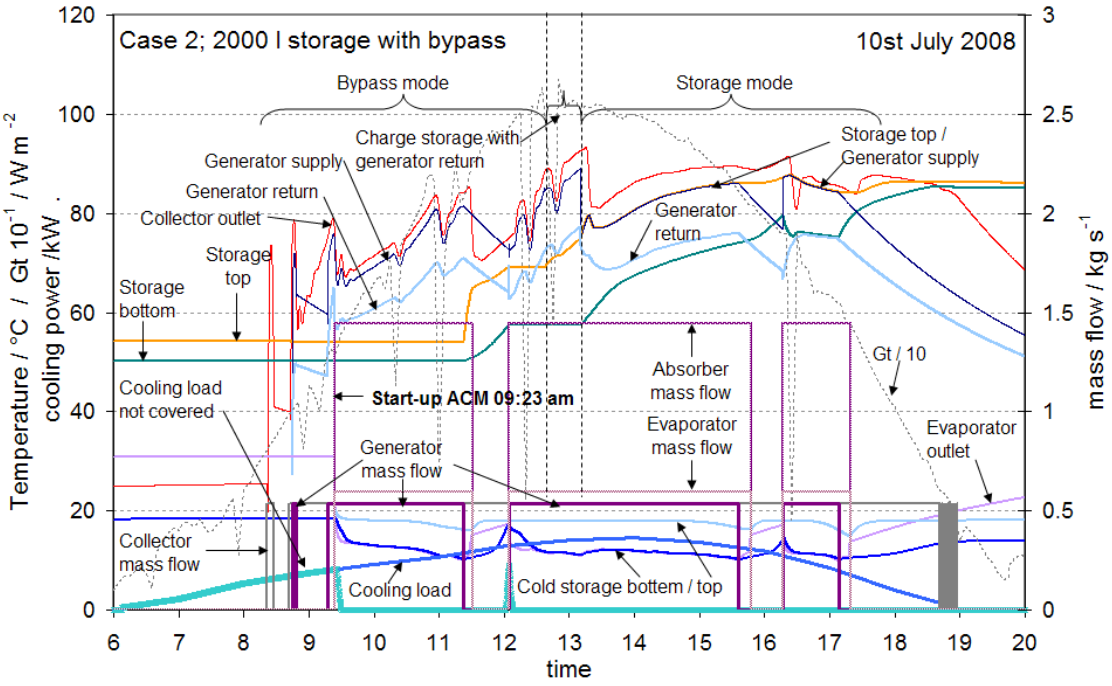

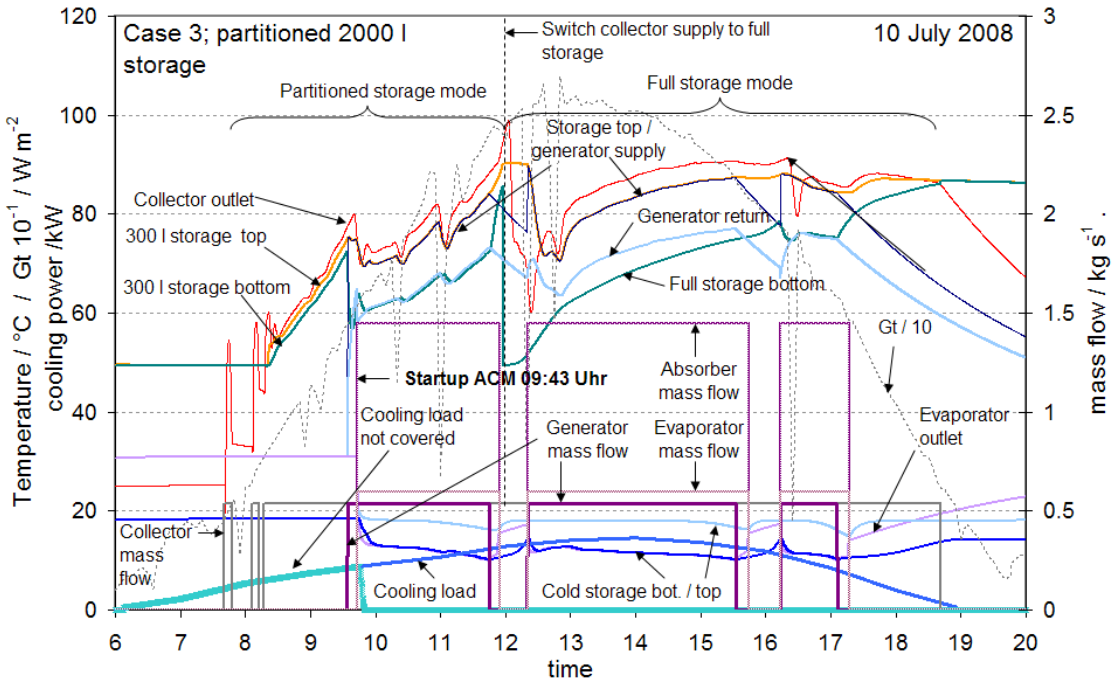
Case 3; partitioned 2000 l storage
10 July 2008
Switch collector supply to full storage
Partitioned storage mode
Full storage mode
Storage top / generator supply
Collector outlet
300 l storage top
300 l storage bottom
Generator return
Full storage bottom
Gt / 10
Startup ACM 09:43 Uhr
Absorber mass flow
Cooling load not covered
Generator mass flow
Evaporator mass flow
Evaporator outlet
Collector mass flow
Cooling load
Cold storage bot. / top
Temperature / °C / Gt 10-1 / W m-2
cooling power /kW
mass flow / kg s-1 .
time

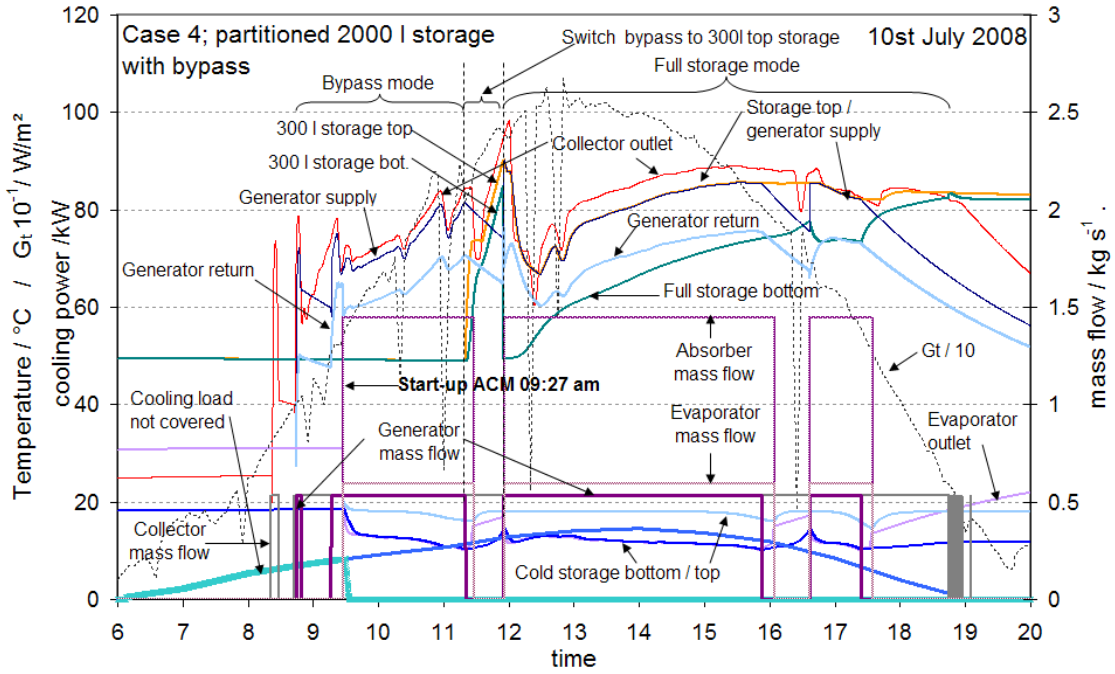
Case 4; partitioned 2000 l storage with bypass
10st July 2008
Switch bypass to 300l top storage
Full storage mode
Bypass mode
Storage top / generator supply
300 l storage top
Collector outlet
300 l storage bot.
Generator supply
Generator return
Full storage bottom
Absorber mass flow
Gt / 10
Start-up ACM 09:27 am
Cooling load not covered
Evaporator mass flow
Generator mass flow
Evaporator outlet
Collector mass flow
Cold storage bottom / top
Temperature / °C / Gt 10-1 / W/m²
cooling power /kW
mass flow / kg s-1 .
time

3. Simulation results for 11th July 2008

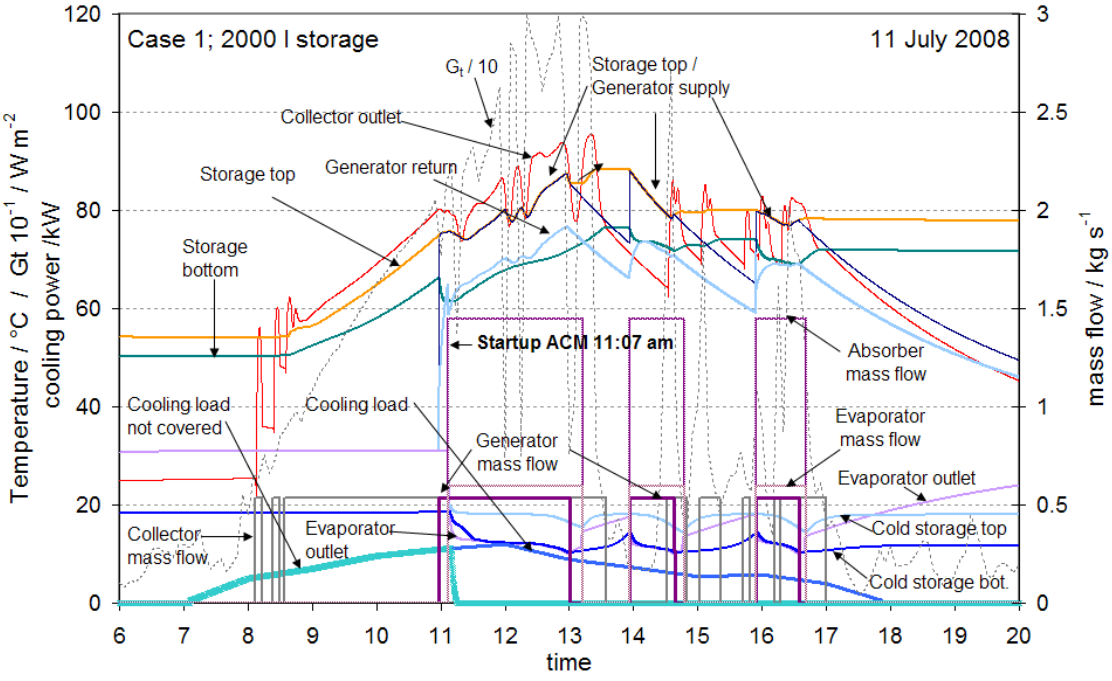

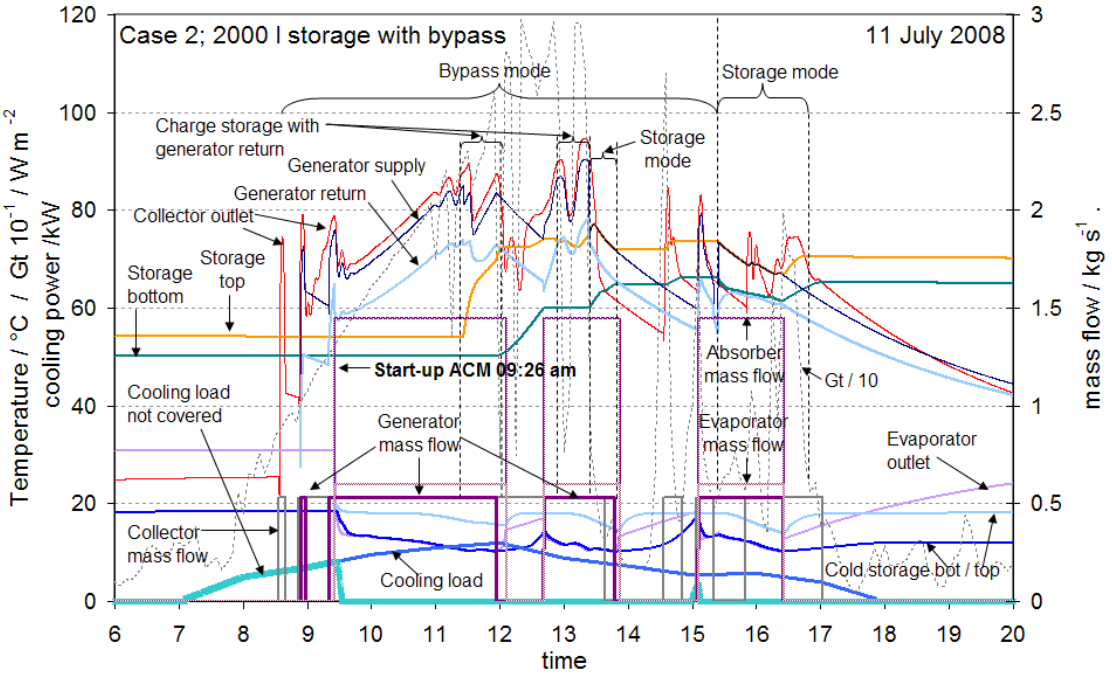

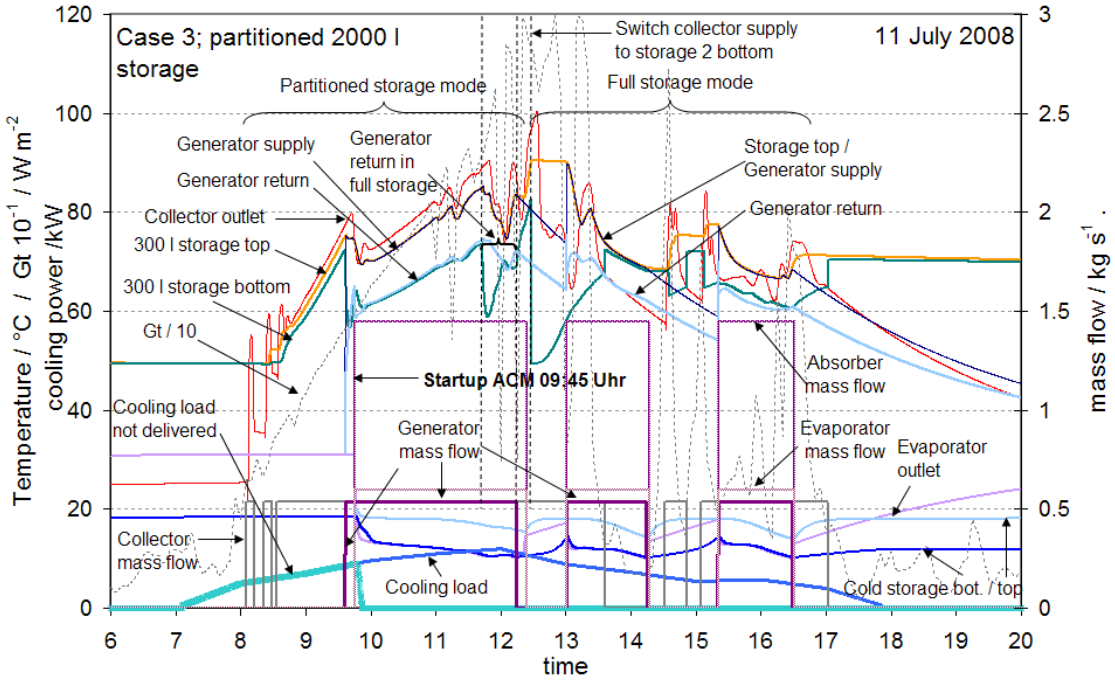
Case 3; partitioned 2000 l storage
11 July 2008
Switch collector supply to storage 2 bottom
Partitioned storage mode
Full storage mode
Generator supply
Generator return
Generator return in full storage
Collector outlet
300 l storage top
300 l storage bottom
Gt / 10
Storage top / Generator supply
Generator return
Absorber mass flow
Startup ACM 09:45 Uhr
Cooling load not delivered
Generator mass flow
Evaporator mass flow
Evaporator outlet
Collector mass flow
Cooling load
Cold storage bot. / top
Temperature / °C / Gt 10-1 / W m-2
cooling power /kW
mass flow / kg s-1 .
time

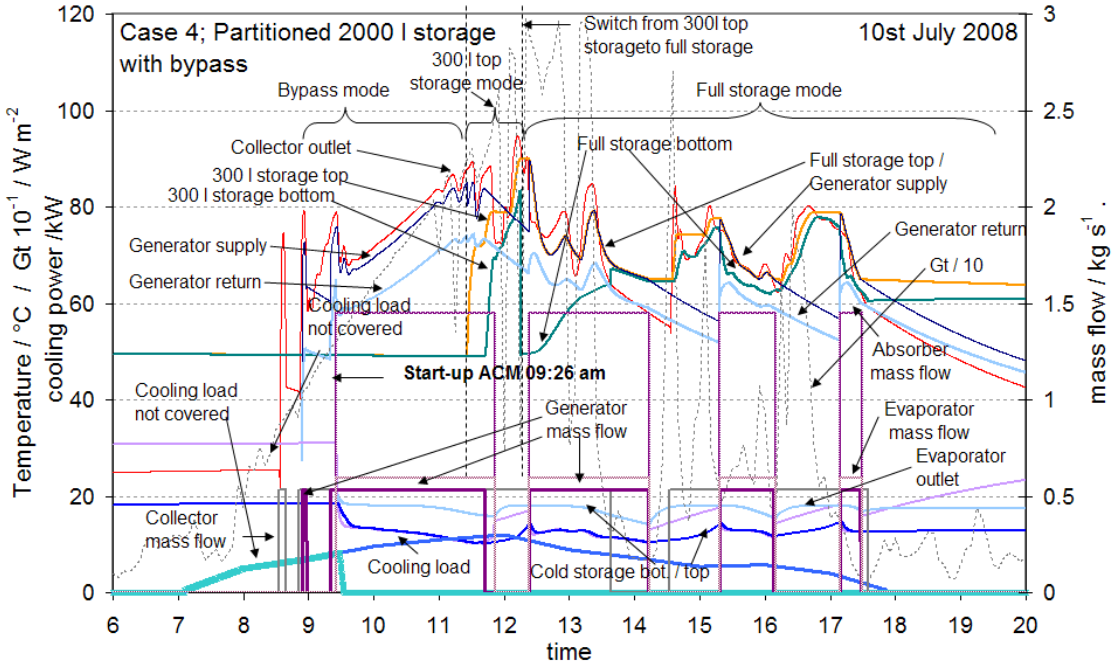
Case 4; Partitioned 2000 l storage with bypass
10st July 2008
Switch from 300l top storageto full storage
300 l top storage mode
Bypass mode
Full storage mode
Collector outlet
300 l storage top
300 l storage bottom
Full storage bottom
Full storage top / Generator supply
Generator supply
Generator return
Generator return
Gt / 10
Cooling load not covered
Absorber mass flow
Start-up ACM 09:26 am
Cooling load not covered
Generator mass flow
Evaporator mass flow
Evaporator outlet
Collector mass flow
Cooling load
Cold storage bot. / top
Temperature / °C / Gt 10-1 / W m-2
cooling power /kW
mass flow / kg s-1 .
time

SIEMENS BPS CONTROL UNIT FOR DEC SYSTEM CONTROL

1. I/O ELEMENT LIST AND SYSTEM SCHEME WITH CONTROL INDICATES

The following list aims to give an overview of the installed I/O elements and the connected sensors or related control functions within the Siemens Visonic BPS control unit. A system scheme shows the position of the Sensors and actuators within the DEC system.

Module Number	Type	Address	Description of function / value
1	2U10	$000 $001	Ambient air temperature at sorption wheel inlet Relative humidity ambient air at sorption wheel inlet
2	2U10	$002 $003	Supply air temperature between sorption wheel and HX Relative humidity supply air between sorption wheel and HX
3	2U10	$004 $005	Return / regeneration air temperature at sorption wheel inlet Relative humidity return air at sorption wheel inlet
4	2U10	$006 $007	Exhaust air temperature Relative humidity exhaust air
5	2U10	$010 $011	Relative humidity ambient air Supply air humidity after heat exchanger
6	2U10	$012 $013	Relative humidity supply air Relative humidity return air
7	2U10	$014 $015	Relative humidity return air between humidifier and HX Relative humidity return air after HX
8	2R1K	$016 $017	Temperature solar storage Nr. 1 Temperature solar storage Nr. 2
9	2Q250-M	$020 $021	On/Off Sorption wheel On/Off Heat exchanger
10	2Q250-M	$022 $023	On/Off Sup fan and Ret fan On/Off Water supply return air humidifier
11	2Q250-M	$024 $025	On/Off pump solar heating coil supply air On/Off pump solar heating coil return air
12	2Q250-M	$026 $027	On/Off Return air humidifier On/Off Electric heating register
13	4D20	$030 $031 $032 $033	Air volume flow observation supply air Air volume flow observation return air Error sorption wheel Error heat exchanger
15	4D20	$034 $035 $036	Error supply air ventilator Error Electric heating register Error supply air ventilator
17	2I420	$040 $041	Air volume flow rate supply air Air volume flow rate air collector
18	2I420	$042 $043	Air volume flow rate return air Global solar irradiation
19	2P100	$044 $045	Ambient air temperature Supply air temperature after HX

Module Number	Type	Address	Description of function / value
20	2P100	$046 $047	Supply air temperature after Solar heating coil Supply air temperature
21	2P100	$050 $051	Return air temperature Return air temperature between humidifier and HX
22	2P100	$052 $053	Return air temperature after heat exchange Return air temperature at air collector outlet
23	2P100	$054 $055	Mixed Return / regeneration air temperature AB-Temperatur nach E-Register
24	2Y10S-M	$056 $057	Setpoint sorption wheel Setpoint heat exchanger
25	2Y10S-M	$060 $061	Setpoint supply air ventilator Setpoint return air ventilator
26	2Y10S-M	$062 $063	Setpoint pump solar heating coil supply air Setpoint pump solar heating coil return air
27	2Y10S-M	$064 $065	Setpoint bypass flap Setpoint collector flap
28	2Y10S-M	$066 $067	Setpoint supply air humidifier Setpoint electronic additional heating devicec

Description of the installed sensors and their accuracy:

- **Temperature sensors:**

  PT1000 temperature sensors 1/3DIN with a measurement accuracy of ± 0,15 K

- **Humidity sensors:**

  Galltec capacity humidity sensors (Galltec PMU-V)

Measurement accuracy:	10..90%rF	± 1.5 % relative humidity
	<10%rF or >90%rF	± 2 % relative humidity
	<10°C or >40°C	additional inaccuracy ± 0.05%/K

- **Air volume flow rate:**

  Micatrone differential pressure sensors (Type Micaflex MF-FD)

  Measurement accuracy: ± 3 % of the measured pressure difference

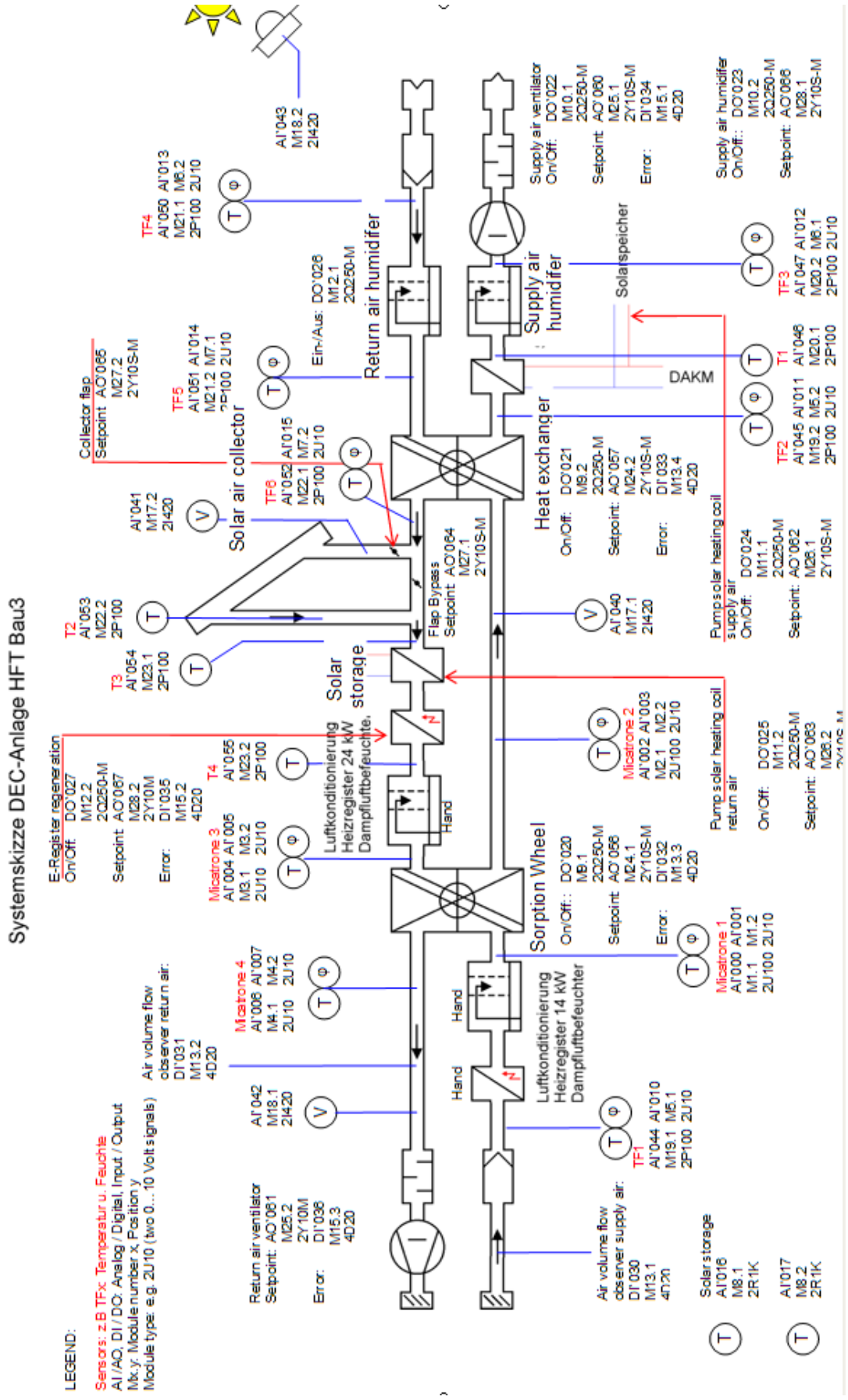
Systemskizze DEC-Anlage HFT Bau3
LEGEND:
Sensors: z.B TFx: Temperatur u. Feuchte
AI/AO, DI / DO: Analog / Digital, Input / Output
Mx.y: Module number x, Position y
Module type: e.g. 2U10 (two 0...10 Volt signals)
Solar air collector
Collector flap
Setpoint AO'065
M27.2
2Y10S-M
TF5
AI'051 AI'014
M21.2 M7.1
2P100 2U10
TF4
AI'050 AI'013
M21.1 M8.2
2P100 2U10
AI'043
M18.2
2I420
Ein-/Aus: DO'026
M12.1
2Q250-M
Return air humidifer
Supply air humidifer
Supply air ventilator
On/Off: DO'022
M10.1
2Q250-M
Setpoint AO'060
M25.1
2Y10S-M
Error: DI'034
M15.1
4D20
Solarspeicher
Supply air humidifer
On/Off:: DO'023
M10.2
2Q250-M
Setpoint: AO'066
M28.1
2Y10S-M
TF3
AI'047 AI'012
M20.2 M8.1
2P100 2U10
DAKM
T1
AI'046
M20.1
2P100
TF2
AI'045 AI'011
M19.2 M5.2
2P100 2U10
Heat exchanger
On/Off: DO'021
M9.2
2Q250-M
Setpoint: AO'057
M24.2
2Y10S-M
Error: DI'033
M13.4
4D20
AI'041
M17.2
2I420
TF6
AI'052 AI'015
M22.1 M7.2
2P100 2U10
T2
AI'053
M22.2
2P100
T3
AI'054
M23.1
2P100
Flap Bypass
Setpoint: AO'064
M27.1
2Y10S-M
AI'040
M17.1
2I420
Pump solar heating coil
supply air
On/Off: DO'024
M11.1
2Q250-M
Setpoint: AO'062
M28.1
2Y10S-M
Solar storage
Luftkonditionierung
Heizregister 24 kW
Dampflufbefeuchte.
Hand
Micatrone 3
AI'004 AI'005
M3.1 M3.2
2U10 2U10
T4
AI'055
M23.2
2P100
Micatrone 2
AI'002 AI'003
M2.1 M2.2
2U100 2U10
Pump solar heating coil
return air
On/Off: DO'025
M11.2
2Q250-M
Setpoint: AO'063
M28.2
E-Register regeneration
On/Off: DO'027
M12.2
2Q250-M
Setpoint AO'067
M28.2
2Y10M
Error: DI'035
M15.2
4D20
Air volume flow
observer return air:
DI'031
M13.2
4D20
Micatrone 4
AI'006 AI'007
M4.1 M4.2
2U10 2U10
Sorption Wheel
On/Off:: DO'020
M8.1
2Q250-M
Setpoint: AO'058
M24.1
2Y10S-M
Error: DI'032
M13.3
4D20
Micatrone 1
AI'000 AI'001
M1.1 M1.2
2U100 2U10
Luftkonditionierung
Heizregister 14 kW
Dampflufbefeuchter
Hand
Return air ventilator
Setpoint: AO'061
M25.2
2Y10M
Error: DI'036
M15.3
4D20
AI'042
M18.1
2I420
Air volume flow
observer supply air:
DI'030
M13.1
4D20
TF1
AI'044 AI'010
M19.1 M5.1
2P100 2U10
AI'016
M8.1
2R1K
AI'017
M8.2
2R1K